MOLECULAR SIEVES

6 *Science and Technology*

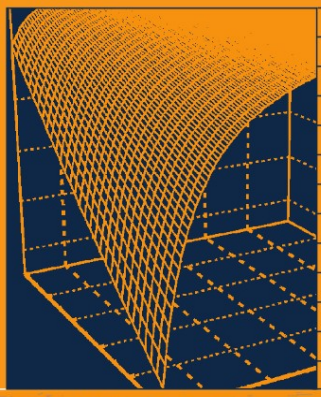

ACIDITY AND BASICITY

Springer

6
Molecular Sieves
Science and Technology

Molecular Sieves

Editors: H. G. Karge · J. Weitkamp

Recently Published and Forthcoming Volumes

Adsorption and Diffusion
Editors: Karge, H. G., Weitkamp J.
Vol. 7, 2008

Acidity and Basicity
Vol. 6, 2008

Characterization II
Editors: Karge, H. G., Weitkamp J.
Vol. 5, 2006

Characterization I
Editors: Karge, H. G., Weitkamp J.
Vol. 4, 2004

Post-Synthesis Modification I
Editors: Karge, H. G., Weitkamp J.
Vol. 3, 2003

Structures and Structure Determination
Editors: Karge, H. G., Weitkamp J.
Vol. 2, 1999

Synthesis
Editors: Karge, H. G., Weitkamp J.
Vol. 1, 1998

Acidity and Basicity

A. Auroux · A. Brait · E. Brunner · F. Fajula
E. Garrone · A. Jentys · J. A. Lercher · H. Pfeifer

Springer

Molecular Sieves – Science and Technology will be devoted to all kinds of microporous crystalline solids with emphasis on zeolites. Classical alumosilicate zeolites as well as microporous silica will typically be covered; titaniumsilicate, alumophosphates, gallophosphates, silicoalumophosphates, and metalloalumophosphates are also within the scope of the series. It will address such important items as hydrothermal synthesis, structures and structure determination, post-synthesis modifications such as ion exchange or dealumination, characterization by all kinds of chemical and physico-chemical methods including spectroscopic techniques, acidity and basicity, hydrophilic vs. hydrophobic surface properties, theory and modelling, sorption and diffusion, host-guest interactions, zeolites as detergent builders, as catalysts in petroleum refining and petrochemical processes, and in the manufacture of organic intermediates, separation and purification processes, zeolites in environmental protection.
As a rule, contributions are specially commissioned. The editors and publishers will, however, always be pleased to receive suggestions and supplementary information. Papers for *Molecular Sieves* are accepted in English. In references *Molecular Sieves* is abbreviated *Mol Sieves* and is cited as a journal.
Springer WWW home page: springer.com
Visit the Molecular Sieves home page at springerlink.com

ISBN 978-3-540-73963-0 e-ISBN 978-3-540-73964-7
DOI 10.1007/978-3-540-73964-7

Molecular Sieves ISSN 1436-8269

Library of Congress Control Number: 2008920329

Typesetting and Production: LE-TEX Jelonek, Schmidt & Vöckler GbR, Leipzig, Germany
Cover Design: WMXDesign GmbH, Heidelberg, Germany

Printed on acid-free paper

9 8 7 6 5 4 3 2 1 0

springer.com

Publisher's Note

Dear Reader

This volume of *Molecular Sieves* on **Acidity and Basicity** may not provide as complete a coverage of the topic as the series editors and Springer usually aspire to. Originally chapters on additional topics had been agreed. However despite all efforts, these chapters were not forthcoming. Some of the present contributions had been published online at SpringerLink.com for some time while waiting for the volume to be completed and published in print. Springer as the publisher of the series has a responsibility towards the authors to publish their contributions. After taking all possible actions Springer finally decided to close this volume and publish all contributions submitted until the end of 2007. With much regret we therefore publish Volume 6 of Molecular Sieves under Springer's name and not in the name of the series editors.

Heidelberg, January 2008

Marion Hertel
Springer-Verlag

Molecular Sieves
Also Available Electronically

For all customers who have a standing order to Molecular Sieves, we offer the electronic version via SpringerLink free of charge. Please contact your librarian who can receive a password or free access to the full articles by registering at:

springerlink.com

If you do not have a subscription, you can still view the tables of contents of the volumes and the abstract of each article by going to the SpringerLink Homepage, clicking on "Browse by Online Libraries", then "Chemical Sciences", and finally choose Molecular Sieves.

You will find information about the

- Editorial Board
- Aims and Scope
- Instructions for Authors
- Sample Contribution

at springer.com using the search function.

Color figures are published in full color within the electronic version on SpringerLink.

Contents

NMR Spectroscopic Techniques for Determining Acidity and Basicity
E. Brunner · H. Pfeifer 1

Acidity and Basicity: Determination by Adsorption Microcalorimetry
A. Auroux 45

Catalytic Test Reactions for Probing the Acidity and Basicity of Zeolites
J. A. Lercher · A. Jentys · A. Brait 153

Acidity and Basicity of Ordered Silica-based Mesoporous Materials
E. Garrone · F. Fajula 213

Author Index Volumes 1–6 269

Subject Index 273

Mol Sieves (2008) 6: 1–43
DOI 10.1007/3829_2007_016

Published online: 17 November 2007

NMR Spectroscopic Techniques for Determining Acidity and Basicity

Eike Brunner[1] (✉) · Harry Pfeifer[2]

[1]Fachrichtung Chemie und Lebensmittelchemie, Bioanalytische Chemie, Technische Universität Dresden, 01062 Dresden, Germany
eike.brunner@tu-dresden.de

[2]Universität Leipzig, Fakultät für Physik und Geowissenschaften, Linnéstraße 5, 04103 Leipzig, Germany

1 Introduction 4

2 Brønsted Acid Sites in Zeolites and Their NMR Spectroscopic Characterization 4
2.1 NMR Spectroscopic Detection of Brønsted Acid Sites 8
2.2 Measurement of the Concentration of Acid Sites 10
2.3 Measurement of the Strength of Acidity of Acid Sites in Activated Samples 11
2.4 Determination of the Accessibility and Strength of Acidity of Acid Sites in Samples Loaded with Probe Molecules 15
2.4.1 NMR of Surface Hydroxyl Groups in Loaded Samples 15
2.4.2 NMR of Probe Molecules 22
2.4.3 NMR Spectroscopic Determination of the Geometry of Adsorption Complexes and of the Mobility of the Probe Molecules . . . 24

3 NMR Spectroscopic Characterization of Lewis Acidity in Zeolites 27
3.1 ^{27}Al NMR Spectroscopy 27
3.1.1 Hydrated Samples 27
3.1.2 Dehydrated Samples 28
3.2 Use of Probe Molecules 30
3.2.1 Slow Exchange 31
3.2.2 Rapid Exchange 32

4 NMR Spectroscopic Characterization of Basicity in Zeolites 36

References 38

Abstract Solid acids and bases have found numerous applications in heterogeneous catalysis. However, the characterization of the acidic and basic properties of solids is relatively complicated compared to that of liquids. This contribution summarizes the state of the art in the spectroscopic determination of acidity and basicity by NMR methods, especially with respect to zeolites. Zeolites are porous inorganic crystals built from TO_4 tetrahedra. In original zeolites, T represents Si or Al. The latter atoms may be replaced to some extent by other elements like B, Ga, Be, Ti etc. Other classes of microporous materials are based, e.g. on $AlPO_4$ compounds. The ability of zeolites to act as acid catalysts had already been described in the early 1960s and has remained an interesting subject of research. In recent years, zeolites have also found increasing interest as basic catalysts. The presence of both acidic and basic sites is responsible for the broad applicability of zeolites as catalysts.

Abbreviations

Symbols

β, B	Parameters
B_0	Magnetic flux density
c_j	Concentration of species j (e.g. Al, B, H etc.)
C_Q	Quadrupole coupling constant
δ	Chemical shift of a NMR signal
δE	Distribution width of the deprotonation energy
δ_H, δ_C etc.	NMR chemical shift of ^1H, ^{13}C etc.
$\langle\delta_H\rangle$	Mean ^1H NMR chemical shift
$\delta_{11}, \delta_{22}, \delta_{33}$	Principal values of the chemical shift tensor
$\delta_{\|\|}, \delta_\perp$	Principal values of a chemical shift tensor of axial symmetry
δ_{SiOH}	^1H NMR chemical shift of non-acidic SiOH
δ_0	Extrapolated value of δ
Δ, Δ^{MAS} etc.	Line widths (in ppm)
$\Delta\delta_H$	Induced ^1H NMR chemical shift
ΔE	Energy difference
ΔE_{DP}	Deprotonation energy
ΔE_{DP}^{SiOH}	Deprotonation energy of non-acidic SiOH
ΔE_{DP}^{O}	Zero-point vibrational energy change of deprotonation
$\Delta\nu_L$	Full width at half maximum of the ^{13}C NMR signal of ^{13}CO adsorbed on Lewis acid sites
$\Delta\nu_{OH}$	Wavenumber shift of a OH stretching vibration IR band
$\Delta\nu_{1/2}$	Full width at half maximum of a NMR signal in Hz
$\Delta\nu_{1/2}^{MAS}$	Full width at half maximum of a MAS NMR signal in Hz
$\Delta\nu_P$	Full width at half maximum of the ^{13}C NMR signal of physisorbed ^{13}CO
$\Delta\nu_{SiOH}$	Wavenumber shift of the stretching IR band due to non-acidic SiOH
$\Delta\omega$	Angular frequency difference
$\Delta\sigma_C$	Chemical shift anisotropy of ^{13}CO
Δt	Uncertainty of time in Heisenberg's uncertainty relation
e	Elementary charge
eq	Electric field gradient
eQ	Electric quadrupole moment
η	Asymmetry parameter
h	Planck's constant
$\hbar$	Planck's constant divided by 2π
I	Spin quantum number
i, j	Indices
J, J_{ref}, etc.	Intensities of NMR signals
K	Equilibrium constant
m	Charge of a cation in units of the elementary charge
M, M_{ref}	Mass of a sample and of a reference sample, respectively
n	Si/Al ratio
ν_{CG}	Centre of gravity of a quadrupolar shifted NMR signal
$\nu_{crit}^{MAS}, \nu_{crit}^{DOR}$	Critical values for sample spinning rates
ν_j	Resonance frequency of a nucleus at an adsorption site j
ν_L	Resonance frequency (Larmor frequency)
ν_{OH}	Wavenumber of the OH stretching vibrations

$\nu_{OH...M}$	Wavenumber of the fundamental stretching vibration of a hydroxyl group influenced by a probe molecule M
ν_Q	Quadrupole frequency
ν_r	Sample spinning rate in MAS experiments
ν_{ri}	Spinning rate of the inner rotor in DOR experiments
ν_{ro}	Spinning rate of the outer rotor in DOR experiments
ν_{sj}	Frequency of the spinning sideband of the order j
ν_0	Centre of gravity of a NMR signal (frequency)
p_j	Relative concentration of a nucleus at an adsorption site j
q_O	Average charge on the framework oxygen atoms
r	Distance between two atoms
$r_{H–C}$	Distance between H of a SiOHAl group and C of an adsorbed CO molecule
$r_{H–O}$	Distance between H of a SiOHAl group and O of an adsorbed CO molecule
S	Sanderson's intermediate electronegativity
S_a	Strength of gas phase acidity
S_{Al}, S_{Si} etc.	Atomic electronegativities of the corresponding atoms
t	Time
τ	Mean residence time
τ_{crit}	Critical value of the mean residence time
τ_j	Mean residence time of a nucleus at an adsorption site j
x_{Al}	Number of Al atoms in the second coordination sphere of a Si atom
$X(i)$	Exchange degree of the cations $Me^{m(i)+}$ divided by $m(i)$
z	Number of H_2O molecules adsorbed per framework Al atom
x, y	Variables

Abbreviations

AlOD	Deuterated hydroxyl group located on non-framework Al species
AlOH	Hydroxyl group located on non-framework Al species
$AlPO_4$	Aluminophosphate
CP	Cross polarization
CRAMPS	Combined rotation and multiple pulse spectroscopy
DOR	Double rotation
HF band	High frequency IR band
H – Y	Proton exchanged Y zeolite
H-ZSM-5	Proton exchanged zeolite of type ZSM-5
IR	Infrared
L	Lewis acid site
LF band	Low frequency IR band
M	Molecule
MAS	Magic angle spinning
Me^{m+}	Cation (with a charge $m \cdot e$)
MQ	Multiple quantum
NMR	Nuclear magnetic resonance
REDOR	Rotational echo double resonance
SEDOR	Spin echo double resonance
SiOD	Deuterated silanol group
SiOH	Silanol group
SiOHAl	Bridging hydroxyl group
T	Framework T-atom (Si, Al etc.)

TRAPDOR	Transfer of populations double resonance
u.c.	Unit cell
0.3 HNa – Y	Y zeolite with a proton exchange degree of 0.3

1 Introduction

Solid acids and bases have found numerous applications in heterogeneous catalysis [1–7]. However, the characterization of the acidic and basic properties of solids is relatively complicated compared to that of liquids. The present contribution summarizes the state of the art in the spectroscopic determination of acidity and basicity by NMR methods, especially with respect to zeolites. Zeolites are porous inorganic crystals built from TO_4 tetrahedra [8–10]. In original zeolites, T represents Si or Al. The latter atoms may be replaced to some extent by other elements like B, Ga, Be, Ti etc. (see, e.g. [11, 12]). Other classes of microporous materials are based, e.g. on $AlPO_4$ compounds [13–15]. The ability of zeolites to act as acid catalysts had already been described in the early 1960s [16, 17] and has remained an interesting subject of research. Zeolites have also found increasing interest as basic catalysts in recent years [4]. The presence of both acidic and basic sites is responsible for the broad applicability of zeolites as catalysts.

2 Brønsted Acid Sites in Zeolites and Their NMR Spectroscopic Characterization

Proton-exchanged zeolites (H-zeolites) exhibit *structural* Brønsted acid sites (bridging hydroxyl groups, see Fig. 1). The chemical composition of a partially proton-exchanged zeolite is given by the formula:

$$H_X{}^{+}Me^{m+}_{\frac{1}{m}(1-X)}\left[(SiO_2)_n AlO_2{}^{-}\right]\left(H_2O\right)_z \ , \tag{1}$$

where n denotes the Si/Al ratio and X is the proton exchange degree given by the ratio $c_{\mathrm{SiOHAl}}/c^{\mathrm{F}}_{\mathrm{Al}}$ of the concentration of bridging hydroxyl groups, c_{SiOHAl}, and the concentration of framework Al atoms, $c^{\mathrm{F}}_{\mathrm{Al}}$. Me^{m+} ($m = 1, 2, \ldots$) denotes exchangeable cations such as Na^+, Mg^{2+} and others. The number of adsorbed water molecules (per framework Al) is given by z.

The catalytic activity of zeolites in Brønsted acid-catalysed reactions should be directly proportional to the concentration of accessible bridging hydroxyl groups, provided that the strength of acidity of the bridging hydroxyl groups is constant. This behaviour was indeed observed for silicon-rich H-ZSM-5 [20] (see Fig. 2). In contrast, however, the catalytic activity of

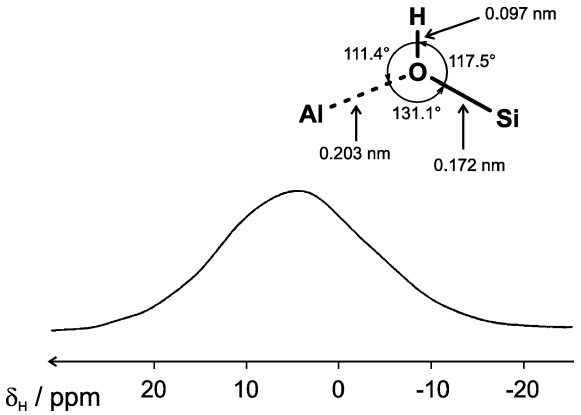

Fig. 1 Structure of a free bridging hydroxyl group in the framework of zeolites, according to a quantum chemical calculation [18] and ^{1}H NMR spectrum of an activated 0.3 HNa – Y zeolite (Si/Al = 2.5) measured at 500 MHz. The spectra were recorded by the use of Hahn's echo in order to avoid problems with the dead time of the receiver [19]. This sample almost exclusively contains free bridging hydroxyl groups

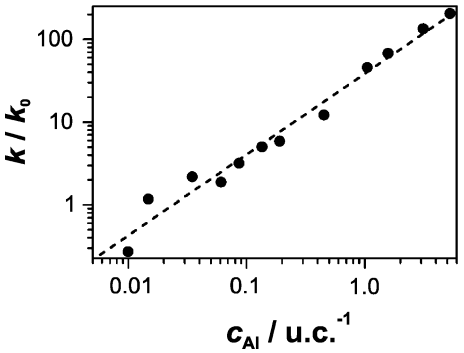

Fig. 2 Relative *n*-hexane cracking activity k/k_0 of H-ZSM-5 as a function of the aluminium concentration c_{Al}. k and k_0 denote the reaction rate constants of the catalyst under study and of a reference catalyst, respectively [20]

X zeolites with $n \approx 1.2$ is lower than the catalytic activity of Y zeolites with $n \approx 2.4$ (see [21, 22]). These observations have led to the conclusion [23] that the strength of acidity increases with decreasing concentration of framework Al atoms for aluminium-rich zeolites ($n < 6$) but remains constant for silicon-rich zeolites. In other words, the strength of acidity of bridging hydroxyl groups must depend on the structural and compositional parameters of the zeolite.

It is apparent that an enhancement of the electronegativity of the zeolite framework $(SiO_2)AlO_2^-$ will reduce the electron density of the O – H bond of a surface hydroxyl group, which should result in an increased strength of

acidity. Sanderson's intermediate electronegativity S [24] is defined as:

$$S = \left(S_{\mathrm{Me}}^{\frac{1}{m}} S_{\mathrm{Al}} S_{\mathrm{O}}^{2n+2} S_{\mathrm{Si}}^{n} \right)^{\frac{1}{3n+4}} \tag{2}$$

with the atomic electronegativites $S_{\mathrm{Al}} = 2.22$, $S_{\mathrm{O}} = 5.21$ and $S_{\mathrm{Si}} = 2.84$ for zeolites of the composition given in Eq. 1. $S_{\mathrm{Me}}^{\frac{1}{m}}$ has to be replaced in Eq. 2 by the expression:

$$S_{\mathrm{Me}}^{\frac{1}{m}} = \prod_{i=1}^{k} \left[S_{\mathrm{Me}(i)} \right]^{X(i)} \tag{3}$$

with:

$$X(i) = \frac{1}{m(i)} \frac{c_i}{c_{\mathrm{Al}}^{\mathrm{F}}} \tag{4}$$

if a zeolite contains two or more different charge compensating cations. $S_{\mathrm{Me}(i)}$ denotes the atomic electronegativity of the cation $\mathrm{Me}(i)^{m(i)+}$ $(i = 1, 2, \ldots, k)$ having a positive charge $m(i) \cdot e$ and c_i is the concentration of the corresponding cations. S_{Me} corresponds to $S_{\mathrm{H}} = 3.55$ $(m = 1)$ for completely proton-exchanged zeolites. Figure 3 exhibits Sanderson's intermediate electronegativity S plotted as a function of the Si/Al ratio n and the proton exchange degree $c_{\mathrm{SiOHAl}}/c_{\mathrm{Al}}^{\mathrm{F}}$ for zeolites containing protons (H^+) and sodium ions (Na^+) as charge compensating cations. Obviously, S reflects the above-described dependence of the strength of acidity on the Si/Al ratio. Therefore, it was suggested that use be made of S as a measure for the (mean) strength of acidity of the bridging hydroxyl groups [25, 26].

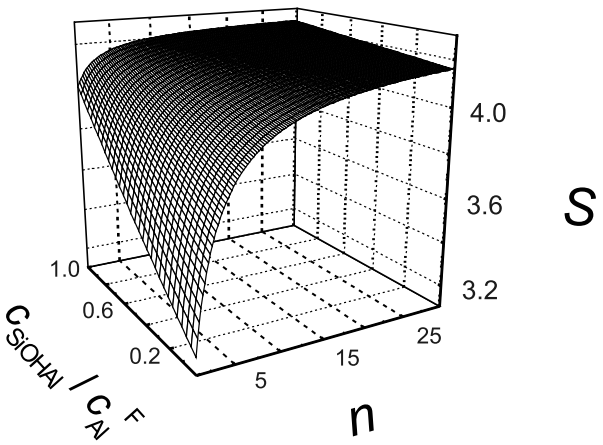

Fig. 3 Values for Sanderson's intermediate electronegativity S as a function of the framework Si/Al ratio n and the proton exchange degree $c_{\mathrm{SiOHAl}}/c_{\mathrm{Al}}^{\mathrm{F}}$ for HNa-zeolites

However, possible distributions of the strength of acidity of bridging hydroxyl groups, which may be caused by the influence of short-range interactions, cannot be described by Sanderson's intermediate electronegativity. Quantum chemical calculations (see, e.g. [27, 28]) give rise to the assumption that the distribution of aluminium atoms in the zeolite framework is the main reason for the distribution of the strength of acidity of bridging hydroxyl groups ("heterogeneity of bridging hydroxyl groups"). In particular, the strength of acidity of a bridging hydroxyl group should depend on the number of neighbouring Al atoms. If we denote the number of Al atoms in the second coordination sphere of the Si atom of a SiOHAl group by $x_{Al} = 1, 2, 3, 4$, the strength of acidity, S_a, should decrease with increasing values of x_{Al} [27]. In addition, the strength of acidity of a SiOHAl site may be influenced by the local geometry of the site, i.e. bond angles and distances [27–30].

Furthermore, it is suggested that the interaction between Brønsted acid sites and Lewis acid sites may lead to the formation of *Brønsted acid sites of enhanced strength of acidity* [31–33]. This suggestion was supported by the observation of an enhanced catalytic activity of H-ZSM-5 with respect to Brønsted acid-catalysed reactions after a hydrothermal treatment [34] (see Fig. 4). Haag et al. [34] suggested the following model for the structure of the Brønsted acid sites of enhanced strength of acidity in H-ZSM-5: One aluminium atom of an Al – O – Si – O – Al site in the zeolite framework is modified by the steaming process. The modified aluminium atom is envisioned as a partially hydrolysed, coordinatively unsaturated Al species of Lewis acid character. This inductively leads to a greater negative charge delocalization in the remaining Si – O – Al bridge, thus creating a Brønsted acid site of enhanced strength of acidity. Since it has been impossible to detect these sites in H-ZSM-5 spectroscopically until now [35–37], an alternative explanation was that the enhanced catalytic activity of "mildly" hydrothermally

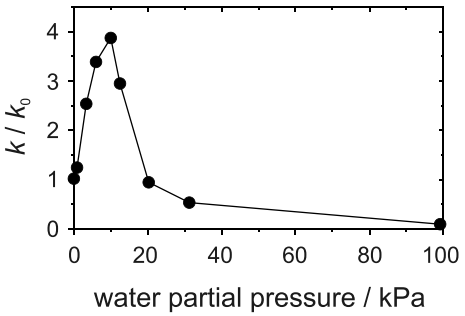

Fig. 4 Relative *n*-hexane cracking activity k/k_0 of H-ZSM-5 hydrothermally treated for 2.5 h at 813 K as a function of the water partial pressure according to [34]. The non-steamed sample was used as reference catalyst

treated H-ZSM-5 may be due to a synergism between Brønsted acid sites of *normal* strength of acidity and neighbouring Lewis acid sites. It should, however, be mentioned that IR-spectroscopic investigations gave evidence for the existence of Brønsted acid sites of enhanced strength of acidity in H – Y zeolites [38].

In the light of these remarks, it becomes quite clear that quantitative spectroscopic methods for determining the Brønsted acidity are a necessary prerequisite for the characterization and understanding of solid catalysts. Quantitative determination of Brønsted acidity, however, means the measurement of (i) the concentration, (ii) the strength of acidity, and (iii) the accessibility of the Brønsted acid sites.

2.1 NMR Spectroscopic Detection of Brønsted Acid Sites

Surface hydroxyl groups can be detected by ^{1}H NMR [19, 39–47] or ^{2}H NMR spectroscopy [48–51]. In order to measure the signals of the pure surface hydroxyl groups, the samples have to be activated in order to completely remove water (see Eq. 1) and other adsorbed molecules. During the measurements, the samples must be isolated from the atmosphere in order to prevent re-adsorption of molecules such as water or oxygen that would perturb the spectra (see below). This can be achieved by sealing the samples in glass ampoules after activation.

In general, ^{1}H and ^{2}H NMR signals of surface hydroxyl groups are strongly broadened (see Fig. 1) by internal magnetic interactions like the homonuclear and heteronuclear magnetic dipole–dipole interaction, the anisotropy of the chemical shift, and – in the case of ^{2}H – by the electric quadrupole interaction. It is, therefore, necessary to apply line narrowing techniques such as magic angle spinning (MAS) [52] or combined rotation and multiple-pulse spectroscopy (CRAMPS) [53–57] in order to obtain highly resolved spectra. The ^{1}H NMR signals of surface hydroxyl groups in zeolites are mainly broadened by inhomogeneous magnetic interactions like the heteronuclear magnetic dipole–dipole interaction and the chemical shift anisotropy. For bridging hydroxyl groups, the heteronuclear magnetic dipole–dipole interaction between ^{1}H and ^{27}Al (see Fig. 1) dominates. Therefore, MAS leads to ^{1}H MAS NMR signals consisting of a narrow central line at the centre of gravity of the signal ν_0 and spinning sidebands at the frequencies:

$$\nu_{sj} = \nu_0 + j\nu_r \,, \tag{5}$$

where $j = \pm 1, \pm 2, \ldots$ denotes the order of the spinning sideband and ν_r is the spinning rate of the sample (see Fig. 5). Within the present work, spinning sidebands will be denoted by an asterisk (*) in all figures. The central line as well as the spinning sidebands may exhibit a characteristic broadening if the NMR signal is additionally influenced by a homogeneous interaction like

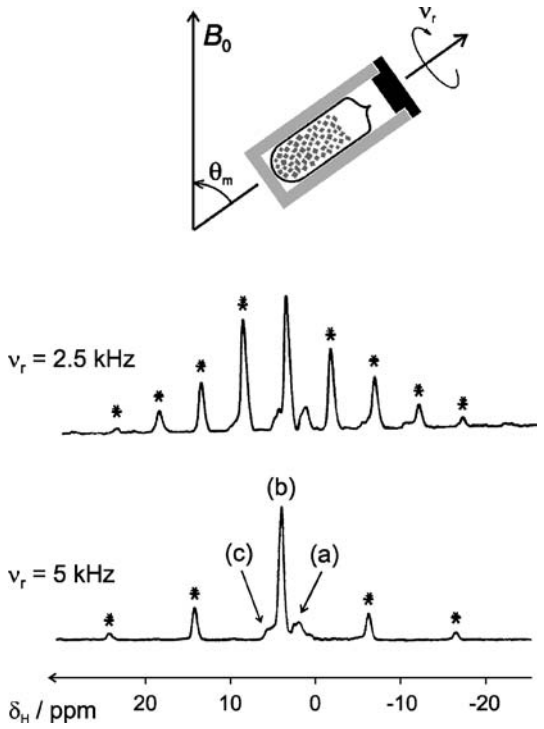

Fig. 5 *Top:* Sketch illustrating magic angle spinning (MAS) of evacuated, sealed samples. The rotor axis is tilted against the external magnetic field B_0 by the magic angle θ_m =54.74°. The powdered sample is activated and then sealed in a glass ampoule under high vacuum. This method has to be applied for the detection of unperturbed surface hydroxyl groups. *Middle and bottom:* ^{1}H MAS NMR spectra of the same sample as in Fig. 1 measured with sample spinning rates of 2.5 kHz and 5 kHz [19]. *Line a* at 2 ppm is due to SiOH groups, *line b* at 3.9 ppm is caused by bridging OH groups in the large cavities and *line c* at 4.9 ppm results from bridging OH groups in the six-oxygen rings

the homonuclear magnetic dipole–dipole interaction between more than two ^{1}H spins [58–63]. The latter effect is preferentially found for H-zeolites with low Si/Al ratio, i.e. high proton density. In contrast, it is negligible for highly siliceous zeolites such as H-ZSM-5.

Since the heteronuclear magnetic dipole–dipole interaction is the dominating line-broadening interaction, NMR spectroscopy allows an accurate measurement of the H – Al distance in bridging hydroxyl groups (see Fig. 1). The H – Al distance can be measured in static experiments by conventional second moment analysis of the broad-line ^{1}H NMR spectrum [64, 65] or by so-called SEDOR (spin echo double resonance [66–68]) experiments [69]. Another method offering an excellent accuracy is the numerical analysis of the spinning sideband patterns of the ^{1}H MAS NMR signals [70]. This method also allows measurement of the chemical shift anisotropy $\Delta\sigma_H$. For the 0.3 HNa – Y

zeolite shown in Figs. 1 and 5, a H – Al distance of 0.245 ± 0.002 nm and a chemical shift anisotropy of 16 ± 2 ppm could be determined [19]. Within this context, it should be noted that the adsorption of oxygen strongly influences the spinning sideband patterns of hydroxyl groups [71, 72]. Even small amounts of the paramagnetic oxygen molecules lead to significantly broadened spinning sideband patterns, especially at low temperatures. This effect results in the disappearance of the signals of bridging hydroxyl groups from the ^{1}H MAS NMR spectra for higher oxygen loadings [71]. In a detailed study of these phenomena, Liu et al. [72] have suggested making use of oxygen in order to probe the accessibility of Brønsted acid sites.

Hydroxyl protons, especially those of the bridging hydroxyl groups are mobile at elevated temperatures [73]. This results in two characteristic effects: (i) a decrease of the intensity of the spinning sidebands and (ii) an increase of the residual line width of the central line [74, 75]. Both effects could be observed especially for bridging hydroxyl groups while the signal due to non-acidic SiOH groups is almost independent of temperature [76–79]. It is assumed that the protons belonging to bridging hydroxyl groups jump between the four oxygen atoms surrounding the Al atom. Activation energies of 20–60 kJ/mol were measured for these proton jumps depending on the structure and Si/Al of the zeolite. For H-ZSM-5, a striking correlation between the Si/Al ratio and the mobility of the protons could be found [79]. So far, it is, however, unclear whether the activation energy of the proton jumps corresponds to an energy barrier or to proton affinity differences between the different oxygen sites.

2.2
Measurement of the Concentration of Acid Sites

The intensity (area) J of an NMR signal, which is directly proportional to the concentration of resonating nuclei, is given by the equation:

$$J = \sum_{j=-\infty}^{\infty} J_j \,. \tag{6}$$

J_0 denotes the intensity of the central line ($j = 0$) and J_j ($j = \pm 1, \pm 2, \ldots$) is the intensity of the spinning sideband of the order j. ^{1}H MAS NMR spectroscopy easily allows the measurement of the numberc_H of a certain proton species per mass unit by the use of an inner or an outer standard with a known proton number c_H^{ref} per mass unit according to the equation:

$$c_H = \frac{M_{ref}}{M} \frac{J}{J_{ref}} c_H^{ref} \,, \tag{7}$$

where M and M_{ref} denote the masses of the sample under study and of the reference sample, respectively. J_{ref} is the intensity of the reference signal.

2.3 Measurement of the Strength of Acidity of Acid Sites in Activated Samples

The strength of gas phase acidity of a surface hydroxyl group was defined as the reciprocal value of the standard Gibbs free energy for deprotonation (see, e.g. [46]). As shown by Sauer [80], the deprotonation energy ΔE_{DP} may be used instead of the standard Gibbs free energy in order to evaluate changes in the strength of gas phase acidity. Therefore, the question arises whether the ^{1}H NMR chemical shift δ_H of surface hydroxyl groups is related to the deprotonation energy. Although it is known from previous NMR measurements performed on hydroxyl groups in solids [46] that no general correlation exists, δ_H and ΔE_{DP} are correlated for surface hydroxyl groups if the following conditions are fulfilled:

- Measurements have to be performed on activated samples since adsorbed molecules may strongly influence δ_H (see below)
- The concentration of surface hydroxyl groups should be relatively low in order to exclude a direct interaction of neighbouring hydroxyl groups
- Additional electrostatic interactions of the hydrogen bonds of the surface hydroxyl groups with the framework must be excluded

The essential point is that the ^{1}H NMR chemical shift δ_H of free bridging hydroxyl groups was shown to be correlated with Sanderson's intermediate electronegativity of the zeolite lattice [41, 42, 46]. On the basis of these experimental results it was suggested [41, 42, 46] to make use of the chemical shift δ_H of free surface hydroxyl groups as a measure for their strength of acidity. This statement is supported by ab initio quantum chemical calculations [81] that have revealed a linear correlation between the deprotonation energy ΔE_{DP} and the chemical shift δ_H for free surface hydroxyl groups in compounds where the first coordination sphere of the T atoms (T = Si, Al, B, P, ...) consists of oxygen atoms only. The slope of ΔE_{DP} amounts to $-84 \pm 12\,\mathrm{kJ\,mol^{-1}\,ppm^{-1}}$. Therefore, the difference $\Delta E = \Delta E_{DP}^{SiOH} - \Delta E_{DP}$ between the deprotonation energy of non-acidic SiOH groups and the considered surface hydroxyl groups can be calculated by:

$$\frac{\Delta E}{\mathrm{kJ\,mol^{-1}}} = 84 \left(\frac{\delta_H}{\mathrm{ppm}} - \frac{\delta_{SiOH}}{\mathrm{ppm}} \right) . \tag{8}$$

It has been found [46, 82] that the chemical shift δ_{SiOH} of terminal SiOH groups in highly siliceous zeolites as well as silica gel is 2.0 ± 0.1 ppm. The experimental error of ± 0.1 ppm corresponds to $\pm 8\,\mathrm{kJ\,mol^{-1}}$. The experimental error of δ_H amounts to ca. ± 0.05 ppm, corresponding to $\pm 4\,\mathrm{kJ\,mol^{-1}}$ [82]. Therefore, ΔE can be measured with an accuracy of $\pm 12\,\mathrm{kJ\,mol^{-1}}$ in favourable cases by this method. Using the value of $\Delta E_{DP}^{SiOH} = 1400 \pm 25\,\mathrm{kJ\,mol^{-1}}$ [83–86] it is then possible to determine the deprotonation energy ΔE_{DP} within an error of ca. $\pm 40\,\mathrm{kJ\,mol^{-1}}$.

The value of the full width at half maximum $\Delta\nu_{1/2}^{MAS}$ of line b (residual line width) achieved for a resonance frequency higher than 500 MHz and sufficiently high sample spinning rates can be used to estimate the upper limit of the distribution width δE_{DP} of the deprotonation energy [19, 82, 87]. Applying Eq. 8 one may write:

$$\frac{\delta E_{DP}}{\text{kJ mol}^{-1}} \leq 84 \times 10^6 \frac{\Delta\nu_{1/2}^{MAS}}{\nu_L} . \tag{9}$$

The residual line width of ca. 300 Hz (0.6 ppm) observed for line b in 0.3 HNa – Y at a resonance frequency (Larmor frequency) ν_L = 500 MHz therefore corresponds to $\delta E_{DP} \leq 50$ kJ mol^{-1}. A distribution width of 10–30 kJ mol^{-1} was determined for bridging hydroxyl groups in the large cavities of HNa – Y zeolites [88] by temperature programmed desorption of NH_3.

The interdependence between the chemical shift δ_H and the wavenumber ν_{OH} of the stretching vibration is shown in Fig. 6 for different types of hydroxyl groups [89]. Data are summarized in Table 1. For surface hydroxyl groups in zeolites this relation is given by:

$$\frac{\delta_H}{\text{ppm}} = 57.1 - 0.0147 \frac{\nu_{OH}}{\text{cm}^{-1}} . \tag{10}$$

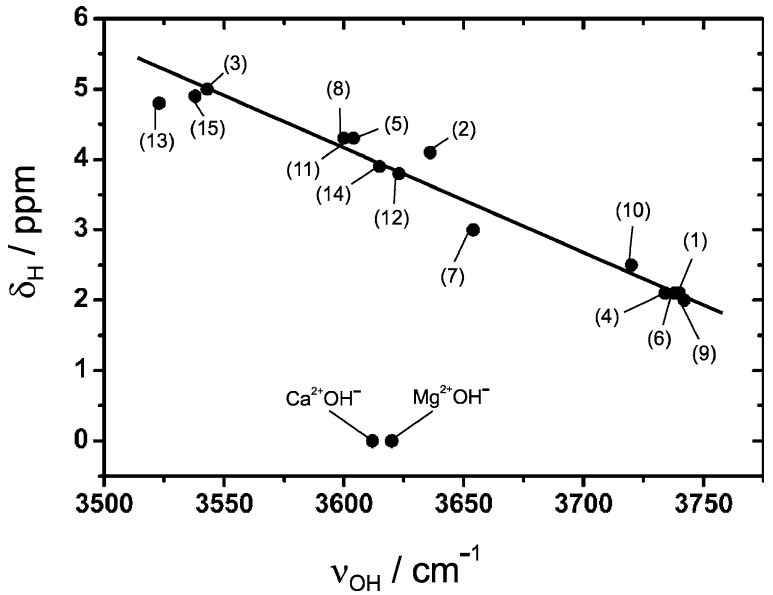

Fig. 6 Correlation between the ^{1}H NMR chemical shift δ_H and the wavenumber ν_{OH} of the fundamental stretching vibration of various surface hydroxyl groups in zeolites [89]. The data are summarized in Table 1

Table 1 Experimental values for the chemical shift δ_H and for the wavenumber ν_{OH} of the stretching vibration of the various OH groups of zeolites [89]

Zeolite	OH group	δ_H ppm	ν_{OH} cm^{-1}	Data point in Fig. 6
H-Y	SiOH	2.0	3742	(1)
	SiOHAl (HF)	4.1	3636	(2)
	SiOHAl (LF)	5.0	3543	(3)
H-ZSM-5	SiOH	2.1	3734	(4)
	SiOHAl	4.3	3604	(5)
H-ZSM-5^{HT}	SiOH	2.1	3738	(6)
	AlOH (non-framework)	3.0	3654	(7)
	SiOHAl	4.3	3600	(8)
H-SABO	SiOH	2.1	3740	(9)
	SiOHB	2.5	3720	(10)
	SiOHAl	4.3	3604	(11)
SAPO-5	SiOH[a]	1.7[s]	3739	–
	POH[a]		3674	–
	SiOHAl(I)	3.8	3623	(12)
	SiOHAl(II)	4.8	3523	(13)
SAPO-11	SiOH[a]	1.9[s]	3741	–
	POH[a]		3671	–
	SiOHAl(I)	3.9	3615	(14)
	SiOHAl(II)	4.9	3538	(15)
Mg – Y[b]	$Mg^{2+}OH^-$	0.0	3620	–
Ca – Y[b]	$Ca^{2+}OH^-$	0.0	3612	–

HF and LF denote bridging hydroxyl groups corresponding to the so-called HF and LF infrared bands in H – Y

[a] Assignment uncertain

[b] SiOH and SiOHAl as in H-Y

[c] NMR signals are the sum of two or more components

A linear dependence also exists for hydrogen bonded protons in various solids, which can be described by [89]:

$$\frac{\delta_H}{\text{ppm}} = 37.9 - 0.0092\frac{\nu_{OH}}{\text{cm}^{-1}} . \tag{11}$$

It has to be mentioned, however, that cationic OH groups such as $Mg^{2+}OH^-$ or $Ca^{2+}OH^-$ significantly deviate from these equations. The linear correlation between ν_{OH} and δ_H for surface hydroxyl groups confirms that both quantities can be used to determine the strength of acidity of free surface hydroxyl groups in zeolites.

It is remarkable that ν_{OH} as well as δ_H are strongly influenced by the formation of hydrogen bonds, which complicates the determination of the strength

of acidity of hydrogen bonded surface hydroxyl groups as can be seen from the following examples.

Bridging hydroxyl groups in the six-oxygen rings of zeolite Y (line c at ca. 5 ppm) exhibit a chemical shift that is ca. 1 ppm higher than the chemical shift of free bridging hydroxyl groups in the large cavities (line b at 3.9–4.1 ppm). The higher chemical shift is due to the electrostatic interaction of these hydroxyl groups with the zeolite lattice [41, 46]. There is, however, no evidence for a higher strength of acidity of the bridging hydroxyl groups in the six-oxygen rings. This effect was also demonstrated by quantum chemical calculations [30]. The electrostatic interaction with the zeolite framework leads to a (calculated) increase in chemical shift of ca. 0.4 ppm for the populated proton positions O1H and O3H, pointing into the large cavities and into the six-oxygen rings, respectively. In contrast, the calculated deprotonation energies differ by only 5 kJ mol^{-1}.

A similar phenomenon could be found for H-ZSM-5 (see Fig. 7) where an additional signal at ca. 7 ppm appears besides the well-known lines at 2.0 and 4.2 ppm. The latter signals are known to be due to SiOH groups and free bridging hydroxyl groups, respectively. It could be shown that the signal at 7 ppm is caused by a second type of bridging hydroxyl group [36, 90, 91] influenced by an additional electrostatic interaction with the zeolite framework [36, 91]. The corresponding IR band occurs at ca. 3250 cm^{-1} [92]. By the application of Eq. 8 and with ΔE_{DP}^{SiOH} = 1400 kJ mol^{-1} one obtains values of ΔE_{DP}(4.2 ppm) = 1215 kJ mol^{-1} and ΔE_{DP}(7 ppm) = 980 kJ mol^{-1} for the deprotonation energy of the bridging hydroxyl groups, giving rise to the signals at 4.2 and 7 ppm, respectively. This result would lead to the conclusion that the latter hydroxyl groups are much more acidic than the former species. In contrast to this (erroneous) conclusion it could be shown, however, that both

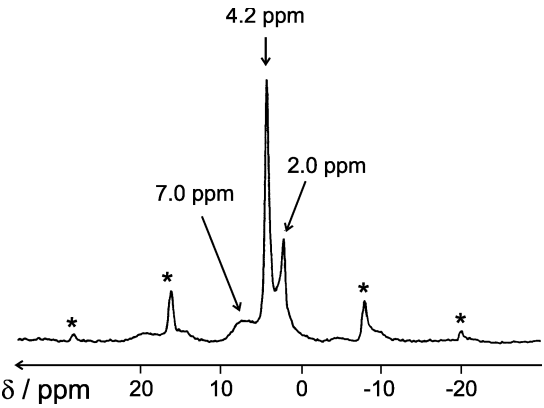

Fig. 7 ^{1}H MAS NMR spectrum of an activated H-ZSM-5 (Si/Al = 15) measured at a temperature of 123 K (–150 °C) and at a resonance frequency of 500 MHz [36]

species exhibit approximately the same strength of acidity [36, 91]. Therefore, it has to be emphasized again that Eq. 8 is exclusively valid for *free* surface hydroxyl groups. This behaviour of the chemical shift δ_H is completely analogous to that of ν_{OH}.

Surface hydroxyl groups can be studied by ^2H NMR spectroscopy in deuterated samples. The corresponding signals are strongly broadened due to the electric quadrupole interaction, giving rise to a broad spinning sideband pattern under MAS conditions. Analysis of line shape allows determination of the quadrupole coupling constant C_Q [48–51]. C_Q decreases with increasing strength of acidity of the (deuterated) bridging hydroxyl groups [50]. On the other hand, it was found that the quadrupole coupling constants of the non-acidic SiOD and the weakly acidic AlOD on non-framework Al species amount to 65 kHz and 67 kHz, respectively, which is much less than the values of 208–236 kHz observed for deuterated bridging hydroxyl groups. This means that no unique correlation between the strength of acidity and the quadrupole coupling constant could be observed. It is, furthermore, known [93, 94] that C_Q is strongly influenced by the formation of hydrogen bonds, as is the case for δ_H and ν_{OH} (see above).

2.4 Determination of the Accessibility and Strength of Acidity of Acid Sites in Samples Loaded with Probe Molecules

In analogy to IR spectroscopy, the accessibility and strength of acidity of a surface hydroxyl group can be investigated by NMR spectroscopy on samples loaded with probe molecules. NMR spectroscopy offers two possibilities for the study of the interaction between accessible surface hydroxyl groups and adsorbed probe molecules: (i) the study of the surface hydroxyl groups influenced by the probe molecules and (ii) the investigation of the probe molecules under the influence of the surface hydroxyl groups. It should be mentioned that NMR spectroscopy also allows the study of the geometry of the adsorption complexes formed in loaded samples, especially the measurement of internuclear distances.

2.4.1 NMR of Surface Hydroxyl Groups in Loaded Samples

Adsorption of probe molecules M results in characteristic changes of the ^1H MAS NMR signals of surface hydroxyl groups. In particular, the value of the ^1H NMR chemical shift of accessible surface hydroxyl groups is usually higher than in the unloaded sample. As already mentioned above, strongly basic probe molecules such as pyridine or ammonia are protonated by acidic surface hydroxyl groups. The ^1H NMR signals of these protonated complexes occur at relatively high chemical shifts. Pyridinium ions give rise to strongly

shifted ^{1}H NMR signals at ca. 16 ppm and ammonium ions at ca. 7 ppm (the chemical shift of bridging hydroxyl groups in unloaded samples amounts to ca. 4 ppm, see [46] and references therein). This means that the accessibility of surface hydroxyl groups can be detected by loading the samples with such strongly basic probe molecules.

The interaction between weakly basic probe molecules and surface hydroxyl groups also leads to an enhanced ^{1}H NMR chemical shift $\delta_H + \Delta\delta_H$ caused by the formation of hydrogen bonds. The question arises whether the so-called induced chemical shift $\Delta\delta_H$ reflects the strength of acidity in analogy to the wavenumber shift $\Delta\nu_{OH} = \nu_{OH...M} - \nu_{OH}$ observed in IR spectroscopy. ν_{OH} and $\nu_{OH...M}$ denote the wavenumbers of the fundamental stretching vibration of a free surface hydroxyl group and a hydroxyl group influenced by a probe molecule M, respectively. Paukshtis and Yurchenko [85, 86] have developed a method for the determination of differences in the deprotonation energy of surface hydroxyl groups that is based on the measurement of $\Delta\nu_{OH}$. The difference $\Delta E = \Delta E_{DP}^{SiOH} - \Delta E_{DP}$ between the deprotonation energy of SiOH groups and the considered surface hydroxyl groups can be calculated according to the formula:

$$\frac{\Delta E}{\text{kJ mol}^{-1}} = \frac{1}{B} \log \frac{\Delta\nu_{OH}}{\Delta\nu_{SiOH}} \tag{12}$$

provided that $|\Delta\nu_{OH}| \leq 400\ \text{cm}^{-1}$ (weak hydrogen bonding) with $B = 0.00226$ and $\Delta E_{DP}^{SiOH} = 1400 \pm 25\ \text{kJ mol}^{-1}$. $\Delta\nu_{SiOH}$ denotes the shift of the OH stretching vibration of non-acidic SiOH groups in silica gel caused by the probe molecules M.

As described in Sect. 2.3, δ_H and ν_{OH} are linearly correlated at least in limited ranges. It is, therefore, tempting to assume a similar correlation between $\Delta\delta_H$ and $\Delta\nu_{OH}$ given by:

$$\frac{\Delta\delta_H}{\text{ppm}} = \beta \frac{|\Delta\nu_{OH}|}{\text{cm}^{-1}} \tag{13}$$

with β values between 0.0092 and 0.0147 (see Eqs. 10 and 11). Provided that this is true, $\Delta\nu_{OH}$ and $\Delta\nu_{SiOH}$ can be replaced by $\Delta\delta_H$ and $\Delta\delta_{SiOH}$ in Eq. 12 in order to determine the deprotonation energy. Here, $\Delta\delta_{SiOH}$ denotes the induced chemical shift of the non-acidic SiOH groups in silica gel caused by the probe molecules M.

The induced ^{1}H NMR chemical shift $\Delta\delta_H$ caused by the adsorption of hydrogen-bond forming probe molecules M on surface hydroxyl groups can be strongly reduced by rapid thermal motions and/or exchange processes of the probe molecules [95]. In most cases it is, therefore, necessary to carry out the corresponding ^{1}H MAS NMR measurements at low temperatures. The influence of small and weakly basic probe molecules on the low-temperature ^{1}H MAS NMR spectra of zeolites was investigated for the first time by White et al. [96]. Table 2 summarizes induced chemical shift values for a variety of

Table 2 Induced ^{1}H NMR chemical shift $\Delta\delta_H$ of bridging hydroxyl groups in H-ZSM-5 for various probe molecules [96]

Loading	$\Delta\delta_H$ for probe molecule M				
	N_2	CO	C_2H_6	C_2H_4	C_2H_2
1 M/Al^F	–	1.8	–	2.7	3.5
2 M/Al^F	0.3	1.8	0.6	2.7	3.9

Loading is given in molecules (M) per framework Al atom (Al^F), and $\Delta\delta_H$ in ppm. Measurements were performed at a temperature of 123 K

probe molecules. Convenient probe molecules should exhibit the following properties:

(i) The induced ^{1}H NMR chemical shift $\Delta\delta_H$ caused by the probe molecules should be high since its relative experimental error is then low

(ii) $\Delta\delta_H$ should remain constant for loadings higher than one probe molecule per surface hydroxyl group. Otherwise, the dependence of $\Delta\delta_H$ on the loading has to be taken into account, which would complicate its use as a measure for the strength of acidity

(iii) The molecules must be chemically stable even in the presence of acid sites in zeolites

Conditions (i) and (ii) are obviously fulfilled for CO and C_2H_4. However, it turned out that C_2H_4 chemically reacts rapidly at room temperature in H-zeolites, which prevents its use as a probe molecule. Two selected examples will be considered for the demonstration of characteristic phenomena caused by the adsorption of small and weakly basic probe molecules on zeolites, namely the adsorption of CO and C_2Cl_4 (instead of C_2H_4).

The data collected in Table 3 show that the induced ^{1}H NMR chemical shift $\Delta\delta_H$ caused by the interaction of surface hydroxyl groups in H-ZSM-5 with CO molecules qualitatively reflects the strength of acidity of the hydroxyls. However, it is not very reasonable that the induced chemical shift of bridging hydroxyl groups in the large cavities of zeolite 0.3 HNa – Y should be smaller than that for the AlOH groups on non-framework Al species in H-ZSM-5. Moreover, the wavenumber shift of the free bridging hydroxyl groups in H-ZSM-5 of ca. 300 cm^{-1} [97–99] would correspond to an induced ^{1}H NMR chemical shift of ca. 2.8–4.4 ppm according to Eqs. 10 and 11, in contrast to the experimental value of only 2 ppm. It turned out that the CO molecules move rapidly even at 123 K [19, 95, 96, 100] so that the induced chemical shift $\Delta\delta$ has not reached its maximum value. ^{13}C NMR spectroscopic studies (see below) have shown that the suppression of the influence of rapid thermal motions and/or exchange processes requires measurement temperatures lower than 60–80 K. It would, therefore, be necessary to use a helium cooled MAS NMR device.

Table 3 Experimental values for the ^{1}H NMR chemical shift δ_H of free surface hydroxyl groups and the induced chemical shift $\Delta\delta_H$ caused by the adsorption of carbon monoxide [100]

Zeolite	OH group	δ_H ppm	$\Delta\delta_H$ ppm
H-ZSM-5 (hydrothermally treated)	Non-acidic SiOH	2.0	0.0
	Weakly acidic AlOH (on non-framework Al)	2.9	1.0
	Acidic SiOHAl (free)	4.2	2.0
0.3 HNa – Y	Acidic SiOHAl (free, in the large cavities)	3.9	0.9

Measurements were carried out at 123 K

Figure 8 shows the ^{1}H MAS NMR spectrum of an activated 0.3 HNa – Y zeolite, which has already been described (see Fig. 5). The total concentration of bridging hydroxyl groups amounts to ca. 17 OH per unit cell (u.c.). More than 90% of the bridging hydroxyl groups are located in the large cavities. Figure 8 exhibits the ^{1}H MAS NMR spectra of the same zeolite loaded

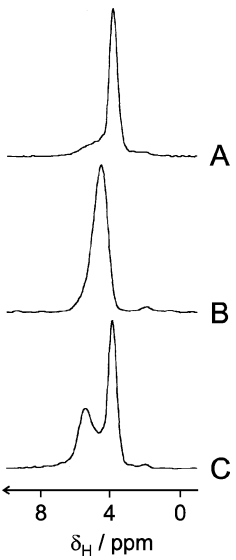

Fig. 8 ^{1}H MAS NMR spectra of zeolite 0.3 HNa – Y [101]. Unloaded sample measured at 293 K (*A*). Sample loaded with $8C_2Cl_4$ per unit cell measured at 293 K (*B*) and at 130 K (*C*). The spectra *B* and *C* are enlarged by a factor of two

with eight molecules of C_2Cl_4 per unit cell measured at 293 K and 130 K, respectively. At a temperature of 293 K the signal due to the bridging hydroxyl groups in the large cavities is broadened and completely shifted from 3.9 ppm to ca. 4.5 ppm despite the fact that the loading is considerably lower than the concentration of bridging hydroxyl groups in the large cavities. Assuming that the C_2Cl_4 molecules exchange rapidly between bridging hydroxyl groups in the large cavities, one expects only a single signal at an averaged position $\langle\delta_H\rangle$ given by (see Sect. 3.2):

$$\langle\delta_H\rangle = \delta_H + p_M\Delta\delta_H \tag{14}$$

p_M is given by the ratio c_M/c_b where c_M denotes the concentration of probe molecules (C_2Cl_4) adsorbed on bridging hydroxyl groups in the large cavities and c_b is the concentration of bridging hydroxyl groups in the large cavities. Since c_M is less than or equal to the total concentration of probe molecules (8 per u.c.) it follows that $p_M \leq 0.5$. Using $\langle\delta_H\rangle = 4.5$ ppm and $\delta_H = 3.9$ ppm (Eq. 14) yields $\Delta\delta_H \geq 1.2$ ppm. For the limiting case of slow exchange (i.e. for sufficiently low temperatures) one therefore expects a line at $\delta_H + \Delta\delta_H \geq 5.1$ ppm caused by bridging hydroxyl groups perturbed by C_2Cl_4 besides the signal at 3.9 ppm due to unperturbed bridging hydroxyl groups in the large cavities. In fact, the spectrum measured at temperatures below 150 K shows two well-resolved signals at $\delta_H = 3.9$ ppm and $\delta_H + \Delta\delta_H = 5.5$ ppm (see spectrum C in Fig. 8). The existence of these two signals indicates that the limiting case of slow exchange is reached for temperatures below 150 K. Therefore, the measurement of $\Delta\delta_H$ should be carried out at temperatures below 150 K in order to suppress the influence of thermal motions and exchange processes of the C_2Cl_4 molecules upon the spectra.

Figure 9 shows the low-temperature ^{1}H MAS NMR spectra of H-ZSM-5 loaded with different amounts of C_2Cl_4. The spectrum of the unloaded sample has already been described (see Fig. 7). A quantitative analysis yields the following concentrations of the different types of surface hydroxyl groups: 0.9 ± 0.2 SiOH per u.c., 3.4 ± 0.4 free SiOHAl per u.c. and 1.8 ± 0.4 SiOHAl of type 2 per u.c. A part of the signal due to free bridging hydroxyl groups is shifted from $\delta_H = 4.2$ ppm to $\delta_H + \Delta\delta_H = 6.1$ ppm after loading with 2 C_2Cl_4 per u.c. (see B in Fig. 9). It could, furthermore, be shown that C_2Cl_4 molecules are adsorbed on bridging hydroxyl groups of type 2 for loadings higher than the concentration of free bridging hydroxyl groups. The corresponding complexes give rise to a "shoulder" at ca. 6.2–6.4 ppm near the described signal at 6.1 ppm (see C in Fig. 9). This means that the bridging hydroxyl groups of type 2 form similar complexes with C_2Cl_4 as the free bridging hydroxyl groups. The additional electrostatic interaction of these hydroxyls with the zeolite framework is cancelled by the interaction with the C_2Cl_4 molecules, as also shown by IR spectroscopy. The same behaviour could be found by IR and ^{1}H MAS NMR spectroscopy using other probe molecules such as

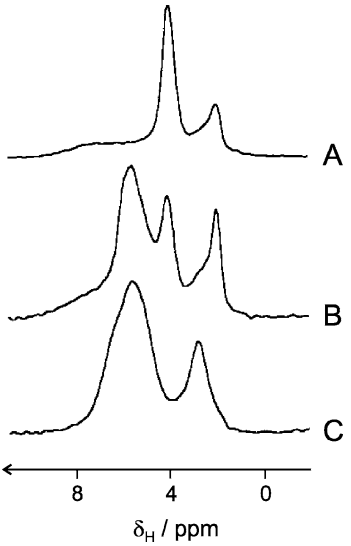

Fig. 9 ^{1}H MAS NMR spectra of H-ZSM-5 measured at 130 K [101]. Unloaded sample (*A*), sample loaded with $2C_2Cl_4$ per unit cell (*B*) and with $12C_2Cl_4$ per unit cell (*C*). The spectra *B* and *C* are enlarged by a factor of two

CO [36, 91, 92]. Furthermore, it is remarkable that the SiOH groups are completely shifted from 2.0 ppm to 2.8 ppm.

Table 4 summarizes values for the induced ^{1}H NMR chemical shift $\Delta\delta_H$ and the wavenumber shift $\Delta\nu_{OH}$ of various free surface hydroxyl groups

Table 4 Values for the wavenumber shift $\Delta\nu_{OH}$ and the induced ^{1}H NMR chemical shift $\Delta\delta_H$ of free surface hydroxyl groups in zeolites using C_2Cl_4 as the probe molecule M [101]

Sample	OH group	$\Delta\nu_{OH}$	$\Delta\delta_H$	ΔE (from $\Delta\nu_{OH}$)	ΔE (from $\Delta\delta_H$)
		cm^{-1}	ppm	kJ mol^{-1}	kJ mol^{-1}
0.3 HNa – Y	SiOHAl (HF)	–155	1.6	127	146
H-ZSM-5	SiOH	–80	0.8	–	–
	SiOHAl (free)	–175	1.9	150	177
H-ZSM-5^{HT}	SiOH	–75	0.8	–	–
	AlOH	–105	1.1	52	74
	SiOHAl (free)	–185	1.9	161	177

The difference $\Delta E = \Delta E_{DP}^{SiOH} - \Delta E_{DP}$ between the deprotonation energy of SiOH in SiO_2 and the corresponding surface hydroxyl groups was determined from $\Delta\nu_{OH}$ and from $\Delta\delta_H$ (instead of $\Delta\nu_{OH}$) by using Eq. 12. Values of $\Delta\delta_{SiOH} = 0.75 \pm 0.07$ ppm and $\Delta\nu_{SiOH} = -80 \pm 7$ cm^{-1} could be determined for SiOH groups in SiO_2. H-ZSM-5^{HT} denotes a hydrothermally treated H-ZSM-5

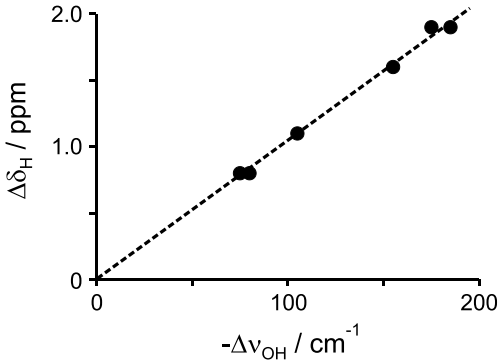

Fig. 10 Correlation between the induced ^{1}H NMR chemical shift $\Delta\delta_H$ and the wavenumber shift $\Delta\nu_{OH}$ caused by adsorbed C_2Cl_4 for various free surface hydroxyl groups in zeolites [101]

in zeolites loaded with C_2Cl_4. It is shown in Fig. 10 that $\Delta\delta_H$ and $\Delta\nu_{OH}$ are linearly correlated as anticipated (see Eq. 13). The slope β amounts to 0.01 ppm cm.

Therefore, ΔE can be calculated on the basis of Eq. 12 by using $\Delta\delta_H$ instead of $\Delta\nu_{OH}$. It can be seen from Table 4 that the values calculated for ΔE by using $\Delta\delta_H$ and $\Delta\nu_{OH}$ are in reasonable agreement. The experimental error of this method will be discussed and compared with the method based on the measurement of δ_H (see Eq. 8) for the following example. For bridging hydroxyl groups in the large cavities of zeolite 0.3 HNa – Y values of $\Delta\delta_H = 1.6 \pm 0.1$ ppm and $\Delta\nu_{OH} = -155 \pm 15$ cm^{-1} were found. Using the wavenumber shifts $\Delta\nu_{OH}$ and $\Delta\nu_{SiOH} = -80 \pm 10$ cm^{-1}, Eq. 12 yields $\Delta E = 127 \pm 35$ kJ mol^{-1}. Replacing $\Delta\nu_{OH}$ and $\Delta\nu_{SiOH}$ in Eq. 12 by the induced ^{1}H NMR chemical shifts $\Delta\delta_H$ and $\Delta\delta_{SiOH} = 0.75 \pm 0.07$ ppm, respectively, it follows $\Delta E = 146 \pm 30$ kJ mol^{-1}. Both these values are in reasonable agreement with $\Delta E = 160 \pm 8$ kJ mol^{-1}, which follows from the difference $(\delta_H - \delta_{SiOH}) = 1.9 \pm 0.1$ ppm using Eq. 8.

In summary, it can be stated that the induced chemical shift obviously reflects the strength of acidity of surface hydroxyl groups. It is possible to calculate the deprotonation energy on the basis of Eq. 12 by exchanging $\Delta\nu_{OH}$ and $\Delta\nu_{SiOH}$ with $\Delta\delta_H$ and $\Delta\delta_{SiOH}$, respectively. The error of the deprotonation energy obtained with both spectroscopic methods is nearly the same if C_2Cl_4 is chosen as the probe molecule. A reduction of this error requires probe molecules causing higher shifts. The measurement of $\Delta\delta_H$ (i.e. the NMR method) would then be preferred to measurement of $\Delta\nu_{OH}$ (IR method of Paukshtis and Yurchenko) since the broadening of the IR bands due to the hydrogen bond formation leads to larger relative experimental errors for $\Delta\nu_{OH}$ than for $\Delta\delta_H$. Promising candidates for such investigations are molecules such as CO [100] or CCl_3CN [102].

However, if it is known that the surface hydroxyl groups under study are free, i.e. that hydrogen bonding can be excluded, the measurement of activated (unloaded) samples would be preferred in any case since the error of the deprotonation energy calculated by the use of Eq. 8 is considerably smaller than the error of both methods based on the use of probe molecules.

2.4.2 NMR of Probe Molecules

The adsorption of the strongly basic pyridine molecules on bridging hydroxyl groups leads to the formation of pyridinium ions. ^{15}N CP MAS NMR spectroscopy allows the detection of the corresponding signal [103, 104] at a position of 88 ± 2 ppm relative to solid pyridine. In contrast, physisorbed pyridine molecules give rise to a signal at a position of -10 ± 10 ppm relative to solid pyridine. The main problem of this method is the necessity of the application of the cross polarization (CP) technique [105, 106]) due to the low natural abundance of the isotope ^{15}N. Therefore, a determination of the concentration of Brønsted acid sites by this method may be connected to large errors since the intensity of the signals strongly depends on different parameters controlling the efficiency of cross polarization [107].

The interaction of trimethylphosphine with bridging hydroxyl groups in zeolites also leads to protonation of the probe molecules. ^{31}P MAS NMR investigations on adsorbed trimethylphosphine [108–110] have shown that the ^{31}P NMR signal of protonated trimethylphosphine occurs at 59 ± 2 ppm relative to liquid trimethylphosphine. The chemical shift of physisorbed trimethylphosphine amounts to 0.7 ± 6 ppm. On the other hand, trimethylphosphine is a rather large molecule and the measurement of the concentration of bridging hydroxyl groups is therefore restricted by the maximum adsorption capacity of the pore system and also by steric hindrances [109].

Recently, Peng et al. [111] have suggested making use of diphosphine molecules to study Brønsted acid sites via ^{31}P MAS NMR spectroscopy of the probe molecules. It could be shown that these molecules are sensitive to the acidity of the acid sites as well as to the distances between the acid sites.

It is assumed that the adsorption of H_2O molecules on bridging hydroxyl groups can lead to the formation of hydrogen bonded adsorption complexes and also to hydroxonium ions. However, the conditions required for the formation of hydroxonium ions are still a subject of discussion. Quantum chemical calculations [112, 113] have shown for low H_2O concentrations (one H_2O molecule per bridging hydroxyl group) that the formation of hydroxonium ions corresponds to a saddle point at the potential energy surface, i.e. to a transition state. In contrast, the neutral hydrogen bonded complex was found to be an energy minimum. For higher loadings (two H_2O molecules per bridging hydroxyl group), the formation of hydroxonium ions was also found to yield a minimum at the potential energy surface [113].

The concentration of hydroxonium ions should depend on both the concentration and the strength of acidity of bridging hydroxyl groups. Therefore, the ratio between the concentration of hydroxonium ions and the total concentration of accessible bridging hydroxyl groups was suggested as a measure of the strength of acidity [114–116]. Unfortunately, the ^{1}H MAS NMR spectroscopic investigation of H_2O molecules adsorbed on zeolites is complicated by three problems:

(i) The Hirschler–Plank mechanism, i.e. the dissociation of H_2O molecules on multivalent non-framework cations (e.g. Ca^{2+}, Al^{3+} etc.) results in the formation of cationic OH groups and bridging OH groups [117, 118].
(ii) Partially hydrated zeolites may exhibit a signal at ca. 6.5 ppm [119], which is ascribed to H_2O molecules adsorbed on Lewis acid sites.
(iii) H_2O molecules can also exist in the physisorbed state (see above). At room temperature, H_2O molecules in the different adsorption states exchange rapidly, which makes the interpretation of the spectra difficult. On the other hand, ^{1}H MAS NMR spectroscopic studies of these exchange processes allow indirect measurement of the concentration of hydroxonium ions [119].

Fraissard et al. [114–116, 120] have developed another method for the determination of the concentration of hydroxonium ions. ^{1}H NMR spectra of hydrated zeolites are measured at 4 K. The above-mentioned thermal motions and exchange processes are then completely suppressed and the spectra are extremely broad due to the homonuclear dipole–dipole interactions among the protons. Therefore, the different species cannot be distinguished by their chemical shift. The spectra have to be decomposed into the contributions of isolated hydroxyl groups (one-spin systems), isolated water molecules (two-spin systems), water molecules hydrogen-bonded to bridging OH groups (isolated systems of three spins at the corners of isosceletal triangles), and hydroxonium ions (isolated systems of three spins at the corners of equilateral triangles). This method fails if there are different types of bridging hydroxyl groups. However, it might be very valuable if it could be shown that its sensitivity is high enough, e.g. to reproduce the well-known dependence of the strength of acidity of bridging hydroxyl groups on the Si/Al ratio of zeolites [46] (see Fig. 3).

A number of papers deal with the adsorption of methanol on bridging hydroxyl groups [121–126]. The existence of an equilibrium of neutral hydrogen-bonded adsorption complexes and methoxonium ions is discussed, e.g. in [126] on the basis of NMR spectroscopic investigations. On the other hand, quantum chemical calculations [123] have shown that the formation of methoxonium ions corresponds to a saddle point in the potential energy surface, i.e. they should only exist as transition states. In contrast, the formation of the neutral hydrogen-bonded adsorption complexes corresponds to a potential energy minimum. Biaglow et al. [127] have suggested making use of the ^{13}C NMR chemical shift of the carbonyl carbon atoms of ace-

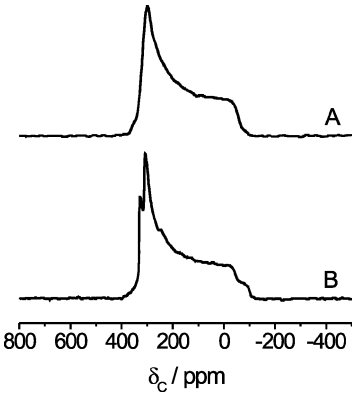

Fig. 11 ^{13}C NMR spectra of ^{13}CO adsorbed on silicalite (*A*) and on zeolite H – Y (*B*) [132]. The measurements were performed at a temperature of 4.5 K and at a ^{13}C resonance frequency of 125.7 MHz. Silicalite was loaded with six ^{13}CO molecules per unit cell. The zeolite H – Y was loaded with 26 ^{13}CO molecules per unit cell, which corresponds to the concentration of bridging hydroxyl groups in the large cavities. Bridging hydroxyl groups in the six-oxygen rings are inaccessible for CO molecules. The spectra were recorded by the use of Hahn's echo in order to avoid problems with the dead time of the receiver

tone molecules adsorbed on bridging hydroxyl groups as a measure of the strength of acidity. A detailed NMR spectroscopic study of the adsorption of acetonitrile in acid zeolites combined with quantum chemical calculations was published by Haw et al. [128]. Furthermore, Nicholas et al. [129] have suggested investigation of the protonation of typical Hammett indicators by NMR spectroscopy in order to determine the strength of acidity of Brønsted acid sites, which may be a promising technique for future experiments.

Finally, Mildner and Freude [130] have studied the proton transfer between Brønsted acid sites in H – Y zeolites and adsorbed benzene molecules via two-dimensional exchange spectroscopy. This exchange can be considered to be the first elementary step of a Brønsted acid-catalysed reaction. The proton exchange rate turned out to depend on the strength of acidity of the Brønsted acid sites. In addition, activation energies of ca. 90–100 kJ/mol could be observed for the proton transfer reaction by this method.

2.4.3 NMR Spectroscopic Determination of the Geometry of Adsorption Complexes and of the Mobility of the Probe Molecules

NMR spectroscopy allows the determination of the geometry of adsorption complexes and of the mobility of the probe molecules. This will be demonstrated for CO molecules adsorbed on bridging hydroxyl groups.

Rigid ^{13}CO molecules should exhibit a broad signal with the typical shape of a line dominated by the chemical shift anisotropy. The principal values of

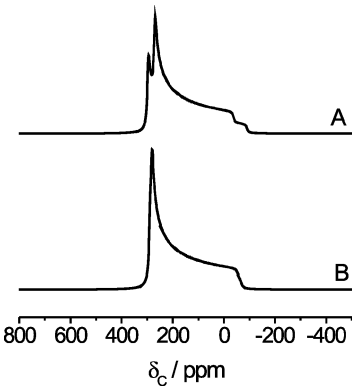

Fig. 12 ^{13}C NMR spectra calculated [132] for the two theoretically predicted linear complexes formed by CO adsorbed on bridging hydroxyl groups: *A* Complex I with r_{H-C} = 0.21 nm and $\Delta\sigma_C \approx 370$ ppm. *B* Complex II with r_{H-O} = 0.21 nm and $\Delta\sigma_C \approx 370$ ppm

the chemical shift tensor of rigid ^{13}CO molecules are $\delta_{11} = \delta_{22} = \delta_{\perp} = 305$ ppm and $\delta_{33} = \delta_{||} = -48$ ppm [131], i.e. the chemical shift anisotropy amounts to $\Delta\sigma_C = \delta_{\perp} - \delta_{||} = 353$ ppm. The corresponding line shape could also be found [132] for the ^{13}C NMR signal of ^{13}CO molecules physisorbed on silicalite measured at 4.5 K (see A in Fig. 11). The ^{13}C NMR spectrum of ^{13}CO molecules adsorbed on a zeolite H – Y measured at 123 K consists of a single narrow line at ca. 185 ppm, which confirms that the CO molecules still move isotropically. At a temperature of 4.5 K, the spectrum exhibits a width corresponding to that expected for rigid ^{13}CO molecules [132] (see B in Fig. 11). The transition from the narrow line observed at 123 K to the broad signal shown in Fig. 11 takes place at temperatures between 60 and 80 K. ^{1}H MAS NMR studies of the interaction between surface hydroxyl groups and CO molecules should, therefore, be carried out at temperatures below 60 K (see above).

It is remarkable that the characteristic line shape shown in Fig. 11 can only be observed for CO loadings not exceeding the concentration of accessible bridging hydroxyl groups. All CO molecules are then adsorbed on bridging hydroxyl groups, as shown by IR spectroscopy. The characteristic features of spectrum B in Fig. 11, namely the two maxima at the left edge of the spectrum and the step at the right edge, vanish for loadings higher than the concentration of accessible bridging hydroxyl groups. In the latter case, IR-spectroscopic investigations reveal the existence of physisorbed CO besides CO molecules adsorbed on bridging hydroxyl groups. Therefore, it has to be concluded that the characteristic shape of spectrum B shown in Fig. 11 is not caused by a superposition of two different signals due to ^{13}CO molecules in different adsorption states. It is known from quantum chemical calculations [133–136] that the adsorption of CO molecules on bridging hydroxyl groups leads to the formation of linear adsorption complexes. The following

two adsorption complexes have to be considered: O – H···^{13}C = O (complex I) and O – H···O = ^{13}C (complex II). It is predicted [133–136] that the equilibrium hydrogen bond distances r_{H-C} and r_{H-O} in complexes I and II amount to 0.20–0.23 nm, respectively. Figure 12 shows the ^{13}C NMR spectra calculated for ^{13}CO in these two complexes. The heteronuclear magnetic dipole–dipole interaction between the proton and the ^{13}C nucleus of the ^{13}CO molecule was taken into account in addition to the chemical shift anisotropy discussed above. The spectrum numerically calculated for complex I using a H – C hydrogen bond distance r_{H-C} of 0.21 nm and a chemical shift anisotropy $\Delta\sigma_C$ of 370 ppm almost perfectly matches the experimentally observed spectrum (see B in Fig. 11). This observation shows that the adsorption of CO on bridging hydroxyl groups leads to the formation of complex I in agreement with ^{1}H MAS NMR [95] and IR- [134, 135] spectroscopic investigations as well as quantum chemical calculations [133–136]. Furthermore, it is remarkable that $\Delta\sigma_C$ increases compared with physisorbed ^{13}CO. It turned out that r_{H-C} is identical for ^{13}CO adsorbed on H – Y and H-ZSM-5 within experimental error, i.e. the hydrogen bond distance cannot be used as a measure of the strength of acidity of bridging hydroxyl groups.

If the NMR spectrum consists of two or more superimposed signals, it may be advantageous to apply the MAS technique in order to resolve the different signals (see above). Structural information, e.g. internuclear distances, may then be obtained by a numerical analysis of the spinning sideband pattern [70].

In contrast to the above-described example (CO on bridging hydroxyl groups), the NMR signals of nuclei in adsorption complexes may exhibit complicated line shapes due to the superposition of various magnetic interactions. This problem often prevents the direct determination of the geometry of the adsorption complexes by line shape analysis or numerical analysis of the spinning sideband pattern. A variety of advanced NMR spectroscopic techniques allowing the measurement of internuclear distances have been developed meanwhile that can be applied in such cases. The measurement of distances between unlike spins may be carried out by the use of double resonance techniques such as SEDOR or REDOR (rotational echo double resonance [137]) if line shape analysis fails. The latter technique is carried out under MAS conditions, which allows different signals to be distinguished while the SEDOR experiment is carried out under static conditions. The geometry of complexes formed by the adsorption of singly ^{13}C-enriched C_2Cl_4 on bridging hydroxyl groups could be determined by SEDOR experiments at low temperatures [138]. The so-called TRAPDOR (transfer of populations in double resonance) technique was applied to the study of the adsorption of monomethylamine on zeolite H – Y [139].

In summary, it can be stated that variable-temperature NMR spectroscopy allows determination of the geometry of the complexes formed by molecules adsorbed on surface hydroxyl groups, and quantitative study of the thermal motions of the molecules [132].

3
NMR Spectroscopic Characterization of Lewis Acidity in Zeolites

In general, it is accepted [140, 141] that Lewis acidity of zeolites and related catalysts (silica-alumina, γ-alumina) is related to the presence of aluminium species on the surface. Therefore, two possibilities exist for the study of Lewis acidity by NMR: (i) an analysis of highly resolved ^{27}Al NMR spectra similar to the ^{1}H MAS NMR spectroscopy described in Sect. 2.1 and (ii) the use of probe molecules such as pyridine or others.

3.1
^{27}Al NMR Spectroscopy

3.1.1
Hydrated Samples

In well-crystallized hydrated zeolites exhibiting no Lewis acidity, aluminium is tetrahedrally oxygen-coordinated. The isotropic ^{27}Al NMR chemical shift of these framework Al atoms was found to be correlated with the mean [Al – O – Si] bond angle and is between 55 and 67 ppm [142, 143] with respect to a dilute aqueous solution of Al^{3+}. After a deep-bed [144] or a hydrothermal treatment, however, non-framework Al species are formed ("true" Lewis acid sites) and the ^{27}Al MAS NMR spectrum becomes more complicated. The intensity of the initial signal at ca. 60 ppm decreases due to the ejection of aluminium from the framework into the intracrystalline space. In hydrated samples, a narrow signal at 0 ppm is often observed, which indicates the presence of some octahedrally oxygen-coordinated Al^{3+} balancing negative framework charges [142]. Tetrahedrally oxygen-coordinated non-framework Al species give rise to relatively broad signals at ca. 30–50 ppm [42, 145, 146]. It could be shown by ^{1}H–^{27}Al cross polarization [147] that these species must exist at least partly as $Al(OH)_i$ species ($i = 1, 2, 3$). Furthermore, it turned out that the broad signal at ca. 30 ppm may also be due to penta-coordinated species [148] in dependence on the sample pretreatment [149]. Multiple-quantum (MQ) MAS NMR spectroscopy has led to a considerably improved resolution for quadrupolar nuclei such as ^{27}Al [150]. By the application of this technique, Menezes et al. [151] could for example show that the signal at ca. 30 ppm in ultrastable Y zeolites is caused by tetrahedrally oxygen-coordinated non-framework Al atoms, which can be removed easily by acid leaching. In contrast, the Lewis acidity of the samples studied in [151] was found to be correlated with the acid-resistant signal at 0 ppm due to octahedrally oxygen-coordinated Al^{3+}. Other non-framework Al species give rise to lines in the interval between –15 and 4 ppm, which were assigned to polymeric aluminium species [152]. In addition, a very broad hump extending from ca. –180 ppm to ca. 230 ppm appears (for an external magnetic field

Table 5 Experimental results for the chemical shift δ_{Al} of ^{27}Al NMR signals observed on zeolites

δ_{Al} ppm	Species	Refs.
0	Octahedrally coordinated non-framework Al (Al^{3+})	[142]
–15 … +4	Polymeric non-framework Al species	[152]
30	Penta-coordinated non-framework Al	[148, 149]
30 (50?)	Tetrahedrally coordinated non-framework Al	[145, 146, 149]
–180 … +230	Non-framework Al of low symmetry ("NMR invisible")	[147]
(B_0 = 7.1 T) 55 … 67	Framework Al	[142]

of 7.1 T) in addition to the described more distinct resonances. As shown in [147], this broad hump merges into the lines near 0.30 and 60 ppm for high sample spinning rates ($\nu_r \geq 18$ kHz). A survey of these experimental results is given in Table 5. The main problem, however, is that hydration of the samples may result in a change of the coordination state of the aluminium species. This means that it is not clear to what extent the results obtained by ^{27}Al NMR spectroscopy on hydrated samples are representative for the dehydrated state.

3.1.2 Dehydrated Samples

In ^{27}Al NMR experiments performed on dehydrated, non-spinning samples in magnetic fields of high magnetic flux densities (B_0 = 11.74 T), the following values for the ^{27}Al quadrupole frequency ν_Q defined by Eq. 17 have been found: 1.02 MHz, 1.91 ± 0.15 MHz and 2.40 ± 0.15 MHz for the framework aluminium nuclei of zeolites Na – Y, H – Y and H-ZSM-5, respectively [50, 51]. Hence, it must be assumed for non-framework aluminium species with a lower symmetry that the values of ν_Q may even exceed 3 MHz. Large values of ν_Q give rise to a large second-order quadrupole shift [153]:

$$\nu_{CG} - \nu_L = -\frac{\nu_Q^2}{30\nu_L}\left[I(I+1) - \frac{3}{4}\right]\left(1 + \frac{\eta^2}{3}\right), \tag{15}$$

where ν_{CG} and ν_L denote the centre of gravity of the signal and the Larmor frequency of the nuclei under study, respectively. I is the spin quantum number ($I = 5/2$ for ^{27}Al) and η the asymmetry parameter ($0 \leq \eta \leq 1$). The quadrupole frequency ν_Q is related to the quadrupole coupling constant:

$$C_Q = \frac{e^2qQ}{h} \tag{16}$$

by the equation:

$$\nu_Q = \frac{3C_Q}{2I(2I-1)} \tag{17}$$

with *eq* and *eQ* denoting the electric field gradient and the electric quadrupole moment, respectively. In addition to this effect (Eq. 15), which must be taken into account for the determination of the "true" chemical shift of a ^{27}Al NMR signal, a strong quadrupole interaction leads to a dramatic broadening of the lines. This broadening cannot be removed completely by MAS. Application of the double rotation (DOR) technique [154–156] may lead to a further suppression of this broadening. The widths of the spectra (in ppm) for a static sample (Δ), for a sample under MAS conditions (Δ^{MAS}), and under conditions of double rotation (Δ^{DOR}) are given by [153, 156, 157]:

$$\Delta = \frac{10^6}{18}\left(\frac{\nu_Q}{\nu_L}\right)^2\left(25 + 22\eta + \eta^2\right) \tag{18}$$

$$\Delta^{MAS} = \frac{10^6}{63}\left(\frac{\nu_Q}{\nu_L}\right)^2\left(36 + 12\eta + \eta^2\right) \qquad \text{if} \quad \nu_r \geq \nu_{crit}^{MAS} \tag{19}$$

$$\Delta^{DOR} = \Delta^C \qquad \text{if} \quad \nu_{ri} = 5\nu_{ro} \geq \nu_{crit}^{DOR} \tag{20}$$

where ν_{ri} and ν_{ro} denote the sample spinning rates for the inner and the outer rotors of the DOR probe, respectively. The critical values of these rates are given by:

$$\nu_{crit}^{MAS} = \Delta^{MAS}\nu_L 10^{-6} \tag{21}$$

$$\nu_{crit}^{DOR} = 5\Delta^D\nu_L 10^{-6} \tag{22}$$

Δ^C denotes the line width (in ppm) due to a distribution of the chemical and/or quadrupole shift and Δ^D the line width (in ppm) due to homonuclear magnetic dipole–dipole interaction. It is the influence of these latter quantities (Eqs. 19–22) that determines the ultimate resolution of ^{27}Al MAS and of ^{27}Al DOR NMR spectra. For a constant magnetic field with $B_0 = 11.74$ T corresponding to $\nu_L = 130.29$ MHz, $\nu_Q = 3$ MHz (aluminium species of low symmetry), $\eta = 0$. For an estimated mean distance of ca. 330 pm between neighbouring Al nuclei (condensed non-framework material), which corresponds to $\Delta^D\nu_L \times 10^{-6} \approx 5$ kHz, the following values can be derived: $\Delta = 736$ ppm (Eq. 18), $\nu_{crit}^{MAS} = 39.5$ kHz (Eqs. 19 and 21) and $\nu_{crit}^{DOR} = 25$ kHz (Eq. 22). An inspection of these values shows that the conditions of Eqs. 19 and 20 cannot be fulfilled experimentally so that we must state that neither the application of ^{27}Al MAS NMR nor of ^{27}Al DOR NMR spectroscopy will allow the detection of condensed non-framework Al species of low symmetry (NMR "invisible" Al).

Interestingly, the degree of proton transfer from a bridging hydroxyl group in a zeolite to an adsorbed molecule was found to be correlated with the line width of the ^{27}Al MAS NMR signal of framework Al species [158]. This effect

could be shown experimentally by single pulse and MQ ^{27}Al MAS NMR spectroscopy of samples loaded with basic probe molecules such as nitromethane, acetone, trimethylphosphine, and pyridine. Quantum chemical calculations have confirmed these experimental observations [158].

3.2 Use of Probe Molecules

In analogy to infrared spectroscopy, probe molecules can be used to study Lewis acid sites. In the case of NMR spectroscopy, however, due to the much smaller resonance frequencies (which correspond to a much longer time scale) exchange effects may lead to an average line instead of the expected separate lines due to molecules adsorbed on the various adsorption sites. From Heisenberg's uncertainty relation:

$$\Delta E \Delta t \geq \hbar \tag{23}$$

together with Planck's equation:

$$\Delta E = \hbar \Delta \omega \tag{24}$$

it follows that the critical value $\tau_{crit} = \Delta t$ of the mean residence time τ between two succeeding exchanges is given by:

$$\tau_{crit} = \frac{1}{\Delta \omega} . \tag{25}$$

For $\tau \ll \tau_{crit}$ the two lines merge into a single line while for $\tau \gg \tau_{crit}$ they can be observed separately. In infrared spectroscopy, the typical bands of pyridine adsorbed on Brønsted and Lewis acid sites appear at ca. 1540 cm^{-1} and 1450 cm^{-1}, respectively, so that the critical value τ_{crit} is ca. 0.06 ps. For the ^{15}N NMR of the same molecule at a magnetic field of 7 T the frequency difference between the two lines is ca. 2 kHz (see Table 6) corresponding to $\tau_{crit} \approx 0.08$ ms, which is nine orders of magnitude larger than the value for the IR bands.

Table 6 Values for the ^{15}N NMR shift of pyridine [103, 104, 159] in different adsorption states relative to the resonance position of solid pyridine

Species	δ_N ppm
Liquid pyridine	–26
Physisorbed pyridine	-10 ± 10
Pyridinium ion (Brønsted acid site)	88 ± 2
Pyridine on tetrahedral Al^{3+} (Lewis acid sites)	22.5 ± 3.5
Pyridine on octahedral Al^{3+} (Lewis acid sites)	46.5 ± 7.7

If one denotes by ν_j, p_j and τ_j, respectively, the resonance frequency, the relative concentration and the mean residence time of a nucleus at an adsorption site j, then the shape of the NMR spectrum for a system with two different sorts of adsorption sites $j = a, b$ with $p_a + p_b = 1$ strongly depends on the quantity:

$$\tau = \left(\frac{1}{\tau_a} + \frac{1}{\tau_b}\right)^{-1} = \tau_a p_b = \tau_b p_a \,. \tag{26}$$

The spectrum consists of well-separated lines at ν_a and ν_b for the limiting case of slow exchange, i.e. for:

$$2\pi\tau\,|\nu_a - \nu_b| \gg 1 \,. \tag{27}$$

In the limiting case of rapid exchange:

$$2\pi\tau\,|\nu_a - \nu_b| \ll 1 \tag{28}$$

the lines merge into a single line at the frequency:

$$\nu = p_a\nu_a + p_b\nu_b \,. \tag{29}$$

Determination of the frequencies ν_j and relative concentrations p_j from the spectra is complicated in the case of intermediate exchange rates, i.e. for:

$$2\pi\tau\,|\nu_a - \nu_b| \approx 1 \,. \tag{30}$$

Therefore, we shall discuss only experiments where the exchange of the probe molecules among the adsorption sites can be assumed to be slow (Eq. 27) or rapid (Eq. 28).

3.2.1 Slow Exchange

The complete suppression of the influence of rapid exchange processes upon the spectra may require measurements at very low temperatures, especially for small probe molecules of high mobility (see Sect. 2.4). In the experiments to be described in this section, the NMR spectra exhibit various lines so that the limiting case of slow exchange can be assumed, at least approximately for the analysis of the spectra.

^{15}N CP MAS NMR spectra of adsorbed pyridine have been studied by Maciel et al. [103] (pyridine on silica-alumina), Ripmeester [104] (pyridine on γ-alumina, mordenite), and by Majors and Ellis [159] (pyridine on γ-alumina). Values for the resonance shift relative to solid pyridine are collected in Table 6. The major drawbacks of these experiments are: (i) an absolute determination of concentrations is connected with large errors due to the strong dependence of the line intensities on parameters controlling the efficiency of cross polarization [107] (see Sect. 2.4), and (ii) it is not certain that the exchange rates of the molecules among the various adsorption sites are

Table 7 Values for the ^{31}P NMR shift of trimethylphosphine physisorbed and adsorbed on Brønsted and Lewis acid sites relative to liquid trimethylphosphine [108–110, 160]

Species	δ_P ppm
Physisorbed trimethylphosphine	0.7 ± 6
Protonated trimethylphosphine (Brønsted acid sites)	59 ± 2
Trimethylphosphine on Lewis acid sites	12 ± 10
Trimethylphosphine on a second type of Lewis acid site in H – Y	30

Note that the chemical shift of liquid trimethylphosphine amounts to –62 ppm relative to 85% H_3PO_4

sufficiently small, so the resonance positions and intensities derived from the spectra may be apparent values only.

Compared with pyridine, phosphines are roughly three orders of magnitude stronger bases. ^{31}P MAS NMR spectroscopic studies of trimethylphosphine adsorbed on zeolite H – Y and on γ-alumina were carried out by Lunsford et al. [108, 109], and of various trialkylphosphines adsorbed on silica-alumina and on γ-alumina by Maciel et al. [110]. Values for the resonance shifts relative to solid trimethylphosphine are given in Table 7. The sensitivity of trimethylphosphine to distinguish between different sorts of Lewis acid sites seems to be less than that of pyridine since only one type of Lewis acid site could be found for γ-alumina (see Table 7). For H – Y zeolites, however, Kao and Grey [160] have observed a new signal at 30 ppm in addition to the signal at 18 ppm due to Lewis acid sites. Both signals are neighbouring Al atoms, as shown by $^{31}P/^{27}Al$ TRAPDOR experiments. The former signal is, therefore, possibly due to a second type of Lewis acid site in H – Y.

3.2.2 Rapid Exchange

Another way to quantitatively study Lewis acidity results from the fact that probe molecules could be found where the resonance shift caused by the Lewis acid sites is much larger than that caused by Brønsted acid sites or by physisorption. This situation can be described by a two-site exchange model. Exchange only takes place between molecules adsorbed on sites a (Lewis acid sites) and b (all other sites including physisorbed molecules). Typical examples are carbon monoxide [161–165] and dinitrogen oxide [166]. Since these molecules exchange between the various adsorption sites at room temperature and above, only a single line is observed for the ^{13}C NMR of carbon monoxide and for the ^{15}N NMR of the terminal nitrogen of dinitrogen oxide. The position of this single line is given by Eq. 29. It is then necessary to

perform a series of experiments in order to determine the two quantities of interest, namely the resonance shift of a molecule adsorbed on a Lewis acid site and the concentration of these sites. An interesting method allowing this analysis has been developed by Borovkov et al. [167]. If c_L, c_{LM} and c_M denote the concentrations of Lewis acid sites, of Lewis acid sites occupied by an adsorbed probe molecule, and of probe molecules M, respectively, one may write:

$$c_{LM} = K\left(c_M - c_{LM}\right)\left(c_L - c_{LM}\right) , \tag{31}$$

where K is the equilibrium constant of the exchange reaction:

$$L + M = LM . \tag{32}$$

On the other hand, Eq. 29 may be rewritten as:

$$\nu = \left(\frac{c_{LM}}{c_M}\right)\nu_{LM} + \left(\frac{c_M - c_{LM}}{c_M}\right)\nu_M \tag{33}$$

or if one introduces the resonance shift δ with regard to the resonance frequency ν_M of the probe molecules which are not adsorbed on Lewis acid sites:

$$\delta = \frac{\nu_M - \nu}{\nu_M} \tag{34}$$

one may write:

$$\delta = \frac{c_{LM}}{c_M}\delta_{LM} \tag{35}$$

with:

$$\delta_{LM} = \frac{\nu_M - \nu_{LM}}{\nu_M} . \tag{36}$$

A combination of Eqs. 31 and Eq. 35 leads to:

$$\frac{\delta}{\delta_{LM}} = \frac{1}{2}\left(1 + \frac{1}{Kc_M} + \frac{c_L}{c_M}\right) \pm \left[\frac{1}{4}\left(1 + \frac{1}{Kc_M} + \frac{c_L}{c_M}\right)^2 - \frac{c_L}{c_M}\right]^{\frac{1}{2}} . \tag{37}$$

Using the value δ_0 of the shift δ extrapolated to $c_M = 0$:

$$\delta_0 = \frac{Kc_L}{1 + Kc_L}\delta_{LM} . \tag{38}$$

Equation 37 may be rewritten as:

$$y = \frac{\delta_{LM}}{\delta_0}x - c_L\left(\frac{\delta_{LM}}{\delta_0}\right)^2 \tag{39}$$

with:

$$y = c_{\mathrm{M}} \frac{\left(\frac{\delta}{\delta_0}\right)^2}{1 - \frac{\delta}{\delta_0}} \tag{40}$$

$$x = c_{\mathrm{M}} \frac{\frac{\delta}{\delta_0}}{1 - \frac{\delta}{\delta_0}} \tag{41}$$

The benefit of this representation (Eqs. 39–41) is that x and y are quantities that can be derived from the experimental data, so that a plot of y versus x should yield a straight line from which one can directly determine the resonance shift δ_{LM} of the probe molecules adsorbed on a Lewis acid site and the concentration c_{L} of these sites. The main disadvantage of this method results from the fact that the signal-to-noise ratio decreases with decreasing loading of the samples ($c_{\mathrm{M}} \to 0$) so that δ_0 cannot be determined exactly. As an example, the ^{13}C MAS NMR signal of carbon monoxide adsorbed on H-ZSM-5 measured at 375 K is shown in Fig. 13 for decreasing values of the loading. Furthermore, it can be seen from Fig. 13 that the signal is broadened considerably for decreasing loading, which can be explained as follows. The residual line width $\Delta\nu_{1/2}^{\mathrm{MAS}}$ of the signal in the ^{13}C MAS NMR spectrum approximately corresponds to the static line width $\Delta\nu_{1/2}$ (i.e. the line width without MAS) for the case of rapid exchange since the MAS technique does

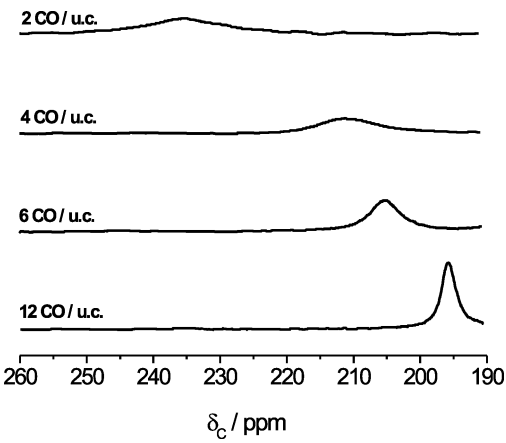

Fig. 13 Dependence of the ^{13}C MAS NMR signal due to CO molecules rapidly exchanging between Lewis acid sites and Brønsted acid sites (and/or the physisorbed state) on the CO loading [165]

not result in a further line narrowing in the presence of rapid thermal motions (see e.g. [75]). Therefore, the formula of Swift and Connick [168]:

$$\Delta\nu_{1/2} = \Delta\nu_P + \frac{c_{LM}}{c_M}\Delta\nu_L \tag{42}$$

also describes the behaviour of the residual line width $\Delta\nu_{1/2}^{MAS}$ under MAS for a temperature of 375 K (rapid exchange). Here, $\Delta\nu_P$ and $\Delta\nu_L$ denote the static line widths of the signals due to physisorbed CO (and/or CO on Brønsted acid sites) and due to CO on Lewis acid sites, respectively. The considerable increase of $\Delta\nu_{1/2}^{MAS}$ for decreasing values of c_M indicates that the line width $\Delta\nu_L$ must be relatively large even at 375 K.

A given error of δ_0 resulting from both the decreasing signal-to-noise ratio and the increasing line width, however, leads to relatively large errors for the quantities of interest (δ_{LM}, c_L). The value of δ_0 and, hence to a much larger extent, the values of δ_{LM} and c_L are connected with large errors especially in cases where the absolute value of the slope for the plot of δ versus c_M increases strongly at the lowest loadings. In general, the described method yields values that are too small. Therefore, the numerical results of 300–400 ppm for δ_{LM} (Table 8), from [162], should be taken as a lower limit. In a subsequent study [163, 164], the method of selective saturation introduced by Forsén and Hoffman [170] has been applied to carbon monoxide adsorbed on various zeolites containing Lewis acid sites. The accuracy for the value of δ_{LM} could be enhanced through measurement of the ^{13}C NMR signal intensity as a function of the frequency of a selective ^{13}C saturation pulse. Values of δ_{LM} between 440 ppm and 590 ppm have been found, with an error of ca. 60 ppm (Table 8) depending on the type of zeolite and on the pretreatment conditions.

Table 9 summarizes values for the resonance shift of dinitrogen oxide physisorbed and adsorbed on Brønsted and Lewis acid sites. The latter value was obtained using the method of Borovkov [167] described above.

Table 8 Values for the ^{13}C NMR shift of carbon monoxide in different adsorption states relative to gaseous CO [161–165]

Species	δ_C ppm
Physisorbed carbon monoxide	-3 ± 2
Carbon monoxide on Brønsted acid sites	-3 ± 2
Carbon monoxide on Lewis acid sites [162]	300–400
Carbon monoxide on Lewis acid sites [163, 164]	$(400–590) \pm 60$

For gaseous CO, chemical shifts of 183.5 ± 0.5 ppm [165] and of 181.3 ppm [169] were determined relative to TMS

Table 9 Values for the ^{15}N NMR chemical shift of dinitrogen oxide in various adsorption states [166] relative to gaseous N_2O

Species	δ_N ppm
Physisorbed dinitrogen oxide	4.5 ± 3
Dinitrogen oxide on Brønsted acid sites	4.5 ± 3
Dinitrogen oxide on Lewis acid sites	50 ± 20

Summarizing the results so far obtained with probe molecules, the following statements can be made:

(i) The accuracy is not sufficient to take the values of the resonance shift for the molecules adsorbed on Lewis acid sites as a measure of their strength of acidity
(ii) Only a semi-quantitative determination of the concentration of Lewis acid sites is possible in those cases where cross polarization must be applied due to a poor signal-to-noise ratio (pyridine)
(iii) Steric effects related to the larger probe molecules may lead to large errors

4 NMR Spectroscopic Characterization of Basicity in Zeolites

Increasing interest is devoted to the properties of zeolites as basic catalysts [4, 171, 172]. It is generally accepted that the strength of basicity of the framework oxygen atoms is determined by the partial charge on the framework oxygen atoms. The average oxygen partial charge can be calculated [24, 173] from Sanderson's intermediate electronegativity S (see Eq. 2) and the atomic electronegativity of oxygen $S_O = 5.21$ by the equation:

$$\frac{q_O}{e} = \frac{S - S_O}{2.08\sqrt{S_O}} . \tag{43}$$

Figure 14 shows the average (negative) oxygen partial charge $-q_O$ calculated according to Eq. 43 as a function of the framework Si/Al ratio for zeolites containing Cs^+, Na^+ and H^+ as charge compensating cations. Obviously, the framework oxygen atoms in typical basic zeolites containing charge compensating cations such as Cs^+ exhibit a considerably higher (negative) average oxygen partial charge $-q_O$ than in the acid proton exchanged zeolites. It should, however, be noted that the strength of basicity, i.e. the partial charge on the framework oxygen atoms, may be different for different oxygen positions [174]. The distances between oxygen atoms and neighbouring charge compensating cations are also discussed as a possible reason for the distribution of the strength of basicity of the framework oxygen atoms. Of course,

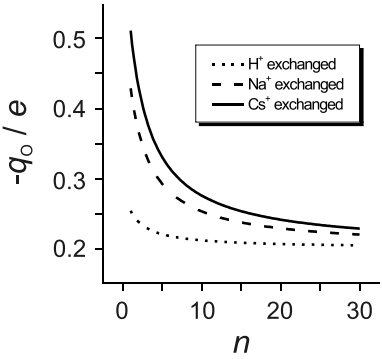

Fig. 14 Average partial charge q_O on the framework oxygen atoms calculated according to Eq. 43 as a function of the framework Si/Al ratio for zeolites exchanged with different charge compensating cations (100% Cs^+, 100% Na^+ and 100% H^+)

these local effects are not described by the average partial charge q_O determined according to Eq. 43 since Sanderson's intermediate electronegativity S is defined as a mean value calculated for the whole zeolite lattice. As an attempt to overcome this problem, a modification of the calculation of the oxygen partial charge was suggested [175] that considers local compositional differences.

So far, the spectroscopic methods for determining acidity of zeolites are much more developed than those for the determination of basicity. The NMR spectroscopic techniques recently available for the characterization of basicity will be described in this section. Zeolites may exhibit structural basic sites (framework oxygen atoms) and Brønsted basic sites (OH^- groups on cations). The following discussion is focused on the characterization of the former species since typical basic zeolites exhibit charge compensating cations such as Cs^+, Rb^+, K^+ or Na^+ where the Hirschler–Plank mechanism leading to the formation of OH^- groups on cations does not occur.

The direct detection of the oxygen atoms, i.e. the structural basic sites in zeolites, is complicated by the strong electric quadrupole interaction of the NMR-active oxygen isotope ^{17}O ($I = 5/2$) and its low natural abundance (0.038%). The former problem could be solved by the development of elegant techniques allowing an effective suppression of the quadrupole interaction, such as DAS, DOR and MQMAS NMR spectroscopy. The low natural abundance requires isotope enrichment of the samples; a problem that has also been solved. Triggered by the initial work of Mueller et al. [176] and Grandinetti et al. [177], an increasing number of ^{17}O MAS NMR spectroscopic studies are being published (see, e.g. [178–182]). Although it may be too early to rationalize these results with respect to the measurement of the strength of basicity, it can be stated that the type of cations, i.e. the charge at the oxygen atoms, is one of the factors determining the ^{17}O NMR chemical

shift. This has been demonstrated, e.g. by Freude et al. [181] and Readman et al. [182]. It is, furthermore, remarkable that the ^{17}O NMR chemical shift is sensitive to the Si – O – Al bond angle [181].

Another NMR spectroscopic method for the determination of basicity in zeolites was suggested by Bosácek [183]. This method is based on measurement of the ^{13}C NMR chemical shift of surface methyl groups. Surface methyl groups can be formed on framework oxygen atoms, here denoted by O^- according to the reaction:

$$CH_3I + O^-Me^+ \rightarrow O - CH_3 + MeI \tag{44}$$

if CH_3I is adsorbed on a zeolite containing charge compensating cations Me^+. The corresponding reaction can also take place on cations Me^{m+} with $m > 1$. It is, however, important to mention that only a small part of the cations should be replaced by methyl groups. Otherwise, the partial charge on the framework oxygen atoms may be changed during the replacement of the cations Me^+ by $CH_3{}^+$ (Eq. 44), which would lead to erroneous conclusions on the basicity of the original zeolite. A linear interdependence between the ^{13}C NMR chemical shift of the surface methyl groups and the partial charge on the oxygen atoms could be observed [183]. Furthermore, it is remarkable that the ^{13}C CP MAS NMR signal of the surface methyl groups in H-ZSM-5 consists of various components, indicating the existence of framework oxygen atoms of different strengths of basicity.

Another method, based on ^{13}C CP MAS NMR spectroscopic studies of nitromethane, was suggested by Kheir and Haw [184] and could be applied to CsX zeolites as well as to other basic catalysts [185].

References

1. Weitkamp J (1991) Stud Surf Sci Catal 65:21
2. Haag WO (1994) Stud Surf Sci Catal 84:1375
3. Naber JE, de Jong KP, Stork WHJ, Kuipers HPCE, Post MFM (1994) Stud Surf Sci Catal 84:2197
4. Barthomeuf D (1994) In: Fraissard J, Petrakis L (eds) Acidity and basicity of solids, NATO ASI Series C, vol 444. Kluwer Academic, Dordrecht, p 181
5. Kouwenhoven HW, Gunnewegh EA, van Bekkum H (1996) In: Weitkamp J, Lücke B (eds) Proceedings 9601 of the DGMK-conference: catalysis on solid acids and bases, Berlin, 14–15 March 1996. DGMK, Hambuerg, p 9
6. Hölderich W, Gallei E (1985) Ger Chem Eng 8:337
7. Tißler A, Müller U, Unger K (1988) Nachr Chem Tech Lab 36:624
8. Breck DW (1974) Zeolite molecular sieves: structure, chemistry and use. Wiley, London
9. Barrer RM (1978) Zeolite and clay minerals as sorbents and molecular sieves. Academic, London
10. Meier WM, Olson DH (1992) Atlas of zeolite structure types, 3rd edn. Butterworth, London

11. Barrer RM (1982) Hydrothermal chemistry of zeolites. Academic, London
12. Bellussi G, Rigutto MS (1994) Stud Surf Sci Catal 85:177
13. Wilson ST, Lok BM, Messina CA, Cannan TR, Flanigen EM (1982) J Am Chem Soc 104:1146
14. Lok BM, Messina CA, Patton RL, Gajek RT, Cannan TR, Flanigen EM (1984) J Am Chem Soc 106:6092
15. Martens JA, Jacobs PA (1994) Stud Surf Sci Catal 85:653
16. Rabo JA, Pickert PE, Stamires DN, Boyle JE (1960) Actes Du Deuxieme Congres International De Catalyse. Paris, p 2055
17. Weisz PB, Frilette VJ (1960) J Phys Chem 64:342
18. Curtiss LA, Brand H, Nicholas JB, Iton LE (1991) Chem Phys Lett 184:215
19. Brunner E (1995) J Mol Struct 355:61
20. Haag WO, Lago RM, Weisz PB (1984) Nature 309:589
21. Ward JW (1970) J Catal 17:355
22. Tsutsumi K, Takahashi H (1972) J Catal 24:1
23. Beaumont R, Barthomeuf D (1972) J Catal 26:218
24. Sanderson RT (1976) Chemical bonds and bond energy. Academic, New York
25. Jacobs PA (1982) Catal Rev-Sci Eng 24:415
26. Jacobs PA, Mortier WJ (1982) Zeolites 2:226
27. Pelmenschikov AG, Paukshtis EA, Stepanov VG, Pavlov VI, Yurchenko EN, Ione KG, Zhidomirov GM (1989) J Phys Chem 93:6725
28. Kramer GJ, van Santen RA (1993) J Am Chem Soc 115:2887
29. Schröder K-P, Sauer J, Leslie M, Catlow CRA, Thomas JM (1992) Chem Phys Lett 188:320
30. Eichler U, Brändle M, Sauer J (1997) J Phys Chem B 101:10035
31. Hopkins PD (1968) J Catal 12:325
32. Lunsford JH (1968) J Phys Chem 72:4163
33. Mirodatos C, Barthomeuf D (1981) J Chem Soc Chem Commun, p 39
34. Lago RM, Haag WO, Mikovsky RJ, Olson DH, Hellring SD, Schmitt KD, Kerr GT (1986) Stud Surf Sci Catal 28:677
35. Brunner E, Ernst H, Freude D, Hunger M, Krause CB, Prager D, Reschetilowski W, Schwieger W, Bergk K-H (1989) Zeolites 9:282
36. Brunner E, Beck K, Koch M, Pfeifer H, Staudte B, Zscherpel D (1994) Stud Surf Sci Catal 84:357
37. Zholobenko VL, Kustov LM, Kazansky VB, Loeffler E, Lohse U, Peuker C, Oehlmann G (1990) Zeolites 10:304
38. Fritz PO, Lunsford JH (1989) J Catal 118:85
39. Freude D, Hunger M, Pfeifer H (1982) Chem Phys Lett 91:307
40. Freude D, Hunger M, Pfeifer H, Scheler G, Hoffmann J, Schmitz W (1984) Chem Phys Lett 105:427
41. Pfeifer H, Freude D, Hunger M (1985) Zeolites 5:274
42. Freude D, Hunger M, Pfeifer H (1987) Z Phys Chemie NF 152:171
43. Engelhardt G, Jerschkewitz H-G, Lohse U, Sarv P, Samoson A, Lippmaa E (1987) Zeolites 7:289
44. Brunner E, Ernst H, Freude D, Hunger M, Pfeifer H (1988) Stud Surf Sci Catal 37:155
45. Pfeifer H, Ernst H (1994) Ann Rep NMR Spectrosc 28:91
46. Pfeifer H (1994) NMR of solid surfaces. In: Diehl P, Fluck E, Günther H, Kosfeld R, Seelig J (eds) NMR basic principles and progress, vol 31. Springer, Berlin, p 31
47. Hunger M (1996) Solid State Nucl Magn Reson 6:1
48. Vega AJ, Luz Z (1987) J Phys Chem 91:365

49. Gluszak TJ, Chen DT, Sharma SB, Dumesic JA, Root TW (1992) Chem Phys Lett 190:36
50. Ernst H, Freude D, Wolf I (1993) Chem Phys Lett 212:588
51. Freude D, Ernst H, Wolf I (1994) Solid State Nucl Magn Reson 3:271
52. Andrew ER, Bradbury A, Eades RG (1958) Nature (London) 182:1659
53. Haeberlen U, Waugh JS (1968) Phys Rev 175:453
54. Schnabel B, Haubenreisser U, Scheler G, Müller R (1976) In: Brunner H, Hausser KH, Schweitzer D (eds) Proceedings 19th Congress Ampere. Heidelberg, 27 Sept–1 Oct 1976. Groupement Ampere, Geneva, p 441
55. Pembleton RG, Ryan LM, Gerstein BC (1977) Rev Sci Instrum 48:1286
56. Ryan LM, Taylor RE, Paff AJ, Gerstein BC (1980) J Chem Phys 72:508
57. Scheler G, Haubenreisser U, Rosenberger H (1981) J Magn Reson 44:134
58. Maricq MM, Waugh JS (1979) J Chem Phys 70:3300
59. Brunner E, Freude D, Gerstein BC, Pfeifer H (1990) J Magn Reson 90:90
60. Brunner E, Fenzke D, Freude D, Pfeifer H (1990) Chem Phys Lett 169:591
61. Brunner E (1990) J Chem Soc Faraday Trans 86:3957
62. Brunner E (1993) J Chem Soc Faraday Trans 89:165
63. Wind R (1991) In: Popov AF, Hallenga K (eds) Modern NMR techniques and their application in chemistry. Dekker, New York, p 125
64. Stevenson RL (1971) J Catal 21:113
65. Freude D, Klinowski J, Hamdan H (1988) Chem Phys Lett 149:355
66. Kaplan DE, Hahn EL (1958) Le Journal de Physique et le Radium 19:821
67. Slichter CP (1978) Principles of magnetic resonance, 2nd edn. Springer, Berlin
68. Wang P-K, Slichter CP, Sinfelt JH (1984) Phys Rev Lett 53:82
69. Kenaston NP, Bell AT, Reimer JA (1994) J Phys Chem 98:894
70. Fenzke D, Hunger M, Pfeifer H (1991) J Magn Reson 95:477
71. Zscherpel D, Brunner E, Koch M (1995) Z Phys Chem 190:123
72. Liu H, Kao H-M, Grey C (1999) J Phys Chem B 103:4786
73. Freude D, Pfeifer H (1980) In: Rees LVC (ed) Proceedings 5th international zeolite conference. Heyden, London, p 732
74. Andrew ER, Jasinski A (1971) J Phys C: Solid State Phys 4:391
75. Fenzke D, Gerstein BC, Pfeifer H (1992) J Magn Reson 98:469
76. Sarv P, Tuherm T, Lippmaa E, Keskinen K, Root A (1995) J Phys Chem 99:13763
77. Baba T, Inoue Y, Shoji H, Uematsu T, Ono Y (1995) Microporous Mater 3:647
78. Baba T, Komatsu N, Ono Y, Sugisawa H, Takahashi T (1998) Microporous Mesoporous Mater 22:203
79. Baba T, Ono Y (1999) Appl Catal A: General 181:227
80. Sauer J (1987) Mol Catal 54:312
81. Fleischer U, Kutzelnigg W, Bleiber A, Sauer J (1993) J Am Chem Soc 115:7833
82. Brunner E, Pfeifer H (1995) Z Phys Chemie 192:77
83. Sauer J (1994) Stud Surf Sci Catal 84:2039
84. Sauer J, Hill J-R (1994) Chem Phys Lett 218:333
85. Paukshtis EA, Yurchenko EN (1983) Usp Khim 52:426
86. Paukshtis EA, Yurchenko EN (1981) React Kinet Catal Lett 16:131
87. Hunger M, Ernst S, Steuernagel S, Weitkamp J (1996) Microporous Mater 6:349
88. Hunger B, von Szombathely M (1995) Z Phys Chemie 190:19
89. Brunner E, Karge HG, Pfeifer H (1992) Z Phys Chemie 176:173
90. Beck LW, White JL, Haw JF (1994) J Am Chem Soc 116:9657
91. Brunner E, Beck K, Koch M, Heeribout L, Karge HG (1995) Microporous Mater 3:395
92. Zholobenko VL, Kustov LM, Borovkov VY, Kazansky VB (1988) Zeolites 8:175

93. Berglund B, Vaughan RW (1980) J Chem Phys 73:2037
94. Sternberg U, Brunner E (1994) J Magn Reson A 108:142
95. Koch M, Brunner E, Fenzke D, Pfeifer H, Staudte B (1994) Stud Surf Sci Catal 84:709
96. White JL, Beck LW, Haw JF (1992) J Am Chem Soc 114:6182
97. Kubelková L, Beran S, Lercher JA (1989) Zeolites 9:539
98. Kustov LM, Kazansky VB, Beran S, Kubelková L, Jirù P (1987) J Phys Chem 91:5247
99. Mirsojew I, Ernst S, Weitkamp J, Knözinger H (1994) Catal Lett 24:235
100. Brunner E (1995) Stud Surf Sci Catal 97:11
101. Sachsenröder H, Brunner E, Koch M, Pfeifer H, Staudte B (1996) Microporous Mater 6:341
102. Jänchen J, van Wolput JHMC, van de Ven LJM, de Haan JW, van Santen RA (1996) Catal Lett 39:147
103. Maciel GE, Haw JF, Chuang I-S, Hawkins BL, Early TA, McKay DR, Petrakis L (1983) J Am Chem Soc 105:5529
104. Ripmeester JA (1983) J Am Chem Soc 105:2925
105. Pines A, Gibby MG, Waugh JS (1973) J Chem Phys 59:569
106. Mehring M (1983) High resolution NMR in solids, 2nd edn. Springer, Berlin
107. Schulze D, Ernst H, Fenzke D, Meiler W, Pfeifer H (1990) J Phys Chem 94:3499
108. Lunsford JH, Rothwell WP, Shen W (1985) J Am Chem Soc 107:1540
109. Lunsford JH, Tutunjian PN, Chu P-J, Yeh EB, Zalewski DJ (1989) J Phys Chem 93: 2590
110. Baltusis L, Frye JS, Maciel GE (1987) J Am Chem Soc 109:40
111. Peng L, Chupas PJ, Grey CP (2004) J Am Chem Soc 126:12254
112. Haase F, Sauer J (1994) J Phys Chem 98:3083
113. Krossner M, Sauer J (1996) J Phys Chem 100:6199
114. Batamack P, Dorémieux-Morin C, Vincent R, Fraissard J (1991) Chem Phys Lett 180:545
115. Batamack P, Dorémieux-Morin C, Fraissard J, Freude D (1991) J Phys Chem 95:3790
116. Batamack P, Dorémieux-Morin C, Vincent R, Fraissard J (1993) J Phys Chem 97:9779
117. Hirschler AE (1963) J Catal 2:428
118. Plank CJ (1964) In: Sachtler WMH, Schuit GCA, Zwietering P (eds) Proceedings 3rd international congress on catalysis, Amsterdam, 1964. North-Holland, Amsterdam
119. Hunger M, Freude D, Pfeifer H (1991) J Chem Soc Faraday Trans 87:657
120. Heeribout L, Dorémieux-Morin C, Nogier J-P, Vincent R, Fraissard J (1998) Microporous Mesoporous Mater 24:101
121. Gale JD, Catlow CRA, Carruthers JR (1993) Chem Phys Lett 216:155
122. Bates S, Dwyer J (1994) J Mol Struct (Theochem) 306:57
123. Haase F, Sauer J (1995) J Am Chem Soc 117:3780
124. Luz Z, Vega AJ (1987) J Phys Chem 91:374
125. Hunger M, Horvath T (1995) Ber Bunsenges Phys Chem 99:1316
126. Thursfield A, Anderson MW (1996) J Phys Chem 100:6698
127. Biaglow AI, Gorte RJ, Kokotailo GT, White D (1994) J Catal 148:779
128. Haw JF, Hall MB, Alvarado-Swaisgood AE, Munson EJ, Lin Z, Beck LW, Howard T (1994) J Am Chem Soc 116:7308
129. Nicholas JB, Haw JF, Beck LW, Krawietz TR, Ferguson DB (1995) J Am Chem Soc 117:12350
130. Mildner T, Freude D (1998) J Catal 178:309
131. Beeler AJ, Orendt AM, Grant DM, Cutts PW, Michl J, Zilm KW, Downing JW, Facelli JC, Schindler MS, Kutzelnigg W (1984) J Am Chem Soc 106:7672

132. Koch M, Brunner E, Pfeifer H, Zscherpel D (1994) Chem Phys Lett 228:501
133. Geerlings P, Tariel N, Botrel A, Lissillour R, Mortier WJ (1984) J Phys Chem 88:5752
134. Bates S, Dwyer J (1993) J Phys Chem 97:5897
135. Neyman KM, Strodel P, Ruzankin SP, Schlensog N, Knözinger H, Rösch N (1995) Catal Lett 31:273
136. Farnworth KJ, O'Malley PJ (1996) J Phys Chem 100:1814
137. Gullion T, Schaefer J (1989) J Magn Reson 81:196
138. Koch M (1996) Thesis, University of Leipzig
139. Kao H-M, Grey CP (1996) J Phys Chem 100:5105
140. Dwyer J (1987) Stud Surf Sci Catal 37:333
141. Karge HG (1991) Stud Surf Sci Catal 65:133
142. Engelhardt G, Michel D (1987) High-resolution solid-state NMR of silicates and zeolites. Wiley, Chichester
143. Lippmaa E, Samoson A, Mägi M (1986) J Am Chem Soc 108:1730
144. Kerr GT (1969) J Catal 15:200
145. Samoson A, Lippmaa E, Engelhardt G, Lohse U, Jerschkewitz H-G (1987) Chem Phys Lett 134:589
146. Grobet PJ, Geerts H, Tielen M, Martens JA, Jacobs PA (1989) Stud Surf Sci Catal 46:721
147. Kellberg L, Linsten M, Jacobsen HJ (1991) Chem Phys Lett 182:120
148. Gilson JP, Edwards GC, Peters AW, Rajagopalan K, Wormsbecher RF, Roberie TG, Shatlock MP (1987) J Chem Soc Chem Commun, p 91
149. Ray GJ, Samoson A (1993) Zeolites 13:410
150. Frydman L, Harwood JS (1995) J Am Chem Soc 117:5367
151. Menezes SMC, Camorim VL, Lam YL, San Gil RAS, Bailly A, Amoureux JP (2001) Appl Catal A: General 207:367
152. Müller D, Gessner W, Behrens H-J, Scheler G (1981) Chem Phys Lett 79:59
153. Freude D, Haase J (1993) Quadrupole effects in solid-state nuclear magnetic resonance. In: Diehl P, Fluck E, Günther H, Kosfeld R, Seelig J (eds) NMR basic principles and progress, vol 29. Springer, Berlin, p 1
154. Samoson A, Lippmaa E, Pines A (1988) Mol Phys 65:1013
155. Samoson A, Lippmaa E (1989) J Magn Reson 84:410
156. Samoson A, Pines A (1989) Rev Sci Instrum 60:3239
157. Woessner DE, Timken HKC (1990) J Magn Reson 90:411
158. Ehresmann JO, Wang W, Herreros B, Luigi D-P, Venkatraman TN, Song W, Nicholas JB, Haw JF (2002) J Am Chem Soc 124:10868
159. Majors PD, Ellis PD (1987) J Am Chem Soc 109:1648
160. Kao H-M, Grey CP (1996) Chem Phys Lett 259:459
161. Michael A, Meiler W, Michel D, Pfeifer H (1981) Chem Phys Lett 84:30
162. Michael A, Meiler W, Michel D, Pfeifer H, Hoppach D, Delmau J (1986) J Chem Soc Faraday Trans I 82:3053
163. Wutscherk T (1990) Thesis, University of Leipzig
164. Brunner E, Pfeifer H, Wutscherk T, Zscherpel D (1992) Z Phys Chemie 178:173
165. Zscherpel D, Brunner E, Koch M, Pfeifer H (1995) Microporous Mater 4:141
166. Mastikhin VM, Mudrakovsky IL, Filimonova SV (1988) Chem Phys Lett 149:175
167. Borovkov VJ, Zhidomirov GM, Kazansky VB (1975) Zhurn Strukt Chim 16:308
168. Swift TJ, Connick RE (1962) J Chem Phys 37:307
169. Ettinger R, Blume P, Patterson A Jr, Lauterbur PC (1960) J Chem Phys 33:1597
170. Forsén S, Hoffman R (1963) J Chem Phys 39:2892
171. Hattori H (1995) Chem Rev 95:537

172. Barthomeuf D (1996) In: Weitkamp J, Lücke B (eds) Proceedings of the DGMK-conference: catalysis on solid acids and bases. Berlin, 14–15 March 1996. DGMK Hamburg, p 65
173. Huang M, Adnot A, Kaliaguine S (1992) J Am Chem Soc 114:10005
174. Uytterhoeven L, Dompas D, Mortier W (1992) J Chem Soc Faraday Trans 88:2753
175. Huang M, Kaliaguine S (1992) J Chem Soc Faraday Trans 88:751
176. Mueller KT, Baltisberger JH, Wooten EW, Pines A (1992) J Phys Chem 96:7001
177. Grandinetti PJ, Baltisberger JH, Farnan I, Stebbins JF, Werner U, Pines A (1995) J Phys Chem 99:12341
178. Bull LM, Cheetham AK, Anupold T, Reinhold A, Samoson A, Sauer J, Bussemer B, Lee Y, Gann S, Shore J, Pines A, Dupree R (1998) J Am Chem Soc 120:3510
179. Amoureux J-P, Bauer F, Ernst H, Fernandez C, Freude D, Michel D, Pingel U-T (1998) Chem Phys Lett 285:10
180. Bull LM, Bussemer B, Anupold T, Reinhold A, Samoson A, Sauer J, Cheetham AK, Dupree R (2000) J Am Chem Soc 122:4948
181. Freude D, Loeser T, Michel D, Pingel U, Prochnow D (2001) Sol State Nucl Magn Reson 20:46
182. Readman JE, Kim N, Ziliox M, Grey CP (2002) Chem Commun, p 2808
183. Bosácek V (1993) J Phys Chem 97:10732
184. Kheir AA, Haw JF (1994) J Am Chem Soc 116:817
185. Lima E, Lasperas M, de Menorval L-C, Tichit D, Fajula F (2004) J Catal 223:28

Mol Sieves (2008) 6: 45–152
DOI 10.1007/3829_008

Published online: 13 January 2006

Acidity and Basicity: Determination by Adsorption Microcalorimetry

Aline Auroux

Institut de Recherches sur la Catalyse, CNRS, 2 avenue Einstein,
69626 Villeurbanne Cedex, France
aline.auroux@catalyse.cnrs.fr

1 Introduction 46

2 Experimental 47

3 Limitations 56

4 Acidity and Basicity in Zeolites 59
4.1 Influence of the Zeolite Structure and Pore Diameter 61
4.2 Influence of the Si/Al Ratio 63

5 Probe Molecules 65
5.1 Acidic Probe Molecules 67
5.2 Basic Probe Molecules 67
5.3 Influence of the Probe Molecule on Adsorption Heats 69

6 Faujasite-Type Zeolites X and Y 73
6.1 Influence of the Probe Molecule 74
6.2 Temperature Dependence of Heats of Adsorption 78
6.3 Thermal Stability of Faujasites 79
6.4 Influence of the Crystallite Size 81
6.5 The Effect of Proton Exchange Level 81
6.6 Substitution by Other Cations 83
6.7 Influence of Occluded Clusters 86
6.8 Influence of Dealumination on H-Y Zeolites 87
6.9 Acidity in Fluid Cracking Catalysts (FCCs) 94

7 ZSM-5 Zeolites 95
7.1 Influence of the Probe Molecule 96
7.2 Effect of Adsorption Temperature 99
7.3 Difference in Preparation Procedures 100
7.4 Effect of Pretreatment 101
7.5 Effect of Proton Exchange Level 101
7.6 Influence of the Si/Al Ratio and Dealumination 102
7.7 Metal-Modified ZSM-5 104
7.8 Effect of Coke Deposition 105
7.9 Isomorphous Silica Molecular Sieves: Silicalite-1 105

8 Mordenites 107
8.1 Influence of the Probe Molecule 108
8.2 Influence of the Adsorption Temperature 109

8.3 Effect of Pretreatment . . . 109
8.4 Influence of the Exchange Level . . . 110
8.5 Influence of Dealumination . . . 113

9 Offretites and Erionites . . . 115

10 Other Zeolites . . . 116
10.1 H-Rho . . . 116
10.2 Ferrierite-Type Zeolites . . . 116
10.3 Mazzite . . . 116
10.4 MCM-22 and MWW-Based Catalysts . . . 117
10.5 Zeolites G, L, ZK-4, ZK-5, and SVK . . . 118
10.6 Beta Zeolites . . . 119

11 Tuning the Acidity . . . 119
11.1 Isomorphous Substitution . . . 119
11.1.1 Trivalent T Atoms . . . 120
11.1.2 Tetravalent T Atoms . . . 122
11.2 Chemical Modification . . . 124
11.3 Aging and Coke Deposition . . . 125
11.4 Additives . . . 126

12 Other Molecular Sieves . . . 130
12.1 Aluminophosphates (VPI, $AlPO_4$) . . . 130
12.2 Silicoaluminophosphates (SAPOs) . . . 132
12.3 Metal Aluminophosphates (MeAPOs) . . . 134
12.4 Mesoporous Materials (such as MCM-41) . . . 136

13 Relationship to Catalytic Activity . . . 138

14 Conclusion . . . 141

References . . . 142

Abstract We review the use of adsorption microcalorimetry for the determination of the surface acidity and basicity of various types of zeolites and related materials, as well as the relationship between the information gathered by this technique and catalytic activity.

1 Introduction

The unique catalytic properties of zeolites are mainly attributed to their acidic properties. However, the characterization of their acidity is difficult because of the possible presence of both Lewis and Brönsted acid sites and the possible existence of a heterogeneous distribution of acid site strengths.

While the acid sites in zeolites have been characterized by numerous investigators using a variety of spectroscopic, sorption, and titration techniques [1, 2], no fully satisfactory technique has emerged yet to provide in-

formation completely consistent with catalytic data. Therefore, sometimes, hydrocarbon reactions proceeding via carbocations may be chosen to characterize zeolite acid strength [2, 3]. While these experiments give reliable and practical information on the catalytic activity of large-pore zeolites and thus on their effective acidity, they provide no information on the range of intrinsic acid strength and on the acid site distribution. Moreover, none of the methods developed to characterize the acid strength in zeolites are able to give absolute values comparable to the scale of p*Ka* for acids in solution, with the possible exception of ab initio determination of the deprotonation energies [4].

The most promising approach to this problem is the use of suitable probe molecules for the quantitative characterization of site density and strength by means of adsorption microcalorimetry. The best-known applications of chemisorption involve the use of bases such as NH_3 or pyridine to probe the acidity of zeolites. Moreover, it is well known that adsorption influences all phenomena depending on surface properties, since it constitutes the primary step for every catalytic reaction involving solid catalysts. Adsorption is generally exothermic ($\Delta H < 0$) and the heat evolved is called heat of adsorption. This heat is related to the ability of the sites to interact with the probe molecule, i.e. to their basic or acidic character.

The number of cases where adsorption microcalorimetry has been successfully applied to this end has increased in recent years, especially in the field of determination of the acidic function of molecular sieves, and extensive reviews of the systems investigated using this methodology have been published [2, 5–18]. In particular, a review has been written [19] summarizing some of the most recently published results concerning the applications of microcalorimetry to the study of the acid/base sites of zeolites and mesoporous materials. The efficiency of thermal analysis techniques for the characterization of the acid/base strength of zeolite materials is discussed, as well as their ability to provide information consistent with catalytic data [19]. The reader is referred to the Atlas of Zeolite Structures [20] for nomenclature used throughout the text.

2 Experimental

The thermochemical techniques most commonly used to investigate the acid/base character of solid surfaces are DTA, TG, DTG, DSC, and calorimetry. These techniques can be used either by themselves, or combined with other techniques (for instance, TG-DSC, calorimetry-volumetry, DSC-chromatography, etc.) [10].

Techniques such as DTA, DTG, or DSC study the thermal behavior of a catalyst as it undergoes heating at a constant rate.

For example, differential thermal analysis (DTA) relies on the recording, as a function of time, of the difference between the temperature of the sample (T_s) and that of a reference material (T_r), upon heating both materials in a furnace. $\Delta T = T_s - T_r$ is related to the heat evolved (or absorbed) by the sample per unit time when the sample undergoes an endothermic or exothermic reaction.

In the differential thermogravimetry (DTG) method, the variation with time of the sample mass (dm/dt) is recorded as a function of temperature, while the sample is heated at a constant rate.

Finally, in the case of differential scanning calorimetry (DSC), the recorded quantity is the heat flow evolved per unit time by the sample as it is being heated at a constant rate.

On the contrary, in the adsorption microcalorimetry technique, the sample is kept at a constant temperature, while a probe molecule adsorbs onto its surface, and a heat-flow detector emits a signal proportional to the amount of heat transferred per unit time.

Values of the enthalpy of adsorption, determined either from the variation of adsorption with temperature (isosteric enthalpy of adsorption) or by direct calorimetric measurements, provide a valuable insight into the mechanism of adsorption. When taken together with data of adsorption isotherms, they provide information which could not be extracted from either set of data alone.

Heats of adsorption and other thermodynamic parameters can be obtained either by direct calorimetric determination, $-\Delta H = f(n_a)_T$ (n_a = adsorbed amount), or by using the Clausius–Clapeyron equation and the data from the isosteric measurements. Isosteric heats of adsorption is calculated from the temperature dependence of the adsorption isotherms, i.e. from the isosteres. Indeed, q_{st} can be computed from the experimental isosteres for each average temperature according to the equation

$$q_{st} = -RT^2(\delta(\ln P)/\delta T)_{n_r} . \quad (1)$$

where T is the absolute temperature, R the gas constant, and n_r the number of reversibly adsorbed molecules.

However, the irreversibility of adsorption in micropores is often reported, and this effect is mostly responsible for the frequently encountered uselessness of adsorption heats calculated from isosteres.

The average errors in evaluation of the differential heats of adsorption estimated by Stach et al. [21] are 1–2% only for the direct measurement and around 5% for the isosteric measurements.

The direct measurement of heats is also more accurate than the computation of energies from TPD data, which quantifies average activation energies of desorption. Whereas calorimetry is capable of yielding the strong acid site distribution in detail, the TPD of ammonia usually yields only an average value [22], except when appropriate kinetic models are employed.

In the direct calorimetric determination, ($-\Delta H = f(n_a)_T$), the amount adsorbed (n_a) is calculated either from the variations of the gas pressure in a known volume (volumetric determination) or from variations of the weight of the catalyst sample in a static or continuous-flow apparatus (gravimetric determination). In a static adsorption system, the gas is brought into contact with the catalyst sample in successive doses, whereas the catalyst is swept by a continuous flow in a dynamic apparatus. Comparative calorimetric studies of the acidity of zeolites by static (calorimetry linked to volumetry) and temperature-programmed (differential scanning calorimetry linked to thermogravimetry) methods of ammonia adsorption and desorption have been performed [23].

Another interesting comparison of various thermal analysis techniques, namely adsorption microcalorimetry, thermoprogrammed desorption, and thermoprogrammed reaction using constant rate thermal analysis (CRTA), has been performed by Fesenko et al. in order to study the reactivity of zeolites in terms of the adsorption or desorption of base probe molecules [24]. As an example, CRTA was applied to the desorption of isopropylamine from Na-Y zeolite and its acidic form HY.

Presently, calorimetry linked to the volumetric technique is still the most commonly used method [18]. Prior to the adsorption, the catalyst is outgassed at the desired temperature and under high vacuum (~ 0.1 mPa) in the calorimetric cell. After cooling to the adsorption temperature and establishing the thermal equilibrium of the calorimeter, a dose of gaseous probe molecules is brought into contact with the catalyst sample, and both the pressure and heat signal are monitored until equilibrium is reached. Then, successive new doses are added and the new equilibrium pressures are recorded together with the corresponding evolved heats. The data obtained directly from adsorption calorimetry measurements can be expressed in different ways (Fig. 1) as follows.

(a) The amount of gas adsorbed at constant temperature plotted as a function of the equilibrium pressure (adsorption isotherm I).

In order to accurately determine the chemisorbed amount from the overall adsorption isotherm, the sample can be outgassed at the same temperature to remove the physically adsorbed amount, after which a new adsorption procedure is carried out to obtain isotherm II. The difference between the first and second isotherm gives the extent of irreversible adsorption (V_{irr}) at a given temperature (Fig. 1a), and can be considered as a measurement of the amount of strong sites in the catalyst. However, in a first approximation, the magnitude of the heat of adsorption can be considered as a simple criterion to distinguish between physical and chemical adsorption.

(b) The corresponding calorimetric isotherms (Q_{int} vs. P) (Fig. 1b).

(c) The integral heats (Q_{int}) as a function of the adsorbed quantities (n_a) (Fig. 1c).

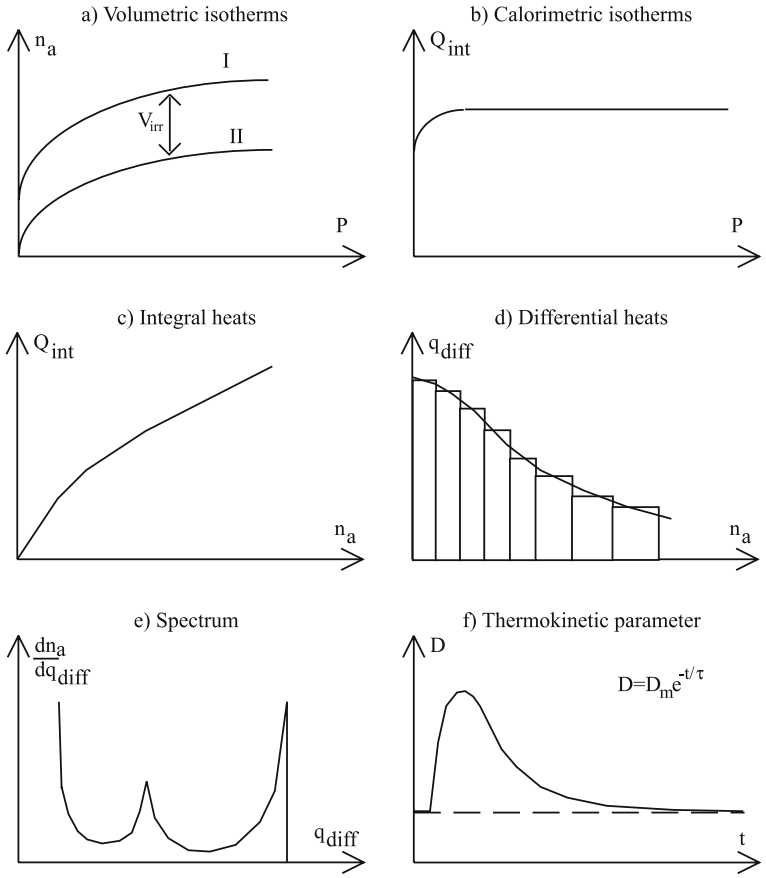

Fig. 1 Calorimetric and volumetric data obtained from adsorption calorimetry measurements

This representation leads to the detection of coverage ranges with constant heat of adsorption, for which the evolved heat is a linear function of the coverage.

(d) The differential heat $Q_{diff} = \partial Q_{int}/\partial n_a$ (molar adsorption heat for each dose of adsorbate) as a function of n_a (Fig. 1d).

The ratio of the amount of heat evolved for each increment to the number of moles adsorbed (in the same period) is equal to the average value of the differential enthalpy of adsorption in the interval of the adsorbed quantity considered. The curve showing the differential heat variations in relation to the adsorbed amount is traditionally represented by histograms. However, for simplification, the histogram steps are often replaced by a continuous curve connecting the centers of the steps. The curves of differential heat of adsorption vs. coverage are generally distinguished by the following features [25] (Fig. 2):

i) an initial region of high heat of adsorption, representing adsorption on the strongest sites which are ascribed mainly to Lewis sites. The initial drop in the curve of Q_{diff} vs. coverage, even in the case of adsorption on apparently homogeneous surfaces, could be ascribed to residual surface heterogeneities. Thus, an exponentially decreasing adsorption energy distribution for 1–5% of the surface exhibiting strong heterogeneity is often observed, especially in the presence of extra-framework aluminum species;
ii) one or more regions of intermediate strength sites which are predominantly Brönsted acid sites. There is always a fairly good relationship between framework aluminum content and population of Brönsted acid sites, provided the framework aluminum atoms are totally accessible to the probe. A region of constant heat in this domain is characteristic of a set of acid sites of homogeneous strength;
iii) a region where heats decrease more or less steeply depending on the heterogeneity of the sites. Sometimes interactions between already adsorbed molecules can create a small heat increase with gas loading;
iv) a heat of adsorption at high coverage approaching a nearly constant value characteristic of hydrogen-bonding between the probe and the sample or physisorption of the probe. This constant value depends on the nature of the probe (i.e. of its enthalpy of vaporization at the adsorption temperature). However, there is also evidence in the literature for weak Lewis acidity giving rise to low heats of adsorption [25]. The heat then falls to a value close to that of the heat of condensation of the adsorbate in liquid phase.

(e) Acidity spectra.

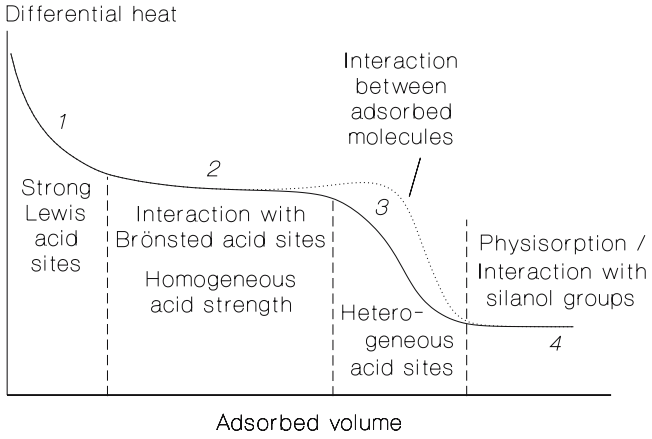

Fig. 2 Regions in a typical curve of differential heat of adsorption versus adsorbed amount

In some cases the variation of the adsorption heats with progressive coverage corresponds to step-shaped curves. Such a behavior may be associated with the discrete surface heterogeneity due to the existence of several energetic levels [26]. In such cases, to describe the change in the adsorption heats with coverage, another approach is to plot acidity spectra (Fig. 1e) : assuming that the variation in the adsorption heats coincides with energy distributions, one may wish to measure the number of sites with the same energy, i.e. sites that give rise to the same differential heat. This is achieved upon plotting $-\mathrm{d}n/\mathrm{d}Q_{\mathrm{diff}}$ as a function of Q_{diff}. The area below the curve included between Q_{diff} and $Q_{\mathrm{diff}} + \mathrm{d}Q_{\mathrm{diff}}$ represents the population of sites of identical strength estimated via Q_{diff}.

(f) Plot of the variation of the thermokinetic parameter as a function of the adsorbed amount of probe.

Heat conduction microcalorimetric output consists of power versus time and hence can undergo analysis to produce not only thermodynamic but also kinetic data. The kinetics of heat release during adsorption can be monitored by the change in the thermokinetic parameter τ [27, 28]. The calorimetric signal decreases exponentially with the adsorption time after the maximum of each adsorption peak (Fig. 1f). This can be approximated by $D = D_{\mathrm{m}} \exp(-t/\tau)$, where D and D_{m} are the deviation at time t and the maximum deviation of the calorimetric signal, respectively. In this expression, the thermokinetic parameter τ, known also as the time constant, can thus be calculated as the reciprocal of the slope of the straight line obtained upon plotting $\log D$ as a function of time [27]. This thermokinetic parameter is indeed not constant and varies with coverage. One can then plot the variations of the thermokinetic parameter with the amount of adsorbed probe (Fig. 3).

For most zeolites, when NH_3 is used as the probe molecule at a given temperature, the time needed to establish thermal equilibrium after each dose at first increases with increasing adsorbed amount, passes through a maximum, then decreases rapidly and finally reaches a value close to the time constant of the calorimeter. For example, Fig. 3 shows the time constant (in seconds) versus the amount of NH_3 adsorbed for samples of H-ZSM-5 (Si/Al = 10.3) pretreated at 673 K or 1073 K and possessing a very small particle size (0.02 to 0.05 μm). The maximum time constant is higher for the sample pretreated at 1073 K than for the sample pretreated at 673 K, because increasing the pretreatment temperature causes dealumination, i.e. creates extra-framework aluminum species which restrict the access to the channels and creates diffusional limitations. The time constant of the calorimeter was close to 300 s. The heat transfer is determined by the mass transfer which becomes slower.

In fact, the establishment of the adsorption equilibrium is monitored both through the change in the heat signal and by the change of the pressure in the system. The time required to establish equilibrium depends on the quantity

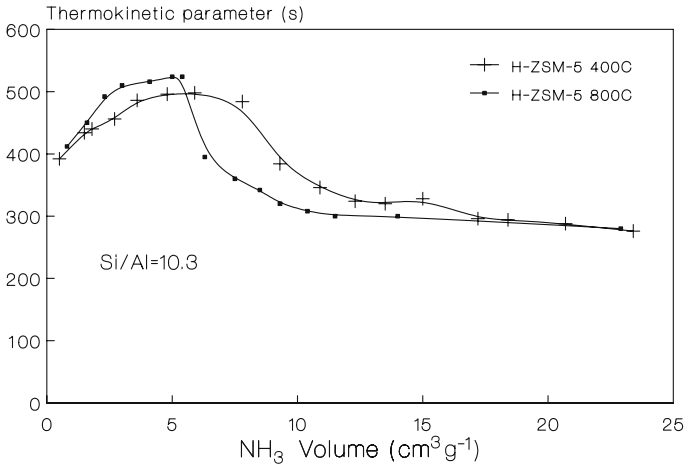

Fig. 3 Variation of the thermokinetic parameter (in seconds) versus the ammonia uptake for a H-ZSM-5 sample (Si/Al = 10.3) pretreated at 673 K (+) and 1073 K (•)

of adsorbed probe, on the temperature, and on the inertia of the calorimeter. At low temperatures, a slower adsorption is observed in covering the strong adsorption centers than at higher temperature. The long time to establish equilibrium is apparently related to a redistribution of the adsorbed probe on the centers that are energetically more favorable [29].

A calorimetric study of ammonia adsorption on zeolites has confirmed that, at 303 K, the adsorption process involves a slow redistribution of adsorbed species, so that a longer time is needed to achieve thermal equilibrium [30]. The rate of heat liberation depends strongly on the amount of ammonia adsorbed. At higher temperature this phenomenon cannot be observed. The data related to the thermokinetic behavior of ammonia adsorbed on faujasite, *L* and mordenite type zeolites are discussed [30]. The position of the maximum on the kinetic curves depends on the chemical composition of the zeolite and on the degree of filling of the cavities of the zeolite by the molecules adsorbed. The slow liberation of the heat is associated with a redistribution of the adsorbed molecules.

When the adsorption temperature is increased to 373 K and then to 473 K, there is a decrease in the time required to establish equilibrium and a decrease in the region of coverage in which slow adsorption is observed [29]. At 573 K and 673 K, equilibrium is established rapidly at all coverages. The time to establish thermal equilibrium in this case is determined solely by the inertia of the calorimeter. When using probes, the molecular diameter of which is much larger than that of NH_3, other diffusional problems also occur.

(g) Estimate of the entropy of adsorption from the adsorption equilibrium constants obtained from adsorption isotherms and heat of adsorption data obtained microcalorimetrically.

The differential molar entropies can be plotted as a function of the coverage. Adsorption is always exothermic and takes place with a decrease in both free energy ($\Delta G < 0$) and entropy ($\Delta S < 0$). With respect to the adsorbate, the gas-solid interaction results in a decrease in entropy of the system. The cooperative orientation of surface-adsorbate bonds provides a further entropy decrease. The integral molar entropy of adsorption S^a and the differential molar entropy S^a_{diff} are related by the formula $S^a_{diff} = \partial(n_a S^a)/\partial n_a$ for the particular adsorbed amount n_a. The quantity S^a can be calculated from

$$\Delta_a S = S^a - S^{g,P} = Q_{int/Tn_a} + R/n_a \int_0^P n_a \mathrm{d}(\ln P)\,, \tag{2}$$

where S^a is the molar entropy of the adsorbed phase, $S^{g,P}$ the molar entropy of the gaseous phase (available from tables), and n_a the adsorbed amount. After integration of the plot of n_a vs. ln(P) between 0 and P from the adsorption isotherm at the temperature T, and of the plot of Q_{diff} vs. n_a between the same boundaries to obtain Q_{int}/n_a, the value of S^a can be obtained, and then that of S^a_{diff}.

As indicated above, the extent of adsorption can also be measured directly by weighing the catalyst sample together with the adsorbed probe molecule by means of a microbalance set inside the calorimeter. The sample is outgassed as previously described and then contacted with successive doses of probe gas. The adsorbed amount is calculated from the weight gain for each dose [10].

An alternative method is flow adsorption microcalorimetry, which involves the use of a carrier gas passing continuously through the adsorption cell [31–34].

In the pulse flow method, the procedure consists of injection of a precise and well-defined gas volume (probe molecule + carrier gas) into the stream which flows through the catalyst bed held on the fritted glass of a specially designed calorimetric cell. For each pulse, the calorimetric signal is recorded and the amount of gas which has not been retained by the catalyst is measured by a gas chromatograph (or mass spectrometer) connected on-line to the calorimetric cell. The major disadvantage of this technique is that the weakly chemisorbed portion of the probe gas is not held by the catalyst and gives rise to an endothermic peak of desorption which follows immediately the exothermic peak of adsorption, and thus necessitates peak deconvolution.

As an illustration, let us mention a study by Brown et al. [31], who investigated by flow adsorption calorimetry the relative accessibilities of acid sites in zeolite Y and K_{10} clay catalysts in both acid and Na^+ forms, reaching the conclusion that, under flow conditions and nitrogen at atmospheric pressure as carrier gas, the sites first covered by ammonia are not necessarily those with the highest heats of adsorption.

Another example is a calorimetric study by Aguayo et al. [33] of the adsorption of different bases (ammonia, *n*-butylamine, *tert*-butylamine, pyridine) from the gas phase on a FCC (H-Y-type) catalyst in flow regime through an isothermal bed of solid; the authors have determined the conditions under which the adsorption is exclusively chemisorption, as well as those under which the adsorption is not limited by the internal diffusion of the base.

Flow microcalorimetry has been compared with batch volumetry and temperature-programmed desorption for the determination of the surface acidity of various porous materials in powder using ammonia chemisorption [35]. Flow-calorimetric measurements of the transfer of matter and thermal effects accompanying one adsorption-desorption cycle of pure ammonia in helium carrier gas at 373 K were carried out on powders of porous materials such as H-Y zeolites with varying Si/Al ratios (H-Y30, H-Y20, H-Y9, H-Y6) and surfactant-templated aluminosilicates (MSA20, MSA10, MSA5). The comparison of the flow-microcalorimetry method with two-cycle ammonia adsorption and thermoprogrammed ammonia desorption revealed some differences in the number of surface acid sites, which could be ascribed to variations in experimental conditions used during desorption or pre-treatment stages in each of these methods. Therefore much attention should be paid to this aspect when comparing the results of surface acidity tests reported in the literature. The same experiments were performed on some selected samples pre-saturated with water vapor, and the non-negligible influence of vicinal water on the results of surface acidity tests was demonstrated [35].

Finally, let us mention that calorimetric measurements can also be used to monitor adsorption phenomena in the liquid phase (in a solvent). For example, the so-called *cal-ad method* [36–38] has been used to measure the adsorption heats evolved upon addition of dilute solutions of pyridine in *n*-hexane to a solid acid (TS, H-ZSM-5) in a slurry with *n*-hexane. The amount of free base in solution is measured separately with a UV-Vis spectrophotometer [36, 37]. Contrary to earlier calorimetric results for H-MFI in vacuum, the authors [36] suggested the presence of two energetically different types of sites, with only the strong sites ($\approx 176\,\mathrm{kJ\,mol^{-1}}$) capable of transferring a proton to the adsorbed base. More recently, De Macedo et al. have characterized Na and proton-exchanged mordenite zeolites by the cal-ad method (calorimetric and adsorption studies of pyridine interaction with the solid in cyclohexane slurry) [39]. A two-site adsorption process has been proposed to describe the acidic sites of H-MOR, with $0.081\,\mathrm{mmol\,g^{-1}}$ of Brönsted sites ($\Delta H_1 = -82.9\,\mathrm{kJ\,mol^{-1}}$) and $0.422\,\mathrm{mmol\,g^{-1}}$ of Lewis sites ($\Delta H_2 = -36.7\,\mathrm{kJ\,mol^{-1}}$). However, Savitz et al. [38] using vapor-phase measurements for the co-adsorption of pyridine and *n*-hexane in H-MFI claimed that equilibrium is not achieved for pyridine titration measurements in a solvent at room temperature and, therefore, that the ability of the cal-ad method

to distinguish Brönsted acid sites of widely different strengths in H-MFI is unproven [38]. Finally, it is also worth mentioning that calorimetric measurements of immersion into water and *n*-butylamine have been used to estimate the hydrophilic and acid-base characters of a series of Zn(II) exchanged Na-X zeolites [40].

Calorimetry is also a suitable technique for co-adsorption studies. For example, it has been shown that the enthalpy change of ammonia adsorption on the remaining sites of an H-mordenite after methanol pre-adsorption is not affected by the irreversibly bound methanol species, but that methanol pre-adsorption has the effect of reducing the number of strong adsorption sites [41].

Another application of the calorimetric technique deals with simultaneous measurements of loading, composition, and heats of adsorption from gaseous mixtures. The components of a binary mixture are dosed alternately, so that the individual differential heats of adsorption can be determined from two successive measurements [42, 43].

3 Limitations

- Wall adsorption, although high mainly in a metallic volumetric system, appears not to result in major problems if a suitable careful calibration is performed. Rapid transfer of heat from the sample to the cell wall is recommended [44].
- Careful heat flow calibrations have to be performed. Chemical calibrations present many disadvantages: they rely on prior results, with no general agreement and no control of rate, and are generally available only at a single temperature. On the contrary, electrical calibrations provide many advantages: the absolute energy input is easy to measure with most modern equipment, the rate of heat input can be easily varied, the magnitude of heat input is readily available, and the calibrations are easy to perform at any temperature.
- It appears that it is often difficult to determine the nature of the adsorbed species, or even to distinguish between the different kinds of adsorbed species from the calorimetric data. In many cases this technique fails to distinguish between cations and protonic sites due to the insufficient selectivity of the adsorption. The experimental data obtained by microcalorimetric measurements of ammonia adsorption are, at low coverages on zeolites, markedly affected by the circumstance that the differential heats of adsorption on strong Lewis centers and strong Brönsted sites are relatively close. This fact might render it difficult in some cases to discriminate Lewis and Brönsted sites solely by the adsorption of basic probe molecules and microcalorimetry if no complementary techniques

are used. As no exact information can be obtained regarding the nature of the acid centers from the calorimetric measurements, suitable IR, MAS NMR, and/or XPS [45] investigations are necessary to identify these sites. However, due to the complex nature of the acid strength distribution, it is currently still not possible to make a detailed correlation between sites of different nature and their strength.

- It is also difficult to find good correlations between the site strength distribution and the activity or selectivity of a catalyst. Indeed, in catalysis only a fraction of the energy spectrum of the surface sites may actually be involved during the catalytic reaction. If the critical size of the reactant molecules is commensurate with the pore dimensions, the rate of conversion may be determined by diffusional limitations and not only by the strength of acid sites [46]. In addition, the interplay of reaction and diffusion depends in fact on the temperature.
- Initial values representing small concentrations of the strongest acid sites can be easily missed in the measurement. It is possible to detect the strong Lewis sites of zeolites even though small in number via adsorption microcalorimetry of NH_3, provided the gas doses are small enough, the adsorption temperature high enough and the gas adsorption system remains stable and leak-free over very long periods of time such as those required for describing the whole coverage, otherwise low equilibrium pressures cannot be accurately determined.
- Another limitation is that the rate of heat liberation depends strongly on the amount of preadsorbed ammonia [47]. In view of the high sensitivity of the calorimeters, heat liberation can be observed for a significantly longer period, but the true time necessary to establish equilibrium cannot be determined accurately because the heat liberation curve approaches the base line asymptotically. However, the use of a highly sensitive and accurate capacitance manometer for the measurement of the equilibrium pressure limits the error on this determination.
- The adsorption of the gas should not be limited by diffusion, neither within the adsorbent layer (external diffusion) nor in the pores (internal diffusion). Should diffusion limitations occur, then adsorption on active but less accessible sites may only occur after better exposed but less active sites have interacted. Diffusion may, thus, cause the "smoothing out" of significant details in the energy spectrum, and the differential heat curves determined under the influence of diffusion phenomena may indicate less surface heterogeneity than actually exists on the adsorbent surface [7].

  The validity of energy distributions derived from heats of adsorption has been examined in the literature [48].

  According to Biaglow et al. [49], there is a possibility that the mobility of molecules larger than NH_3, such as pyridine, can be limited even at weaker sites. Molecules may not be able to migrate to the strongest sites;

in such a case, migration of the adsorbate between crystallites in the bed is not possible and the initial heats are simply a statistical average of the sites which are first exposed. A way to get around this is to increase the mobility of the probe molecule by increasing the calorimeter temperature, but this might be limited by the thermal stability of the probe in the presence of the sample.

External diffusion is especially a serious problem with adsorption calorimeters which contain a thick bed of adsorbent. The adsorption of very small doses of gas may help to solve diffusion problems if the number of molecules in the dose is small enough compared to the number of readily accessible reactive sites. The admission of small doses, which prevents the rapid increase of the equilibrium pressure, favors the reaction of the gas with the most active surface sites. However, it is evident that the detailed analysis of the surface sites by means of adsorption calorimetry is then very time-consuming.

- Microcalorimetry can give erroneous results if adsorption equilibration is too slow, a particularly serious problem if one works at low temperatures. If, for example, a fraction of the adsorbate molecules do not reach the aluminum sites of the framework during the time of the experiment, the measured heats will not be indicative of the strong Brönsted acid sites [50]. The temperature has to be chosen according to a systematic study of the temperature dependence of the heat curve of probe molecule chemisorption. At low temperature, no selective sorption preferring the stronger acid sites occurs, but random distribution of the gaseous molecules on acid and non-acid sites is simultaneously observed. It follows that temperatures high enough to avoid steric hindrance or diffusional limitations should be used for the acidity determinations [51].

  It is worth noting that the literature contains some controversial articles on this subject [52]. Generally speaking, the adsorption temperature should not be too low, in order to allow the detection of differences among the sites; otherwise, under certain circumstances the measured evolved heat can be just an average value. Another important issue is that one must ensure that chemisorption predominates over physisorption.
- The absence of a plateau of constant heat in the differential heat curve can be the result of molecular interactions between molecules adsorbed at neighboring sites rather than a true indication of differences between sites [49]. This matter can be checked by varying the probe size or the site density.

4
Acidity and Basicity in Zeolites

The high variability of the *acidic properties* of these materials is caused by the existence of crystallographically non-equivalent sitings and different local environments of the framework atoms.

The Brönsted acidity in zeolites is assigned to the tetracoordination of isomorphously substituted Al in a tetrahedral SiO_2 framework which results in a negatively charged AlO_4^- anion: this charge is compensated by cations and particularly by protons, the latter resulting in the so-called Brönsted acidity that plays a very important role in the catalytic activity of zeolites.

The differential heats of adsorption on Brönsted sites and Lewis sites (cationic species) are not easily comparable [53]. For the former it is the difference between the enthalpy of dissociation of the acidic hydroxyl and the enthalpy of protonation of ammonia, while for Lewis sites the differential heat of adsorption represents the energy associated with the transfer of electron density towards an electron deficient, coordinatively unsaturated site, and probably an energy term related to a relaxation of the strained surface. Microcalorimetric studies of several zeolites (H-mordenite, USY, H-ZSM-5) treated in such a way as to contain a noticeable amount of extra-framework aluminum have shown that the distribution of the sites with respect to the differential heats of NH_3 adsorption is exponential for the Lewis sites (Freundlich isotherm) and linear for the Brönsted sites (Temkin isotherm) [53].

In most cases, the catalytic activity is related to the number of Brönsted sites rather than Lewis acid sites. However, the influence of acidic Lewis sites in catalytic reactions over zeolites is still controversial and cannot be neglected. Therefore, it appears necessary to develop methods to identify and characterize the acid strength of Lewis sites by more selective probes.

Energetic surface heterogeneity is, first of all, a consequence of the structural surface heterogeneity which is one of the fundamental features of real solid surfaces. It seems, therefore, reasonable to assume that there should exist correlations between structural and energetic heterogeneities. Indeed, the adsorption energies on given acidic sites are related to the nature of their nearest-neighbors or even next-nearest neighbors [54].

Thus, the sites of varying strength in a given zeolite may be a reflection of aluminum *topology*, i.e. the number of next-nearest neighbors (NNN) or more distant Al atoms. In zeolites, an Al atom cannot be connected directly to another Al atom through oxygen, so the nearest neighbor tetrahedral sites (T sites: Si or Al) are all Si. The adsorbed molecules are usually assumed to be localized, and each one occupies a single adsorption site. Furthermore, only the lateral interactions of the NNN pairs are considered.

Consequently, Brönsted sites of different strength can be observed. These Brönsted acid sites may be Si – OH – Al species having different numbers of NNN Al-centered tetrahedra or tetrahedral Al. In the literature, evidence is

provided that isolated Al framework atoms (having no next-nearest Al neighbors) have the highest strength and that, as the number of next-nearest Al atoms increases, the acid strength is likely to decrease [55]. Zeolites having high Si/Al ratios, where the Si – OH – Al species are widely separated and can be considered to be isolated, will give rise to a homogeneous site distribution (occurrence of a heat plateau), provided the absence of extra-framework aluminum species (EFAL). On the contrary, zeolites with high Al contents contain large and variable numbers of Al atoms in NNN positions. The number of isolated framework aluminum atoms and the relationship with the Brönsted acidity in dealuminated acid zeolites can be obtained from theoretical calculations [56]. Considering the topological aluminum density for different zeolites, Barthomeuf [57] calculated the corresponding limit value m_{lim} of the aluminum molar fraction, $m = Al/(Si + Al)$, which depends on the density of T atoms in the framework. Below the limit value m_{lim}, no Al atom has another Al atom as a next-nearest neighbor, and therefore all acid sites show a high acid strength. Above the limit m_{lim}, there are Al atoms in the second coordination sphere, with the consequence that not all Brönsted sites have a strong acidity (although the total number of acid sites is still increasing with the total number of Al atoms in the unit cell), and the concentration of strong sites decreases with increasing Al content of the framework [58].

The way the differential heats of adsorption change with coverage illustrates quite clearly the distribution of surface sites with respect to a given adsorbate and their varying reactivity on given adsorbents. The shape of the differential heat curves versus coverage demonstrates quite explicitly that the number, the reactivity, and the distribution of surface sites are significantly modified when the composition or the pretreatment of the samples are changed.

Apart from plain hydrogen bonding, three main modes of adsorption of basic probe molecules have been identified by adsorption calorimetry, namely adsorption on surface silanol groups, adsorption on cations, and adsorption on acid sites that are associated with protons occupying non-framework cationic positions. Adsorption may also occur on Al-containing non-framework species which are not cationic in nature, e.g., oxidic species.

The role of *basicity* in catalysis has been less studied than acidity. However, a demand for a deeper knowledge is now required in the field of catalysis, as basic catalysts begin to play an important role in many reactions (e.g., aldolization, transesterification, Michael and Knoevenagel reactions, etc.). A comprehensive review about basicity and the basic properties of zeolites has been given by Barthomeuf [59].

The basicity of the framework in molecular sieves corresponds to anions such as O^{2-}, AlO_4^- or OH^-. In Si – Al zeolites, the framework oxygen bears the negative charge, and when this charge is compensated by cations with low electronegativity (such as alkali cations), the charge may become high enough

to create basic properties. The cation then acts as a Lewis acid while the associated framework oxygens act as Lewis bases. Thus, the base strength in zeolites can also be expressed by the negative charges of framework oxygen atoms, which are calculated from the Sanderson electronegativity equivalence method [60]. In principle, a clear distinction between basic sites of different strengths should be expected in basic zeolites. It is well-known that the charge on the framework oxygen varies depending on the Si – O – Al angle and the T – O distance, and simultaneously on the O – M distance (where M is the exchanged alkali cation), the charge increasing as the O – M distance decreases. A distribution of intrinsic basic site strength is generated as a function of the different cation locations (or different O – M distances).

Basic strength and the density of the basic sites decrease with an increase in the framework Si/Al ratio, while the basic strength increases with an increase in electropositivity of the countercation in zeolites [60].

In the determination of acidity by microcalorimetry, several factors play an important role, such as the adsorption temperature, the pretreatment temperature, and the choice of probe molecule. Other factors, more specific to zeolites, are the topology, the Si/Al ratio, the chemical composition, and the modifications to which the samples have been subjected. These various factors will be examined in what follows, for the various families of studied zeolites. However, the main two factors are the zeolite structure and the framework aluminum content. Most of the studies described herein are summarized as reference tables in a review by Cardona-Martinez et al. [5].

4.1
Influence of the Zeolite Structure and Pore Diameter

It is well known that under identical conditions of adsorption on molecular sieves of the same chemical composition but different pore systems, the structure of the pore system and the diameters of the pores of the microporous adsorbents are responsible for the phenomenon of selective adsorption. The intensity of the electrostatic field is also determining.

In acid-catalyzed reactions, zeolites often show shape selectivity because of their unique pore structure. Outer surface acidity, however, diminishes this important property, and can even cause pore blocking by coke formation.

Table 1 summarizes the pore diameters, the variety of *n*-oxygen-membered rings, the network dimensionality, and the chemical formulae of various zeolites. Table 1 also gives the average differential heats of ammonia adsorption corresponding to the main site populations of these zeolites in their H-form. Figures 4 to 6 display the differential heats of ammonia adsorption versus coverage on samples of these different types of zeolites, which all presented very few extra-framework aluminum species. The Si/Al ratio, the activation temperature, and the adsorption temperature are given for each sample in the figure captions.

Table 1 Different zeolite structures (cf. [20])

Type	Samples	Pore diameter (nm)	Oxygen rings	Network dimensionality	Chemical composition	NH3 Average heat (kJ mol^{-1})
Small pores	Linde A	0.41	8	III	$(Na_{12}(Al_{12}Si_{12}O_{48}), 27H_2O)_8$	—
	Erionite	0.36×0.51	8	III	$(Na_2, Ca)_{3.5}K_2(Al_9Si_{27}O_{72}), 27H_2O$	160
	Ferrierite	0.34×0.48	8	I	$Na_2Mg_2(Al_6Si_{30}O_{72}), 18H_2O$	150
		0.43×0.55	10	I		
	ZK-5	0.39	8	III	$Na_{30}(Al_{30}Si_{66}O_{192}), 98H_2O$	—
Medium pores	ZSM-5	0.53×0.56	10	III	$Na_n(Al_nSi_{(96-n)}O_{192}), 16H_2O$ $(n < 27)$	160
		0.51×0.55	10	III		
	ZSM-11	0.53×0.54	10	III	$Na_n(Al_nSi_{(96-n)}O_{192}), 16H_2O$ $(n < 16)$	155
Large pores	Offretite	0.36×0.49	8	II	$(Ca, Mg)_{1.5}K(Al_4Si_{14}O_{36}), 14H_2O$	155
		0.67	12	I		
	Mordenite	0.7×0.65	12	I	$Na_8(Al_8Si_{40}O_{96}), 24H_2O$	160–170
		0.26×0.57	8	I		
	Faujasite X	0.74	12	III	$Na_{88}(Al_{88}Si_{104}O_{384})$	100
	Y				$(Na_2, Ca, Mg)_{29}(Al_{58}Si_{134}O_{384}), 240H_2O$	120–140
	Beta	0.76×0.64	12	I	$Na_n(Al_nSi_{64-n}O_{128}), n < 7$	130
		0.55×0.55	12	II		
	Mazzite	0.74	12	I	$(Na_2, K_2, Ca, Mg)_5(Al_{10}Si_{26}O_{72}), 28H_2O$	200
		0.34×0.56	8	I		

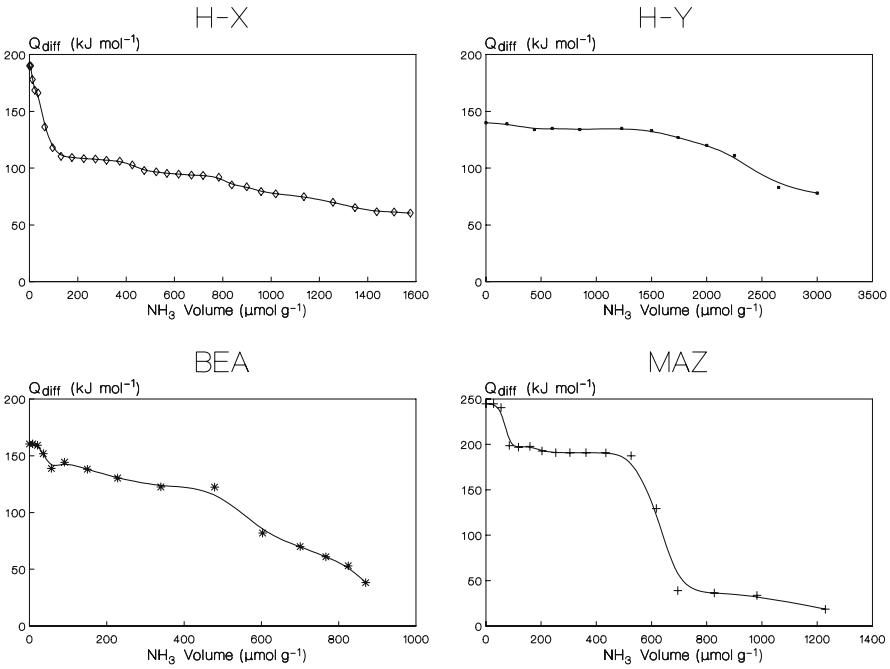

Fig. 4 Differential heat of adsorption vs. NH_3 uptake for a H-X zeolite (Si/Al = 1.25, pretreatment at 573 K, adsorption at 353 K), a H-Y zeolite (Si/Al = 2.4, 80% exchange, pretreatment at 673 K, adsorption at 423 K), a Beta zeolite (Si/Al = 10, pretreatment at 773 K, adsorption at 423 K) and a mazzite zeolite (Si/Al = 12, pretreatment at 673 K, adsorption at 423 K)

A comparison of the acidic characters of amorphous and crystalline aluminosilicates has been performed using ammonia adsorption calorimetry [61]. H-ZSM5, H-MCM-22, H-β samples with similar Si/Al ratios (Si/Al $\approx$ 13) were found to display plateaus of constant adsorption heats near 150 kJ mol^{-1}, while the silica-alumina samples gave rise to continuously decreasing heats starting from 150 kJ mol^{-1} at zero coverage, due to their surface heterogeneity.

4.2 Influence of the Si/Al Ratio

The Si/Al ratio plays a significant role, since the aluminum atom is directly related to the acidic site and accounts for the formation of carbenium and/or carbonium ions or possibly cation radicals inside the zeolite. Dealumination processes can promote porous structure modifications, which may improve some interesting properties of zeolites, like thermal and hydrothermal stability, acidity, catalytic activity, resistance to aging and low coking rate, and

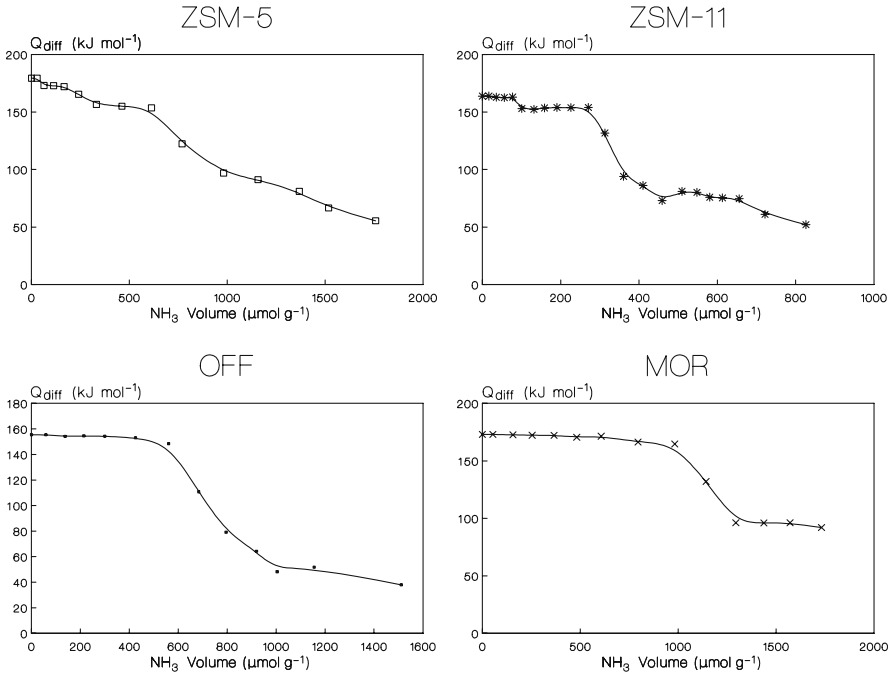

Fig. 5 Differential heat of adsorption vs. NH_3 uptake for a ZSM-5 zeolite (Si/Al = 13.3, pretreatment at 673 K, adsorption at 393 K), a ZSM-11 zeolite (Si/Al = 20, pretreatment at 673 K, adsorption at 423 K), an offretite (Si/Al = 3.9, pretreatment at 673 K, adsorption at 423 K), and a mordenite (Si/Al = 16.2, pretreatment at 673 K, adsorption at 423 K)

material transfer. However, a severe dealumination may also cause a loss of crystallinity.

Different dealumination processes have been proposed, namely steaming and acid treatments, as well as reactions with $SiCl_4$ or SiF_6^{2-}. From many experimental and theoretical investigations of the acidity of zeolites with different aluminum contents of the framework, it has been concluded that the number of bridging hydroxyl groups increases with rising number of Al atoms in the lattice [62]. In contrast, the dependence of the acid strength on the aluminum content is more complicated, since from theoretical considerations an increasing acid strength with a decreasing number of aluminum atoms is expected, whereas from studies of the Al topology in the framework a curve often presenting a maximum was derived from the number of strong sites [62, 63]. The effect of steaming on the number and strength of acid sites is apparent from a comparison of the differential heat curves for the dealuminated zeolites. The microcalorimetric curves also show that the strength of sites corresponding to the intermediate plateau region first increases and then progressively decreases with steaming severity. The dependence of the acid strength distribution of dealuminated mordenites (Fig. 7a) and dealumi-

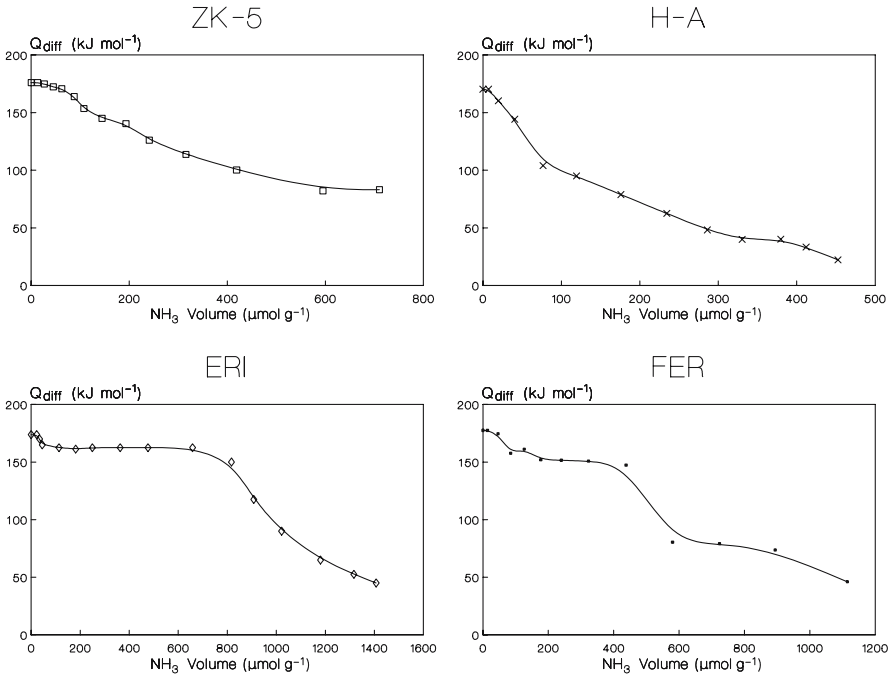

Fig. 6 Differential heat of adsorption vs. NH_3 uptake for a ZK-5 (Si/Al = 3.36, pretreatment at 673 K, adsorption at 423 K), a H-A (Si/Al = 1, pretreatment at 573 K, adsorption at 353 K), an erionite (Si/Al = 3.5, pretreatment at 673 K, adsorption at 423 K), and a ferrierite (Si/Al = 15, pretreatment at 673 K, adsorption at 423 K)

nated faujasites (Fig. 7b) on the Si/Al ratio is depicted in Fig. 7. The number of strong acid sites presents a distinct maximum. The abscissa of the maximum corresponds to an Al content of 4.6/u.c. (and Si/Al ratio equal to 9.5) for dealuminated mordenites, and an Al content of about 29/u.c. (and Si/Al ratio around 5.5) for dealuminated Y zeolites. These values are in good agreement with the ones predicted by Barthomeuf [57] who calculated the limit value, m_{lim}, for mordenite and H-Y zeolites, and found that it corresponds to $m_{lim} = 0.096$ (or Si/Al = 9.4) for mordenite and $m_{lim} = 0.150$ (which corresponds to Si/Al = 5.8) for H-Y zeolites.

5 Probe Molecules

As calorimetry gives the total number of adsorption sites and possibly catalytically active centers, the obtained values depend on the nature and size of the probe molecule. In zeolites of the alumino-silicate type, the negatively charged aluminum atoms in the framework generate an electrostatic field,

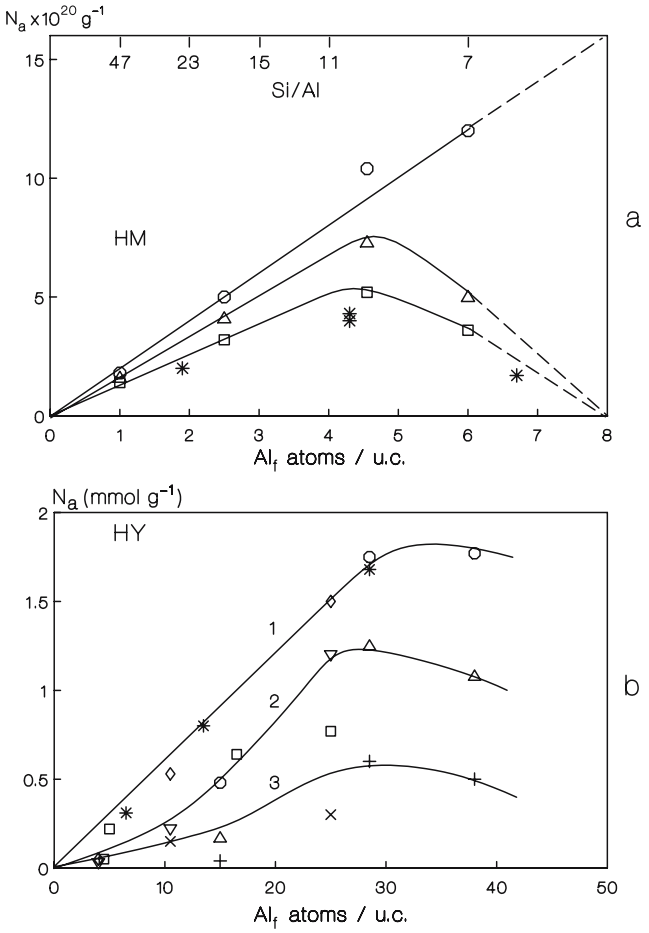

Fig. 7 **a** Acid strength distribution dependence on Al(IV) content per unit cell of dealuminated H-mordenites. N_a number of acid sites in molecules g^{-1} with $Q > 80$ kJ mol^{-1} (○), with $Q > 100$ kJ mol^{-1} (△), with $Q > 120$ kJ mol^{-1} (□, ∗) from [63]. Differential molar heats of ammonia adsorption were measured at 423 K. **b** Acid strength distribution dependence on the framework aluminum content per unit cell in dealuminated Y zeolites. *Curve 1*: total number of acid sites with $Q > 80$ kJ mol^{-1} (∗, ○, ◊). *Curve 2*: number of acid sites with $Q > 100$ kJ mol^{-1} (△, ▽). *Curve 3*: number of acid sites with $Q > 120$ kJ mol^{-1} (+, ×, □) from [62]. Differential molar heats of ammonia adsorption were measured at 423 K

making zeolites capable of interacting strongly with polar molecules. On the other hand, non-polar molecules can be adsorbed on zeolites via van der Waals interactions as well as pore filling [64].

Appropriate probe molecules to be selected for adsorption microcalorimetry should be stable with time and with temperature. Furthermore, they should be small enough to readily penetrate into the intracrystalline space of

most zeolites. The probe adsorbed at a given temperature should also have sufficient mobility to equilibrate with active sites. For example, the heats of adsorption of CO_2 and NH_3 are extremely sensitive to changes in the chemistry and geometry of the surface of the void spaces and channels in zeolites, since the significantly large quadrupole (CO_2) and dipole (NH_3) moments cause a very significant contribution of specific interactions to the total energy of adsorption of these molecules [65].

Moreover, repulsive interactions between adsorbate molecules could arise from the ionic repulsion of two positively charged adsorbates, or from changes in a protonic site due to adsorption at adjacent sites [49].

5.1 Acidic Probe Molecules

For basicity measurements, the number of acidic probes able to cover a wide range of strength is rather small [59]. Moreover, a difficulty stems from the fact that some acidic probe molecules may interact simultaneously with cations (such as Na^+). The ideal probe molecule should be specific to basic sites and should not be amphoteric. It should not interact with several types of basic sites or give rise to chemical reactions [59]. For instance CO_2 ($pKa = 6.37$) is commonly chosen to characterize the basicity of zeolites but it may either be adsorbed on the cations or physisorbed, or may react with hydroxyls and framework oxide ions to give carbonated species. However, the energetic aspect of the adsorption of CO_2 on various molecular sieves in a large domain of temperature and pressure can provide interesting information on the nature of the adsorbate-adsorbent interactions [66]. The heats of adsorption of the quadrupolar molecule CO_2 increase in the order silicalite < H-ZSM-5 < Na-ZSM-5 < Na-X [67].

The same problems may arise when using SO_2 as an acidic probe, despite the fact that SO_2 ($pKa = 1.89$) is more acidic than CO_2 and, thus, more likely to probe the total basicity of the surface. Carboxylic acids such as acetic acid can also be used but dimers can be formed, particularly at high coverage. Pyrrole may also be used, particularly at low adsorption temperature, but has sometimes shown some amphoteric character. The model of pyrrole chemisorbed on a basic site consists of a bonding between the framework oxygen (Lewis basic site) and the H atom of the NH group of the pyrrole molecule.

5.2 Basic Probe Molecules

Heats of adsorption of strong bases are related both to the intrinsic acidity of the site and the interaction energy between the deprotonated zeolite and the protonated base.

Ammonia (pKa = 9.24, proton affinity in gas- phase = 857.7 kJ mol^{-1}) and pyridine (pKa = 5.19, proton affinity in gas-phase = 922.2 kJ mol^{-1}) are the favored molecules to probe the overall acidity of a zeolite, since both Lewis and Brönsted acid sites retain these molecules. As indicated above, the use of infrared spectroscopy is necessary to distinguish qualitatively and unambiguously between these two types of sites. The use of substituted pyridines (2,6-dimethylpyridine) has also been considered in order to probe specifically the Brönsted sites [68].

Reviews by Gorte et al. [69, 70] deal with the adsorption complexes formed by strong and weak bases with acid sites in zeolites. Among strong bases, they examine the thermochemistry and adsorption enthalpies of a series of molecules similar to ammonia, i.e. alkylamines, but also pyridines and imines. Concerning weak bases, studies of the adsorption properties of water, alcohols, thiols, olefins, aldehydes, ketones, and nitriles are taken into account. The authors report a poor correlation between the differential heats of adsorption on H-MFI and enthalpies of protonation in aqueous solutions, but a much better correlation with gas-phase proton affinities [70].

Ammonia is among the smallest strongly basic molecules, and its diffusion is hardly affected by the porous structure. This makes it the most commonly used probe in calorimetry. One proton is transferred from the zeolite hydroxyl site to ammonia upon adsorption, i.e. ammonia is adsorbed as an ammonium ion. The heat of ammonia adsorption depends both on the proton mobility and on the affinity of ammonia for the proton. Ammonia adsorption isotherms are of type I.

The adsorption capacities of large pore zeolites for benzene and pyridine vapors are practically equal. The adsorption rate of pyridine is substantially lower than the adsorption rate of benzene due to its electronic structure. A comparison of the adsorption heats of pyridine and benzene makes it possible to conclude that the unshared pair of electrons and the large dipole moment of pyridine both make an important contribution to the energy of reaction of pyridine with zeolites [26]. Most linear and branched amines have also been used to titrate the acid sites in zeolites.

Acetonitrile is an interesting molecule for probing the acid sites in zeolites [52, 71–73]. It is a weak base, so no protons are abstracted and actual hydroxyl groups can be observed. It allows also the investigation of both Lewis and Brönsted acidity. While it is normally considered to be a weak base, it actually has a moderately high proton affinity (798 kJ mol^{-1}, compared to 857 kJ mol^{-1} for ammonia and 773 kJ mol^{-1} for methanol). Unlike the stronger bases ammonia and pyridine, which are completely protonated by Brönsted acid sites, acetonitrile forms strong hydrogen bonds with the zeolite lattice. Since these hydrogen bonds perturb the CN group, it should be possible to characterize the acid site by examining the hydrogen bond [71].

Calorimetric data of acetonitrile adsorption on the acidic forms of various high-silica zeolites having the MFI (ZSM-5), CHA (chabazite), MOR

(mordenite), TON (ZSM-22), MTW (ZSM-12), FER (ferrierite), and FAU (faujasite) structures have been reported by Yang et al. [74], with adsorption heats that were independent of the structure within experimental error, the differential heats for the 1 : 1 adsorption complexes all being $100 \pm 10\,\mathrm{kJ\,mol^{-1}}$. A possible explanation lies in the additional orientation-dependent interaction resulting from hydrogen bonding. On the contrary, calorimetric measurements of CH_4 and O_2 adsorption at 210 K showed that structure affects the adsorption properties in a manner which depends on the pore dimensions [74].

Other nitriles and alcohols have also been used to probe the acid sites of zeolites [75, 76].

NO can be employed as a probe to identify Lewis acid sites and characterize their density and strength [77]. However, NO may disproportionate into N_2O and oxygen and is also very likely to form multi nitrosyl complexes with transition metal ions when present. From a different point of view, calorimetric measurements of CO and N_2 adsorption [78] at low temperature also provide a powerful tool for characterizing zeolites (Li-, Na-, K-MFI and H-MFI), by probing the cations and providing information on their nature and accessibility [79].

5.3 Influence of the Probe Molecule on Adsorption Heats

Because of their strong basicity, ammonia and pyridine are adsorbed very strongly even on the weakest acid sites. As a consequence, their interactions with surface acid sites are relatively unspecific. Therefore, a significant number of studies using these probe molecules report a homogeneous acid site strength [55, 80].

In any case, the size and the strength of the probe molecule are important parameters and have to be carefully considered when performing adsorption studies.

As shown in the case of many zeolites (ZSM-5, mordenite, H-Y) [68, 81], it is difficult to compare adsorption of ammonia and pyridine, because of their difference in basicity and the specific interactions of each of these molecules with the host zeolite. The adsorption heats should indeed be correlated not to the basicity of the probe molecules in liquid phase or in aqueous solutions (where NH_3 is more basic than pyridine by about $20\,\mathrm{kJ\,mol^{-1}}$, since the p*Ka* values are 9.3 and 5.2, respectively) but to their basicity in the gas phase, which can be expressed in terms of the proton affinities (PA). In the gas phase, pyridine is a stronger base than ammonia: the PA value of pyridine is ca. $922.2\,\mathrm{kJ\,mol^{-1}}$, while that of ammonia is only ca. $857.7\,\mathrm{kJ\,mol^{-1}}$. The other parameters, which have to be taken into account, are size (the kinetic diameters of pyridine and ammonia are 0.533 and 0.375 nm, respectively) and the secondary interactions between these adsorbates and the zeolite struc-

ture (hydrogen bonds may lead to the formation of a monodentate with pyridine and a bidentate with ammonia), as shown by Parillo et al. [81, 82]. These differences are reflected in the adsorption heats, which are usually 20–30 kJ mol^{-1} higher in the case of pyridine than in the case of ammonia; a similar difference is observed for the chemisorption limit [68, 80].

Adsorption enthalpies have been measured for ammonia, pyridine, and isopropylamine as a function of coverage at 480 K by Parrillo et al. [80], on several high silica zeolites, including H-ZSM-5, H-ZSM-12, H-mordenite (H-M, Si/Al = 15), and H-Y. Except for isopropylamine in H-ZSM-5, each adsorbate exhibited a constant heat of adsorption up to a coverage of one molecule per Brönsted acid site, followed by a sharp drop in the measured heats. For isopropylamine in H-ZSM-5, the results were found to depend on the Si/Al ratio and synthesis procedures, and it appears that hydrogen bonding between the adsorbate molecules affected the measured heats. For ammonia, the adsorption enthalpies were 150 kJ mol^{-1} for H-ZSM-5, H-ZSM-12, and H-Y, and 160 kJ mol^{-1} for H-M. Adsorption enthalpies for pyridine were between $\sim$ 190 and 210 kJ mol^{-1} for H-ZSM-5, H-ZSM-12, and H-M, but only $\sim$ 180 kJ mol^{-1} for H-Y. Heats of adsorption for isopropylamine tended to be slightly higher than those for pyridine on each sample (between 200 and 240 kJ mol^{-1} for H-ZSM-5 [83]), but appeared to depend on site concentrations. As the various structures exhibited almost the same adsorption energies, the authors suggested that the isolated Brönsted acid sites in high silica materials are almost identical [80].

A comparison of the adsorption energies of the complexes formed by ammonia, pyridine, and isopropylamine with a simple potential-energy model, which assumes that the heat of adsorption linearly scales with gas-phase proton affinities, suggests that proton transfer dominates the interaction between the adsorbate and the acid site [83].

In another study by Parrillo et al. [82] on a H-ZSM-5 sample, the average heats of adsorption in the low coverage regime were as follows: ammonia (145 kJ mol^{-1}), methylamine (185 kJ mol^{-1}), ethylamine (195 kJ mol^{-1}), isopropylamine (205 kJ mol^{-1}), *n*-butylamine (220 kJ mol^{-1}), dimethylamine (205 kJ mol^{-1}), trimethylamine (205 kJ mol^{-1}) and pyridine (200 kJ mol^{-1}). Again a good correlation was found between these heats and gas-phase proton affinities. The heats of adsorption increase in increments that are identical to the gas-phase proton affinity differences, except for relatively small deviations with trimethylamine and *n*-butylamine. The deviations for trimethylamine and *n*-butylamine imply that there are some specific interactions between these amines and the zeolite [82]. The deviation for trimethylamine could be explained by a decrease in the ability of this molecule to form hydrogen bonds, while the deviation for *n*-butylamine could be due to interactions between the alkyl groups and the zeolite walls. In contrast to the excellent correlation between heats of adsorption and gas-phase acidity scales, the correlation with solution-phase acidities (p*Ka*) is very poor [82].

The microcalorimetric technique has also been applied to investigate the adsorption of acetonitrile, dimethylether, water, pyrrole, and ammonia on ferrierite, a small pore zeolite [84]. This investigation showed that the results of the determination of the site strength distribution are dependent on the strong or weak basicity of the probe, on the acidity and porosity of the acid solid, and on the adsorption temperature. A similar calorimetric investigation of the acidity of dealuminated Y-type zeolites was performed using the same various basic probes [85].

The data concerning the adsorption of different bases indicate that the sorbed bases interact with zeolites more strongly than hydrocarbons of similar structure and molecular weight [26]. A comparison of adsorption heats of various bases such as ammonia, pyridine, *n*-butylamine with benzene on A, X, Y and mordenite zeolites modified by ion exchange and aluminum extraction was carried out by Klyachko et al. [26]. Surprisingly, it was found that the heats of pyridine adsorption are virtually the same on sodium and hydrogen zeolites. Furthermore, the sorbed amounts of large molecules such as pyridine and *n*-butylamine are very limited by the finite void volume of zeolites. In the case of ammonia, some complications could arise because of penetration of NH_3 into the small cages.

An important observation is that it is possible to quantitatively evaluate the location of acid sites by using different probe molecules, e.g., on one hand ammonia, which is able to reach all acid sites, and on the other hand pyridine, cyclohexane, benzene, etc., probes that can only attach to sites in the main channels.

It is worth noticing that the sorption properties and associated enthalpies of many aliphatic and aromatic compounds have been shown to vary in accordance with the size of the sorbate molecules and the pore size distribution of the sorbant [86–89]. For example, a study of the adsorption of benzene and benzene derivatives onto zeolite H-Y at 323 K [86] has revealed that the ΔH values corresponding to interaction with acidic Brönsted sites vary between 66 and 125 kJ mol^{-1} and increase in the following order: benzene < ethylbenzene < 1,4-diethylbenzene $\approx$ 1,3-diethylbenzene. Benzene exhibited a constant adsorption enthalpy over a wide range of sorbate loadings, while the substituted benzene atoms showed gradual increases in ΔH_{ads} with coverage, indicating mutual interaction between sorbate molecules. In the case of alkane sorption in molecular sieves, Eder et al. [90] have estimated the contribution of the direct interaction between the alkane and the acid sites to the adsorption heat to be around 10 kJ mol^{-1} for MFI and 6 kJ mol^{-1} for FAU, while the heats of adsorption were found to decrease in the sequence H-MFI > H-MOR > H-FAU [91]. A similar study was performed on zeolites theta 1, ferrierite, and ZK-5 [90].

Jänchen et al. [72] have reported that the heats of adsorption of acetonitrile on mesoporous (MCM-41) and microporous (FAU and MFI) molecular sieves are mainly influenced by a specific interaction with the acidic sites,

while the adsorption heats of a non-polar molecule like *n*-hexane are determined by the pore size or density of those materials. However, a pore size effect affecting the heats of acetonitrile adsorption on acidic molecular sieves has to be taken into account when employing those heats as a measurement of acidic strength. The contribution of the pore size-governed dispersion interaction in MCM-41 is ca. 15 kJ mol^{-1} less than that in the narrow channels of MFI.

Finally, it is worth mentioning that water can be used as a probe molecule to provide knowledge of hydration enthalpies, which is of considerable interest when assessing the hydrophilic or hydrophobic character of zeolites [92].

For example, adsorption of water vapor on X and Y zeolites exchanged with barium (Ba-X, Ba-Y) has been studied by thermogravimetry and calorimetry [93]. The faujasite zeolite was found to exhibit a stronger adsorption affinity for water molecules when exchanged with barium than with sodium or potassium.

Monitoring by microcalorimetry of the adsorption of molecules of different sizes has also been used to assess the micropore network of zeolites (micropore sizes, channels, presence of cavities, etc.) and to determine the topology of a zeolite.

For example, it has been shown that the adsorption of molecules of different sizes (toluene, xylenes, etc.), and the consecutive adsorption of these same molecules, studied by adsorption microcalorimetry together with reaction tests, can provide useful indications of the pore geometry and reactant accessibility of new zeolitic materials such as MCM-22 [94] or ZSM-11, SSZ-24, ZSM-12, H-M, and CIT-1 [95].

Similarly, insight into the pore structure of zeolites of type MWW, ITQ-2, and IM-5 has been gained through microcalorimetric studies of *n*-hexane, toluene, *m*- and *o*-xylenes, 1,2,4- and 1,3,5-trimethylbenzene adsorption [87, 96]. In another study [97] it was shown that the γ-cages of H-ZK-5 and K-ZK-5 are the preferred adsorption sites for propane and *n*-butane because of the more favorable heats of adsorption.

As a last example, it has been reported that the heats of adsorption of dichloromethane on Na-Y samples decrease from 72 kJ mol^{-1} initially to 54 kJ mol^{-1} after adsorption of 0.2 molecule per supercage, then remain constant up to a value of 5.5 molecules per supercage, i.e., close to that corresponding to a complete filling of supercages: 6 molecules per supercage [98].

In conclusion, the choice of a suitable probe molecule depends on the physico-chemical characteristics of the studied samples, such as the pore size distribution, aluminum content, etc.

6
Faujasite-Type Zeolites X and Y

In order to understand the complexity of the determination of the acid strength distribution in a zeolite, we will first focus on the most studied zeolites, the faujasites (X and Y). Figure 8 presents the differential heats of ammonia adsorption versus coverage for various H-Y zeolites. The initial

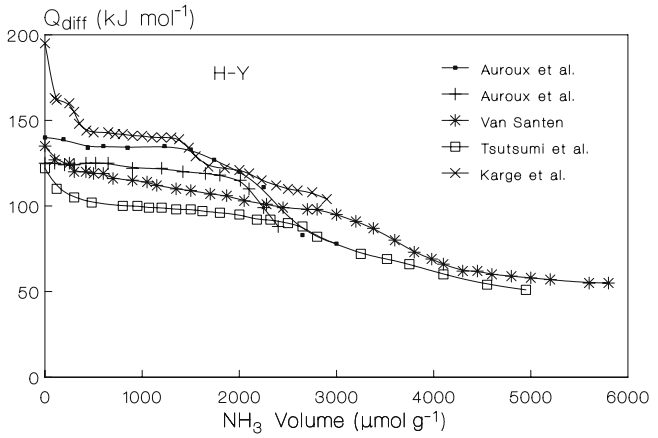

Fig. 8 Differential molar heats of ammonia adsorption versus coverage for various H-Y zeolites: × from [99], • from [23], + from [104], ∗ from [106], □ from [102]. See Table 2 for the composition, activation, and adsorption temperatures of the corresponding samples

Table 2 Comparison of various H-Y zeolites

Refs.	Si/Al	% Exchange	Activation temp. (K)	Adsorption temp. (K)	Initial heat (kJ mol^{-1})	Average heat at plateau (kJ mol^{-1})
[99]	2.54	98.6	675	425	200	140
[106]	2.4	100	673	423	133	120
[108]	2.4	85	673	423	114	110
[100]	2.4	82	723	423	130	115
[107]	2.42	85.7	673	423	113	110
[101]	2.4	80	753	573	110	110
[102]	2.5	83	673	473	125	100
[105]	2.56	79	673	353	150	130
[23]	2.4	80	673	423	140	140
[104]	2.43	85	675	416	125	125

NH_4-Y samples were all produced by repeated exchange of an original sample of Na-Y. These samples display very similar Si/Al ratios and exchange levels above 80%, and were pretreated and studied at similar temperatures. However, the curves show completely different profiles, and the average heat at the plateau varies from 100 to 140 kJ mol^{-1}. The differences in volumes can be easily explained by the uncertainty of the mass of the samples, depending on whether one starts from a hydrated sample or not, and whether or not dealumination could take place during the heat pretreatment (deep bed/shallow bed) or whether or not the samples maintain their crystallinity, which is not always indicated in the corresponding literature (see Table 2). Still, the results show that tiny variations in the exchange level, Si/Al ratio, or adsorption temperature can create important differences in the acidity of a system. The differences in the reported results may also be attributed to other factors, such as different operating conditions or sample crystallite sizes.

6.1 Influence of the Probe Molecule

The differential heats of *ammonia* adsorption on an H-Y sample (Si/Al = 2.54, 98.6% exchange) after activation at 675 K and at an adsorption temperature of 425 K were studied by Karge et al. [99] with respect to the amount of NH_3 adsorbed. The curve obtained indicated a small number of strong sites with Q_{diff} ranging from approximately 200 to 140 kJ mol^{-1} and extending to 0.5 mmol g^{-1} of adsorbed NH_3 (see Fig. 8). These sites were identified because of their strength as Lewis sites. In this portion, the curve dropped steeply between 200 and 170 kJ mol^{-1}, followed by a pseudo-plateau over a small coverage at 165–160 kJ mol^{-1} and then fell again to a more recognizable plateau at 140 kJ mol-1. This part of the curve amounted to 1.5 mmol g^{-1} of adsorbed ammonia (corresponding to a total of 30 NH_3 molecules per u.c.), showing the homogeneity of the acidic strength of these particular sites. The curve then began to drop again, as ammonia started covering sites which were weaker in energy (i.e. Q_{diff} = 140–100 kJ mol^{-1}) and also had a wider distribution. This last series of sites was assigned to OH groups of the supercages.

A H,Na-Y zeolite sample (Si/Al = 2.4) having 82% of the Na exchange cations replaced by protons was studied by microcalorimetry of NH_3 adsorption by Spiewak et al. [100] at 423 K. An initial heat of adsorption of 130 kJ mol^{-1} was observed. Using this probe, the authors showed a heat decrease to a plateau at 115 kJ mol^{-1}, indicating that ca. 750 μmol/g of the sites were relatively homogeneous in strength. After ca. 1000 μmol/g of NH_3 were adsorbed on the surface, the heat gradually decreased to a value of 70 kJ mol^{-1}, which corresponds to hydrogen bonding of ammonia to non-acidic hydroxyl groups.

The reaction of NH_3 with various kinds of acidic centers on Y zeolites (Si/Al = 2.4) at 573 K was also studied by Kapustin et al. [101] by adsorption microcalorimetry. It was determined that the heats of adsorption of ammonia on the Brönsted acid centers of Y zeolites were 110–90 kJ mol^{-1}. These values were closer to those obtained by Tsutsumi et al. [102, 103], and can also be compared with those of Auroux et al. [23, 104], Huang et al. [105], van Santen [106], Stach et al. [107], and Lohse et al. [108], which can be found in Table 2.

These findings can be compared with the results obtained by Chen et al. [55], who adsorbed *pyridine* at 473 K on a H-Y sample with a Si/Al ratio of 2.4. They observed acidic sites with a broad distribution of energies ranging from 250 to 100 kJ mol^{-1}, but did not see any single plateau indicating sites with homogeneous strength. However, Chen et al. [55] reported that the total coverage was only half of that expected from the Si/Al ratio. The authors described sites with heats of adsorption greater than 180 kJ mol^{-1} to be predominantly Lewis acid sites. The absence of a plateau can be explained by the fact that the bulky pyridine molecules are unable to interact (at 473 K) with the OH groups located in the small cavities, whereas these sites are available for ammonia and produce the plateau at $\sim$ 140 kJ mol^{-1}. Studies of aluminum distribution in Y zeolite suggest that there should be four different acid strengths corresponding to aluminum atoms with 0, 1, 2, or 3 Al next-nearest neighbors. Thus, another explanation for the heterogeneity in acid strength distribution for this H-Y zeolite is that the studied sample possibly had a Si/Al ratio higher than the reported value of 2.4.

Adsorption enthalpies have been measured by Parrillo et al. [80] for *ammonia*, *pyridine*, and *isopropylamine* as a function of coverage at 480 K on a high silica H-Y (Si/Al = 30) pretreated at 750 K. The authors found that each adsorbate exhibited a constant heat of adsorption up to the coverage of one molecule per Brönsted acid site, followed by a sharp drop in the measured heats. The adsorption enthalpies were respectively 150 kJ mol^{-1} for ammonia, $\sim$ 180 kJ mol^{-1} for pyridine, and slightly higher ($\sim$ 190 kJ mol^{-1}) for isopropylamine. Their results suggest that the isolated Brönsted acid sites in high silica faujasite are almost identical.

The acidic properties of hydroxyl sites of H-Y zeolite were also measured at 473 K by adsorption calorimetry of various bases (*piperidine*, *pyridine*, and *ammonia*) by Tsutsumi et al. [109]. The difference in heats of adsorption between the OH sites was explained by a positional difference between the OH sites, molecular size of the titrating bases, and proton mobility induced by strong bases. The order of strength of bases was determined by replacing a base molecule by another one (for adsorption on H-Y zeolite) as follows: piperidine ($Q_{init} \approx 165$ kJ mol^{-1}) > pyridine ($Q_{init} \approx 160$ kJ mol^{-1}) > ammonia ($Q_{init} \approx 125$ kJ mol^{-1}). This order differs from the order expected from their p*Ka* values in solution. Heats of adsorption were measured over a wide range of coverage in the case of ammonia, but only below ca. 3 mmol g^{-1} in the

cases of pyridine and piperidine. The shapes of the curves also differed considerably with the different probes. The combined use of calorimetric and IR measurements allowed the authors to separate the heats of adsorption into heats evolved from OH sites associated with bands at 3640 cm^{-1} and 3550 cm^{-1}. No Lewis acid sites on H-Y were detected on the spectra between 1800–1200 cm^{-1} after adsorption of bases, although the calorimetric curves displayed a sharp decrease at very low coverage before reaching a plateau at respectively 160, 145, and ca. 100 kJ mol^{-1} for piperidine, pyridine, and ammonia.

According to Brueva et al. [110], the high heats of adsorption (measured at 303 K) of *n-butylamine* on Na-forms of Y-type zeolites are due to the formation of a coordination bond between the NH_2 group and Na^+ ions. On H-forms of zeolites, the heats of adsorption of *n*-butylamine are substantially higher, while the rate of establishment of the adsorption equilibrium is lower than on Na-forms, which is probably associated with the formation of $C_4H_9NH_3^+$ ions.

For *acetonitrile*, adsorption experiments on zeolite H-Y gave heats of chemisorption of 80 kJ mol^{-1} at 303 K, characteristic of the H-complex of acetonitrile on Brönsted acid sites [111]. After careful shallow-bed dehydroxylation of this H-Y at 870 K, the adsorption heat for the strongest sites amounted to ca. 90 kJ mol^{-1}. This was most probably due to Lewis sites created by dehydroxylation.

Microcalorimetric measurements of *ammonia*, *pyrrole*, *dimethylether*, and *acetonitrile* adsorption unveiled various strength distributions among the acid sites population of Y-type zeolites with various Si/Al ratios [85]. Ammonia proved to be a reliable probe when only Brönsted acid sites were investigated. Dimethylether, a very weak base, did not appear to be any better than ammonia to reveal the inhomogeneity of one particular acid sites population, whereas pyrrole appeared as a rather acidic probe which helped visualize the basicity difference between the parent material and the dealuminated samples. Acetonitrile proved to be a reliable probe to monitor quantitatively and qualitatively Lewis acidity.

Thermodynamic parameters of the adsorption of *hydrocarbons*, especially of normal paraffins, olefins, and cyclic hydrocarbons, on highly dealuminated Na-Y zeolites, and for comparison on silicalite $(SiO_2)_{96}$, have been measured by Stach et al. [21, 112]. The dealuminated Na-Y named US-Ex $(Na_2(AlO_2)_2(SiO_2)_{190})$ presented mesopores with diameters between 3 and 10 nm besides the unchanged micropore structure of the parent Na-Y material. Dealuminated zeolites showed less energetic heterogeneity in the adsorption of hydrocarbons than Na-X and Na-Y zeolites. A comparison of the equilibrium data of hydrocarbons adsorbed on highly dealuminated zeolites revealed a strong influence of the diameters of the pore systems on the thermodynamic parameters. While the electrostatic fields within the pore systems of the zeolites influenced the heats of adsorption of hydrocarbons, no such in-

fluence on the entropy values was found [21]. In the case of *n*-paraffins, the heat increased with the number *n* of carbon atoms of the chain of the adsorbed *n*-paraffins. Moreover, the enthalpy values of *n*-paraffins adsorbed in faujasite increased with the number of adsorbed molecules, attained a maximum and then decreased [21].

The adsorption heats of *n-paraffins* (ethane, *n*-butane, *n*-hexane, *n*-decane), *benzene*, *cyclohexane* and *water* were also measured by Stach et al. [112] and Jänchen et al. [113] on US-Ex, and an empirical equation was derived for the initial heats of adsorption of the *n*-alkanes.

Differential heats of adsorption have been determined calorimetrically for *n-butane* and *but-1-ene* on molecular sieves US-Ex and silicalite by Thamm et al. [114]. It was shown that on US-Ex but-1-ene isomerized, whereas on silicalite it was physically adsorbed.

The isosteric heats of adsorption of *n-hexane* and *3-methylpentane* in zeolites Na-Y and H-Y have been reported by Pires et al. [115]. The difference between the heats of adsorption of *n*-hexane on the Na^+ ($56\,kJ\,mol^{-1}$) and the H^+ forms ($58\,kJ\,mol^{-1}$) of Y zeolites was within the range of experimental error, but a significant difference between the heats of adsorption of 3-methylpentane on Na-Y ($51\,kJ\,mol^{-1}$) and H-Y ($57\,kJ\,mol^{-1}$) was observed. These results were compared with those obtained on a ZSM-20. The adsorption of both molecules with a higher energetic effect on Y zeolite relative to ZSM-20 reflected structural effects, in agreement with the existence of larger supercages in ZSM-20 than in Y zeolite, and hence a higher confinement effect for the sorbate molecules in zeolite Y [115].

A calorimetric study was realized to characterize the contributions of the different interactions of *aromatic molecules* adsorbed by various exchanged Y zeolites (Na-Y, K-Y, Ba-Y) [80]. The interactions, which affected the energy of adsorption, involved the methylenes, methyl groups, and aromatic rings. These contributions were evaluated from the adsorption data of benzene, toluene, *p*-xylene, *m*-xylene, and *p*-dimethylcyclohexane on the cation-exchanged zeolites (Na^+, K^+, Ba^{2+}) at 298 K and 423 K [116–118]. The strength of interaction between an aromatic cycle and the cation increased, when the cation varied from K^+ to Na^+ and from Na^+ to Ba^{2+}. The adsorption heats also increased with the number of methyl groups, and the methyl/framework interaction was independent of the cation nature. The adsorption heats of *p*-xylene and *m*-xylene were of the same order of magnitude, except at high filling of Na-Y which led to adsorption heats slightly greater with *m*-xylene than *p*-xylene [116–118]. The results did not show any significant effect of the dipolar moment of *m*-xylene [119].

Trichloroethylene (TCE) adsorption in faujasite-type zeolites was also studied [120]. At fixed loading, initial heats of adsorption of TCE increased in the sequence of host basicity and cation content: siliceous faujasite ($\approx 40\,kJ\,mol^{-1}$) < Na-Y ($\approx 55\,kJ\,mol^{-1}$) < Na-X ($\approx 80\,kJ\,mol^{-1}$).

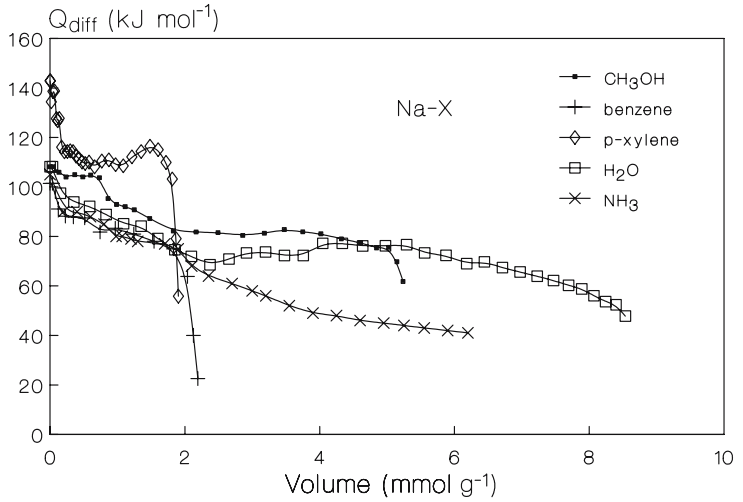

Fig. 9 Calorimetric differential molar heats of adsorption of various probe molecules versus coverage for Na-X zeolite: ammonia (× from [65], activation at 673 K, adsorption at 308 K), water (□, activation at 593 K, adsorption at 298 K), methanol (●, activation at 623 K, adsorption at 298 K), benzene (+, activation at 623 K, adsorption at 298 K), and *p*-xylene (◇, activation at 623 K, adsorption at 303 K)

The number and kind of cation sites affects also the adsorptivity of *propyne* [81], and this molecule interacts strongly with the cations at 303 K. In the case of a H-Y (Si/Al = 2.8), Tsutsumi et al. [121] observed an initial heat of adsorption of about 170 kJ mol^{-1}, whereas in the case of Na-Y (Si/Al = 2.8) it was only 77 kJ mol^{-1}, with the presence of a plateau in both cases. The heats increased with the number of proton sites when the Si/Al ratio increased from 2.8 to 385.

As a final example, Fig. 9 presents the differential heats of adsorption of *ammonia*, *p-xylene*, *benzene*, *methanol*, and H_2O at about 300 K on a Na-X zeolite sample pretreated at about 623 K in vacuo. This figure clearly indicates how the choice of a polar or non-polar probe molecule results in different interactions and thus different heats.

6.2
Temperature Dependence of Heats of Adsorption

Heats of adsorption of ammonia and pyridine on H-Y zeolites (Si/Al = 2.5) pretreated at 673 K were measured by Tsutsumi et al. [102] using a microcalorimeter in the temperature range of 313 to 673 K. The heats of adsorption appeared to depend on temperature in two different ways. One was that heats of adsorption on H-Y did change with coverage to a greater extent at high temperature (above 473 K) than low temperature, and more for

pyridine than for ammonia. The difference in the shape of the heat curves was attributed to the difference in the selectivity of adsorption at different temperatures, that is, adsorption at higher temperatures occurred preferentially on stronger acidic sites, while adsorption on weaker or non-acidic sites also took place in the low temperature range. The other kind of temperature dependence was a slight decrease in heats of adsorption with a temperature rise, which was observed in cases of ammonia adsorption on H-Y zeolites above 473 K and on Na-Y above 313 K, while the shapes of heat curves were similar irrespective of the adsorption temperature. Such a decrease may be attributed to the fact that the temperature dependence of the heat of adsorption is thermodynamically defined by the difference in molar heat capacity between adsorbed state and gaseous state [102]. It was also concluded that the strength of acid sites should preferably be determined by the heat curve obtained at 473 K rather than at 313 K because of more selective adsorption. Similar conclusions were derived by Stach et al. [107] for the chemisorption heats of NH_3 on H-Y zeolite (Si/Al = 2.4) measured at different temperatures. The authors suppose that at the low temperature of 303 K equilibrium was never reached but a stationary state was measured.

It can be concluded that adsorbed ammonia has sufficient mobility at 423 K to equilibrate with the catalyst surface on the time scale of microcalorimetric measurements, and these measurements provide an effective method for quantifying acid site distributions of solid acid catalysts. However, when using pyridine it is preferable to choose a higher temperature, e.g., around 573 K.

6.3 Thermal Stability of Faujasites

Once a methodology (probe molecule and temperature of adsorption) has been chosen, the calorimetric determination of the acidity of faujasites depends on the characteristics of the sample itself.

The acidic properties of zeolites are dependent on their pretreatment and particularly on their activation temperature, which are closely related to the mechanism of generation of acid sites.

A chemical technique used for the activation of a zeolite to turn it into an acidic solid consists of calcining the ammonium form. In the case of Y-type zeolites, acidic sites are created by the decomposition of ammonium Y-zeolites (NH_4-Y). Thus, Brönsted acid sites are formed by the decomposition of ammonium ions as formulated (Scheme 1).

The decomposition of NH_4-Y to obtain the proton form (H-Y) occurs around 550 K. Heating H-Y at 773 K leads to the loss of Brönsted acid sites because of dehydroxylation of the zeolites [122] (Scheme 2).

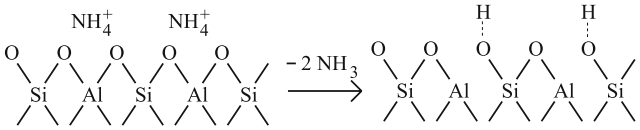

Scheme 1

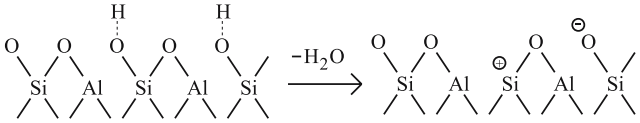

Scheme 2

The tricoordinated aluminum in the dehydroxylated zeolites is unstable and may be dislodged from the zeolitic framework, after which it remains in the zeolite cavity as cationic species (Lewis acid site) [123, 124]. Thus, keen attention must be paid to pretreatment conditions when discussing acidic properties of zeolites, since dealumination easily occurs under ordinary pretreatment conditions.

Calcination changes the acid site strength distribution, and high-temperature calcination is a method of reducing total acidity via dehydroxylation and dealumination while increasing the number of Lewis acid sites. Faujasites pretreated at temperatures between 673 and 1273 K present thermal stability increasing with decreasing Al content or with increasing Si/Al ratio, as shown by, e.g., Mishin et al. [125].

For zeolites with Si/Al less than 2.8, temperatures as low as 773–823 K are sufficient to cause the onset of structural degradation. By contrast, the structure of the siliceous varieties with Si/Al > 2.8 disintegrates only above 973 K. The thermal stability remains essentially unaltered for faujasites with N_{Al} less than 30 atoms per u.c. In such zeolites, the proportion of isolated (0 NNN) AlO_4 tetrahedra rapidly increases, and the strength of Al – O bonds increases accordingly.

On the basis of calorimetric measurements, Kapustin et al. [101] have shown that the thermal dealumination of Y zeolites leads to the appearance of sites with heats of adsorption of NH_3 which increased from about 110 to about 120 kJ mol^{-1}. A high-temperature dehydroxylation at 873 K of the parent zeolite H-Y (Si/Al = 2.4) increased the initial heat of NH_3 adsorption to 170–180 kJ mol^{-1} [101], while the number of centers associated with high heats of adsorption sharply decreased. The latter values are typical of the reaction of ammonia with the Lewis acid centers on which its dissociation takes place.

In another study, Shannon et al. [126] have shown that dehydroxylation of H-Y zeolite at 923 K resulted in the destruction of most of the acid sites of

medium strength (75–140 kJ mol^{-1}) and replacement by fewer but stronger (150–180 kJ mol^{-1}) ones.

6.4 Influence of the Crystallite Size

An important question concerns the relative contributions of the short range and long range factors influencing the Lewis acidity in zeolites. To examine the long-range effects in zeolite crystals, a series of Na-zeolites (Na-X, Na-Y, Na-A) with different degrees of crystal collapse was prepared using the high-energy ball milling method [127, 128]. The acidity and basicity of these samples was studied by microcalorimetry of ammonia and sulfur dioxide adsorption. A thermodynamic scale of the strength of Lewis acid and Lewis base sites was obtained. The collapse of the zeolite crystal caused a decrease in the number and strength of both Lewis acids and Lewis bases. It was, however, observed that the Lewis acid strength is strongly crystallinity-dependent, whereas the Lewis base strength is less so. The extra-framework Lewis acids (Na cations) are remarkably influenced by the long-range stabilization effect of the zeolite crystal, yielding then a higher Lewis acid strength.

Similarly, a thermodynamic scale of the strength of the acid sites of H-X, H-Y, and H-A zeolites after progressive milling was established [105]. In that case, the collapse of the zeolite crystal caused a decrease in the number and strength of the acid sites and it was found that the Brönsted acid strength is strongly crystallinity-dependent. The destruction of a long-range crystal order induced an increase of the population of weak Brönsted acid sites and a decrease of the population of strong Brönsted acid sites. Both calorimetric and infrared results suggested that the supercage structure was destroyed first during the decrystallization process of H,Na-Y. The evaluation of the thermokinetic parameter of heat release during ammonia adsorption is also a good tool to study the destruction of the crystal upon milling [27].

6.5 The Effect of Proton Exchange Level

The effect of proton exchange level, or sodium content, on H-Y zeolites has been the subject of numerous studies [55]. The acid form is mostly obtained by decomposing the ammonium form obtained from the Na form by cation exchange, so that the acidity varies with the exchange level. Generally, an increase in acidity with increasing proton exchange was measured; however, uncertainty exists as to the strength of the acid sites introduced at different exchange levels.

The differential heat curves for pyridine adsorption at 473 K on Na,H-Y zeolites with various Na contents (84%, 68%, and 39% levels of proton exchange, respectively) were studied by Chen et al. [55]. Increasing the pro-

tonation level from 39% to 68% of exchange resulted in a fairly uniform generation of acid sites with strength above 110 kJ mol^{-1}. Upon decreasing the sodium content from 68% to 84% of exchange, the last sites to be proton-exchanged were slightly more energetic than those previously formed, around 130 kJ mol^{-1}. However, one might question the suitability of the probe for this study since, as said above, some hydroxyl groups are inaccessible to pyridine adsorption because of their location in the H-Y lattice.

The interaction of ammonia with zeolite Y (Si/Al = 2.4) was also compared at 100% proton exchange and 85% proton exchange by van Santen [106]. One noted a significant increase (of 20 kJ mol^{-1}) in the initial heat of adsorption due to protonation of ammonia.

The effect of exchange degree on the heterogeneity of acid sites in decationed faujasites was also studied by Mishin et al. [129]. The strength of acid sites was evaluated from the differential heats of adsorption of ammonia measured at 303 K after the samples were first evacuated at 673 K. It was shown that acidity and catalytic activity appeared relatively slowly until the first half of the Na^+ cations was removed, but after reaching a decationization level of 50%, both the number of acid sites and activity increased much more rapidly. The parent Na-Y zeolite adsorbed NH_3 with heats lower than 85 kJ mol^{-1}, where with the main portion of ammonia adsorption was characterized by heats of 75–50 kJ mol^{-1}, indicating interaction of Na^+ cations with NH_3 molecules. Heats higher than 90 kJ mol^{-1} appeared upon decationization, and all the sites adsorbing NH_3 with $Q_{diff} > 90$ kJ mol^{-1} could be related to the acidic OH groups. Acid sites characterized by heats around 110–120 kJ mol^{-1} were observed in the samples with exchange degrees of 30 and 56%, but their contents were far below the amounts of sodium ions removed. Up to about 60% exchange, the number of acid sites present in the zeolites was four-times lower than that of sodium replaced. At higher extents of decationization, the density of acid sites increased rapidly and approached the theoretical value. Figure 10 shows that the number of medium and strong sites increased with decationization, and mostly above 60% of exchange, while the number of weaker sites decreased continuously. No satisfactory explanation has been advanced yet to clarify the discrepancy found at lower exchange levels between the number of cations removed and the number of acid sites generated. To rationalize the observed acidity-exchange level profile a model was developed that extended the neutralizing effect of a single Na^+ cation to several neighboring AlO_4 tetrahedra.

N-butylamine was also used by Brueva et al. [130] to determine the number and strength of the acid centers of Na,H-Y zeolites with various amounts of Na^+ ions. The differential adsorption heats, measured at 303 K after outgassing at 753 K, all presented a wide plateau of heats before a sharp decrease. The initial adsorption heat increased from 105 to 155 kJ mol^{-1} as the degree of decationization increased up to 80%. This increase was not proportional to the amount of removed Na^+ ions. A strong increase of the adsorption

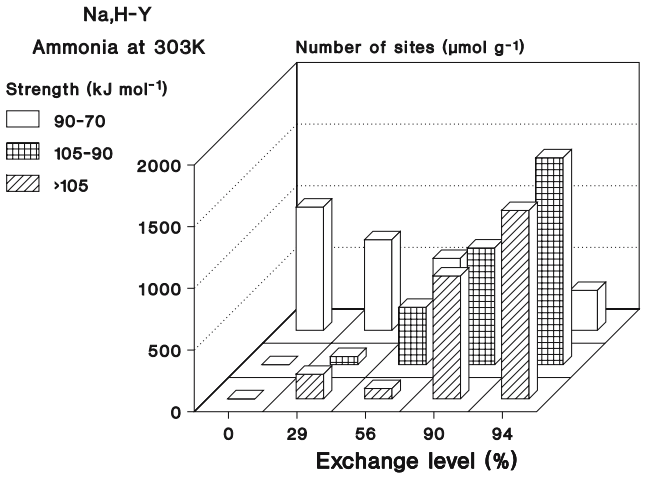

Fig. 10 Dependence of the acid strength distribution on the exchange level for Na,H-Y zeolites. Ammonia adsorption at 303 K, pretreatment at 673 K (from [129])

heat occurred from 20 to 45% of exchange, whereas the removal of the first 20% of Na^+ ions or an increase from 45 to 80% had little effect on the heat.

Specific distributions of acid sites according to their strength can be related to the activity-exchange level profiles observed for faujasites [46]. For Y zeolites, the increase in the catalytic activity in octane cracking and ethylbenzene disproportionation was found to be parallel to the increase both in the number and in the strength of acid sites [46]. On removal of sodium from Y zeolites a low activity was observed, until 60% of the Na^+ cations were removed. At higher exchange levels, both the number of the acid sites with $Q_{diff} > 90$ kJ mol^{-1} and the activity in the cracking of *n*-octane increased strongly. The increase in cracking activity for hydrogen faujasites with progressive sodium removal was related more to the increase in the number of strong acid sites than to the increasing activity per site [46].

In conclusion, progressive exchange of the sodium ions to produce the acidic form results in an increase in the number of adsorption sites and in their strength, although the observed increase is not always proportional to the decrease of the sodium content.

6.6 Substitution by Other Cations

The nature of the exchanged cation is one of the key points that determine acidity in zeolites.

In the low coverage region, the heats of ammonia adsorption by Li zeolites observed by Khvoshev et al. [65] were substantially higher than those for

adsorption by Na zeolites. The basic features of the variation of heats of adsorption as a function of coverage were preserved when the change was made from Na to Li zeolites. These results were explained using concepts such as the possible non-identity of the effective charges of Na^+ and Li^+ cations in zeolites, and also on the basis of an analysis of the different positions of the cations in their crystal lattice. The heat of NH_3 adsorption on Na-X zeolites was greater than that on Na-Y over the entire range of coverage [65].

The differential heats of adsorption of pyridine at 303 K were measured on zeolites Na-X and Ca-X, with an SiO_2/Al_2O_3 ratio = 2.5, and on Ca-Y and H-Y, with an SiO_2/Al_2O_3 ratio = 4.2 [131]. The initial heats for zeolites Na-X and Ca-X were very close, viz. about 121 kJ mol^{-1}. The adsorption heats displayed little change with an increase in the amount of adsorbed pyridine. Replacing the Na^+ ions by Ca^{2+} did not cause any important change in the relation between the adsorption heats and degree of filling. The capacity of zeolite Ca-X for pyridine adsorption was somewhat lower than that of zeolite Na-X. For zeolites of the Y type, the initial heats were equal to about 130 kJ mol^{-1}. In the case of zeolite Ca-Y the initial heat gradually decreased to 95 kJ mol^{-1} with increase in the degree of filling [131].

The acidic properties of calcium-exchanged Na-Y zeolite were also investigated by means of *n*-butylamine desorption using differential scanning calorimetry [132]. The enthalpies of these processes were shown to be proportional to the acid strength in each specific temperature range.

The heats of adsorption of ammonia at 303 K on Linde molecular sieve X (Na-X and Ca-X) were also measured by Stone et al. [133]. Ca-X displayed higher heats of ammonia adsorption than the corresponding sodium zeolite at all coverages, the latter being represented by a homogeneous site population with an adsorption energy of around 47 kJ mol^{-1}.

A La,Na-Y sample (73% La exchange) was studied by Karge et al. [99] after activation at 675 K and at an adsorption temperature of ammonia of 425 K. The differential heat curve showed a few strong Lewis sites (Q_{diff} > 150 kJ mol^{-1}) but no obvious plateau of differential heat appeared. The continuously decreasing part of the curve with Q_{diff} = 150 to 80 kJ mol^{-1} was ascribed to the interaction of NH_3 with Brönsted acid OH groups in the supercages, in analogy with the results obtained on H-Y, but these were in a considerably lower amount than found with H-Y.

The basic properties of a series of X faujasites exchanged with Li, Na, K, Rb, Cs were studied by adsorption microcalorimetry using carbon dioxide as acidic probe. The heat of CO_2 adsorption was observed to decrease from Li to Cs in the alkaline series of X zeolites and to increase when Na^+ ions were replaced by Ca^{2+} [134]. It decreased as coverage increased [135], except for very low coverages for which a maximum was observed [66]. Unfortunately, it is not possible to draw definite conclusions about basic strength since simultaneous interaction of CO_2 with cations (Na^+, Li^+, ...) and basic sites did occur.

Chemisorption of CO_2 on cation exchanged zeolites A and X, studied by calorimetry at different temperatures [136], gave rise to relatively high initial heats, in particular for high contents of Na^+, Li^+, or Ca^{2+}.

The acid-base properties of alkali-metal ion exchanged X and Y zeolites were also investigated by ammonia and sulfur dioxide adsorption microcalorimetry, in parallel with the study of a catalytic reaction, viz. 4-methylpentan-2-ol conversion [137]. The X zeolites were pretreated at 553 K and the Y zeolites at 673 K; the adsorption temperature was 353 K for NH_3 and 423 K for SO_2. Li and Na zeolites presented much higher heats of NH_3 adsorption and greater coverage at the same pressure than the other zeolites. The acidic strength of X zeolites differed by only a few kJ mol^{-1} from that of the corresponding Y zeolites. The amounts of SO_2 adsorbed were very similar for all the Y zeolites except for Li-Y, on which the amount adsorbed was smaller. X zeolites adsorbed higher amounts of SO_2 than Y zeolites at the same temperature and most of the X samples had centers possessing a strong basicity (Q_{diff} > 150 kJ mol^{-1}). The main product from 4-methylpentan-2-ol, for both X and Y catalysts, was 4-methylpent-2-ene; on Y zeolites, which exhibited a higher catalytic activity, a larger amount of other isomers was generally formed. The heats of adsorption and adsorption capacities of the samples for 4-methylpentan-2-ol were also investigated, leading to a plateau of heats around 140 kJ mol^{-1} for Y zeolites and 150 kJ mol^{-1} for X zeolites. In the case of Cs-exchanged X, excess cesium oxide was also added by impregnation with cesium acetate. Microcalorimetric measurements indicated that the extra-framework cesium oxide provided even stronger basic adsorption sites. The catalytic runs showed that a significant amount of 4-methylpent-2-ene

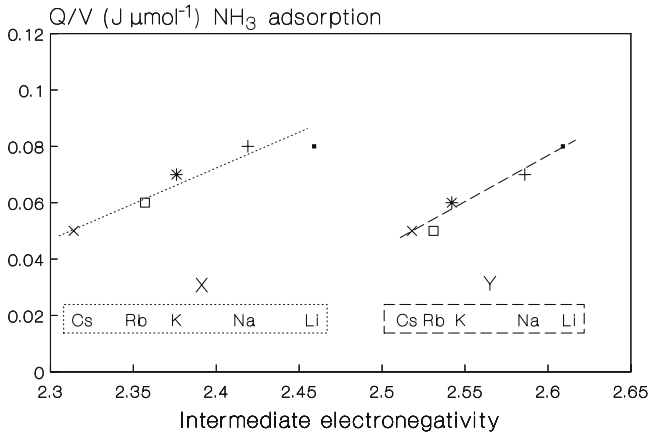

Fig. 11 Heats of ammonia adsorption evolved per acid site versus the intermediate electronegativity on alkali-exchanged X and Y zeolites (from [137]). Adsorption temperature: 353 K, pretreatment temperature: 673 K (Y zeolites) or 553 K (X zeolites)

was produced only on Cs-X containing excess Cs oxide. Linear correlations were found between the heat of NH_3 adsorption evolved per site and the intermediate electronegativity (Fig. 11), and between the irreversibly adsorbed volume of SO_2 and the partial oxygen charge [137].

To examine the interaction between basic sites and adjacent cations, a series of alkali-exchanged X zeolites was employed in calorimetric experiments [60, 127] using pyrrole to probe the basicity. Although pyrrole is too large to enter the sodalite cages, it has access to all the framework oxygens and can potentially interact with all the basic oxygens adjacent to the exchanged cations. A linear relationship was observed between the negative charge on oxygen and the differential heat value responsible for the maximum of the $-\mathrm{d}n/\mathrm{d}Q_{\mathrm{diff}}$ versus Q_{diff} curve. In general, the amount of chemisorbed pyrrole decreased with an increase in the cation size, except for the Li-X sample which exhibits a volume smaller than expected from its small cation size. To summarize, the Lewis basicity in alkali-exchanged zeolites is a local property, strongly influenced by the adjacent alkali cation, and basicity is more determined by the local environment than by the bulk composition.

In conclusion, these results emphasize the necessity of finding an acidic probe able to distinguish the alkali cations from the basic sites.

6.7 Influence of Occluded Clusters

Solid basic catalysts such as K-X zeolite and Cs-loaded K-X zeolite have been studied by CO_2 adsorption microcalorimetry [138]. Carbon dioxide adsorbed on K-X with a ΔH_{ads} of about $70\,\mathrm{kJ\,mol^{-1}}$ up to a loading of about $80\,\mu\mathrm{mol\,g^{-1}}$. The addition of cesium to K-X zeolite increased both the heat of adsorption (to more than $100\,\mathrm{kJ\,mol^{-1}}$) and the maximum CO_2 uptake. Nonetheless, the heats of carbon dioxide adsorption on Cs/K-X zeolites remained $50\,\mathrm{kJ\,mol^{-1}}$ lower than on, for example, MgO or Cs/Al_2O_3. The stronger basicity of Cs/K-X compared to K-X can be attributed to the occluded alkali metal oxide species, which may be either cesium or potassium oxide. The values of ΔH_{ads} on Cs/K-X samples were similar to those reported previously for Cs-loaded into Cs-X using analogous synthesis procedures [139].

In another study, cesium and potassium oxides were synthesized in the supercages of zeolite X by impregnation and decomposition of acetate precursors [140]. The basic sites of the alkali-loaded zeolites were characterized at 373 K by enthalpies of CO_2 adsorption of about $80-100\,\mathrm{kJ\,mol^{-1}}$. The strength and the number of basic sites increased upon the occlusion of CsO_x clusters. The CsO_x occluded in supercages of Cs-X was a slightly stronger base than CsO_x occluded in K-X or KO_x occluded in K-X.

Adsorption microcalorimetry using carbon dioxide as a probe gas has also revealed the formation of new sites of higher strength on Na-X by occlusion

of sodium metal clusters or sodium oxide clusters [141]. Increasing the loading of each of the occluded species resulted in an increase of the number of CO_2 adsorption sites, but did not significantly increase the highest strength of the sites formed on the catalyst. For similar loadings of sodium species, the strength of the CO_2 adsorption sites of zeolites that contained occluded sodium metal clusters was greater than for the zeolites containing occluded sodium oxide clusters prepared via controlled thermal decomposition of either impregnated sodium azide or sodium acetate salts.

6.8 Influence of Dealumination on H-Y Zeolites

The removal of aluminum from Y zeolite crystals leads to products with high framework Si/Al ratios. The dealumination may be performed using one of the following procedures: thermochemical treatment of NH_4,Na-Y (steaming and acid treatments), aluminum extraction from Na-Y with EDTA in aqueous solutions, isomorphous substitution with $(NH_4)_2SiF_6$, aluminum substitution by silicon through treating Na-Y with $SiCl_4$ vapor at high temperature. Some of the aluminum atoms are released from the framework and form non-framework aluminum-containing species. The Si/Al ratio of the framework must be determined not by chemical analysis but by nuclear magnetic resonance (NMR) or infrared spectroscopy. The non-framework aluminum species can be eliminated by treatment with dilute hydrochloric acid.

The dealumination process is associated with a change in the porosity within the crystals and may sometimes cause a drastic loss of crystallinity. The microporous adsorbents of the faujasite type are so arranged that the Si/Al ratio increases as the number of cations and the average electrostatic field within the framework decrease. To assess the effect of the Si/Al ratio on the activity and acidity of Y zeolites, it is desirable to compare samples with similar extents of exchange, since the degree of exchange has a significant influence on the catalytic and acidic properties of faujasites.

Steam dealumination of H-Y zeolite is known to cause a progressive destruction of weak and intermediate sites while producing new stronger sites. Microcalorimetric measurements of ammonia and pyridine adsorption have shown the presence in samples containing extra-framework aluminum of sites with adsorption heats that are much higher than those observed for samples containing only framework Al [142–145]. Moreover, steamed samples possess sites presenting a wide distribution of acid strength. The high initial heats of ammonia or pyridine adsorption that can be observed on steamed zeolites in comparison to unsteamed samples may be attributed to Lewis acid centers or to a combination of Lewis and Brönsted sites [145, 146].

The acidity of H-Y zeolites with different Si/Al ratios (2.4, 5.6 and 12.0) was characterized by calorimetric measurements of ammonia chemisorption at 423 K by Stach et al. [107]. Dealumination of Y zeolites was found to de-

crease the total number of acid sites and to generate very strong acid sites with $Q_{diff} > 120\,kJ\,mol^{-1}$. The relative proportion of these very strong acid sites went through a maximum.

In a study by Brueva et al. [147], the calorimetric values obtained by ammonia adsorption at 573 K over hydrogen forms of H-Y zeolites suggested that in parent H-Y the strong sites were mainly in the range 105–110 kJ mol^{-1}, whereas dealumination of faujasites resulted in the appearance of stronger acid sites with $q > 120\,kJ\,mol^{-1}$ [147]. Relationships between acidity and catalytic activity were also discussed.

Microcalorimetric studies by Auroux et al. [146] of dealuminated Y zeolites prepared by *steaming* and subsequent acid leaching in order to remove (partially or totally) the extra-framework species generated by steaming, have attributed the initial strong sites to Lewis acidity (alumina phases or non-framework aluminum). This result agrees with most IR studies which confirm that a fraction of the Lewis acid sites generated by dealumination are stronger than the Brönsted acid sites of pure Y zeolites. The samples, which had similar total (chemical analysis) and framework (NMR) Si/Al ratios, showed the occurrence of a plateau in their acid strength distribution, whereas the other samples showed a more heterogeneous distribution [146]. An important increase of the initial heat values and of the site strength heterogeneity was observed for samples presenting many extra-framework aluminum species. Samples subjected to a moderate dealumination and nearly total removal of extra-framework aluminum displayed a homogeneous acid strength, slightly but significantly higher than that of the parent H-Y material (150 kJ mol^{-1} instead of 140). The number of acid sites was of course reduced in accordance with the dealumination level. The residual structural acid sites remained essentially equivalent, even though alteration of their local environment inevitably resulted in a faint acid strength enhancement, well below that observed when guest aluminum species were present (in which case heats might attain 200 kJ mol^{-1}). Further dealumination generated samples characterized by heat curves presenting a narrower plateau. At high Si/Al ratios (> 50) the acidity was weakened; this suggests that extreme rarefaction of the structural sites greatly depressed their strength. Thus, it appears that an optimum site density is a prerequisite for strong acidity [146].

Increasing severity of steam treatment of H-Y was associated with decreases in total acidity by all reported studies. In particular, the correlation observed in the above-mentioned study by Auroux et al. [146] between an increasing steam dealumination and a decrease in the number of sites exhibiting intermediate strength is confirmed by the results of Chen et al. [25]. Moreover, the heat of ammonia adsorption at zero coverage, measured at 423 K, first increased with Si/Al ratio and then decreased upon further dealumination beyond Si/Al ratios of 10. The strength of intermediate sites, corresponding to Brönsted acid sites, also passed through a maximum at an Si/Al ratio equal to 10.

The reason for the decrease in Brönsted acid strength with severe steam treatment is not very clear. For faujasite type zeolites, Barthomeuf [148], using the topological density theory, obtained Si/Al(F) (Si/Al ratio of the framework) values of about 6 at which point framework Al would have 0 NNN. For this value, the Al atoms should be far enough from each other, so that the interactions would be negligible. Y zeolites with higher Si/Al(F) ratios would, therefore, be expected to have constant Brönsted acid strength, which is not the case in most of the calorimetric studies [25, 146, 149, 150]. This is, however, not surprising because the topological density theory addresses ideal distribution of aluminum all over the crystal. Yet it is known from various ESCA studies that crystals are frequently far more aluminum rich at the surface than expected. Incorporation of aluminum is favored at the latest stages of crystallization. Therefore, dealumination, except at very high levels, does not yield homogeneously dispersed aluminum throughout the crystals. Since the surface is much more Al-rich, the overall Si/Al is well above the actual one at the surface.

Macedo et al. [151], also studying H-Y zeolites dealuminated by *steaming*, found that the strength of intermediate sites decreased with increased dealumination for Si/Al ratios from 8 to greater than 100. For comparison, isomorphously substituted H-Y, which is free of extra-framework cationic species, possesses more acid sites than conventionally dealuminated solids with a similar framework Si/Al ratio [151]. This is because some of the extra-framework aluminum species act as charge-compensating cations and therefore decrease the number of potential acid sites.

The acidity of a series of Y zeolites dealuminated by *steaming* and of the corresponding acid-leached samples free from non-framework aluminum was studied by calorimetric measurements of NH_3 chemisorption at 423 K by Lohse et al. [108]. A stepwise decreased acid strength was found for H-Y and moderately dealuminated samples, the zeolites with relatively high framework aluminum content behaving in the neutralization process as a solid polyfunctional acid. With increasing Si/Al ratio non-acidic hydroxyl groups became acidic, whereas the acid strength spectrum was not changed significantly. The distribution of acid strengths became more diffuse at higher degrees of dealumination, which was explained by the variation of the local geometry of acid sites due to the disturbance of the structure [108]. Only a very small number of acid sites was generated by non-framework aluminum species.

The number of very strong acid sites was found to rise, pass through a pronounced maximum and then decrease with increasing aluminum content in the framework [62] (see Fig. 7b). These results are in good agreement with those of Macedo et al. [151] and the concept of aluminum topological density of zeolites [152].

Dealuminated faujasites with Si/Al ratios ranging from 2.3 to 67 were obtained by Shibuichi et al. [153], and the molar differential heats of adsorption of ammonia were measured at relatively high temperature (473–623 K) after

pretreatment at 723 K. The amount adsorbed at saturation decreased with increasing Si/Al ratio, reflecting the decrease in the number of aluminum atoms in the framework. The adsorption occurred on both acidic and non-acidic sites; the adsorption on the former was completed at low equilibrium pressure. The adsorption on "non-acidic sites" existed even at 623 K [153], however, the corresponding amount adsorbed decreased with an increase in the adsorption temperature. The adsorbed amount with heats of adsorption higher than 80 kJ mol^{-1} corresponded to the number of acidic sites calculated from the structural formula. With an increase in the Si/Al ratio, the initial heats of adsorption increased, suggesting the formation of the stronger acid sites, and concomitantly the acidic sites became inhomogeneous from the viewpoint of their adsorption energy. This may result from the formation of several kinds of acidic sites by dealumination [153].

Kuehne et al. [154] have compared the acidic strength distributions for H-Y and two dealuminated H-Y zeolites with similar framework Al contents, namely H-DY dealuminated by *ammonium hexafluorosilicate* and a (H, NH_4)-USY zeolite dealuminated by steaming. All samples possessed mostly Brönsted acid sites and only very few Lewis acid sites. The authors found the differential heats of NH_3 adsorption on these zeolites to be nearly constant: about 120 kJ mol^{-1} for H-Y and H-DY, and approximately 7 kJ mol^{-1} higher for the (H, NH_4)-USY. The same authors have also compared the acidic properties of steamed dealuminated USY zeolites presenting various framework Al contents per unit cell. H-USY, with both Brönsted and Lewis sites, had a heterogeneous acid strength distribution, whereas zeolites containing only Brönsted sites had a homogeneous acid strength [155].

The effects on acidity of *post-synthesis treatments* on H-Y-type zeolites have been studied using microcalorimetry experiments at 423 K with ammonia as the probe molecule [156, 157]. Post-synthesis treatment of Na-Y crystals with ammonium salts and reaction of NH_4-Y with ammonium fluorosilicate solutions followed by calcination can be used to generate silica-enriched faujasite frameworks. In the temperature range studied (1033–1088 K), the strength of the strongest acid sites in the reference H-Y (LZY-82) remained practically unaffected after a 5 h hydrothermal treatment with 100% steam at 1 atm. As the framework Si/Al molar ratio increased, the decreased acid site (Brönsted + Lewis) densities were attributed to losses of framework SiOHAl units, while the increased strength of the strongest sites was attributed mainly to the removal of most of the residual charge compensation Na ions.

Shi et al. [158] measured the strength of H-Y zeolites dealuminated *by treatment with* $SiCl_4$ for Si/Al ratios ranging from 4.2 to 37.1, and they also found a decrease in the number of sites possessing intermediate strength with increasing dealumination. As the Si/Al ratio increased, the initial heat of adsorption, presumably corresponding to a few Lewis sites present in the samples, first increased and then passed through a maximum at an Si/Al

ratio equal to 36. The heats of adsorption at the plateau of Brönsted acid sites passed through a maximum at a Si/Al ratio of about 7. The acidity of these dealuminated Y zeolites was also investigated using basic probes other than ammonia [85]. Pyrrole, dimethylether, and acetonitrile unveiled various strength distributions among the acid population of these samples. The same samples were subsequently subjected to an acid leaching, giving rise to a more heterogeneous distribution of the acid sites [158].

The acidic properties of (Na,H)-Y zeolites prepared by dealumination of Na-Y by $SiCl_4$ treatment and transformed into the acidic form have been determined by adsorption calorimetry using *n*-butylamine as a probe molecule [159]. The samples presented Si/Al ratios ranging between 2.5 and 20, and the heats of *n*-butylamine adsorption were determined at 405 K. The highest heat of adsorption was found with the non-dealuminated sample. Surprisingly, the heat of adsorption decreased slowly with increasing dealumination, and simultaneously the total amount of adsorbed *n*-butylamine went down. The calorimetric curves of samples with Si/Al ratios 3.4, 5.1, and 5.75 were close to each other, with the occurrence of a plateau around 170 kJ mol^{-1}. The acid strength of the Brönsted sites was mostly homogeneous, while that of the Lewis centers was heterogeneous. In the individual samples of those zeolites, the decrease in number of acid sites followed the decrease of aluminum content. Assuming that two Brönsted centers provide after dehydroxylation one Lewis center, the sum B+2L for the parent zeolite (Si/Al = 2.5) should be comparable with the theoretical number of OH groups. The difference between the two values was 6%. The same kind of comparison could not be made for the other samples because, as mentioned by the authors, there was no determination of how much extra-lattice aluminum, which may be a source of electron-acceptor sites, took part in the compensation of the lattice charge and in which form [159].

Tsutsumi et al. [103] studied H-Y zeolites with Si/Al ratios greater than 2.5, prepared by extracting Al atoms from NH_4-Y zeolite with *EDTA*. The differential heat of NH_3 adsorption at 298 K decreased with the increase in surface coverage, the acid sites on the surface becoming stronger (Q_{diff} up to 113 kJ mol^{-1}) when the Si/Al ratio increased.

Mitani et al. [149] studied H-Y zeolites dealuminated by *EDTA* for Si/Al ratios from 2.5 to 5.1 using adsorption microcalorimetry at 473 K. In this range, they found a moderate increase in the initial heat (up to 170 kJ mol^{-1} for pyridine adsorption and 130 kJ mol^{-1} for ammonia adsorption) and in the heat characterizing the plateau of intermediate strength sites, with increasing dealumination [149]. The heat of pyridine adsorption on Brönsted sites of intermediate strength ranged from 145 to 160 kJ mol^{-1}, in good agreement with the values found in the study of Chen et al. [25].

Dealumination generally brings about a decrease in the acid site concentration. However, the extent of the indicated decrease varies with the kind of

base probe, and a significant change was observed in the above-mentioned study by Mitani et al. [149] in the ratio of acid site concentrations when titrated with pyridine instead of ammonia. Moreover, the catalytic activity for cumene cracking increased with dealumination, which agreed with the acidity determined by the adsorption of pyridine rather than ammonia. All the data led to the notion that the activity for acid-catalyzed reactions should be discussed in relation to the surface acidity only in cases in which the basic molecule used has a size similar to that of the reactant and selectively interacts with active sites.

Mishin et al. [150] reported the heats of adsorption of ammonia and the catalytic activity in isooctane cracking for high silica Y zeolites dealuminated to different extents, obtained by treating Na-Y zeolites with $SiCl_4$ *vapors* and by extracting aluminum with *EDTA*. Ultrastable Y zeolites prepared by *steaming and acid leaching* of hydrogen zeolites were also investigated. All samples were first outgassed at 673 K, and the heats of adsorption of NH_3 were measured at 303 K and 573 K. Zeolites with increased Si/Al ratios showed stronger acid sites than the parent faujasites. The strong impact of the framework Si/Al ratio on the acidity of faujasites was supported by the calorimetric results obtained for adsorption of NH_3 at 573 K on dealuminated faujasite with Si/Al ratios varying from 2.4 to 43. The parent Y zeolite adsorbed NH_3 with an initial heat of ca. 112 kJ mol^{-1}, giving rise to a large plateau which stayed above 90 kJ mol^{-1} up to 1.8 mmol/g of NH_3 adsorbed. After dealumination, the total number of these acid sites decreased but stronger acid sites ($Q_{diff} \geq 140$ kJ mol^{-1}) were evidenced. A minor increase in the Si/Al framework ratio (from 2.4 to 3.9) resulted in an increase in the bond strength between NH_4^+ ions and the lattice. The number of these sites decreased but the strength (determined at 303 K) increased from approximately 110 to 120 kJ mol^{-1} [150]. An increase in the strength of acid sites could be seen up to a limiting value of $N_{Al} \approx 25$ to 30 Al atoms per u.c. Consequently, the dependence of the number of strong acid sites on the aluminum content was described by a curve with a maximum at Si/Al $\approx$ 5 to 7, corresponding to 50% dealumination. These results were in agreement with the catalytic activity. As the Si/Al ratio exceeded 3, the strongest acid sites associated with isolated AlO_4 tetrahedra appeared. Dealumination beyond 50% resulted in extraction of the isolated AlO_4 tetrahedra, which provided sites of constant acidity. The destruction of these strongest acid sites caused a decline in total acidity and catalytic activity, but not in the strength of the initial heats of adsorption which were still increasing or at least remained very high (above 140 kJ mol^{-1}).

For the dealuminated zeolites produced by exposing Na-Y to an $SiCl_4$ *stream*, an enhanced concentration of extra-framework aluminum species (EFAL) inside the zeolite crystal was discovered, and heats > 130 kJ mol^{-1} were observed in the $SiCl_4$-treated samples. This was not the case on faujasites dealuminated with EDTA, which showed a lower concentration of strong

acid sites. Explanations for this low concentration of strong acid sites in the EDTA-treated Y zeolites assume that the dislodgement of Al is not always concerted with silicon replacement, or that the very strong acid sites associated with frameworks containing 25–30 Al/u.c. would be confined to a thin layer of the interior of the zeolite, giving rise to a non-uniform distribution of Al atoms [150].

Biaglow et al. [49] have performed microcalorimetry measurements for pyridine and isopropylamine adsorption on a series of *steamed* and chemically dealuminated faujasites. They reported a considerable heterogeneity in the strength of the sites in studying a H-Y sample (bulk Al/u.c. = 43) based on pyridine adsorption, while the sites appeared to be relatively uniform on another H-Y sample (bulk Al/u.c. = 12). Though an NMR study indicated the presence of significant amounts of extra-framework Al, the authors assumed that the observed heterogeneity was the result of strong repulsive interactions between adsorbate molecules at neighboring sites, rather than a true indication of differences between the sites. They explained this situation by the fact that the initial heats on sample (Al = 43/u.c.) were similar to those found on the other sample (Al = 12/u.c.). The difference between the two samples was, firstly, that the differential heats on sample (Al = 43/u.c.) fell with coverage. Secondly, the apparent site heterogeneity in sample (Al = 43/u.c.) was much lower for isopropylamine than for pyridine. Thus, they concluded that, if one were observing only changes in site strengths, one should expect a similar decrease for both adsorbates [49].

A series of dealuminated commercial H-Y zeolites (Si/Al varying from 2.6 to 24) containing variable amounts of extra-framework aluminum species was studied using adsorption microcalorimetry of various probe molecules such as ammonia, pyridine, and 2,6-dimethylpyridine at 393 K [68]. The combination of microcalorimetry with several other techniques has shown the existence of three different regions of acid strength. The weak sites associated with heats of NH_3 adsorption between 70 and 130 kJ mol^{-1} were of Lewis and Brönsted types, the former being predominant in the dealuminated zeolites. The sites of intermediate strength were essentially the bridging hydroxyl groups of the framework (heats between 130 and 150 kJ mol^{-1}). The strong sites (heats above 160 kJ mol^{-1}) contained a significant number of extra-framework Lewis type sites, but also Brönsted sites. The strength of these sites seemed to be due to mutual interactions between Lewis and Brönsted sites. The use of 2,6-dimethylpyridine furthermore showed that this probe only titrates Brönsted sites and the Lewis sites associated with pentacoordinated aluminum, while it cannot reach the Lewis sites associated with octahedral or tetrahedral aluminum. However, this is an hypothesis which needs to be confirmed by further studies.

The acidity of commercial dealuminated H-Y zeolites (USY) has been studied by ammonia adsorption calorimetry and single ammonia TPD runs by Handy et al. [160]. All TPD profiles were represented by models consisting

of two or three distinct types of sites, while the differential heat plots implied a continuous distribution of sites in the 160–80 kJ mol^{-1} range for all catalysts. A dealumination of increased severity resulted in a decrease in total site density for sites of strength less than 100 kJ mol^{-1}. A general correlation could be established between the amount adsorbed with heats of adsorption greater than 100 kJ mol^{-1} and the framework Al^{3+} site density, although the ratio of the amount of ammonia adsorbed per framework Al^{3+} site was less than one.

The acid properties of non-dealuminated and dealuminated commercial H-Y were also determined by Colon et al. [161] and Ferino et al. [28], using pyridine adsorption microcalorimetry at 423 K.

Adsorption of water depends also significantly on the Si/Al ratio in highly siliceous faujasites as shown by Tsutsumi et al. [64]. As the ratio increased, the adsorbed amount decreased, which can be explained by the decrease in the electrostatic field on the surface. On the other hand, the adsorption of chloroform decreased slightly with an increase in the ratio, suggesting that the field-dipole interaction became less significant. When the Si/Al ratio exceeded about 10, the zeolite could be regarded as hydrophobic.

6.9 Acidity in Fluid Cracking Catalysts (FCCs)

Dealuminated Y zeolites exhibit greatly increased hydrothermal stability, and are accordingly called ultrastable Y zeolites (USY). The incorporation of rare earth (Re) elements also enhances the stability of a Y zeolite. Today, USY or partially exchanged Re-USY zeolites are the key active components of fluid cracking catalysts (FCCs). The main other components in FCCs are usually a binding matrix, and an acidic component consisting of a small amount of H-ZSM5 zeolite in order to enhance the octane number of gasoline.

The determination of acidity in fluid cracking catalysts (FCCs) from adsorption microcalorimetry of probe molecules was the object of a review article by Shen and Auroux [162]. The catalytic activity of such materials is due to the presence of acidic sites and is determined by the zeolite content and by the types of zeolite and matrix in the FCC catalyst. The catalytic selectivity is among other factors determined by the zeolite type, the nature (Brönsted or Lewis), strength, concentration and distribution of the acid sites, the pore size distribution, the matrix surface area and the presence of additives or contaminants. Stability is affected by both the composition and the structural characteristics of the catalyst components. Therefore, the acidity of FCC catalysts is designed to meet specific requirements, and a full characterization of the acidity is necessary; this gives a great deal of importance to the information gathered by direct methods such as the monitoring by microcalorimetry or by temperature-programmed desorption (TPD) of the adsorption or desorption of gaseous bases, particularly ammonia or pyridine.

The distribution of acid site strengths for two Y-based FCC catalysts (USY) was determined by Yaluris et al. [163] from microcalorimetric measurements of differential heats of ammonia adsorption at 423 K. One catalyst (Si/Al = 8.3) was calcined at 840 K for 2 h, and the other (Si/Al = 27.9) was calcined and then steamed for 2 h at 1060 K. The results showed that, when the catalyst was steamed, the acid site strength distribution shifted toward weaker sites. The relative number of sites that adsorbed NH_3 with a differential heat of about 130 kJ mol^{-1} was reduced by about 60%, while the relative number of stronger sites was also reduced. The sites, the number of which increased after steaming, were weaker ones that adsorbed NH_3 with a differential heat of about 110 kJ mol^{-1} and lower. Steaming resulted in the preferential loss of Brönsted acid sites corresponding to NH_3 adsorption with a differential heat of about 130 kJ mol^{-1}. This conclusion agrees well with earlier work [25] indicating that the sites of intermediate strength in Y zeolites are predominantly Brönsted acids, and shows that their number and strength are reduced by steaming [163]. Adsorption microcalorimetry results obtained using ammonia as a probe molecule reveal that, as long as Lewis acid sites with strength greater than 100 kJ mol^{-1} are present and as long as these sites are available to gas oil, FCCs can retain their useful cracking activity and selectivity properties [164]. The effect of aging and regeneration on the acidity of Y-based FCC catalysts has also been studied by Occelli et al. [165, 166] using ammonia and pyridine as probe molecules.

7
ZSM-5 Zeolites

Microcalorimetry has been extensively used to characterize the acid centers in ZSM-5 zeolites, and for comparison in its completely dealuminated form, silicalite-1. No electron donor (basic) sites have been evidenced [167]. Ammonia adsorption experiments have shown that there exists a strong acidity in H-ZSM-5 zeolite which exceeds that present in H-Y zeolite [104].

Figure 12 represents the differential heats of NH_3 adsorption versus coverage for ZSM-5 samples studied by various authors [50, 168–170]. All these samples presented similar Si/Al ratios (between 33.4 and 34.5) and were studied at similar adsorption temperatures (between 423 and 480 K). Two studies evidenced the presence of a small amount of very strong sites (above 150 kJ mol^{-1}), then all samples displayed a plateau of heats around 150 kJ mol^{-1}, followed by a sharp decrease (sharper when measured at 473–480 K than at 423 K). The heats were altogether very similar to each other, but the adsorbed volumes differed slightly.

H-ZSM-11 samples were found to be also very strongly acidic, but slightly less than the corresponding H-ZSM-5 samples [167, 171].

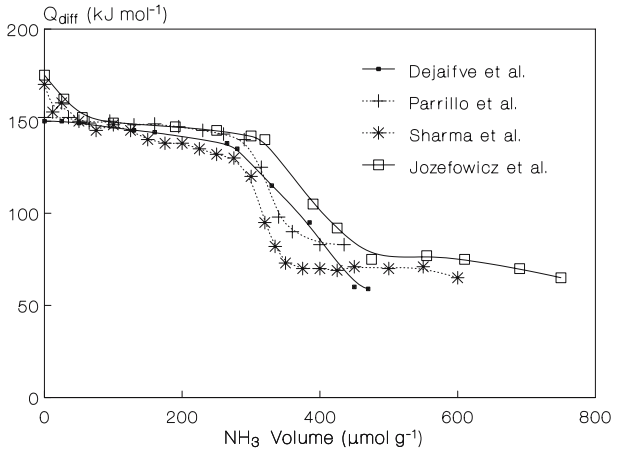

Fig. 12 Differential molar heats of ammonia adsorption versus the adsorbed volume for ZSM-5 zeolites: • from [170], Si/Al = 34.5, activation at 673 K, adsorption at 423 K; + from [50], Si/Al = 34, activation at 770 K, adsorption at 480 K; ∗ from [168], Si/Al = 34, activation at 723 K, adsorption at 473 K; □ from [169], Si/Al = 33.4, activation at 673 K, adsorption at 423 K

7.1 Influence of the Probe Molecule

The combination of thermogravimetry, microcalorimetry (at 473 K), and infrared spectroscopy studies of *pyridine* adsorption has been used by Gonzalez et al. [172] to characterize the acidity of a ZSM-5 catalyst (Si/Al = 33). The infrared spectra collected at low pyridine coverages suggested that the majority of the strong acid sites ($Q_{diff} > 140$ kJ mol^{-1}) were Lewis acid centers (associated with non-framework Al), while the plateau corresponding to heats of pyridine adsorption equal to 140 kJ mol^{-1} was attributed to Brönsted acid centers associated with framework Al species. Non-framework Al species produced both strong Lewis acid sites as well as weak adsorption sites (e.g., weak Brönsted acid sites or hydrogen bonding sites) [172]. However, equilibration of the adsorbate between sites is questionable in this study because of the low value of the differential heats (140 kJ mol^{-1} for the plateau) which was not in agreement with an earlier study by the same authors [55]. This demonstrates that equilibrium is not easily achieved using pyridine, as the plateau of Brönsted sites was observed at 140 kJ mol^{-1} [172], 160 kJ mol^{-1} [55], and even 200 kJ mol^{-1} [50].

Another ZSM-5 sample (Si/Al = 34) was studied by Sharma et al. [168] both by microcalorimetric measurements at 473 K and temperature-programmed desorption experiments. This zeolite possessed a relatively homogeneous distribution of acid strengths with occurrence of a plateau of adsorption heats of *ammonia* around 150 kJ mol^{-1}. For *pyridine* adsorption on the

same sample, Chen et al. [55] found a large number of sites of nearly constant strength around 160 kJ mol^{-1} attributed to Brönsted acid centers. Some strong sites were also present, evidenced by the initially high differential heats, which may be associated with non-framework aluminum species. At high coverages, weaker adsorption sites exhibiting heats of adsorption near 100 kJ mol^{-1} were neutralized, resulting from hydrogen bonding [55]. This weaker interaction was of the same strength as for pyridine adsorption on silica.

Using also H-ZSM-5, Parrillo et al. [80] have demonstrated that the differential heats of adsorption for *ammonia* and *pyridine* are constant up to a coverage of one molecule per Al site, and that the differential heats for coverages below one/Al are 145 ± 5 kJ mol^{-1} for ammonia and 200 ± 5 kJ mol^{-1} for pyridine.

Microcalorimetry was used by Chen et al. [41] to determine the differential enthalpy changes of adsorption at 473 K versus coverage on H-ZSM-5 (Si/Al = 35) of *dimethylether*, *ammonia*, *monomethylamine*, and *dimethylamine*. The heats of adsorption on Brönsted acid sites varied linearly from 90 to 250 kJ mol^{-1} with the gas-phase proton affinities of these basic molecules. The strong sites had an average enthalpy change of ammonia adsorption of 151 ± 11 kJ mol^{-1}, and the weak sites of 69 ± 3 kJ mol^{-1}. On H-ZSM-5, the majority of the strong sites caused an enthalpy change upon monomethylamine adsorption between 230 and 180 kJ mol^{-1} with an average value around 204 kJ mol^{-1}, upon dimethylamine adsorption equal to 245 kJ mol^{-1}, upon *trimethylamine* adsorption around 155 kJ mol^{-1}. The differential enthalpy changes upon dimethylether adsorption on H-ZSM-5 showed an initial region of strong adsorption followed by adsorption on sites effecting an enthalpy change equal to 91 kJ mol^{-1}. *Higher enthalpy changes were observed for molecules with higher proton affinities, trimethylamine being the notable exception*. Ammonia and methylamines adsorbed on Brönsted acid sites to form positively charged ammonium species. It was shown by Parrillo et al. [173] that the acidity of H-ZSM-5 was due to identical sites exhibiting a coverage of one probe molecule per framework Al atom and that the differential heats for a series of bases (NH_3, *methylamine*, *ethylamine*, *isopropylamine*, *n-butylamine*, *dimethylamine*, *trimethylamine*, *pyridine*) adsorbed at the Al sites correlated very well with gas-phase proton affinities [82].

Lee et al. [174] have used microcalorimetry to measure the differential heats of adsorption of both a series of *alkylamines* and a series of *substituted pyridines* in H-ZSM-5. With few exceptions, the differential heats were approximately constant up to coverages close to the expected Brönsted site concentration. The authors observed a strong correlation between gas-phase proton affinities and differential heats of adsorption of amine and pyridine bases but no useful correlation with aqueous base strengths, this contrast implying that the Hammett H_0 value is probably not a meaningful description of zeolite acid strength.

Measurements of the differential enthalpy change of *methanol* adsorption versus coverage on H-ZSM-5 at 373 K showed strong sites that adsorbed methanol with an enthalpy change of ca. 80 kJ mol^{-1}, while the weak sites had an enthalpy change near 66 kJ mol^{-1}. With *water* on H-ZSM-5 at 373 K, the differential heats were nearly constant with respect to coverage, with an average heat of adsorption close to 60 kJ mol^{-1}, with the exception of several points at low coverage from ca. 110 to ca. 65 kJ mol^{-1} [41]. Differential heats of adsorption of water were also measured by Lee et al. [75] on a H-ZSM-5 sample ([Al] bulk = 630 μmol/g). The heats started at ca. 100 kJ mol^{-1} and remained at ca. 80 kJ mol^{-1} at a coverage of 400 μmol/g. The heats remained relatively high even at coverages above the Brönsted site density. This was probably due to clustering of water molecules around the Brönsted sites [75].

Microcalorimetry measurements have also been used to characterize the strength of the hydrogen bond of *acetonitrile* in H-ZSM-5 [71–73, 75]. The differential heats of adsorption on H-ZSM-5 were approximately constant at 105 kJ mol^{-1} up to a coverage of one molecule per framework Al, after which the heats dropped. For comparison, on silicalite the differential heats were also constant at ca. 60 kJ mol^{-1}, suggesting that the strength of the hydrogen bond in H-ZSM-5 is at least 45 kJ mol^{-1}.

The adsorption enthalpies of Ar, N_2, CO, H_2O, CH_3CN, and NH_3 on H-MFI zeolites have been measured calorimetrically at 303 K in order to assess the energetic features of Lewis and Brönsted acidic sites [175]. Both the uptakes and enthalpy changes correlated well with the proton affinities and polarizabilities of the probes. Whereas CO and N_2 were found to single out contributions from Lewis and Brönsted acidic sites, Ar was only sensitive to confinement effects. H_2O, CH_3CN, and NH_3 were not preferentially adsorbed on Lewis sites, suggesting that the adsorption on Brönsted sites is competitive with Lewis sites [176, 177]. With the exception of H_2O, the heats of adsorption at zero coverage of the different probes on the various systems studied were found to correlate well with the proton affinities (PA) of the molecular probes [176, 177].

The differential heats of adsorption of *acetone* adsorbed on H-ZSM-5 (at 360 K) and silicalite (at 350 K) over a wide range of surface coverage were reported by Sepa et al. [76]. The results were compared with ab-initio calculations of the reaction of acetone with model zeolite structures to form a stoichiometric hydrogen-bonded cluster-molecule complex [76]. The differential heats of acetone adsorption on H-ZSM-5 were approximatively constant around 130 kJ mol^{-1} up to a coverage of one molecule per Al, after which the heats dropped to ca. 105 kJ mol^{-1} [71], while on silicalite the heats of adsorption were constant over the entire range examined and equal to ca. 67 kJ mol^{-1}.

Differential heats of adsorption have also been measured for a series of *alcohols*, a series of *nitriles* and *diethylether* in H-ZSM-5 and for comparison in silicalite [75]. Most of the measurements were carried out at 400 K, with

the exception of trifluoroethanol and trichloroacetonitrile which were measured at 350 K. For the nitriles and diethylether, the differential heats were approximately constant up to a coverage of one molecule per site, after which the heats fell to the level observed on silicalite. However, for the alcohols, the heats did not fall at a coverage of one molecule per site, the alcohols being both hydrogen bond acceptors and donors and giving rise to the formation of adsorbate clusters. The implications of these results for understanding zeolite acidity were discussed [75].

Differential molar heats of sorption have been determined calorimetrically by Thamm et al. [178] for *benzene* and *cyclopentane* on H-ZSM-5 type zeolites with different aluminum contents. The results showed that the structural OH groups represent energetically preferred sorption sites for benzene and presumably also for cyclopentane. The occurrence of inflection points in the sorption isotherms as well as of pronounced maxima in the heat of sorption curves of benzene and cyclopentane on the Al-poor H-ZSM-5 samples indicated that the influence of sorbate-sorbate interactions on the state of the sorbed molecules rose with decreasing Al content. Heats of adsorption of *benzene* and *ethylbenzene* were also measured by Nießen et al. [179] on a H-ZSM-5 sample (Si/Al = 33.6) and were 64.5 and 86.5 ± 5 kJ mol^{-1}, respectively.

Adsorption heats of gaseous *p-xylene* molecules have been calorimetrically measured as a function of adsorbed amounts at 298, 333, and 352 K on various ZSM-5 zeolites [180]. They were determined to be around 85 kJ mol^{-1} at the plateau at 352 K for samples with Si/Al ratios of 26 and 40.

Differential microcalorimetry has also been used to study the adsorption of *tetrachloroethene* at 298 K on three ZSM-5 zeolites with Si/Al ratios of 26.5, 339, and 500. The diameter of this non-polar molecule is very close to the pore opening of the adsorbents. The differential molar enthalpies continuously increased with increasing coverage up to the value of 4 molecules per unit cell, and then showed from this value on a stepwise increase of about 10 kJ mol^{-1}. Subsequently, the heat curves were almost horizontal, before abruptly decreasing to the value of the heat of vaporization of tetrachloroethene when approaching micropore saturation [181].

7.2 Effect of Adsorption Temperature

The effect of temperature on ammonia adsorption by ZSM-5 samples has been investigated by microcalorimetry, varying the adsorption temperature from 423 K up to 673 K [51, 167]. The initial heats of adsorption were independent of temperature, at least up to 573 K. When the adsorption temperature increased, there was a competition between the formation of ammonium ions on Brönsted sites and their decomposition. The total number of titrated sites decreased with increasing adsorption temperature. Room temperature

adsorption did not allow us to differentiate strong and weak acid sites, and above 573 K the decomposition of ammonium ions became predominant. It appeared that an adsorption temperature between 423 K and 573 K is appropriate for these calorimetric experiments.

7.3 Difference in Preparation Procedures

Acidic and basic properties of solid materials are greatly influenced by the preparation method and pretreatment conditions. The Al distribution within the zeolite microcrystals has been shown to depend on the synthesis procedure and to be more or less regular, which results in differences in the strength and the distribution of the acid sites [167]. The acidification procedure or chemical treatment may also be important in the distribution of acid sites within the channels. Particularly, the materials might behave differently if protons stemming from the decomposition of tetrapropyl ammonium ions are exchanged by Na^+ or neutralized by NH_3 gas prior to acidification via exchange by ammonium salt or by HCl. The difference in calorimetric curves when comparing the two acidification procedures, with or without neutralizing H^+ from TPA decomposition, has been evidenced by Vedrine et al. [167], while noticeable differences in catalytic properties were also observed.

The effect of the synthesis medium, OH^- or F^-, on the nature and amount of acid sites present in Al,Si-MFI zeolites, has also been examined by microcalorimetry of NH_3 adsorption and infrared spectroscopy [182]. Both techniques revealed that H-MFI (F^-) with Si/Al < 30 contained extra-framework aluminum species. Such species were responsible for the presence of Lewis acid sites and poisoning of the Brönsted acidity. In contrast, MFI (F^-) characterized by Si/Al > 30 behaved very much as H-MFI (OH^-) [182].

Calorimetric measurements of acidity of H-ZSM-5 zeolites synthesized by hydrothermal processes with and without the aid of a template, with various Si/Al ratios (17, 41, 54, 73, 111), have shown a higher acidity of the non-templated samples in number and strength, especially for low Si/Al ratios, while the two series of samples exhibited close behaviors when Si/Al $\geq$ 37. This can be explained by the possible presence of more Lewis acid sites in the non-templated zeolites [183, 184].

Nicolaides et al. [185] have synthesized ZSM-5-based materials that are substantially amorphous or partially crystalline, obtained by varying the hydrothermal synthesis temperature from 298 K to 463 K. Ammonia adsorption microcalorimetry studies have shown that for these ZSM-5-based materials, whose crystallinities as determined by XRD varied from 3 to 70%, the number of strong Brönsted acid sites, i.e. those with a ΔH_{ads} between 120 and 140 kJ mol^{-1}, increases with increasing XRD crystallinity. A strong correlation was observed between the catalytic activity of these zeolite-based materials in the *n*-hexane cracking reaction and the number of strong acid sites. How-

ever, for samples with XRD crystallinities below 30%, the number of strong acid sites is disproportionately low, and the catalytic activity only becomes significant at crystallinities above this level [185].

7.4 Effect of Pretreatment

High-temperature calcination is a well-known method of reducing total acidity via dehydroxylation and dealumination. In principle, calorimetry should make it possible to determine the number of "strong" Brönsted sites, assuming that activation at 673 K before NH_3 adsorption gives rise to a maximum in H^+, i.e. that no dehydroxylation occurs at that temperature. This is a crude approximation but can be considered as valid for comparison of different samples. After calcination at increasing temperatures, dehydroxylation of the zeolite is observed: above 675 K, the number of Brönsted acid sites decreases, while that of strong Lewis acid sites increases. However, a limited dealumination occurs and the constraining character of the intracrystalline voids increases. Microcalorimetric studies of ammonia adsorption confirm the very strong acidic character of the acid sites and shows their dependence in strength and heterogeneity upon calcination temperature [51, 167, 186].

It has been established that calcination at 1073 K before NH_3 adsorption leads to the presence of fewer acid sites but that the remaining ones are stronger [167]. Moreover, when the samples were further rehydrated at room temperature and outgassed again at 673 K, the original curve obtained after pretreatment at 673 K was not restored. It was concluded that such a heat treatment had irreversibly modified the material [167]. These results were confirmed by Jozefowicz et al. [169] who have shown that, upon dehydroxylation at 1073 K, all the ZSM-5 samples studied had lost a considerable proportion of Brönsted sites, and there were no Brönsted sites of homogeneous energy distribution (plateau at 150 kJ mol^{-1}) left. Only the acidic sites of broad energy distribution remained unaffected by high temperature treatment, i.e. the sites with heats of adsorption between about 135 and 80 kJ mol^{-1} [169].

7.5 Effect of Proton Exchange Level

In a study by Muscas et al., Na,H-ZSM-5 zeolites with varying extent of Na exchange were subjected to adsorption of various probe molecules in order to determine the selectivity of adsorption on their acid centers of variable nature, such as Na^+ in Na forms and acidic OHs in the corresponding H forms [187]. Using ammonia as a basic probe at 423 K, the number of acid sites increased quasi linearly with the exchange level, while the acid strength remained almost constant over a wide range of exchange levels. The acidic

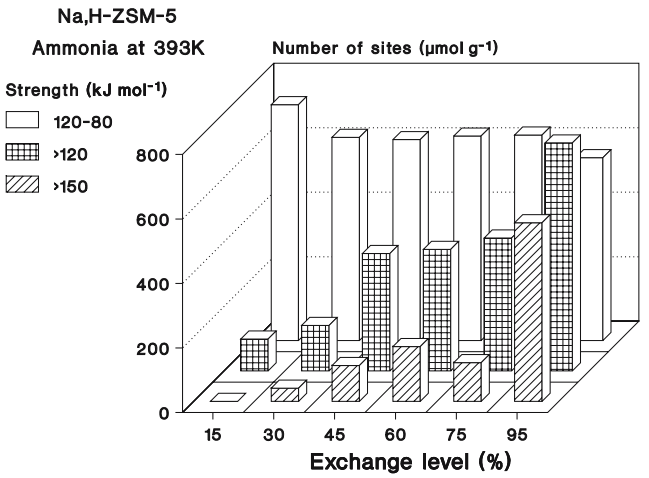

Fig. 13 Acid site strength distribution of Na,H-ZSM-5 zeolites as a function of the exchange level. Ammonia adsorption at 393 K, pretreatment at 673 K (from [187])

strength, however, dramatically increased when 80% of the original Na^+ ions were removed. The removal of the residual Na^+ ions not only generated much stronger sites but resulted also in a general increase of the acid site population (Fig. 13). Figure 13 clearly shows that at low exchange levels most of the acid sites were rather weak sites. While this population of weak sites remained almost constant as the exchange level increased, the population of stronger sites increased progressively up to the point where, for extensively exchanged samples, the strongest sites became predominant. The population of sites, the heat of adsorption of which was above 150 kJ mol^{-1}, illustrated the effect of removal of the very last sodium ions on the acid strength, not only on that of newly created sites but also on that of preexisting ones.

By contrast, butane adsorption resulted in an opposite behavior. Not only did the adsorbed volume decrease as the exchange level increased, but also the initial heat of adsorption declined steadily (from 90 kJ mol^{-1} to 65 kJ mol^{-1}) as the sodium content decreased. All the samples showed a plateau of differential heat of butane adsorption around 60–65 kJ mol^{-1}. This contrasting behavior towards strong and weak bases can be interpreted on the basis of hard-hard and soft-soft acid-base interaction [188].

7.6 Influence of the Si/Al Ratio and Dealumination

The acidity of H-ZSM-5 zeolites synthesized with different Al contents has been characterized by the microcalorimetric measurement of the differential heats of adsorption of ammonia [51]. The strength of the strongest acid sites

increased with the Al content to a maximum for Si/Al = 17.5 and then decreased notably. The total acidity increased regularly with Al content. Therefore, the importance of a proper selection of appropriate Si/Al ratios for specific catalytic applications is obvious.

The spatial distribution of acidity in acid-treated ZSM-5 zeolite is not uniform [104], the most acidic sites, and particularly Lewis sites, being located within the channel structure of the material where they are not always readily accessible to ammonia molecules at 416 K.

Three samples of H-ZSM-5 prepared with varying aluminum content and by different synthesis methods were examined by Parrillo et al. [50] using microcalorimetry of ammonia and pyridine adsorption. Two samples with bulk Si/Al ratios equal to 34 and 58 were prepared employing a TPA-Br template in hydrothermal solution, the third sample (Si/Al $\sim$ 26) was synthesized without a template. The results showed that the heats of adsorption for both ammonia and pyridine were constant with values of 145 kJ mol^{-1} for ammonia and 200 ± 5 kJ mol^{-1} for pyridine up to a coverage of one molecule per framework Al, and were, in fact, independent of the Si/Al ratio. From these results, the authors suggested that the Brönsted acid sites in unsteamed H-ZSM-5 are independent of the sample and equal in concentration to the framework aluminum content.

Microcalorimetric measurements of the differential heats of adsorption of NH_3 at 423 K were performed by Witzel et al. [77] on H-ZSM-5 samples with various Si/Al ratios (22.5, 33.6, and 33.3) activated in high vacuum at high temperature (1075 K). The heat values reported were respectively 175, 168, and 160 kJ mol^{-1}.

A highly crystalline H-ZSM-5 zeolite (Si/Al = 33.4 from chemical analysis and NMR) containing very few Lewis sites was compared with three other H-ZSM-5 zeolites containing increasing amounts of intrinsic strong Lewis sites [169] (Si/Al global/NMR = 33.7/44.9, 20.9/43.8, 13.9/17.7). True Lewis sites were also induced in all of those zeolites by a high-temperature dehydroxylation in vacuum effected at 1073 K instead of a standard activation at 673 K. The strong Lewis sites were found to be associated with differential heats of ammonia adsorption between 185 and 160 kJ mol^{-1}, and the Brönsted site acid strength was characterized by heats of the order of 157–140 kJ mol^{-1}. Most of these Brönsted sites were of homogeneous acidic strength, but where the curve dropped, there were some sites which had a wide energy distribution, i.e. from 140 to 80 kJ mol^{-1}. In the 80 kJ mol^{-1} region, the heats that were evolved from H-ZSM-5 zeolites tended to be representative of physisorption and indicated the interaction of silanol groups and cations with ammonia. Thus, the presence of strong Lewis centers is the reason for the striking difference between the last three samples on the one hand (decrease of the differential adsorption heats even at low doses, heterogeneity of acidic site strength) and the first sample on the other hand (initial plateau of differential heats, homogeneity of strength distribution).

The effect of the Si/Al ratio (ranging from 24 to 154) of H-ZSM-5 zeolites on acidity was also studied by Gayubo et al. [189]. The distribution of the surface acidic strength was studied by measuring the differential adsorption heats of ammonia and *tert*-butylamine, using a combination of differential scanning calorimetry and gas chromatography in order to measure the heat of neutralization of the acidic sites and the amount of base chemically adsorbed, respectively. It was observed that, as the Si/Al ratio increased, the total acidity decreased, even though a small number of stronger acidic sites were generated. The relative proportion of weakly acidic sites noticeably decreased. It was further observed that *tert*-butylamine can give rise to adsorption heats above 200 kJ mol^{-1} for a sample with Si/Al = 154. The total amount of chemisorbed base was similar for NH_3 and *tert*-butylamine.

7.7 Metal-Modified ZSM-5

The effect of surface acidity on the behavior of Fe-MFI zeolite catalysts with different Si/Al and Si/Fe ratios for benzene hydroxylation to phenol has been studied by Selli et al. [190] using FTIR and microcalorimetric analysis of adsorbed pyridine. The behavior of the catalysts in terms of activity and deactivation rate is discussed in relation to the nature, concentration and strength of the surface acid sites. Surface acidity, though not involved directly in the hydroxylation reaction, plays a major role in determining the lifetime of the catalyst.

The acidity and strength distribution of acid sites of a ZSM-5 prepared by hydrothermal synthesis, and zinc and gallium incorporated ZSM-5 catalysts prepared by incipient wet impregnation were compared to those of homologues prepared by a co-synthesis method. Ammonia adsorption microcalorimetry showed that samples prepared by co-synthesis exhibited lower acidity values when compared to the others [191].

A calorimetric and IR study of the adsorption of N_2O and CO at 303 K on Cu(II)-exchanged ZSM-5 zeolites with different copper loadings has been performed by Rakic et al. [192]. The active sites for both N_2O and CO are Cu(I) ions, which are present as a result of the pre-treatment in vacuum at 673 K. The measured amounts of chemisorbed species in the investigated systems and the values of differential heats of adsorption of both nitrous oxide (between 80 and 30 kJ mol^{-1}) and carbon monoxide (between 140 and 40 kJ mol^{-1}) demonstrate the dependence of the adsorption properties on the copper content. The samples were additionally characterized by ammonia adsorption microcalorimetry at 423 K [192].

A calorimetric and spectroscopic study of the coordinative unsaturation of copper(I) and silver(I) cations in ZSM-5 zeolite has been performed by Bolis et al. [193] using adsorption of NH_3 at room temperature. Adsorption microcalorimetry made it possible to characterize both quantitatively

and energetically the amino-complexes formed at the cationic sites. The heats of formation of the different amino-complexes were found to be in the 130–50 kJ mol^{-1} interval for both kinds of Me(I) sites, depending on the number of ligands progressively bound, in spite of the different stoichiometries of the species formed.

CO adsorption microcalorimetry has been used in combination with the IR technique to picture the bonding nature of silver ion-exchanged ZSM-5 type zeolites (Ag-ZSM-5) [194]. CO adsorption at 301 K gave rise to a large heat evolution, in the range of 100–80 kJ mol^{-1}, silver ions exchanged for protons (acting as Brönsted acid sites) being responsible for these strong adsorption sites. These adsorption energies are nonetheless lower than in the case of CO adsorption on copper ion-exchanged ZSM-5 (Cu-ZSM-5) (i.e., 140–110 kJ mol^{-1}).

7.8
Effect of Coke Deposition

In order to understand the effects of acidity and acid strength distribution on the nature of coke formed over ZSM-5 zeolite during the reaction of *n*-heptane aromatization, a series of ZSM-5 samples dealuminated to different degrees by steaming have been prepared and studied by microcalorimetry [195]. Microcalorimetric ammonia adsorption studies carried out at 448 K indicated the presence of very strong acid sites ($\Delta H > 140$ kJ mol^{-1}) in the catalysts steamed at 573 and 673 K. Steam treatment of the samples at various temperatures resulted in changes in initial heats of adsorptions to 148, 155, 133, and 135 kJ mol^{-1}, respectively, for steaming temperatures increasing from 573 to 873 K. These variations in acidity influenced the rate and composition of the coke deposits. The aromatic nature of the coke was found to depend mainly on the density of acid sites rather than on the strength distribution.

Calorimetric measurements performed on ZSM-5 samples used for methanol, C_2H_4 and $C_2H_4 + CH_3OH$ conversions have shown that no strong acidic sites remained accessible to NH_3 if C_2H_4 conversion was performed, while acid sites were still accessible after CH_3OH or $C_2H_4 + CH_3OH$ reactions [167]. This was presumably due to the formation of linear polymeric residues which filled the channels when C_2H_4 was used alone. These results also explained the rapid deactivation of the ZSM-5 zeolite sample for the C_2H_4 conversion.

7.9
Isomorphous Silica Molecular Sieves: Silicalite-1

The all-silica analogues of many zeolites can be synthesized, silicalite-1 being a prime example of the aluminum-free form of ZSM-5.

Silicalite is a microporous crystalline silica, i.e., an aluminium-free zeolite, belonging to the MFI-type structure and being the $Si/Al \rightarrow \infty$ limit of the ZSM-5 zeolite. The nature, population, and acidic properties of the hydroxylated species (hydroxyl nests) present in the nanocavities of variously prepared defective silicalites have been characterized by adsorption of NH_3 at room temperature, monitored through the combined use of microcalorimetry and IR spectroscopy [196]. It was found that a "perfect" silicalite sample exhibits a very low activity towards NH_3, confirming the almost complete absence of defects. The energetics of the interaction indicated that the (mild) acidity of silanols increases as far as the extension of the silanol patches increases.

A drop of the *ammonia* adsorption heats from 60 to 25 kJ mol^{-1} has been observed on a silicalite-1 [107]. This may be explained by an interaction of the basic molecules with terminal hydroxyl groups. Adsorption heats higher than 60 kJ mol^{-1} were only observed for very small adsorbed amounts, and there is strong evidence for physical adsorption in silicalite-1 [107].

Differential heats of adsorption have been determined calorimetrically by Thamm [197] for *benzene*, *n-*, *iso-* and *cycloalkanes*, *but-1-ene*, and *alcohols* on silicalite-1. It was shown that for small molecules, as well as for the flexible straight chain paraffins and *n*-alcohols, silicalite-1 may be regarded as an energetically homogeneous adsorbent, whereas molecules with sizes very close to the pore diameters of silicalite-1 revealed energetically different adsorption sites. The heat of adsorption for but-1-ene on silicalite-1 was found to be lower than the heat of adsorption for *n*-butane [114] and corresponded to physical adsorption only. The enhanced differential heats of benzene adsorption on silicalite-1 at low coverage were attributed to chemical or structural irregularities of the silicalite framework. A subsequent increase of the adsorption heats following a pseudo plateau was ascribed to a probe-probe interaction superimposed to the probe interaction with weaker sites as coverage increased [197].

On silicalite-1, the differential heats of adsorption of *acetone* and *diethylether* are approximately constant at ca. 67 kJ mol^{-1} and ca. 70 kJ mol^{-1}, respectively [76].

With *water*, the heats have been found to decrease continuously from 65 to 20 kJ mol^{-1} [75]. It is likely that the initial heats may be due to traces of Al, hydroxyl defects, or other impurities. Differential heats of adsorption have also been measured for a series of *alcohols* and a series of *nitriles* by Lee et al. [75]. The heats increased from 65 to 90 kJ mol^{-1} when going from methanol to propanol, and from 60 to 85 kJ mol^{-1} when going from acetonitrile to butyronitrile. The results were discussed in comparison to those obtained with a ZSM-5 sample.

The differential heats of adsorption of *n-paraffins* (ethane, *n*-butane, *n*-hexane, *n*-decane) on silicalite-1 were measured by Stach et al. [198]. An empirical equation was derived for the initial heats of adsorption of

n-alkanes. The adsorption behavior of *n*-hexane and benzene on the high-silica molecular sieves silicalite-2 (which displays no zig-zag channels) and ZSM-50 was also investigated [199] and compared with the results obtained on silicalite-1. In contrast to silicalite-1, no adsorption site heterogeneity was observed for benzene adsorption on silicalite-2 and ZSM-50. The initial heats of adsorption at 303 K on the three molecular sieves are very similar (around 74 kJ mol^{-1} for *n*-hexane and 60 kJ mol^{-1} for benzene), due to comparable framework densities and average electronegativities [199].

Finally, the calorimetric heats of adsorption of quadrupolar (CO_2) and non-polar (CH_4, C_2H_6, SF_6) gases on silicalite were determined by Dunne et al. [200], who studied the effect of adsorbate size and polarity on the energetics of adsorption.

8 Mordenites

The interaction energy of ammonia and therefore the acid strength of mordenite at low coverages are higher than the corresponding data for H-Y molecular sieves [63, 104]. The overall initial acid strengths of the H forms of mordenite, ZSM-5 and faujasite may be arranged in the following order: HM > H-ZSM-5 > H-Y.

On a H-mordenite sample (Si/Al = 13) most of the acid sites were found to have a differential enthalpy change for ammonia adsorption equal to about 160 kJ mol^{-1} [168]. In addition, this H-mordenite sample had a small number of stronger adsorption sites that were titrated at low ammonia coverage (ca. 0–100 μmol/g). These sites were related to non-framework aluminum species present in the sample. However, a similar H-mordenite (Si/Al = 13) studied by Spiewak et al. [100] showed, when determined at 423 K, only a uniform acid strength with a plateau of nearly constant differential heat of ammonia adsorption at 155 kJ mol^{-1} [100]. The value of 155 kJ mol^{-1} for the heat of ammonia adsorption agrees well with the value of 160 kJ mol^{-1} determined microcalorimetrically by Parrillo et al. [80]. A similar behavior was observed for pyridine adsorption on this sample [55], for which a large number of sites at about the same strength was observed, characterized by heats of adsorption near 200 kJ mol^{-1}, this value being about 40 kJ mol^{-1} higher than that of sites of H-ZSM-5. There was also evidence for a small number of sites indicated by heats greater than 200 kJ mol^{-1}, as well as weak sites with Q_{diff} near 110 kJ mol^{-1} [55]. These characteristics have also been described in a previous microcalorimetric study by Klyachko et al. [201]. Similarly, Auroux et al. [146] have observed a plateau of nearly constant heat of adsorption of ammonia versus coverage (ca. 170 kJ mol^{-1}) for a non-dealuminated sample (Si/Al = 15).

It was found by Kapustin et al. [101] that the heats of adsorption of ammonia on a mordenite sample (Si/Al = 9) at 573 K and after pretreatment at 703 K were between 160 and 140 kJ mol^{-1}. The initial heat of NH_3 adsorption was 165 kJ mol^{-1}, then it decreased to 148 kJ mol^{-1} and remained at that level up to a coverage of 0.4 mmol g^{-1}. Then another level of heat of adsorption appeared, at 140 kJ mol^{-1} and finally a smooth decrease to 100 kJ mol^{-1} at 1.2 mmol/g of coverage.

The heats of NH_3 adsorption at 473 K on a sample of H-mordenite (Si/Al ca. 10) evacuated at 773 K were measured by Tsutsumi et al. [202]. They were about 170 kJ mol^{-1} at zero coverage, decreased slowly to 150 kJ mol^{-1} up to a coverage of ca. 1100 μmol/g and then sharply decreased to about 80 kJ mol^{-1} [202].

8.1 Influence of the Probe Molecule

Microcalorimetry was used by Chen et al. [41] to determine the heats of adsorption of *dimethylether*, *ammonia*, *monomethylamine*, and *dimethylamine* at 473 K on H-mordenite (Si/Al = 13). The average enthalpy change of ammonia adsorption equaled 158 ± 8 kJ mol^{-1} and the weak sites adsorbed ammonia at 72 ± 2 kJ mol^{-1}. The average enthalpy changes of adsorption for the strong sites were 219, 207, and 140 kJ mol^{-1} with monomethylamine, dimethylamine, and trimethylamine, respectively. The differential enthalpy changes upon dimethylether adsorption on H-mordenite showed an initial region of strength adsorption (around 113 kJ mol^{-1}) followed by a plateau with an enthalpy change of adsorption equal to 87 kJ mol^{-1} [41]. Then the enthalpy change of adsorption decreased gradually with coverage to 60 kJ mol^{-1}. Except for trimethylamine, the enthalpy changes of adsorption on Brönsted sites were found to vary linearly with the gaseous proton affinities of these basic molecules.

The differential enthalpy changes for *methanol* adsorption on strong and weak sites were close to 100 kJ mol^{-1} and 70 kJ mol^{-1}, respectively [41]. The differential enthalpy change of adsorption of *water* on H-mordenite at 423 K showed an initial decrease in adsorption heats at low coverages, followed by a broad plateau with an average enthalpy change of adsorption equal to ca. 75 kJ mol^{-1} [41].

In another study, Lee et al. [174] have observed a strong correlation between gas-phase proton affinities and differential heats of adsorption of a series of *alkylamines* and a series of *substituted pyridines* in H-mordenite.

Concerning co-adsorption studies, ammonia adsorption was studied at 473 K on an H-mordenite previously contacted with *methanol* at 473 K and subsequently evacuated at 548 K. Compared to ammonia adsorption on clean H-mordenite, methanol preadsorption followed by evacuation had the effect of reducing the number of strong adsorption sites. The enthalpy change of

adsorption on the remaining sites was not affected by the irreversibly bound methanol species. The effect of dimethylether preadsorption on ammonia adsorption was similarly studied and gave the same behavior as methanol preadsorption [41].

8.2 Influence of the Adsorption Temperature

Adsorption of ammonia on mordenites has been shown to be significantly influenced by the adsorption temperature [202]. Non-selective adsorption was observed below 373 K, and the measured heats of adsorption were found to be an average between those on the most energetic (acidic) sites and those on the least energetic ones. The molecules adsorbed on the latter migrated at higher temperatures. Consequently, adsorption above 423 K was required to characterize the acidity of mordenites. Since no diffusion limitation was observed in the adsorption of ammonia on faujasites above room temperature [102] and on ZSM-5 above 373 K, this phenomenon may result from the peculiar channel structure and the opening diameter of mordenites [202].

Adsorption calorimetry has also been used by Kapustin et al. [29] to measure the differential heats of adsorption of NH_3 on wide-pore Na-mordenite (Si/Al = 5) between 303 and 673 K after pretreatment at 753 K. As the temperature was increased, the initial heat of adsorption dropped from 109 to 80 kJ mol^{-1}. At all temperatures, there was a stepwise change in the heats of adsorption with increasing coverage due to adsorption on the Na cations. On narrow-pore mordenite, there was no change in the heat with increasing temperature. It was concluded that the significant decrease in the heat of adsorption with increasing temperature is related to the specific properties of the wide-pore mordenite as an adsorbent [22].

8.3 Effect of Pretreatment

The effect of high temperature calcination in air at 1008 K on H-mordenite (Si/Al = 13) has been studied by Chen et al. [55] using adsorption microcalorimetry of pyridine at 473 K. This treatment caused a significant reduction in the total number and in the strength of the acid sites. The plateau characteristic of a large number of sites of uniform strength (near 200 kJ mol^{-1}), observed on the sample pretreated at 673 K, also disappeared. High-temperature calcination is known to induce dealumination and dehydroxylation, both of which are expected to reduce the number of acid sites [55].

Dehydroxylation of an H-mordenite sample at 923 K caused the appearance of centers with heat of NH_3 adsorption of 175–170 kJ mol^{-1} which

were not present in the same sample pretreated at 703 K. Increasing the dehydroxylation temperature to 1023 K increased the concentration of centers characterized by a heat of ammonia adsorption of 175–170 kJ mol^{-1} to 0.2 mmol g^{-1}, and sharply decreased the concentration of centers generating 160–130 kJ mol^{-1} [101]. It was shown that the latter values are typical of the dissociation of ammonia over Lewis acid centers.

The acidic properties of a mordenite zeolite with an Si/Al ratio of 10 were analyzed by Tsutsumi et al. [202] using calorimetric measurements at 473 K of the heats of ammonia adsorption on samples evacuated at temperatures varying from 703 K to 1073 K. Drastic energy changes were observed between low coverage and high coverage, with the exception of the sample evacuated at 1073 K. Both the number of the more energetic sites and their energy increased with an increase in the evacuation temperature, and reached a maximum at 773 K (around 170–175 kJ mol^{-1}). Then a decline was observed. The heat curve of the sample evacuated at 1073 K did not exhibit a plateau, and its initial value was much less than those of the other samples (160 kJ mol^{-1} instead of 175 kJ mol^{-1}). This may be attributed to the breakdown of part of the mordenite structure and/or to the local formation of amorphous species [202].

A sample of mordenite (98% degree of ammonium-ion exchange) deammoniated at various temperatures from 693 K to 923 K was studied at 573 K by NH_3 adsorption microcalorimetry by Bankos et al. [203]. On increasing the pretreatment temperature, the number of acid sites passed through a maximum at 753 K as a result of simultaneous decationation and dehydroxylation. The heat of adsorption of NH_3 on Brönsted acid sites formed by decationation was 110–160 kJ mol^{-1}. During dehydroxylation, two types of Lewis sites were formed, characterized by heats of NH_3 adsorption of 170–185 kJ mol^{-1} and 95–100 kJ mol^{-1} respectively, and on which dissociative chemisorption of ammonia was evidenced by IR [101].

8.4 Influence of the Exchange Level

When NH_3 reacts with Na^+ cations in mordenite, the heat of adsorption is much lower than in the case of H-mordenite [204, 205]. The differential heats of adsorption of NH_3 at 573 K after outgassing at 753 K for sodium small-pore mordenite and for decationated samples with different residual sodium contents were measured by Mishin et al. [46]. The initial Na-form adsorbed NH_3 with heats of 85–75 kJ mol^{-1} showing little change with coverage. After exchange with NH_4^+ and subsequent decationation, sites with $Q_{diff} > 90$ kJ mol^{-1} appeared. Because these centers could not be detected on the Na-form, they were related to Brönsted acid sites. Increasing the exchange level increased the acid strength, and removal of the last Na^+ ions resulted in sites with $Q_{diff}(NH_3) = 130–160$ kJ mol^{-1}. The sites having $Q_{diff} = 140$ kJ mol^{-1}

could be detected in the samples of small-pore mordenites, while those with a heat of adsorption equal to 150–160 kJ mol^{-1} were found in the large-pore zeolites, the initial heats even attaining values ranging from 170 to 180 kJ mol^{-1} [46]. The number of acid sites, as determined from calorimetric measurements, increased nearly linearly with an increase in the exchange level. The difference between the number of sodium ions removed and the number of Brönsted sites created was equal to the number of weak acid sites, as measured by the amounts of NH_3 molecules adsorbed with relatively low heat evolution [46].

Comparing the activities of faujasites and mordenites in cracking of *n*-octane, the reaction rates over mordenites were found to be nearly ten times greater than those over Y zeolites. At the same time, faujasite exchanged to 90% contained twice as many strong acid sites with $Q_{diff} >$ 90 kJ mol^{-1} as mordenite with the same extent of decationation. On going from H-mordenite to H-Y, the fraction of the strong acid sites with $Q >$ 110 kJ mol^{-1} decreased from ca. 50% to < 10%, and this decrease outweighed the increase in the total acidity [46].

Microcalorimetric studies of the adsorption of NH_3 on H,Na-mordenites at 573 K were also performed by Klyachko et al. [26, 206] and Bankos et al. [203]. The acid strength distribution was observed to be heterogeneous. Well-defined steps were clearly seen on the curves of differential heat versus coverage, indicating the presence of a few different types of adsorption centers. On increasing the degree of decationization, not only the number but also the strength of acid sites increased (Fig. 14). The total amount of acid centers changed practically linearly with the degree of decationiza-

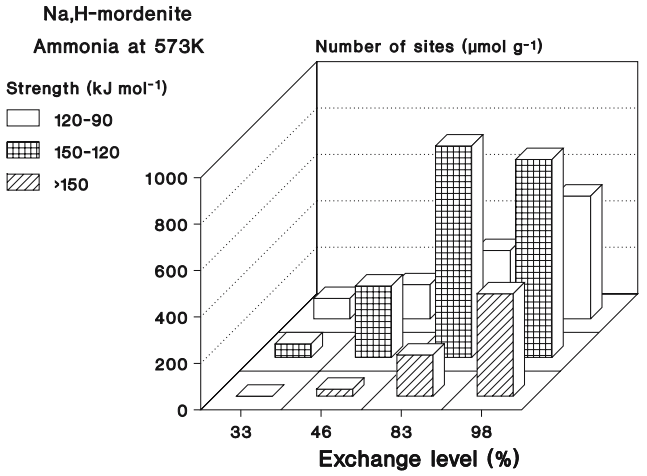

Fig. 14 Acid site strength distribution of Na,H-mordenites as a function of the exchange level. Ammonia adsorption at 573 K, activation at 753 K (from [203])

tion. However, the concentration of acid sites determined by calorimetry was much smaller than the calculated value [206]. Correlations were found between the number of acid sites of different strengths and the catalytic activity as well as the selectivity for xylene isomerization and disproportionation [203, 207].

Contrarily to ammonia, pyridine, which is a larger molecule, can titrate only OH groups located in large channels. Heats of adsorption of pyridine were measured at 573 K on a series of Na-exchanged mordenites [208]. The curves of differential heat of adsorption versus pyridine coverage were composed of roughly three regions. At the very beginning a sharp decrease in Q_{diff} was observed, which should be assigned to the adsorption on a few very strong Lewis acid sites. In the next region, a wide plateau of constant heat values around 180–190 kJ mol^{-1} corresponded to the heats released during adsorption on the predominant Brönsted acid sites. Then a sharp decrease of Q_{diff} with the adsorbed volume was observed for all samples except the least exchanged one, for which the heats of adsorption were much lower and decreased continuously with coverage without the appearance of a plateau. The strength of the predominant population of sites became much less affected by the exchange degree above 47%. The number of acid sites increased nearly linearly with an increase in the exchange level up to 50% and then remained constant above this value. These results suggest that, as long as new hydroxyls are formed in large channels, their average acidic strength increases (probably because more strongly acidic hydroxyls are formed at higher exchange degrees). Above 47% of exchange, the acidic strength of hydroxyls in the large channels remains constant, which indicates that the formation of hy-

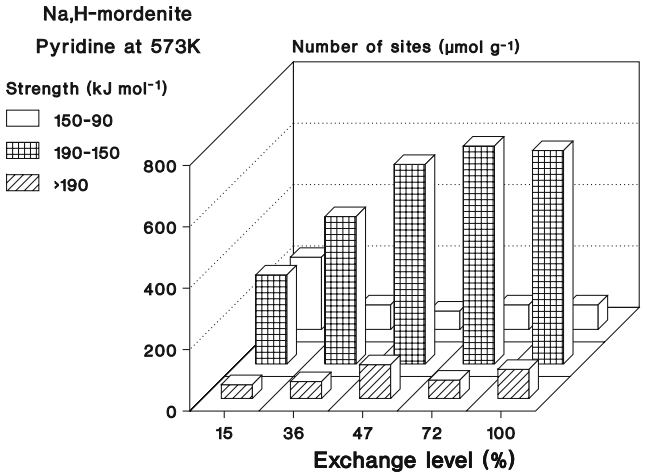

Fig. 15 Acid site strength distribution of Na,H-mordenites as a function of the exchange level. Pyridine adsorption at 573 K, activation at 773 K (from [208])

droxyls taking place in side pockets (above 50% of cation exchange) does not influence the properties of hydroxyls in large channels. For most of the acidic sites (OH groups), the differential heats of pyridine adsorption were found not to depend on pyridine loading. This constant value of adsorption heat suggests that either OH groups in the large channels of mordenite form a homogeneous population or pyridine molecules react with all the accessible hydroxyls without selecting the most acidic ones.

These results are shown in Fig. 15 which represents the spectrum of the acidic strength as a function of the exchange level: the three populations mentioned above are better recognized, viz. above 190 kJ mol^{-1}, within 190–150 kJ mol^{-1}, and within 150–90 kJ mol^{-1}. A moderate increase of the very strong sites (heat above 190 kJ mol^{-1}) is apparent in this figure, whereas the number of sites with Q_{diff} values lying between 190 and 150 kJ mol^{-1} increases considerably with the exchange degree up to 50% and then remains approximatively constant beyond 50% exchange. Concomitantly, the number of sites which display a moderate strength between 150 and 90 kJ mol^{-1} decreases and then remains constant [208].

The heats of adsorption of *n*-butylamine and pyridine on Na- and H-forms of mordenite were also studied by Klyachko et al. [26]: the heats were greater on the H-form of the zeolite and greater than on the corresponding forms of type Y zeolite.

8.5 Influence of Dealumination

The molar differential heats of adsorption of ammonia on mordenites with various Si/Al ratios (from ca. 5 to 10, evacuated at 773 K) were measured at 473 K by Tsutsumi et al. [202]. Heat curves obtained for Na-type mordenites exhibited homogeneity of acid strength irrespective of the Si/Al ratio. In protonated mordenites, the initial heats of adsorption increased with an increase in the Si/Al ratio and reached a maximum (about 170–175 kJ mol^{-1}) for Si/Al $\approx$ 10. The number of acid sites calculated from the heat curves (number of ammonia molecules which adsorbed with heats of adsorption above 80 kJ mol^{-1}) was plotted against the theoretical number of protons (aluminum atoms) per unit cell of mordenites. Although they correlated well, the slope deviated a little from unity, and more for low Si/Al than high Si/Al ratios. This result suggests that the framework aluminum atoms participate in the formation of acid sites and that some of the generated Brönsted acid sites are converted to Lewis acid sites. However, the displacement of aluminum atoms from the framework may also be responsible for the deviation [202]. A similar study was performed at 303 K on mordenites (dealuminated by hydrochloric acid treatment) with Si/Al ratios of 6.3, 10, and 24 by Rukhadze et al. [209]. Dealumination was found to reduce the total number of acid centers and increase their strength [209]. The initial heat of adsorption increased

from about 110 to 145 kJ mol^{-1} with increasing Si/Al ratio. Such a behavior was explained by two opposing effects resulting from Al extraction: the increase of acid strength of protonic sites and the decrease of the number of sites.

The acidity of a series of mordenites dealuminated by acid refluxing (Si/Al ratios between 7 and 48) was studied by Stach et al. [58, 63] by calorimetric measurements of the NH_3 chemisorption at 423 K. Starting with a low Al content (a high Si/Al ratio), the number of strong acidic sites increased with an increasing number of framework Al up to 4.6 Al atoms/u.c. (Si/Al ratio of 9.5) and then decreased. The decrease of the strong acidity above 4.6 atoms/u.c. may be explained by the appearance of an aluminum atom in the second coordination sphere of the Si – OH – Al group. The experimentally found value of the maximum in the curve of the strong acidity versus the aluminum molar fraction coincides with the value (Si/Al = 9.4) calculated by Barthomeuf [57] from the topological Al density of mordenite, thus confirming her theoretical concept of zeolite acidity [48, 63] (see Fig. 7a). Calorimetric measurements by Klyachko et al. [26] are in coincidence with these data. Although progressively increasing the Si/Al ratio led to an increase in initial heats, it also led to a more rapid decrease of the differential heats with filling.

Brueva et al. [147] have studied the acidity of hydrogen mordenites using NH_3 adsorption calorimetry at 573 K. The initial heats were in the range 140–145 kJ mol^{-1} for the parent NH_4-M sample. Dealumination was found to result in the appearance of sites with adsorption heats greater than 165 kJ mol^{-1}.

In another study investigating a series of dealuminated samples [146], greater initial differential heats compared to the parent sample (Si/Al = 15) were observed at a low dealumination level but not at a higher one. The increase of the acid site strength was accompanied by a heterogeneous strength distribution, as a result of dealumination [146].

The surface acidity of three commercial mordenite (MOR) zeolites with Si/Al ratios of 10, 60, and 80 has been evaluated by adsorption microcalorimetry at 423 K, using pyridine as a probe molecule [210]. As could be expected from the Si/Al ratios, the total pyridine uptakes varied in the order MOR-10 > MOR-60 > MOR-80. The initial differential heats of adsorption were in the range 215–220 kJ mol^{-1}. After a sudden drop, Q_{diff} changed slightly and stepwise over a relatively wide range of pyridine uptake (at least for MOR-10) and then steeply decreased. The site-energy distributions and the thermokinetic parameters versus coverage were also determined [210].

Stach et al. [211] found a linear relationship between the adsorbed amounts of ethane and the differential molar heats of adsorption over three dealuminated mordenites. The heats of ethane adsorption on the different mordenites increased with decreasing Si/Al ratio, i.e. with increasing aluminum content of the framework.

The acidic properties of highly siliceous mordenites were also investigated by Shibuichi et al. [153], showing that the homogeneity of acidic strength is decreased by dealumination.

Finally, the acidity of commercial mordenites has also been studied using pyridine adsorption microcalorimetry by Ferino et al. [28].

9 Offretites and Erionites

The acid strength distributions of H-offretites (fresh catalyst and aged samples) have been determined at 423 K using ammonia as a basic probe [212] and compared to other zeolites (ZSM-5, ZSM-11, mordenite). The acidity of offretite dealuminated by hydrothermal treatment has also been characterized by microcalorimetry of NH_3 adsorption at 420 K. It was observed that dealumination up to ca. 50% primarily decreased the number of sites of medium acid strength of offretite and left part of the strong acid sites unaffected [213]. The parent and dealuminated samples displayed very similar initial heats of adsorption (ca. 180 kJ mol^{-1}) when the Si/Al ratio increased from 4.3 to 9.7, followed by a plateau of heats between 170 and 150 kJ mol^{-1} and then a continuous decrease to ca. 70–50 kJ mol^{-1}. Two kinetic regimes of heat evolution were observed for the starting offretite which perhaps arose from two differently accessible types of sites presumably located in the cages and channels. Only one type was observed for dealuminated samples.

Heat-flow microcalorimetry has been used to measure the heat of adsorption of NH_3 and pyridine at 423 K on zeolites with variable offretite-erionite character [214]. The offretite sample (Si/Al = 3.9) exhibited only one population of sites with adsorption heats near 155 kJ mol^{-1}. The presence of erionite domains in the crystals provoked the appearance of different acid site strengths and densities, as well as the presence of very strong acid sites attributed to the presence of extra-framework Al. In contrast, when the same chemisorption experiments were repeated using pyridine, only crystals free from stacking faults, such as H-offretite, sorbed this probe molecule (plateau at 200 kJ mol^{-1}). The presence of erionite domains in offretite drastically reduced pyridine chemisorption. In crystals with an erionite character, pyridine uptake could not be measured. Thus, it appears that chemisorption experiments with pyridine could serve as a diagnostic tool to quickly prove the existence of stacking faults in offretite-type crystals [214].

Methanol adsorption on erionites containing K^+, Na^+, and Li^+ cations has also been studied by calorimetry at 303 K and IR spectroscopy. An increase in the content of Na^+ ions in the crystals and the substitution of Na^+ ions by Li^+ ions were shown to result in the increase of the heat of CH_3OH adsorption in a wide range of coverage [215].

10
Other Zeolites

10.1
H-Rho

Microcalorimetric studies of ammonia adsorption were used to investigate the acidic properties of the small-pore zeolite H-Rho [216]. Shallow-bed calcination of NH_4-Rho at 673 K or 773 K produced a nearly pure H-Rho with highly acidic framework hydroxyls as Brönsted acid sites having an initial heat of adsorption of ammonia of about 170 kJ mol^{-1} [217]. Shallow-bed calcination at 873 K and 973 K destroyed ca. 25% and ca. 50% of the framework hydroxyls, respectively, producing a small number of strongly acidic Lewis sites (ca. 185 kJ mol^{-1}) but also weakly acidic sites having a heat of adsorption of ammonia of ca. 60 kJ mol^{-1} [216].

10.2
Ferrierite-Type Zeolites

Ferrierite samples with two aluminum contents (Si/Al = 15.4 and 7.8) were synthesized. The first sample (Si/Al = 15.4) was pure ferrierite, whereas the second (Si/Al = 7.8) was a mixed ferrierite + mordenite phase [218]. Acidic properties, as evidenced by microcalorimetry of ammonia adsorption at 423 K, corresponded to strong acidity. The essential feature of the pure ferrierite acidity was a strong constant differential heat of 160 kJ mol^{-1} over a large range of coverage indicating a homogeneous number of strong sites. This plateau was followed by a sharp and sudden drop in acid strength. The intimate mixture with mordenite in the second sample resulted in a severe limitation of the adsorption and diffusion properties. Steaming and acid leaching treatment resulted in a decrease in the number but not the strength of acidic sites [219].

The microcalorimetric technique was also applied to investigate the adsorption of acetonitrile, dimethylether, water, pyrrole, and ammonia at 296 K on a small-pore type ferrierite (Si/Al = 15.4) [84]. The acidity spectra collected from the calorimetric measurements showed that the distribution of site strengths was much dependent on the strong or weak basicity of the probe, on the acidity and porosity of the acid solid and on the adsorption temperature [84].

10.3
Mazzite

The acidity of a series of dealuminated mazzites with Si/Al ratios varying from 5 to 23, prepared by combined steam-acid leaching and ion-exchange

procedures, all obtained from the same parent zeolite (Si/Al = 4), has been studied using heat-flow microcalorimetry [220, 221] with particular emphasis on the evaluation of the influence of framework and non-framework aluminum species on the nature, strength, and accessibility of the acid sites. Mazzite samples covering a broad range of overall and framework compositions were prepared for this purpose. It was shown that the strong acid sites present in dealuminated mazzite were associated with the framework aluminum atoms, whereas non-framework species contributed essentially to the weaker acidity. Initial and intermediate heats of adsorption of ammonia were higher (by about 10 to 20 kJ mol^{-1}) than those usually reported for dealuminated zeolites. The initial heats of NH_3 adsorption were around 200 kJ mol^{-1}. The samples presenting non-framework aluminum displayed a heterogeneous distribution of acid sites, with a continuous decrease of the differential heat versus coverage, whereas the samples presenting no extra-framework species displayed a very homogeneous heat of adsorption (presence of a plateau at around 180 kJ mol^{-1}).

10.4 MCM-22 and MWW-Based Catalysts

Ammonia adsorption calorimetry has been applied to investigate the acid properties of MWW-based catalysts with different framework topologies and crystallinities [222]. It was established that the acidic properties of the MCM-22 family depend mainly on the Al-content of the solid (the Si/Al ratio varied from 9.1 to 46.0). Delamination of the MCM-22 precursor, which yields ITQ-2, resulted in a decrease of the total acidity and an increase of the concentration of intermediate acid sites, while the pillaring process, which yields MCM-36, affected mainly the total concentration of acid sites, the acid strength distribution being similar to the corresponding MCM-22 zeolite.

In another study, three H-MCM-22 zeolite samples with total Si/Al ratios of 10, 14, and 30, calcined at 823 K, were characterized by microcalorimetry of pyridine adsorption at 423 K [223]. These experiments showed the presence of very strong acid sites, particularly on the most dealuminated sample (initial heat of 230 kJ mol^{-1}) and a significant increase of the acid strength with the Si/Al ratio of the zeolite.

MCM-22 presents an unusual pore network since its characteristics are between those of large and medium pore zeolites. MCM-22 contains both 10 and 12-membered ring channels. The differential heats of adsorption of toluene at 315 K on MCM-22 (Si/Al = 15) as a function of coverage were studied by Corma et al. [224] on a fresh sample and on a sample after preadsorption of *m*-xylene, *o*-xylene, and 1,2,4-trimethylbenzene. From the kinetic diameters of the adsorbates, the dimensions of the channels and cavities were estimated.

The sorption of light alkanes on the protonic form of MCM-22 and MCM-36 was investigated by calorimetry [225]. On the basis of the MCM-

22 precursor, MCM-36 was produced by swelling and pillaring techniques. As alkanes were sorbed in the same local environment in both samples, identical enthalpies of adsorption were observed. Silica pillaring increased the concentration of terminal Si – OH groups compared with MCM-22. However, the number of Brönsted acid sites determined at 373 K by NH_3 adsorption calorimetry was lower in MCM-36 than in MCM-22. This was attributed to the dealumination induced by the synthesis process [226].

10.5 Zeolites G, L, ZK-4, ZK-5, and SVK

Acidic properties of L zeolite were shown by Tsutsumi et al. [227] to correlate well with its structural disorder. The differential molar heats of adsorption of ammonia at 623 K on a $H_{7.25}K_{2.25}Al_{9.5}Si_{26.5}O_{72}$ sample changed step-wise with coverage, reflecting the difference in the acid strength of protons located at structurally different sites. Adsorption at lower temperatures also yielded step-wise but less distinct variations, which indicated diffusion limitations in the microporous adsorbents at lower temperatures. High-silica L zeolites were also investigated [153]. Their acid strength became less homogeneous after dealumination.

Measurements of the heat of carbon dioxide adsorption have been made at 303 K by Vasiljeva et al. [228] on type A, G, L, and ZK-4 sodium and lithium zeolites pretreated at 673 K. A partial substitution of Na by a low amount of Li led to a reduction of the initial heat of adsorption of CO_2 on type A and ZK4, according to the fact that reducing the radius of the alkali metal cation decreases the excess negative charge of the basic oxygens of the framework. However, this tendency was reversed when the amount of lithium became much larger than that of remaining sodium, leading to initial heat values much higher than on the initial sodium zeolites. Moreover, the initial heat of adsorption of carbon dioxide on type G and L zeolites was markedly increased when replacing most of the sodium ions with lithium ions. In any case, the total number of sites titrated by CO_2 decreased when Li^+ ions displaced the Na^+ ions, for all four studied zeolites.

ZK-5 (KFI) is a high alumina zeolite with a high free pore volume. Microcalorimetry, temperature-programmed desorption (TPD), and FTIR spectroscopy have been applied to get more insight into the adsorption properties of water, methanol, and acetonitrile in the KFI structure [229]. The integral heats of adsorption of water, related to the amount of adsorbent, were found to be higher than those of the larger molecules (methanol and acetonitrile), though the integral molar heat of adsorption of water was the lowest of the three. The differential molar heats of adsorption of methanol and acetonitrile in H-ZK-5 showed a stepwise decrease with increasing loading.

The acidity of SVK zeolites was studied by Klyachko et al. [230] using calorimetry of NH_3 adsorption at 573 K after pretreatment at 753 K. The spec-

tra of acidity were obtained by graphical differentiation of the experimental heat curves and allowed to establish the contributions of different centers to the total activity of catalysts. In agreement with their low aluminum content, these zeolites differ from mordenites by their smaller number of acid centers.

10.6
Beta Zeolites

The surface acidity of a series of Beta zeolites with different Si/Al ratios has been assessed by adsorption calorimetry at 423 K using pyridine as a probe molecule. The site energy distribution was discussed in relation with FTIR results [231]. Differential heats of adsorption of pyridine on Beta zeolites (Si/Al $\approx$ 15) were also measured at 473 K by Diaz-Mendoza et al. [232].

11
Tuning the Acidity

The acid/base properties of zeolites can be systematically changed by acting on various factors: nature of the exchange cation, cation loading, decationation, dealumination, which have been discussed in the previous section, and introduction of various elements (Ge, B, P, Ga, ...) into the crystal framework, the effects of which we will now describe in more detail.

11.1
Isomorphous Substitution

The first synthetic molecular sieves were zeolites with only aluminum and silicon as tetrahedrally coordinated cations. However, several other elements of similar electronic configuration and size can be substituted either for aluminum or silicon.

In the first instance, one considers other trivalent cations that fit well into the tetrahedral oxygen environment, such as Fe, Ga, and possibly also B. The first question to be addressed is whether such elements have indeed been incorporated as "defects" in the zeolite lattice or whether they are present as a separate impurity. In many cases it has been concluded that, up to a certain concentration, incorporation into the zeolite framework had indeed occurred.

The nature and the strength of the bridging hydroxyl groups (Si – OH – T, T = Al, Fe, Ga, B, ...) depend on T, and the proton-T distance, at comparable bond angles, decreases in the order Fe, Ga, Al. This means that the electrostatic repulsion between the proton and T increases in the same way, and that the acidity is expected to increase in the same order.

The use of organic templates has rendered possible the substitution of many other elements, including other trivalent (Cr^{3+}), bivalent (Be^{2+}), and tetravalent ions (Ge^{4+}, Ti^{4+}). Most of these metallosilicate compositions have been synthesized with ZSM-5 crystal structure.

11.1.1 Trivalent T Atoms

Boron-Substituted Zeolites

A co-incorporation of aluminum and boron in the zeolite lattice has revealed weak acidity for boron-associated sites [233] in boron-substituted ZSM-5 and ZSM-11 zeolites. Ammonia adsorption microcalorimetry gave initial heats of adsorption of about 65 kJ mol^{-1} for H-B-ZSM-11 and showed that B-substituted pentasils have only very weak acidity [234]. Calcination at 1073 K increased the heat of NH_3 adsorption to about 170 kJ mol^{-1} by creation of strong Lewis acid sites. The lack of strong Brönsted acid sites in H-BZSM-11 was confirmed by poor catalytic activity in methanol conversion and in toluene alkylation with methanol.

Gallium-, Iron-, and Indium-Substituted Zeolites

Gallium has been successfully introduced into numerous zeolite frameworks (Beta, MFI, offretite, faujasite, ...). The Ga^{3+} ions in zeolites can occupy tetrahedral framework sites (T) and non-framework cationic positions. The isomorphous substitution of gallium into aluminosilicate zeolites results in modified acidity and subsequently modified catalytic activity such as enhanced selectivity towards aromatic hydrocarbons.

Microcalorimetric experiments with ammonia and pyridine as probe molecules have been used to investigate the effects of framework Ga on the acidic properties of several zeolites [235–241].

Experiments of NH_3 adsorption microcalorimetry, together with FTIR results from pyridine thermodesorption, have shown that the isomorphous substitution of Al by Ga in various zeolite frameworks (offretite, faujasite, beta) leads to reduced acid site strength, density, and distribution [236–239]. To a lesser extent, a similar behavior has also been observed in the case of a MFI framework [240, 241].

A drastic reduction in the acid site density of H,Ga-offretites has been reported, while the initial acid site strength remained high [236, 238].

With Ga-Beta it was found that, when the Si/Ga ratio increased from 10 to 40, the number of strong sites decreased drastically for Si/Ga between 10 and 25 and then reached a plateau above Si/Ga = 25 [235].

The strength and density of acid sites in H-(Ga,La)-Y have also been found to be lower than those in H-Y crystals of the type used in FCC preparation (LZY-82) [237].

Parrillo et al. [242] have used microcalorimetric measurements of ammonia and pyridine adsorption to compare the acid sites in H-[Fe]ZSM-5, H-[Ga]ZSM-5, and H-[Al]ZSM-5. On each of the molecular sieves, the differential heats of adsorption for both ammonia and pyridine were constant up to a coverage of one molecule per Brönsted site. The differential heats at coverages below 1 : 1 were identical on each of the materials, with values for ammonia of 145 ± 5, 150 ± 5, and 145 ± 5 kJ mol^{-1} on H-[Fe]ZSM-5, H-[Ga]ZSM-5, and H-[Al]ZSM-5, respectively, and for pyridine of 195 ± 5, 200 ± 5, and 200 ± 5 kJ mol^{-1} on H-[Fe]ZSM-5, H-[Ga]ZSM-5, and H-[Al]ZSM-5, respectively. The authors [242] concluded that the microcalorimetric heats of adsorption for ammonia and pyridine at Brönsted acid sites formed by framework Fe(III) and Ga(III) were very similar to heats of adsorption at Al(OH)Si sites, and that the three samples were effectively equivalent proton donors. In contrast, they found very different reactivity measurements for *n*-hexane cracking and propene oligomerization on the same materials. The authors claimed that heats of adsorption for strong bases do not reflect differences in inherent acid strength and may not be related to catalytic activity in any simple manner.

Iron silicates of MFI structure with various Si/Fe ratios have also been studied by NH_3 adsorption microcalorimetry in [241, 243] and compared with the Al and Ga analogues. The intermediate strength sites (predominantly Brönsted sites) were found to correspond to a plateau around 145 kJ mol^{-1} for H-[Al]-ZSM-5 (Si/Al = 19), 140 kJ mol^{-1} for H-[Ga]-ZSM-5 (Si/Ga = 22), and 135 (Si/Fe = 41), 125 (Si/Fe = 26), or 120 (Si/Fe = 12) kJ mol^{-1} for H-[Fe]-ZSM-5, respectively.

The adsorption of acetonitrile on H-[Fe] ZSM-5 and H-[Al] ZSM-5 has been studied using microcalorimetry at 400 K [73]. The heats of formation of the complexes were found to differ slightly, ca. 95 kJ mol^{-1} on H-[Fe] ZSM-5 compared to ca. 110 kJ mol^{-1} on H-[Al] ZSM-5, suggesting that the hydrogen bonds at FeOHSi sites may be slightly weaker.

Ga- and Fe-substituted MFI zeolites have been investigated using adsorption microcalorimetry of different alkanes at 353 K by Auroux et al. [244]. The acid strength of the zeolite protons decreased following the sequence H-[Al]MFI > H-[Ga]MFI > H-[Fe]MFI. The heats of adsorption decreased with the basicity of the alkane in the order *n*-butane > isobutane > propane.

The active sites of isomorphously substituted MFI structures activated at 673 K have been characterized by Jänchen et al. [245] using microcalorimetric measurements carried out at 423 K with ammonia as a probe. Because of decreasing heats of NH_3 adsorption, the Brönsted acid site strength of the modified MFI was reported to decrease in the sequence Al > Fe > In > silicalite. In

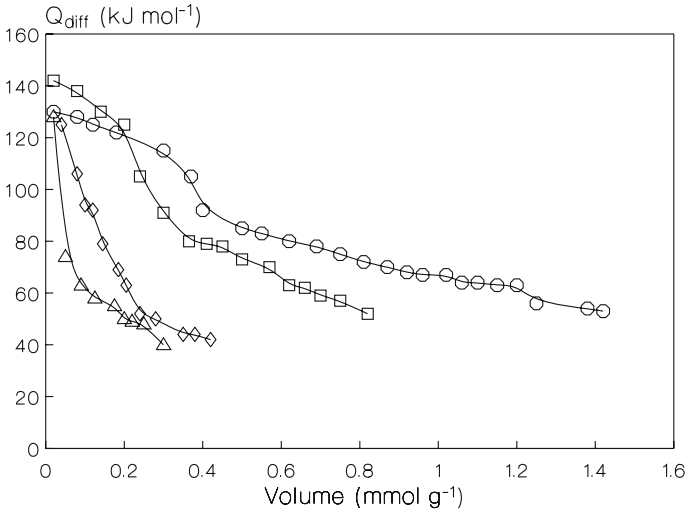

Fig. 16 Differential molar heats of ammonia chemisorption at 423 K on MFI zeolites as a function of the adsorbed amount: □ Al-Sil, ○ Fe-Sil, ◇ In-Sil, △ silicalite. Pretreatment temperature 673 K (from [245])

addition to these strong sites, weaker Lewis centers due to the non-framework material were found (Fig. 16).

Crystalline MFI-type indosilicates containing indium ions in framework positions were hydrothermally synthesized by Vorbeck et al. [246] and characterized by adsorption microcalorimetry of NH_3 at 423 K (after activation of the sample at 670 K). They exhibited rather weak acidity attributed to Brönsted sites. However, the number of acid sites with a sorption heat between 80 and 110 kJ mol^{-1} was significantly higher than for silicalite [246].

11.1.2 Tetravalent T Atoms

Titanosilicate (TS-1)

Titanium-substituted silicalite can be prepared with a homogeneous distribution of Ti ions in the crystal. The Ti ions seem to be all Ti^{4+} surrounded by four NNN Si ions and, thus, the catalytic site is an isolated Ti^{4+} ion.

For TS-1, relatively low heats of adsorption due to coordinatively bonded ammonia were detected by Jänchen et al. [245]. Moreover, the amounts of adsorption with heats higher than found for silicalite correlated with the amount of Ti in the sample [245].

Similarly, the acidity of titanium-silicalites with different titanium contents was characterized by adsorption calorimetry at 353 K of various probe molecules by Muscas et al. [247]. These molecular sieves had a molar compo-

sition $x\mathrm{TiO_2}(1-x)\mathrm{SiO_2}$, where x ranged from 0 to 0.02. Subjected to ammonia adsorption, these solids showed an acidic character compared to a pure silicalite-1 sample. A small amount of titanium induced a high increase in the strong acid sites ($Q_{\mathrm{init}} = 160–170\ \mathrm{kJ\ mol^{-1}}$ instead of 75 for silicalite-1). The integral heat and the total amount of acid sites increased with increasing titanium loading and then reached a plateau for $x \geq 0.014$. All the curves showed a sharp decrease in Q_{diff} at very low coverages. The next region corresponded to a plateau with heats evolving around $70\ \mathrm{kJ\ mol^{-1}}$ instead of $40\ \mathrm{kJ\ mol^{-1}}$ for silicalite-1. Other basic probes such as pyridine and substituted pyridines (DMP) were also used in an attempt to identify by selective adsorption the different sites of these catalysts [247]. The heats and amounts adsorbed were in the order: pyridine > 3.5 lutidine > 2.6 lutidine.

The adsorption properties of titanium silicalites-1 synthesized via two different routes, viz. in the presence or the absence of sodium in the precursor gel, have been compared by Auroux et al. [248]. Adsorption calorimetric measurements of a basic probe (NH_3) and an acidic probe (SO_2) showed that these solids were very acidic compared to a silicalite-1 sample. The presence of Na in the different samples decreased the number and the strength of the acid sites. The modification strongly depended on the synthesis procedure [248].

The treatment of Ti-silicalite-1 (TS-1) and silicalite by aqueous solutions of ammonium acetate has been shown to suppress the most energetic sites on these two catalysts, as evidenced by the heats of adsorption which were much lower for the treated samples than for the untreated ones [249], while the number of NH_3 molecules absorbed per Ti atom was unaffected by the treatment in the case of TS-1.

In another study, the heterogeneity of framework Ti (IV) in Ti-silicalite (TS-1) was studied by NH_3 adsorption calorimetry [250] and compared to a Ti-free silicalite taken as reference material. The evolution of the heat of adsorption with coverage was found to be typical of heterogeneous surfaces, due not only to the presence of sites active towards ammonia on the silicalite matrix but also to the heterogeneous distribution of Ti (IV) sites. This suggests that a considerable number of framework sites (among the 12 available in the MFI framework) are occupied in a nearly equally distributed manner.

Engelhard Titanosilicate-10 (ETS-10)

ETS-10 is a titanosilicate with a three-dimensional 12-ring pore system and a very high ion-exchange capacity. Differential heats of ammonia adsorption versus coverage, determined at 423 K, show a plateau of heats around $80\ \mathrm{kJ\ mol^{-1}}$ [251].

Alkali (K, Cs)- and alkaline earth (Mg, Ca, Ba)-exchanged ETS-10 zeolite catalysts have been studied for the cycloaddition of carbon dioxide to propylene oxide [252]. Adsorption microcalorimetry of CO_2 was used to cor-

relate reactivity to the strength and number of CO_2 adsorption sites. The alkali metal-exchanged catalysts were significantly more active than the alkaline earth-exchanged catalysts on a per gram basis, due to stronger CO_2 adsorption sites as indicated by adsorption calorimetry.

Sodium oxide (NaO_x)-impregnated titanosilicate 10 (ETS-10) molecular sieve catalysts were prepared to enhance the basicity associated with ETS-10, and were subsequently investigated for the same reaction [253]. Microcalorimetry of CO_2 adsorption indicated that, at loadings less than 2.0 NaO_x per unit cell, the total number of CO_2 adsorption sites was less than in the parent ETS-10 material. At higher levels of NaO_x occlusion, the total uptake and strength of the adsorption sites exceeded those observed for the parent ETS-10 material, but the activity decreased, due to the reduced pore volume and surface area. It appears that precise tuning of both the surface acidity and basicity is crucial in creating an effective acid-base bifunctional ETS-10 catalyst for the cycloaddition reaction investigated.

Ti-Beta Zeolites

Toluene and water adsorption microcalorimetry experiments have shown the strictly hydrophobic nature of pure SiO_2 zeolite Beta synthesized in F^- medium, while evidencing a slight increase in the hydrophilicity of the materials upon incorporation of Ti into the framework. This was found to be due to the relatively strong adsorption of precisely one H_2O molecule per Ti site. In contrast, materials synthesized in OH^- medium showed an enhanced hydrophilicity [254].

11.2 Chemical Modification

Phosphorus-Modified Zeolites

H-ZSM-5 zeolite modified by phosphorus was studied by means of adsorption microcalorimetry of ammonia for acidity characterization [255]. It was found that phosphorus neutralizes acidic sites primarily at the entrance of the channels of the zeolite particles. However, the strongest acid sites remained unmodified, which suggested that the aluminum distribution and consequently the distribution of acid site strengths along the zeolite channels was heterogeneous.

Boron-Impregnated Zeolites

A microcalorimetric investigation of NH_3 adsorption at 423 K was applied to characterize the modified acidity of ZSM-5 zeolite impregnated with increasing amounts of H_3BO_3 and pretreated at two different temperatures (673 K

and 1073 K) [256]. The former pretreatment was responsible for removing part of the Brönsted sites, while the latter also induced pore plugging, which therefore drastically reduced the indicated overall zeolite acidity. Zeolite impregnation with increasing amounts of H_3BO_3 contributed to an increased loss of acidity.

Modification with Fluorine

H-mordenite modified using ammonium fluoride solutions and gaseous CHF_3 has been studied by Becker et al. [257]. During treatment, some of the acidic OH groups were substituted with fluorine and the acid strength of the remaining hydroxyls was enhanced because of the inductive effect of fluorine. This was reflected in the higher catalytic activity of the samples for cumene cracking and the higher values of the heats of ammonia adsorption. The heats of ammonia adsorption at low surface coverages were significantly higher for the fluorinated sample than for the initial H-mordenite [257].

11.3 Aging and Coke Deposition

The deposition of carbonaceous residues, leading to aging and modification in the acidic properties of three zeolite samples differing by the size and shape of their interconnecting channel networks (ZSM-5, offretite, and mordenite), has been investigated by Dejaifve et al. during the conversion of methanol to hydrocarbons [170]. The initial coking activities were directly related to the availability of acidic sites, while the subsequent coking and aging rates depended on the pore size and the nature of the channel network. No restriction of access to the acid sites (by ammonia) was observed for H-ZSM-5 and H-offretite, but obstructions appeared for H-mordenite. Acid strength distributions were altered in all cases. However, in the particular case of H-ZSM-5, the strongest acidic sites were still present, which indicated that they were located in the intracrystalline volume of the crystallites where little coke was formed due to shape-selective restrictions.

Microcalorimetry experiments using ammonia and pyridine have shown that after aging either under microactivity test (MAT) conditions or in a fluid cracking catalyst unit, a fresh fluid cracking catalyst (FCC) undergoes severe losses in acid site density while retaining most of the strength of its strongest Lewis acid sites. The presence of these sites, and the retention of an open micro- and mesoporous state, are believed to be responsible for the cracking activity of aged FCCs. Moreover, an increase in acidity and microporosity is consistent with the observed enhanced cracking activity, under MAT conditions, of a regenerated FCC [166]. Adsorption microcalorimetry has been also used to characterize some of the effects of coke deposition on a fluid cracking catalyst during gas oil cracking [258].

In another study, microcalorimetric measurements of the differential heats of pyridine adsorption were used to probe the changes in acidic properties caused by the deactivation processes in REY, USY, and Beta zeolites [232]. Coke formation during the isobutane/butene alkylation reaction significantly decreased the acidity and acid strength of the zeolites studied. A fraction of the sites with intermediate strength was lost for all deactivated catalysts. The best catalytic performance and the slowest deactivation were achieved with Beta zeolite, followed by REY and USY. However, the concentration of strong acid sites was found to vary in the opposite order, USY having the strongest acid sites.

11.4 Additives

Zeolites may sometimes contain a metal additive, such as nickel, copper, or a noble metal (Pt), usually for the purpose of improving their performance in hydrogenation–dehydrogenation reactions.

Bifunctional catalysts very often involve a metallic function (alternatively an oxide function). Metal-loaded zeolites are prime examples of bifunctional catalysts for the conversion of linear alkanes into branched alkanes to improve their octane number (RON, MON). Typically, the linear alkanes are dehydrogenated into the corresponding olefins, which are in turn isomerized (over acid sites of the acid function) and subsequently rehydrogenated into the corresponding isoparaffins. However, the presence of olefins over the acidic zeolite matrix is likely to deactivate the zeolite, hence a significant hydrogen pressure is used, so as to hydrogenate possible coke fragments. Because of the presence of hydrogen, however, the first dehydrogenation step:

$$n\mathrm{C}_p\mathrm{H}_{2p+2} \longleftrightarrow n\mathrm{C}_p\mathrm{H}_{2p} + \mathrm{H}_2 \tag{3}$$

is shifted backward, and little olefin is present to be protonated by the acid sites and subsequently isomerized.

$$n\mathrm{C}_p\mathrm{H}_{2p} + \mathrm{ZOH} \longleftrightarrow \mathrm{ZO}^- + n\mathrm{C}_p\mathrm{H}^+_{2p+1} \tag{4}$$

$$\mathrm{ZO}^- + n\mathrm{C}_p\mathrm{H}^+_{2p+1} \longleftrightarrow \mathrm{ZO}^- + i\mathrm{C}_p\mathrm{H}^+_{2p+1} \tag{5}$$

$$\mathrm{ZO}^- + i\mathrm{C}_p\mathrm{H}^+_{2p+1} \longleftrightarrow \mathrm{ZOH} + i\mathrm{C}_p\mathrm{H}_{2p} \tag{6}$$

$$i\mathrm{C}_p\mathrm{H}_{2p} + \mathrm{H}_2 \longleftrightarrow i\mathrm{C}_p\mathrm{H}_{2p+2}\,. \tag{7}$$

Hence, the formation of the carbenium ion is essentially determined by the strength of the acid site, since the concentration of the olefin is always very low due to the hydrogen pressure. Indeed, an increase of the steady state olefin pressure would require a substantial temperature increase, which would be thermodynamically detrimental to isomerization and favorable to cracking of the carbenium ion.

Therefore, highly acidic components have been sought to be associated with the platinum usually thought of as the best dehydrogenation–rehydrogenation function.

Dealuminated H-Y and rare earth Y-type zeolites were first used, and a low platinum content was achieved via cation exchange and subsequent hydrogen reduction [259]. The chemical composition of the samples investigated by Auroux et al. [259] is given in Table 3. The acidity of such catalysts was measured and compared to that of the parent material. The differential heats of NH_3 adsorption as a function of NH_3 coverage over USY and Pt/USY and over RE-Y and Pt/RE-Y are shown in Fig. 17. As can be seen, there was little difference between the parent zeolites and the platinum-loaded ones. On the other hand, quite a large difference was observed both in the adsorption capacity and in the differential and integral heats of adsorption between Pt/USY and Pt/RE-Y, indicating both a higher proton content of Pt/USY and, most interestingly, a higher overall acid strength. These two features may be safely ascribed to the lower cation content of Pt/USY, particularly as far as Na^+ is concerned, and a higher Si/Al ratio.

This difference in acidity was reflected in the hydroisomerization properties of the two catalysts [259]. On the average, temperature increments of 60 K were needed to achieve identical conversions over Pt/RE-Y compared to Pt/USY, in line with the fact that the overall reaction rate is determined by the protonation of the intermediate olefin.

Furthermore, alkane hydrogenolysis, an undesired side reaction, is often encountered over pure platinum particles. It is known that hydrogenolysis is a demanding reaction requiring at least two adjacent platinum atoms. Therefore, alloying the noble metal by an inactive metal such as copper appeared as an appropriate solution to this problem. In addition, because alloying did not modify the size of the bimetallic particles, it increased the total number of those particles and, therefore, the overall number of isolated surface platinum atoms.

Since the acidity is the rate-determining function (because the dehydrogenation equilibrium is achieved very rapidly over the metallic function), it

Table 3 Chemical composition (wt %) of USY, RE-Y (Si/Al = 2.8) and corresponding mono- or bimetallic catalysts (from [259])

	Na	Rare Earth	Pt	Cu
USY	0.15	0	0	0
RE-Y	2.89	13.49	0	0
Pt/USY	0.12	0	0.97	0
Pt/RE-Y	2.20	10.82	0.80	0
Pt,Cu/USY	0.12	0	1.06	0.86
Pt,Cu/RE-Y	1.63	10.82	0.73	0.52

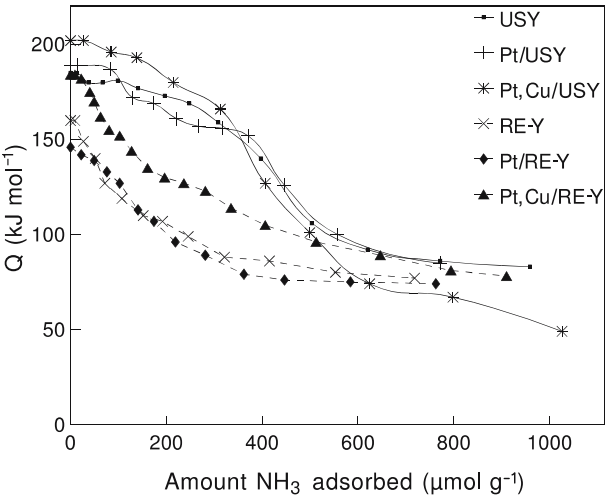

Fig. 17 Differential molar heats of ammonia adsorption on the USY and RE-Y parent zeolites, and the Pt and Pt – Cu modified catalysts (from [259]) versus the adsorbed amount

was interesting to investigate the modification of the acidity of Cu,Pt/USY and Cu,Pt/RE-Y.

The results are shown in Fig. 17. In the case of Cu,Pt/RE-Y a significant increase was observed in both the number and strength of the acid sites, presumably due to further exchange of the Na^+ ions by the Cu^{2+} ultimately converted to $Cu^\circ + 2H^+$ by hydrogen. The increased acid strength may be attributed to the decreased Na^+ content, since Na^+ ions are known to poison one acid site per ion and to strongly moderate the acid strength of vicinal acid sites. However, both the number of acid sites (per unit cell) of Cu,Pt/RE-Y and their strength were lower than those of Cu,Pt/USY. This acidity difference was also reflected by the conversions achieved over these two catalysts [259].

It has been found that introducing certain amounts of Ni, Co, or Cu into a ZSM-5 sample by ion exchange did not enhance markedly the number and strength of the acid sites of the parent zeolite [260]. Co and Ni created some more acid sites in the 100–140 kJ mol^{-1} domain (Fig. 18).

For all these samples, little acidity change could be ascribed to the generation of metallic particles. However, mazzite-supported platinum catalysts have recently been proposed for the hydroisomerization of *n*-alkanes [220, 221]. The variation of the differential heats of adsorption of NH_3 as a function of coverage over H-Mazzite and Pt/H-Mazzite of the same Si/Al ratio has been studied by Auroux et al. [220] at 423 K after activation at 673 K. It was reported that a significant increase of the acid strength was produced by the presence of the metal particles, since the residual Na^+ content was identical for both samples, as was the framework Si/Al ratio [220].

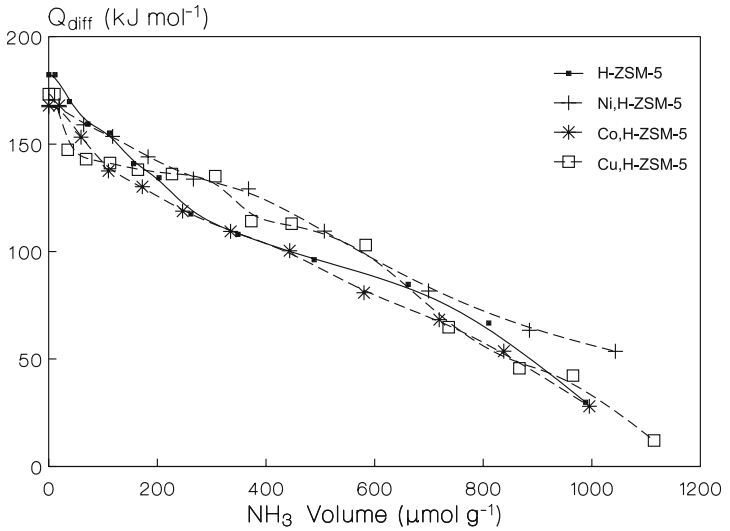

Fig. 18 Differential molar heats of ammonia adsorption at 353 K versus coverage for an H-ZSM-5 zeolite (■) (Si/Al = 28.35) and the corresponding Ni (+), Co (∗) and Cu (□) exchanged zeolites (6.46 wt % Cu, 5.16 wt % Co and 5.84 wt % Ni, respectively). Pretreatment temperature: 623 K (from [260])

This is the first example where the presence of noble metal particles has been claimed to increase the acid strength and consequently the overall number of acid sites of a given strength. The reasons for such an acidity enhancement are not yet known. It could only be speculated that they are probably inherent to the mazzite structure, since it is the only zeolitic matrix where such an effect has been observed. It is also specific to small metal particles, since a low dispersion of the platinum does not induce such an acidity enhancement. Therefore, this phenomenon may be due to an interaction of the acid sites with the metal particles increasing the proton mobility. Such an interaction has been postulated by Sachtler et al. [261], who assumed a total abstraction of the proton from the structural bridging OH (Si – OH...Al) of the zeolite to be transferred over the metal particle to form $(M_nH_p)^{p+}$ particles. The authors have suggested that, if such were the case, these protons would be particularly mobile and would generate higher heats upon NH_3 adsorption.

In another study, a Pt – Zn/X zeolite prepared by sequential addition of Zn and Pt to a 13X zeolite support has been characterized by microcalorimetric measurements of the adsorption of H_2 and C_2H_4 at 300 K and tested in isobutene dehydrogenation [262]. The initial heats of H_2 and C_2H_4 adsorptions were found to be 75 and 122 kJ mol^{-1} respectively.

12
Other Molecular Sieves

Crystalline aluminophosphates, silico-aluminophosphates, and isomorphously substituted aluminophosphates represent a new class of molecular sieves which are considered as potential catalysts and adsorbents [111].

Aluminophosphate molecular sieves exhibit a number of novel crystalline structures as well as analogues of topologies found in zeolites, with a large variety of pore sizes and compositions.

12.1
Aluminophosphates (VPI, $AlPO_4$)

Even though the AlPO lattice is electrically neutral and contains no extra-framework cations, and hence is not expected to exhibit any acidity, the surface hydroxyl groups (Al – OH and P – OH) may possess some residual hydrophilic and acidic character, due to the local electronegativity differences between Al^{3+} and P^{5+}.

Compared to zeolites, aluminophosphate-based molecular sieves seem to have a larger variety of acid sites and a broader acid site distribution. Among the known aluminophosphate molecular sieves, $AlPO_4$-5 and $AlPO_4$-11 have gained considerable attention on account of their straight channel system. $AlPO_4$-5, $AlPO_4$-11, and $AlPO_4$-34 display respectively large-, medium-, and small-sized pores.

VPI-5 is an aluminum phosphate molecular sieve that contains extra-large pores circumscribed by 18-membered oxygen rings with a free diameter of approximately 1.2 nm. VPI-5 is characterized by the absence of an electric field.

Figure 19 displays the differential heats of ammonia adsorption measured at 353 K on an $AlPO_4$-5 sample pretreated at 723 K. Except for the heat at zero coverage, which is around 120 kJ mol^{-1}, the heats range around 60 kJ mol^{-1} and correspond mostly to reversible adsorption at this temperature ($V_{irr} \approx 70$ μmol/g), indicating the absence of strong acid sites on its surface [263].

The differential molar adsorption heats of non-polar molecules such as ethane, *n*-butane, *n*-pentane, and *n*-hexane on $AlPO_4$-11, $AlPO_4$-5, and VPI-5 activated at 670 K have been measured at a temperature of 303 K by Stach et al. [211]. The initial adsorption heats of *n*-paraffins increased with increasing density of the T-atoms (or decreasing pore diameter), and also increased step-by-step with increasing number of CH_2 groups of the probe molecules.

The increase in the zero-coverage heat (Q_0) with an increasing number of CH_2-groups of the adsorbed molecules was found to follow the equation: $Q_0 = 7.0 + 5.75n_C$ (in kJ mol^{-1}) (for VPI-5) where n_C is the number of the C

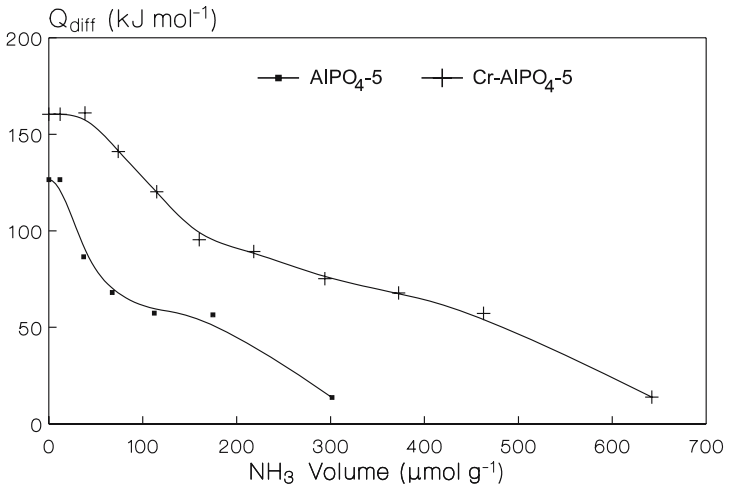

Fig. 19 Differential molar heats of ammonia adsorption at 353 K versus the adsorbed amount for an $AlPO_4$-5 sample (■), P/Al = 1, and a Cr – $AlPO_4$-5 sample (+), P/Al = 1.04, P/Cr = 28, 1.5 wt % Cr. Pretreatment temperature: 723 K (from [263])

atoms of the *n*-paraffins. This linear relationship between the zero-coverage heat of adsorption and the number of C atoms of *n*-paraffins applied also for the adsorption of *n*-paraffins on $AlPO_4$-5 and $AlPO_4$-11 [264]. The corresponding equations were $Q_0 = 7.0 + 8.31n_C$ ($AlPO_4$-5) and $Q_0 = 7.0 + 11.50n_C$ ($AlPO_4$-11). The $AlPO_4$ with the lowest framework density (VPI-5) exhibited the smallest energy of interaction with the *n*-pentane molecules. The $AlPO_4$ with the highest framework density ($AlPO_4$-11) showed the largest heats of adsorption and the smallest adsorption entropies for the *n*-pentane molecules [264].

In the adsorption of non-polar molecules (ethane, *n*-butane, *n*-hexane, benzene, cyclohexane), $AlPO_4$-5 behaves like a homogeneous adsorbent [112]. A linear relationship was found between the adsorption heats of non-polar molecules (ethane, *n*-hexane, and benzene) measured at 303 K and the average effective electronegativity for uncharged microporous solids such as aluminophosphate-type molecular sieves and all-silica molecular sieves. Correlations were confirmed to exist between the initial differential heat, the Gibbs free enthalpy, and the entropy of adsorption on the one hand, and the framework density on the other. An increasing framework density, smaller pore size, and decreasing effective framework electronegativity of molecular sieves increased the heat of adsorption considerably [265]. The adsorption properties of $AlPO_4$-5 and $AlPO_4$-11 were comparable to those of a highly dealuminated mordenite and to silicalite, respectively, because of the similar pore diameters [266].

The sorption of alkanes at 323 K on $AlPO_4$-11 (AEL), $AlPO_4$-5, and its all-silica analogue SSZ-24 (AFI) has been studied by means of combined gravimetry and calorimetry and compared to the sorption on silicalite and highly siliceous faujasite [267]. The samples were pretreated at 673 K. The heats of adsorption of all the alkanes investigated (propane, *n*-butane, *n*-pentane, *n*-hexane, isobutane, isopentane) were identical on the isostructural aluminophosphate and the all-silica samples of AFI, both showing some contribution of intermolecular interactions of the sorbate. This suggested that the sorption of alkanes is mainly governed by the microporous structure and that the chemical composition has only a minor impact on the energetics of sorption. As with acidic samples, the sorption enthalpy increased with decreasing pore diameter and with increasing framework density for all-silica and aluminophosphate-based molecular sieves. Sorption enthalpies of *n*-alkanes exhibited the highest values on $AlPO_4$-11, indicating an excellent fit between the alkanes and the elliptical pores of this structure [267].

Calorimetric measurements at 303 K of the adsorption heats for polar molecules (water, methanol, ethanol) on VPI-5 and $AlPO_4$-11 were performed by Jänchen et al. [268], and the results were compared with the corresponding data on $AlPO_4$-5, two silica molecular sieves, and Na-X. From the measured data, it followed that the adsorption heats on the investigated aluminophosphates were smaller than on the hydrophilic Na-X and larger than on the hydrophobic SiO_2 molecular sieves. Electrically neutral aluminophosphates exhibited a medium hydrophilic character. The stepwise course of the heat curves and isotherms of the polar molecules on VPI-5 may be related to the structure of the as-synthesized VPI-5 as an aluminophosphate dihydrate phase, in accordance with MAS NMR results.

Finally, it is worth noticing that the acidity of thermally stable mesoporous aluminophosphates and silicoaluminophosphates has also been studied by microcalorimetry [269]. By contrast with microporous crystalline aluminophosphate molecular sieves, mesoporous compounds are amorphous and characterized by Al/P ratios greater than 1. These particularities are responsible for a strong Lewis acidity, making these mesoporous materials more acidic than the microporous analogues, with an amount of strong acid sites that increases with the silicon content.

12.2 Silicoaluminophosphates (SAPOs)

In AlPOs, the partial replacement of P^{5+} by Si^{4+} results in a negatively charged framework. This charge deficiency may be compensated by protons, yielding bridging hydroxyl groups as in aluminosilicates, or by exchangeable cations giving rise to the formation of Lewis acid sites.

This is confirmed in Fig. 20, which presents the heats of NH_3 adsorption measured at 423 K on a SAPO-5 ($Si/(Si + Al + P) = 0.077$) and a SAPO-37

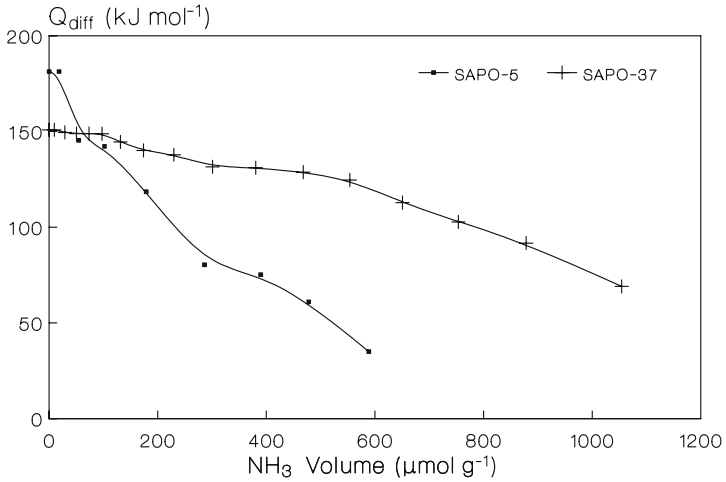

Fig. 20 Differential molar heats of ammonia adsorption at 423 K versus the adsorbed amount for a SAPO-5 sample (Si/(Si + Al + P) = 0.077, 1.85 Si/u.c.) and a SAPO-37 sample (Si/(Si + Al + P) = 0.20, 38 Si/u.c.). Pretreatment temperature: 773 K (from [270])

(Si/(Si + Al + P) = 0.20) after activation at 773 K [270]. SAPO-37 has the same structure as faujasite (3D), while SAPO-5 has an AFI-type structure (1D) with similar pore diameters of 0.74 and 0.73 nm. As can be seen in Fig. 20, the crystalline silico-aluminophosphate SAPO-5 contains rather strong Brönsted acid sites in contrast to aluminophosphate $AlPO_4$-5. The structural OH groups differ in their accessibility to adsorbed ammonia. SAPO-37 displays a broad range of Brönsted sites exhibiting heats of adsorption between 150 and 130 kJ mol^{-1}, showing a rather homogeneous distribution of its acidic sites.

The amounts of strong sites correlate with the concentration of Si in the molecular sieves. Isostructural faujasite (X, Y) and SAPO-37 make it possible to study the influence of the incorporation of P into a framework on its acidity and to compare it with H-Y. The acid strength of SAPO-37 is lower than for the corresponding USY zeolites (see Figs. 17 and 20).

Calorimetric measurements of the heats of ammonia chemisorption have shown that the numbers of Brönsted acid sites and the acid strengths of SAPO-5, SAPO-11, SAPO-17, SAPO-31, and SAPO-34 are different, and in the cases of SAPO-5 and SAPO-34 comparable with the corresponding data for H-ZSM-5 [271]. The density of the Brönsted sites was found to vary in the order SAPO-34 > SAPO-5 > SAPO-11 > SAPO-17. While the heat curves for SAPO-34 and SAPO-5 indicated a stepwise decrease with increasing adsorbed amount, the heat curves of SAPO-11 and SAPO-31 were smoothly decreasing with ammonia coverage. The adsorption heats of the strongest acidic sites in the investigated SAPOs corresponded to those found for H-ZSM-5, exceeding the strength of those of H-Y zeolites. The initial heats of adsorption were about 140 kJ mol^{-1} for SAPO-34 and SAPO-5 and around 130 kJ mol^{-1}

for SAPO-11, -17 or -31 [271]. The maximum number of acid sites varied from 0.3 mmol g^{-1} (for SAPO-31) to 1.1 mmol g^{-1} (for SAPO-34) which corresponded to the number of acid sites found for a H-ZSM-5 sample with a Si/Al ratio of 20. Calorimetric measurements of the heats of adsorption on SAPO-17 with various silicon contents in the framework showed that, while the acid strength did not change, the number of acid sites increased with rising Si content [271].

The measured acidity depends very likely on the Si content (1.85 Si/u.c. for SAPO-5 and 38 Si/u.c. for SAPO-37) but also on experimental conditions changing from one study to another. With regard to the effect of Si content on acidity, a first point is that the number of protons cannot be deduced simply from the chemical analysis, i.e. from the Si content. More work is needed in order to be able to correlate exactly the acidic properties with the Si location in the lattice. The acidity (amount and strength) depends not only on the considered structural type but also on the mode of substitution of Si. At high Si levels, SAPO-5 contains a large amount of Si in siliceous patches; it may thus be expected that the number of protons is lower than that of Si atoms.

SAPO-44 samples prepared with different silicon contents up to 34.3 wt % SiO_2 have been characterized by NH_3 sorption microcalorimetry at 423 K. The number of acid sites was found to be independent of the SiO_2 content of the samples, and three plateaus of constant interaction energy could be distinguished, in accordance with the number of acid sites per unit cell [272].

12.3 Metal Aluminophosphates (MeAPOs)

The framework of metal aluminophosphates contains a metal (e.g., Cr, Co, Mn, etc.) in addition to Al and P. The replacement of aluminum by bivalent cations such as Mg^{2+}, Mn^{2+}, Co^{2+}, or Zn^{2+} in aluminophosphate molecular sieves gives rise to the formation of acidic sites.

The differential heats of adsorption of NH_3 on a CrAPO sample are plotted versus coverage in Fig. 19, comparatively to the AlPO sample previously described and explored under the same conditions [263]. The amount of NH_3 irreversibly adsorbed at 353 K approached 300 μmol/g for this sample and the initial heats were around 160 kJ mol^{-1}.

Measurements by Jänchen et al. [273] of the heats of adsorption of acetonitrile at 295 K on metal-substituted $AlPO_4$-5 and $AlPO_4$-11 (Me = Mg^{2+}, Mn^{2+}, Co^{2+}, or Zn^{2+}) in comparison to the pure AlPOs indicated the formation of strong acidic sites. Besides these strong sites, some weaker acidic centers, probably P – OH groups, were found [273]. It follows from these results that the incorporation of Me^{2+} into AFI and AEL structures results in the formation of strong adsorption sites (above 75 kJ mol^{-1}) which are not present in the pure AlPOs. The differential heat curves evidenced the presence of two distinguishable types of acid sites. The heats of the strongest

centers of each MeAPO-5 amounted to 100–85 kJ mol^{-1}, higher than found for the Brönsted sites in SAPO-5 or H-Y (80 kJ mol^{-1}) with the same probe molecule. The second type of acid sites generated heats of approximately 70–50 kJ mol^{-1}, probably due to weak acidic P – OHs which were additionally formed by the Me^{2+} incorporation. In comparison, $AlPO_4$-5 was found to possess only weak P – OH sites. The authors [273] also suggested that the slightly higher chemisorption heats of the AEL in comparison to the AFI samples were related to the smaller AEL pores compared to AFI. The amount of the strong acid sites correlated with the concentration of Me^{2+} in the molecular sieves.

The acidity of MgAPO molecular sieves of CHA and AFI structures has been studied by Lohse et al. [274]. The characteristics of the differential heat curves of NH_3 adsorption at 423 K as determined by microcalorimetry were found to agree with those observed for SAPO-44 and H-Y. These results also provide evidence for the existence of isolated bridging hydroxyls. The number of acid sites created by the Mg^{2+} incorporation was determined assuming that the number of acid sites is equal to the number of Mg atoms on tetrahedrally coordinated lattice positions.

Calorimetric measurements of adsorption of NH_3 at 300 K in $AlPO_4$-5 and FAPO-5 molecular sieves have also been reported [275].

The acidic properties of cobalt and silicon-substituted AlPO-5, -11, and -44 have been characterized by Jänchen et al. [111, 276] by adsorption calorimetry of acetonitrile at 303 K, after activation at 720 K. Adsorption calorimetric measurements indicated that the adsorption potential of the samples for acetonitrile was enhanced upon cobalt incorporation. The heat curves exhibited at least two steps indicating the existence of acid sites of different strengths. The heats of adsorption indicated the formation of strong acid sites, due to the cobalt incorporation, as well as the presence of weaker acid sites, probably terminal P – OH groups.

The heat curves of the CoAPOs showed a stepwise course which was also observed for the sorption of ammonia on Y zeolites and SAPO-5. The heat curve of CoAPO-11 was shifted by ca. 15 kJ mol^{-1} towards higher heats compared with CoAPO-5, probably due to the smaller pore diameter of CoAPO-11. It was suggested that this difference in the heats of acetonitrile chemisorption could be due to different terms of the dispersion interaction of these two molecular sieves and not to differences in acidic strength of the centers [276]. The acidic sites found on CoAPO-5 (100 kJ mol^{-1}) and CoAPO-11 (110 kJ mol^{-1}) were stronger than the bridging hydroxyl groups or the Lewis sites in H-Y. The second step in the heat curves of the CoAPOs, beginning at 70 kJ mol^{-1} (CoAPO-5) and 80 kJ mol^{-1} (CoAPO-11), was due to medium-strength sites, probably P – OH, which are known to be weaker than bridging OH but stronger than silanols [111].

AFI materials have also been studied by microcalorimetry using ammonia as a probe molecule at 423 K by Yuen et al. [277]. The results indicated

differences in the acid strength and relative populations for four AFI materials (BSSZ-24, Al-SSZ-24, SAPO-5, and MAPO-5). Both SAPO-5 and MAPO-5 showed weaker sites which were not detected in the Al-SSZ-24. The divalent Mg cations generated Lewis acidity and were able to interact with NH_3.

12.4 Mesoporous Materials (such as MCM-41)

Since their relatively recent discovery, ordered mesoporous materials have attracted much interest because of their high surface area and uniform distribution of mesopore diameters. Because of its hexagonal array of uniform one-dimensional mesopores, varying in diameter from 1.5 to 10 nm, MCM-41 is a potentially interesting catalyst for converting large molecules of nondistillable feeds to fuels and other products. To impart the desired catalytic activity to the inert silicate framework, synthesis conditions have been modified to introduce the desired Al concentration into the wall of the different nanostructures. The amount of Brönsted acid sites in MCM-41 is lower than in USY zeolite (see Figs. 17 and 21).

The methods for measuring the acidity of nanoporous aluminosilicates such as MCM-41 have been reviewed by Zheng et al. [278], including microcalorimetric measurement of the heats of adsorption of probe molecules.

Acetonitrile adsorption studies on ordered mesoporous molecular sieves (MCM 41) with varying Si/Al ratios have been performed by Jänchen

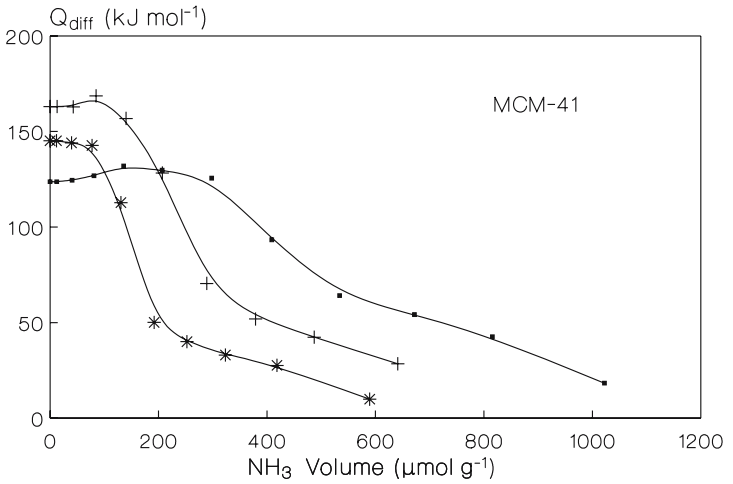

Fig. 21 Differential molar heats of ammonia adsorption at 353 K versus the adsorbed amount for MCM-41 samples. Pretreatment temperature: 673 K. • prepared from Al isopropoxide, Si/Al = 4.4, + prepared from $NaAlO_2$ (Si/Al = 20), ∗ prepared from $NaAlO_2$ (Si/Al = 33) (from [280])

et al. [279]. The combined study by microcalorimetry and FTIR, using acetonitrile as a probe, showed a few strong Lewis sites and only weak Brönsted acidity. The concentrations of both kinds of sites corresponded approximately to the amount of Al in the MCM 41 samples.

Acidity measurements of MCM-41 samples with Si/Al ratios varying from 4 to 30 have been performed at 353 K after pretreatment at 673 K using NH_3 adsorption microcalorimetry by Occelli et al. [280]. The initial heats of ammonia adsorption varied from 165 to 120 kJ mol^{-1} depending on the source of aluminum used for synthesis (Al hydroxide, Al isopropoxide or sodium aluminate) and on the Al(VI)/Al(IV) ratio in the material. For samples prepared using Al hydroxide, a fairly heterogeneous distribution of sites was observed. The high initial heats (ca. 150 kJ mol^{-1}) were attributed to extra-framework aluminum species and correlated with Al(IV)/Al(VI) values. The acid site strength monotonically decreased with coverage. Samples prepared using sodium aluminate or Al isopropoxide gave differential heat profiles different from that obtained when Al hydroxide was used, with a large plateau of initial heats of adsorption (between 120 and 160 kJ mol^{-1}). In these samples, there was no evidence of NH_3 chemisorption by extra-framework Al species (Fig. 21).

Let us also mention a combined microcalorimetry and adsorption study aimed at characterizing the surface acidity of a series of MCM-41 aluminosilicates (referred to as $SiAl_xC_n$, where x is the molar Si : Al ratio and n the chain length of the surfactant template). With the exception of $H-SiAl_{32}C_{14}$ and $SiAl_8C_{14}$, all samples were found to present low surface acidity [281]. The behavior of these materials in liquid phase (adsorption of 1-butanol and immersion in various solvents) has also been studied [282].

Isosteric heats of water adsorption on MCM-41 have been measured at 287 and 397 K [283] and were found to increase with uptake to a value of around 58 kJ mol^{-1}, which is somewhat higher than the enthalpy of liquefaction (44 kJ mol^{-1}). The authors suggested that initially a hydrophobic water-MCM41 interaction occurred, followed by a more important water-water interaction.

The isomorphous substitution of Si with Ti and Zr in mesoporous silicates with MCM-41 structure has also been studied by means of NH_3 microcalorimetry experiments [284]. These materials are weakly acidic solids, and the introduction of Ti or Zr into the mesoporous silicate framework has been found to increase the acidity in the order: silica-gel $\ll$ Si-MCM-41 < (Si,Zr)-MCM-41 < (Si,Ti)-MCM-41. However, this acidity remains significantly lower than that of the corresponding mesoporous aluminosilicates.

The acid properties of Al-, Ga-, and Fe-substituted MCM-41-type mesoporous silicates have been probed using ammonia adsorption at 423 K [285]. Substitution led to the formation of Brönsted and Lewis acid sites of different type and strength. Initial heats of ammonia chemisorption decreased in the same order (185 (Al) > 162 (Ga) > 144 (Fe) kJ mol^{-1}) as the degree of isomorphous substitution of framework silicon by trivalent atoms. The ratio of strong to medium-strong Brönsted sites fell in the same order.

A similar study performed on Al-, Ga-, and Fe-MCM-48 molecular sieves confirmed the existence of a correlation between the acid strength of Brönsted sites and the nature of the substituting element [286]. The average acidic strength of sites was found to be lower than that observed for acidic zeolites. The majority of the sites presented a medium-to-weak strength, but very weak (< 50 kJ mol^{-1}) and strong (140 to 155 kJ mol^{-1}) sites were also present. On pure siliceous MCM-48, the mean value of the heat of ammonia adsorption amounted to 50 kJ mol^{-1}.

The acidity of a series of MCM-41 mesoporous materials has been investigated by microcalorimetry using ammonia adsorption at 423 K [287], giving rise to the following acid strength sequence: H-[AlSi]-MCM-41 > [AlSi]-MCM-41 > [FeSi]-MCM-41 > [LaSi]-MCM-41.

Other types of mesoporous materials have also attracted attention. For example, HMS (hexagonal mesoporous silicate) materials may be prepared with different Al contents, similarly to common zeolites. HMS samples with an Si/Al ratio = 2.5, either in the H form or after partial exchange with Li^+ or Na^+ cations, exhibit much less marked acidic/basic properties than comparable zeolites, though their chemical composition is close to that of Y zeolites [288]. Differential heats of CO_2 adsorption at low coverage of 32 and 26 kJ mol^{-1} were measured on the Li and Na-exchanged samples respectively. This feature is ascribed to the amorphous nature of the walls, to be contrasted with the crystalline structure of zeolites [288].

13
Relationship to Catalytic Activity

In acid catalysis, the catalytic activity is usually related to the number of Brönsted sites rather than to that of Lewis acid sites. However, the influence of acidic Lewis sites in catalytic reactions over zeolites is still controversial and cannot be neglected. Moreover, it is important to discriminate between the strength of given categories of acid sites and the total acidity. For example, the total acidity must be sufficient for the catalytic process to take place, but in order to prevent an excessive polymerization the presence of very strong acid sites must be avoided.

It is well known that coke formation significantly decreases the acidity and acid strength of catalysts. However, it is not so easy to find direct correlations between the heats of adsorption and the catalytic behavior (activity and/or selectivity) of the samples. Some attempts establishing such correlations have been reported in the literature.

For instance, the combination of microcalorimetric measurements with kinetic studies performed over acidic zeolites for methylamine disproportionation reactions, methanol dehydration, and reactions of methanol and dimethylether with methylamines suggests that acid sites are required in

these reactions for the strong adsorption of ammonia and methylamines, while weak adsorption sites are required to facilitate desorption of adsorbed amine species from the acid sites [289].

The variation of cracking selectivity in the conversion of alkanes over various substituted MFI zeolites has been correlated with the basicity of the C – C bond of the alkane, while the selectivity towards dehydrogenation was found to be related to the attenuation of the acid strength of the zeolite [244].

Catalytic tests of Prins condensation of isobutylene with formaldehyde over iron-substituted MFI catalysts have shown that medium to weak acid strength sites favor the selectivity to isoprene [241]. [Ga]-ZSM5 was also tested as a catalyst for this condensation, but its catalytic selectivity was rather close to that of [Al]-ZSM5 [241].

Microcalorimetric measurements of the differential heats of pyridine adsorption have also been used to probe the changes in acid properties caused by the deactivation processes occurring on a series of zeolites (RE-Y, USY, Beta) during the isobutane/butene alkylation reaction. Brönsted sites with intermediate acid strength appeared to be the appropriate sites for maintaining good catalytic performance in alkylation [232].

NH_3 adsorption microcalorimetry has been used to characterize the acid sites of an H-USY zeolite and another USY sample in which the strong Lewis acid sites were poisoned with ammonia. It was found that poisoning of the Lewis acid sites did not affect the rate of deactivation, the cracking activity, and the distribution of cracked products during 2-methylpentane cracking. Thus, strong Lewis acid sites do not seem to play any important role in the cracking reactions [290].

The effect of the Si/Al ratio of H-ZSM-5 zeolite-based catalysts on surface acidity and on selectivity in the transformation of methanol into hydrocarbons has been studied using adsorption calorimetry of ammonia and *tert*-butylamine. The observed increase in light olefin selectivity and decrease in methanol conversion with increasing Si/Al ratio can be explained by a decrease in total acidity [189].

However, it is worth noticing that experiments aimed at directly comparing the cracking activity and the enthalpy of adsorption of basic probe molecules have sometimes failed to make correlative conclusions. For example, Gorte et al. [242] detected no difference in the enthalpies of ammonia or pyridine adsorption on H-[Al]-ZSM-5, H-[Ga]-ZSM-5, and H-[Fe]-ZSM-5 samples, the cracking activities of which were quite different. Likewise, in a study on dealuminated Y zeolites, no significant differences in the highest enthalpies of adsorption could be detected by microcalorimetry for samples of different cracking activities [49]. Kuehne et al. [155] confirmed these conclusions by the results of another study where a $57\,kJ\,mol^{-1}$ difference in the enthalpy of ammonia adsorption was detected between H-Y and an (H, NH_4)-USY sample, although the latter was 33 times more active than H-Y in 2-methylpentane cracking.

The acid/base properties of zeolites are often studied by controlling the selectivity to the different products in the decomposition of alcohols and particularly isopropanol. The rate of propene formation can very often be correlated to the number of acidic sites determined from ammonia adsorption.

For instance, two series of alkali-metal ion-exchanged zeolites have been investigated in order to analyze the possible correlations between the acidity and basicity of the X and Y zeolite structures and their catalytic properties [137]. The catalytic results for the 4-methylpentan-2-ol conversion show that activity and selectivity are both affected to some extent by the acid-base character of the catalysts. The activity was found to increase from Cs to Li for both X and Y zeolites. The dehydrogenation reaction occurred only on Cs-X+Cs_2O, which presents very strong basicity. The product selectivity of the reaction was found to depend on both Lewis acidity and basicity; Lewis basic or acidic sites of zeolites can be considered as acid-base pairs, in which both basic framework oxygens and neighboring cations are important [137].

Among the various catalysts investigated in the literature, the copper-exchanged ZSM5 zeolite has generated a great deal of interest as a potential catalyst for NO_x removal. The differences in the activity of the copper sites have been determined by studying the adsorption properties of the catalysts (copper-exchanged ZSM-5 and ETS-10) towards NO and CO probes and the corresponding adsorption energies. Carbon monoxide was found to strongly adsorb preferentially on Cu^+ ion species [291], while NO could be more specifically adsorbed on isolated Cu^{2+} species. The samples presenting the best NO adsorption properties were also the most active in the reaction of NO reduction by hydrocarbons [251, 292]. The energy distribution of the copper sites towards NO adsorption has also been determined using the method of isosteres [293, 294].

The interaction energies of NH_3 with Cu^+ and Ag^+ metal cations dispersed in ZSM-5 zeolites have been studied by means of adsorption calorimetry [295]. Two different families of coordinatively unsaturated metal cations were evidenced. A (rather heterogeneous) fraction of the reversibly bound ligands were found to be more energetic, their interaction with the sites giving rise to a heat comprised in the 100–150 kJ mol^{-1} interval. The other ligands interacted more weakly with the metal sites, with a nearly constant heat of ca. 50 kJ mol^{-1} [295].

The acidic function of bifunctional catalysts (Pt – Cu alloys in REY and USY zeolites) has also been studied by microcalorimetry, using ammonia as the probe, in relation to the catalytic conversion of *n*-alkanes to isoalkanes or cracked products. Although the acidity and the bifunctional catalytic performances of the copper-exchanged Pt-REY are improved, these materials are much less efficient than the corresponding USY samples. The activation of USY and the reduction of the Pt – Cu-USY catalysts generate in all cases the same number of protons [259].

14 Conclusion

This survey has demonstrated that adsorption microcalorimetry may be used successfully in order to probe acid site strengths, to obtain the relative populations of Brönsted and Lewis acid sites, and to determine their number quite exactly. However, a closer correlation between site strength and site type (preferably by combining microcalorimetry with IR spectroscopy) would result in a clearer description of the acidity of zeolites.

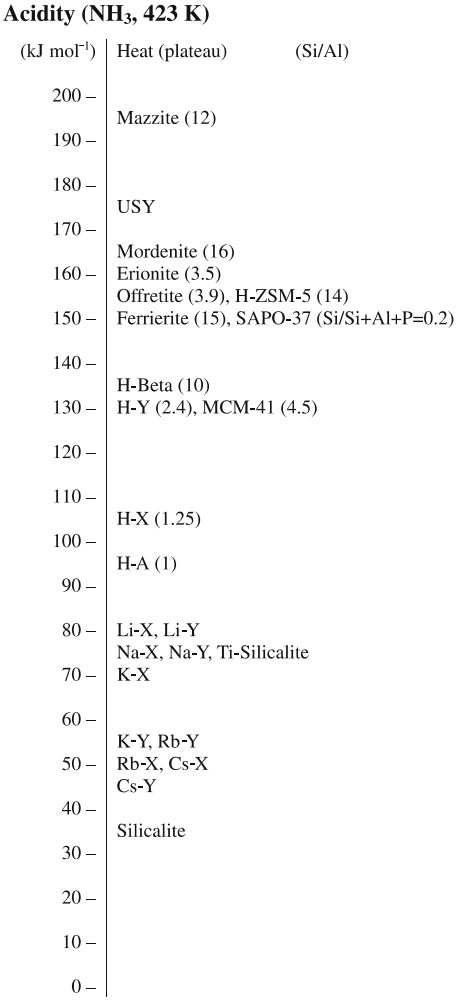

Fig. 22 Scale of acid strength of various zeolites as determined by ammonia adsorption microcalorimetry at 423 K (from [296])

The information that is presently available on the heat of adsorption of gases and vapors by zeolites is very extensive, but only a small part of the experimental data are sufficiently reliable to be regarded as thermodynamic constants characterizing the equilibrium in zeolite/adsorbate systems.

At present, the available results tend to indicate that the chemical composition is more important than the structure of the zeolite lattice.

Precise measurements of the numbers of acid sites of a variety of zeolites and dealuminated zeolites, as obtained from ammonia adsorption experiments, reveal that acid site amounts in zeolites are sometimes not simply correlated with the framework Al content. Therefore, it appears necessary to clarify the relationship between the acid site density and the framework Al content in zeolites and, ultimately, establish a better conceptual understanding of the acidity of zeolites.

Nonetheless, an attempt has been made at establishing a scale of strength of the acid/base sites of various zeolites as determined by ammonia adsorption calorimetry: see Fig. 22 [296].

References

1. Rabo JA, Gajda GJ (1989–1990) Catal Rev Sci Eng 31:385
2. Farneth WE, Gorte RJ (1995) Chem Rev 95:615
3. Guisnet M (1985) In: Imelik B, Naccache C, Coudurier G, Ben Taarit Y, Vedrine JC (eds) Catalysis by Acids and Bases. Proc Int Symp, Ecully (Lyon), September 26–27, 1984. Elsevier, Amsterdam, 1985, p 283; Stud Surf Sci Catal 20:283
4. Eichler U, Braendle M, Sauer J (1997) J Phys Chem B 101:10035
5. Cardona-Martinez N, Dumesic JA (1992) Adv Catal 38:149
6. Andersen PJ, Kung HH (1995) Catalysis. Royal Society of Chemistry 11:441
7. Gravelle PC (1972) Adv Catal 22:191
8. Gravelle PC (1977) Catal Rev Sci Eng 16:37
9. Gravelle PC (1985) Thermochim Acta 96:365
10. Auroux A (1994) In: Imelik B, Vedrine JC (eds) Catalyst characterization: Physical techniques for solid Materials. Plenum Press, New York, p 611
11. Auroux A (1997) Topics in Catalysis 4:71
12. Fubini B (1988) Thermochim Acta 135:19
13. Della Gatta G (1985) Thermochim Acta 96:349
14. Cerny S, Ponec V (1968) Catal Rev 2:249
15. Solinas V, Ferino I (1998) Catal Today 41:179
16. Spiewak BE, Dumesic JA (1996) Thermochim Acta 290:43
17. Spiewak BE, Dumesic JA (1998) Thermochim Acta 312:95
18. Parillo DJ, Gorte RJ (1998) Thermochim Acta 312:125
19. Auroux A (2002) Topics in Catal 19:205
20. Baerlocher C, Meier WM, Olson DH (1996) Atlas of zeolite framework types, 5th edn. Elsevier, Amsterdam, p 302
21. Stach H, Lohse U, Thamm H, Schirmer W (1986) Zeolites 6:74
22. Klyachko AL, Brueva TR, Mishin IV, Kapustin GI, Rubinshtein AM (1978) In: Fejes P (ed) Proc Int Symp Zeolites. Szeged, Hungary, Sept 11–14, 1978; Acta Phys et Chem Nova Series XXIV:183

23. Auroux A, Jin YS, Védrine JC, Benoist L (1988) Appl Catal 36:323
24. Fesenko EA, Barnes PA, Parkes GMB, Brown DR, Naderi M (2001) J Phys Chem B 105:6178
25. Chen D, Sharma S, Cardona-Martinez N, Dumesic JA, Bell VA, Hodge GD, Madon RJ (1992) J Catal 136:392
26. Klyachko AL, Brueva TR, Mishin IV, Kapustin GI, Rubinshtein AM (1978) Acta Phys Chem 24:183
27. Auroux A, Huang M, Kaliaguine S (1996) Langmuir 12:4803
28. Ferino I, Monaci R, Rombi E, Solinas V (1998) J Chem Soc Faraday Trans 94:2647
29. Kapustin GI, Brueva TR, Klyachko AL, Rubinshtein AM (1981) Kinet Katal 22:1247
30. Brueva TR, Kapustin GI, Mishin IV (2001) Thermochim Acta 379:35
31. Brown DR, Groszek AJ (2000) Langmuir 16:4207
32. Groszek AJ (1998 and 1999) Thermochim Acta 312:133; In: Dabrowski A (ed) (1999) Adsorption and its application in industry and environmental protection. Stud Surf Sci Catal 120A:143
33. Aguayo AT, Gayubo AG, Erena J, Olazar M, Arandes JM, Bilbao J (1994) J Chem Tech Biotechnol 60:141
34. Sinev MY, Bychkov VY (1999) Kinet Catal 40:819
35. Zajac J, Dutartre R, Jones DJ, Rozière J (2001) Thermochim Acta 379:123
36. Drago RS, Dias SC, Torrealba M, de Lima L (1997) J Am Chem Soc 119:4444
37. Drago RS, Dias SC, Mc Gilvray JM, Mateus ALML (1998) J Phys Chem B 102:1508
38. Savitz S, Myers AL, Gorte RJ, White D (1998 and 1999) J Am Chem Soc 120:5701 and Micropor Mesopor Mat 31:211
39. De Macedo JL, Dias SCL, Dias JA (2004) Micropor Mesopor Mat 72:119
40. Silvestre-Albero J, Sepulveda-Escribano A, Rodriguez-Reinoso F (2002) In: Rodriguez-Reinoso F, McEnaney B, Rouquerol J, Unger KK (eds) Proc 6th Int Symp on the Characterization of Porous Solids (COPS-VI), Alicante, Spain, May 8–11, 2002. Elsevier, Amsterdam, p107; Stud Surf Sci Catal 144:107
41. Chen DT, Zhang L, Chen Yi, Dumesic JA (1994) J Catal 146:257
42. Siperstein F, Gorte RJ, Myers AL (1999) Langmuir 15:1570
43. Dunne JA, Rao M, Sircar S, Gorte RJ, Myers AL (1997) Langmuir 13:4333
44. Coker EN, Karge HG (1997) Rev Sci Instrum 68:4521
45. Guimon C, Martinez H (2003) Recent Res Develop Catal 2:99
46. Mishin IV, Klyachko AL, Kapustin GI, Karge HG (1993) Kinet Catal 34:828
47. Klyachko AL, Brueva TR, Rubinshtein AM (1979) Kinet Catal 20:1256
48. Mitani Y, Tsutsumi K, Takahashi H (1986) Colloid Polym Sci 264:445
49. Biaglow AI, Parrillo DJ, Kokotailo GT, Gorte RJ (1994) J Catal 148:213
50. Parrillo DJ, Lee C, Gorte RJ (1994) Appl Catal A-Gen 110:67
51. Auroux A, Gravelle PC, Védrine JC, Rekas M (1980) In: Rees LVC (ed) Proc 5th Int Zeolite Conf, Naples, Italy, June 2–6, 1980, LV, Heyden, London, p 433
52. Babitz SM, Williams BA, Kuehne MA, Kung HH, Miller JT (1998) Thermochim Acta 312:17
53. Auroux A, Muscas M, Coster DJ, Fripiat JJ (1994) Catal Lett 28:179–186
54. Rudzinski W, Everett DH (1992) In: Adsorption of gases on heterogeneous surfaces. Academic Press, London, p 608
55. Chen DT, Sharma SB, Filimonov I, Dumesic JA (1992) Catal Lett 12:201
56. Levitz P, Blumenfeld AL, Fripiat JJ (1996) Catal Lett 381:11
57. Barthomeuf D (1987) In: Ward JW (ed) (1988) Catalysis 1987, Proc 10th North Am Meeting of the Catalysis Society, San Diego, CA, USA, May 17–22, 1987. Elsevier, Amsterdam, p 177; Stud Surf Sci Catal 38:177

58. Stach H, Jänchen J (1992) Zeolites 12:152
59. Barthomeuf D (1988) Mater Chem Phys 18:553
60. Huang M, Kaliaguine S, Muscas M, Auroux A (1995) J Catal 157:266–269
61. Dragoi B, Gervasini A, Dumitriu E, Auroux A (2004) Thermochim Acta 420:127
62. Stach H, Jänchen J, Lohse U (1992) Catal Lett 13:389
63. Stach H, Jänchen J, Jerschkewitz HG, Lohse U, Parlitz B, Hunger M (1992) J Phys Chem 96:8480
64. Tsutsumi K, Kawai T, Yanagihara T (1994) In: Hattori T, Yashima T (eds) (1994) Proc Int Symp on Zeolites and Microporous Crystals, Nagoya, Japan, August 22–25, 1993. Elsevier, Amsterdam, p 217; Stud Surf Sci Catal 83:217
65. Khvoshchev SS, Vasil'eva EA (1982) Izvest Akad Nauk SSSR Ser Khim 5:973
66. Cartraud P, Chauveau B, Bernard M, Cointot A (1977) J Therm Anal 11:51
67. Dunne JA, Rao M, Sircar S, Gorte RJ, Myers AL (1996) Langmuir 12:5896
68. Boreave A, Auroux A, Guimon C (1997) Micropor Mat 11:275
69. Gorte RJ, White D (1997) Topics in Catal 4:57
70. Gorte RJ (1999) Catal Lett 62:1
71. Sepa J, Lee CC, Gorte RJ, White D (1996) In: Hightower JW, Delgass WN, Iglesia E, Bell AT (eds) Proc 11th Congress on Catalysis, Baltimore, Maryland, USA, June 30–July 5, 1996, PO 144
72. Jänchen J, Stach H, Busio M, van Wolput JHMC (1998) Thermochim Acta 312:33
73. Kotrla J, Kubelkova L, Lee CC, Gorte RJ (1998) J Phys Chem B 102:1437
74. Yang L, Trafford K, Kresnawahjuesa O, Sepa J, Gorte RJ, White D (2001) J Phys Chem B 105:1935
75. Lee CC, Gorte RJ, Farneth WE (1997) J Phys Chem B 101:3811
76. Sepa J, Lee C, Gorte RJ, White D, Kassab E, Evleth EM, Jessri H, Allavena M (1996) J Phys Chem 100:18515
77. Witzel F, Karge HG, Gutsze A (1992) In: von Ballmoos R, Higgins JB, Treacy MMJ (eds) (1993) Proc 9th Int Zeolite Conf, Montreal, Canada, July 5–10, 1992. Butterworth-Heinemann, Boston, Vol II, p 283
78. Llewellyn PL, Coulomb JP, Grillet Y, Patarin J, André G, Rouquerol J (1993) Langmuir 9:1852
79. Savitz S, Myers AL, Gorte RJ (2000 and 1999) Micropor Mesopor Mat 37:33; J Phys Chem B 103:3687
80. Parrillo DJ, Gorte RJ (1993) J Phys Chem 97:8786
81. Lee C, Parillo DJ, Gorte RJ, Farneth WE (1996) J Am Chem Soc 118:3262
82. Parrillo DJ, Gorte RJ, Farneth WE (1993) J Am Chem Soc 115:12441
83. Parrillo DJ, Gorte RJ (1992) Catal Lett 16:17
84. Auroux A (1988) In: Grobet PJ, Mortier WJ, Vansant EF, Schulz-Ekloff G (eds) Innovation in zeolite materials science, Proc Int Symp, Nieuwpoort, Belgium, September 13–17, 1987. Elsevier, Amsterdam, p 385; Stud Surf Sci Catal 37:385
85. Auroux A, Shi ZC, Echoufi N, Ben Taarit Y (1989) In: Karge HG, Weitkamp J (eds) Zeolites as catalysts, sorbents and detergent builders; Proc Int Symp, Würzburg, Germany, September 4–8, 1988. Elsevier, Amsterdam, p 377; Stud Surf Sci Catal 46:377
86. Coker EN, Jia C, Karge HG (2000) Langmuir 16:1205
87. Corma A, Fornes V, Guil JM, Pergher S, Maesen ThLM, Buglass JG (2000) Micropor Mesopor Mat 38:301
88. Mellot C, Simonot-Grange MH, Pilverdier E, Bellat JP, Espinat D (1995) Langmuir 11:1726

89. Guil JM, Guil-Lopez R, Perdigon-Melon JA (2000) In: Corma A, Melo FV, Mendioroz S, Fierro JLG (eds) Proc 12th Int Congress on Catalysis, Granada, Spain, July 9–14, 2000. Elsevier, Amsterdam, p 2927; Stud Surf Sci Catal 130:2927
90. Eder F, Lercher JA (1997) Zeolites 18:75; (1997) J Phys Chem B 101:1273
91. Eder F, Stockenhuber M, Lercher JA (1997) J Phys Chem B 101:5414
92. Yang S, Navrotsky A (2000) Micropor Mesopor Mat 37:175
93. Moïse JC, Bellat JP, Méthivier A (2001) Micropor Mesopor Mat 43:91
94. Corma A, Corell C, Perez-Pariente J, Guil JM, Guil-Lopez R, Nicolopoulos S, Gonzalez Calbet J, Vallet-Regi M (1996) Zeolites 16:7
95. Guil JM, Guil-Lopez R, Perdigon-Melon JA, Corma A (1998) Micropor Mesopor Mat 22:269
96. Corma A, Chica A, Guil JM, Llopis FJ, Mabilon G, Perdigon-Melon JA, Valencia S (2000) J Catal 189:382
97. Van Well WJM, Jänchen J, de Haan JW, van Santen RA (1999) J Phys Chem B 103:1841
98. Pinard L, Mijoin J, Magnoux P, Guisnet M (2003) J Catal 215:234
99. Karge HG, Jozefowicz LC (1994) In: Weitkamp J, Karge HG, Pfeifer H, Hölderich W (eds) Zeolites and related microporous materials: State of the art, 1994. Proc 10th Int Zeolite Conf, Garmisch-Partenkirchen, July 17–22, 1994. Elsevier, Amsterdam, p 685; Stud Surf Sci Catal 84:685
100. Spiewak BE, Handy BE, Sharma SB, Dumesic JA (1994) Catal Lett 23:207
101. Kapustin GI, Kustov LM, Glonti GO, Brueva TR, Borovkov VY, Klyachko AL, Rubinshtein AM, Kazanskii VB (1984) Kinet Katal 25:959
102. Tsutsumi K, Mitani Y, Takahashi H (1983) Bull Chem Soc Japan 56:1912
103. Tsutsumi K, Koh HQ, Hagiwara S, Takahashi H (1975) Bull Chem Soc Japan 48:3576
104. Auroux A, Bolis V, Wierzchowski P, Gravelle PC, Védrine JC (1979) JCS Faraday Trans II 75:2544–2555
105. Huang M, Auroux A, Kaliaguine S (1995) Micropor Mat 5:17–27
106. van Santen RA (1994) In: Jansen JC, Stöcker M, Karge HG, Weitkamp J (eds) Advanced zeolite science and applications. Elsevier, Amsterdam, p 273; Stud Surf Sci Catal 85:273
107. Stach H, Wendt R, Lohse U, Jänchen J, Spindler H (1988) Catal Today 3:431
108. Lohse U, Parlitz B (1989) J Phys Chem 93:3677
109. Mitani Y, Tsutsumi K, Takahashi H (1983) Bull Chem Soc Japan 56:1917
110. Brueva TR, Klyachko-Gurvich AL, Mishin IV, Rubinshtein AM (1974) Izvest Akad Nauk SSSR Ser Khim 6:1254
111. Jänchen J, Peeters MPJ, van Wolput JHMC, Wolthuizen JP, van Hooff JHC (1994) J Chem Soc Faraday Trans 90:1033
112. Stach H, Thamm H, Fiedler K, Grauert B, Wieker W, Jahn E, Öhlmann G (1986) In: Murakami Y, Iijima A, Ward JW (eds) New developments in zeolite science and technology; Proc 7th Int Zeolite Conf, Tokyo, Japan, August 17–22, 1986. Elsevier, Amsterdam, p 539; Stud Surf Sci Catal 28:539
113. Jänchen J, Stach H (1986) Adsorpt Sci Technol 3:3
114. Thamm H, Stach H, Fiebig W (1983) Zeolites 3:95
115. Pires J, Brotas de Carvalho M, Ramoa Ribeiro F, Derouane E (1989) Appl Catal 53:273
116. Bellat JP, Simonot-Grange MH, Jullian S (1995) Zeolites 15:124
117. Bellat JP, Simonot-Grange MH, Jullian S (1995) Zeolites 15:219
118. Simonot-Grange MH, Pilverdier P, Bellat JP (1996) Proc AFCAT and GEFTA meeting, 24–26 Sept, 1996, Freiburg, Germany. GEFTA Office, Freiburg, pp 85, 177
119. Simonot-Grange MH, Bertrand O, Pilverdier E, Bellat JP, Paulin C (1997) J Therm Anal 48:741

120. Mellot CF, Cheetham AK, Harms S, Savitz S, Gorte RJ, Myers AL (1998) Langmuir 14:6728
121. Matsumoto A, Tsutsumi K (1995) J Chem Soc Faraday Trans 91:1707
122. Uytterhoeven JB, Christner LG, Hall WK (1965) J Phys Chem 69(6):2117
123. Kühl GH (1977) J Phys Chem Solids 38:1259
124. Sendoda Y, Ono Y (1988) Zeolites 8:101
125. Mishin LV, Pál-Borbely G, Karge HG (1995) In: Beyer HK, Karge HG, Kiricsi I, Nagy JB (eds) Catalysis by microporous materials; Proc ZEOCAT '95, Szombathely, Hungary, July 9–13, 1995. Elsevier, Amsterdam, p 294; Stud Surf Sci Catal 94:294
126. Shannon RD, Gardner K, Staley RH, Bergeret G, Gallezot P, Auroux A (1985) J Phys Chem 89:4778
127. Huang M, Kaliaguine S, Auroux A (1995) In: Bonneviot L, Kaliaguine S (eds) A refined tool for designing catalytic sites; Proc Int Symp, Québec, Canada, October 15–20, 1995. Elsevier, Amsterdam, p 311; Stud Surf Sci Catal 97:311
128. Auroux A, Huang M, Kaliaguine S (1995) J Phys Chem 99(24):9952
129. Mishin IV, Klyachko AL, Brueva TR, Nissenbaum VD, Karge HG (1993) Kinet Catal 34:835
130. Brueva TR, Klyachko AL, Mishin IV, Rubinshtein AM (1975) Izvest Akad Nauk SSSR Ser Khim 4:939
131. Brueva TR, Klyachko-Gurvich AL, Rubinshtein AM (1972) Izvest Akad Nauk SSSR Ser Khim 12:2807
132. de Araujo AS, Fernandes VJ Jr, Fernandes GJT (1997) J Therm Anal 49:567
133. Stone FS, Whalley L (1967) J Catal 8:173
134. Barrer RM, Gibbons RM (1965) Trans Faraday Soc 61:948
135. Khvoshchev SS, Skazyvaev VE, Vasil'eva EA (1980) In: Rees LVC (ed) Proc 5th Int Zeolite Conf, Naples, Italy, June 2–6, 1980, LV, Heyden, London, p 476
136. Amari D, Lopez Cuesta JM, Nguyen NP, Jerrentrup R, Ginoux JL (1992) J Therm Anal 38:1005
137. Auroux A, Artizzu P, Ferino I, Monaci R, Rombi E, Solinas V (1997) Micropor Mat 11:117
138. Tu M, Davis RJ (2001) J Catal 199:85
139. Bordawekar SV, Davis RJ (2000) J Catal 189:79
140. Li J, Davis RJ (2003) Appl Catal A-Gen 239:59
141. Doskocil EJ, Mankidy PJ (2003) Appl Catal A-Gen 252:119
142. Auroux A, Ben Taarit Y (1987) Thermochim Acta 122:63
143. Biaglow AI, Parrillo DJ, Kokotailo GT, Gorte RJ (1994) J Catal 148:213
144. Chen D, Sharma S, Cardona-Martinez N, Dumesic JA, Bell VA, Hodge GD, Madon RJ (1999) J Catal 136:392
145. Williams BA, Babitz SM, Miller JT, Snurr RQ, Kung HH (1999) Appl Catal A-Gen 177:161
146. Auroux A, Ben Taarit Y (1987) Thermochim Acta 122:63
147. Brueva TR, Mishin IV, Kapustin GI (2001) Thermochim Acta 379:15
148. Barthomeuf D (1988) In: Ward JW (ed) Catalysis 1987. Proc 10th North Am Meeting of the Catalysis Society, San Diego, CA, USA, May 17–22, 1987. Elsevier, Amsterdam, p 177; Stud Surf Sci Catal 38:177 (cf. [57])
149. Mitani Y, Tsutsumi K, Takahashi H (1983) Bull Chem Soc Japan 56:1921
150. Mishin IV, Klyachko AL, Brueva TR, Tkachenko OP, Beyer HK (1993) Kinet Catal 34:502
151. Macedo A, Auroux A, Raatz F, Jacquinot E, Boulet R (1988) In: Flank WH, Whyte TE (eds) Perspectives in molecular sieve science. ACS Symposium Series 368:98

152. Barthomeuf D (1987) Mat Chem Phys 17:64
153. Shïbuichi S, Nishino H, Tsutsumi K, Nishimiya K, Yoashida A (1993) In: von Ballmoos R, Higgins JB, Treacy MMJ (eds) Proc 9th Int Zeolite Conf, Montreal, Canada, July 5–10, 1992. Butterworth-Heinemann, Boston, RP 134
154. Kuehne MA, Babitz SM, Kung HH, Miller JT (1998) Appl Catal A-Gen 166:293
155. Kuehne MA, Kung HH, Miller JT (1997) J Catal 171:293
156. Auroux A, Occelli ML (2001) In: Galarneau A, di Renzo F, Fajula F, Vedrine J (eds) Zeolites and mesoporous materials at the dawn of the 21st century. Proc 13th Int Zeolite Conf, Montpellier, France, July 8–13, 2001. Elsevier, Amsterdam, p 2007; Stud Surf Sci Catal 135:2007
157. Occelli ML, Auroux A, Kalwei M, Wolker A, Eckert H (2001) In: Occelli ML, O'Connor P (eds) Fluid Catalytic Cracking V. Elsevier, Amsterdam, p 41; Stud Surf Sci Catal 134:41
158. Shi ZC, Auroux A, Ben Taarit Y (1988) Can J Chem 66:1013
159. Krívánek M, Thiet Dung N, Jirú P (1987) Thermochim Acta 115:91
160. Handy BE, Jacobo A, Cardenas Galindo MG, Gonzalez M, Llanos ME, Guzman M, Hernandez F (2002) Topics in Catal 19:249
161. Colon G, Ferino I, Rombi E, Selli E, Forni L, Magnoux P, Guisnet M (1998) Appl Catal A-Gen 168:81
162. Shen J, Auroux A (2004) Stud Surf Sci Catal 149:35
163. Yaluris G, Rekoske JE, Aparicio LM, Madon RJ, Dumesic JA (1995) J Catal 153:65
164. Occelli ML, Olivier JP, Petre A, Auroux A (2003) J Phys Chem B 107:4128
165. Occelli ML, Auroux A, Baldiraghi F, Leoncini S (1998) In: Occelli ML, O'Connor P (eds) Fluid Cracking Catalysts. Marcel Dekker, p 203
166. Occelli ML, Kalwei M, Wölker A, Eckert H, Auroux A, Gould SAC (2000) J Catal 196:134
167. Védrine JC, Auroux A, Coudurier G (1984) In: (eds) Catalytic materials, relationship between structure and reactivity. ACS Symposium Series 248, 13:254
168. Sharma SB, Meyers BL, Chen DT, Miller J, Dumesic JA (1993) Appl Catal A-Gen 102:253
169. Jozefowicz LC, Karge HG, Coker EN (1994) J Phys Chem 98:8053
170. Dejaifve P, Auroux A, Gravelle PC, Védrine JC, Gabelica Z, Derouane E (1981) J Catal 70:123
171. Védrine JC, Auroux A, Coudurier G, Engelhard P, Gallez JP, Szabo G (1983) In: Olson D, Bisio A (eds) Proc 6th Int Zeolite Conf, Reno, USA, July 10–15, 1983. Butterworths, Guildford, Surrey, UK, p 497
172. Gonzalez MR, Sharma SB, Chen DT, Dumesic JA (1993) Catal Lett 18:183
173. Parrillo DJ, Biaglow A, Gorte RJ, White D (1994) In: Weitkamp J, Karge HG, Pfeifer H, Hölderich W (eds) Zeolites and related microporous materials: State of the art 1994; Proc 10th Int Zeolite Conf, Garmisch-Partenkirchen, July 17–22, 1994. Elsevier, Amsterdam, p 701; Stud Surf Sci Catal 84:701
174. Lee C, Parillo DJ, Gorte RJ, Farneth WE (1996) J Am Chem Soc 118:3262
175. Bolis V, Broyer M, Barbaglia A, Busco C, Foddanu GM, Ugliengo P (2003) J Mol Catal A-Chem 204–205:561
176. Busco C, Barbaglia A, Broyer M, Bolis V, Foddanu GM, Ugliengo P (2004) Thermochim Acta 418:3
177. Bolis V, Barbaglia A, Broyer M, Busco C, Civalleri B, Ugliengo P (2004) Origins of life and evolution of the biosphere 34:69
178. Thamm H, Jerschkewitz HG, Stach H (1988) Zeolites 8:151
179. Nießen W, Karge HG, Jozefowicz L (1993) In: Suzuki M (ed) Proc IVth Int Conf on Fundamentals of Adsorption, Kyoto, Japan, May 17–22, 1992. Kodansha, Tokyo, p 475

180. Takaishi T, Tsutsumi K, Chuubachi K, Matsumoto A (1998) J Chem Soc, Faraday Trans 94:601
181. Weber G, Bouvier F, Simonot-Grange MH (1996) In: (eds) Proc of AFCAT and GEFTA Meeting, 24–26 Sept, 1996, GEFTA Office, Freiburg, Germany, 1996, pp 85, 177
182. Joly JF, Auroux A, Lavalley JC, Janin A, Guth JL (1993) In: von Ballmoos R, Higgins JB, Treacy MMJ (eds) Proc 9th Int Zeolite Conf, Montreal, Canada, July 5–10, 1992. Butterworth-Heinemann, Boston, Vol II, p 235
183. Narayanan S, Sultana A, Mériaudeau P, Naccache C, Auroux A, Viornery C (1996) Appl Catal A-Gen 143:337
184. Narayanan S, Sultana A, Le QT, Auroux A (1998) Appl Catal A-Gen 168:373
185. Nicolaides CP, Kung HH, Makgoba NP, Sincadu NP, Scurrell MS (2002) Appl Catal A-Gen 223:29
186. Védrine JC, Auroux A, Bolis V, Dejaifve P, Naccache C, Wierzchowski P, Derouane EG, van Hoff JCH (1979) J Catal 59:248
187. Muscas M, Dutel JF, Solinas V, Auroux A, Ben Taarit Y (1996) J Mol Catal A-Chem 106:169–175
188. Pearson RG (1986) Proc Natl Acad Sci USA 83:8440
189. Gayubo AG, Benito PL, Aguayo AT, Olazar M, Bilbao J (1996) J Chem Tech Biotechnol 65:186
190. Selli E, Rossetti I, Meloni D, Sini F, Forni L (2004) Appl Catal A-Gen 262:131
191. Viswanadham N, Muralidhar G, Prasada Rao TSR (2004) J Mol Catal A-Chem 223:269
192. Rakic V, Dondur V, Gajinov S, Auroux A (2004) Thermochim Acta 420:51
193. Bolis V, Bordiga S, Turnes Palomino G, Zecchina A, Lamberti C (2001) Thermochim Acta 379:131
194. Kuroda Y, Onishi H, Mori T, Yoshikawa Y, Kumashiro R, Nagao M, Kobayashi H (2002) J Phys Chem B 106:8976
195. Sahoo SK, Viswanadham N, Ray N, Gupta JK, Singh ID (2001) Appl Catal A-Gen 205:1
196. Bolis V, Busco C, Bordiga S, Ugliengo P, Lamberti C, Zecchina A (2002) Appl Surf Sci 196:56
197. Thamm H (1987) Zeolites 7:341
198. Stach H, Jänchen J, Thamm H, Stiebitz E, Vetter RA (1986) Adsorpt Sci Technol 3:261
199. Jänchen J, Stach H, Uytterhoeven L, Martens JA, Jacobs PA (1993) In: von Ballmoos R, Higgins JB, Treacy MMJ (eds) Proc 9th Int Zeolite Conf, Montreal, Canada, July 5–10, 1992. Butterworth-Heinemann, Boston
200. Dunne JA, Mariwala R, Rao M, Sircar S, Gorte RJ, Myers AL (1996) Langmuir 12:5888
201. Klyachko AL, Kapustin GI, Brueva TR, Rubinshtein AM (1987) Zeolites 7:119
202. Tsutsumi K, Nishimiya K (1989) Thermochim Acta 143:299
203. Bankós I, Valyon J, Kapustin GI, Kallo D, Klyachko AL, Brueva TR (1988) Zeolites 8:189
204. Kapustin GI, Brueva TR, Klyachko AL, Rubinshtein AM (1981) Kinet Katal 22:1561
205. Kapustin GI, Brueva TR, Klyachko AL, Rukadze AD, Rubinshtein AM (1982) Kinet Katal 23:972
206. Klyachko AL, Bankés I, Brueva TR, Kapustin GI (1985) React Kinet Catal Lett 29:451
207. Bankós I, Klyachko AL, Brueva TR, Kapustin GI (1986) React Kinet Catal Lett 30:297
208. Auroux A, Datka J (1997) Appl Catal A-Gen 165:473
209. Rukhadze AD, Kapustin GI, Brueva TR, Klyachko AL, Rubinshtein AM (1981) Kinet Catal 22:362

210. Cutrufello MG, Ferino I, Monaci R, Rombi E, Solinas V, Magnoux P, Guisnet M (2003) Appl Catal A-Gen 241:91
211. Stach H, Fiedler K, Jänchen J (1993) Pure and Appl Chem 65:2193
212. Auroux A, Védrine JC, Gravelle PC (1982) In: Rouquerol J, Sing KSW (eds) Adsorption at the gas-solid and liquid-solid interface; Proc Int Symp, Aix-en-Provence, France, September 21–23, 1981. Elsevier, Amsterdam, p 305; Stud Surf Sci Catal 10:305
213. Fernandez C, Auroux A, Védrine JC, Grosmangin J, Szabo G (1986) In: Murakami Y, Iijima A, Ward JW (eds) New developments in zeolite science and technology; Proc 7th Int Zeolite Conf, Tokyo, Japan, August 17–22, 1986. Elsevier, Amsterdam, p 345; Stud Surf Sci Catal 28:345
214. Auroux A, Occelli ML (1994) In: Weitkamp J, Karge HG, Pfeifer H, Hölderich W (eds) Zeolites and related microporous materials: State of the art 1994; Proc 10th Int Zeolite Conf, Garmisch-Partenkirchen, July 17–22, 1994. Elsevier, Amsterdam, p 693; Stud Surf Sci Catal 84:693
215. Shapoval YV, Karetina IV, Shubaeva MA, Khvoshchev SS (1997) Kinet Catal 38:129
216. Shannon RD, Staley RH, Auroux A (1987) Zeolites 7:301
217. Shannon RD, Staley RH, Vega AJ, Fischer RX, Baur WH, Auroux A (1985) J Phys Chem 93:2019
218. Jin YS, Védrine JC, Auroux A (1988) Appl Catal 37:1
219. Jin YS, Védrine JC, Auroux A (1988) Appl Catal 37:21
220. Viornery C, Auroux A, Fajula F, Schulz P (1996) In: Weitkamp J, Lücke B (eds) Catalysis on solid acids and bases, Proc of the DGMK Conf, Berlin, Germany, March 14–15, 1996. DGMK, Hamburg, p 41
221. McQueen D, Chiche BH, Fajula F, Auroux A, Guimon C, Fitoussi F, Schulz P (1996) J Catal 161:587
222. Dumitriu E, Meloni D, Monaci R, Solinas V (2005) Comptes Rendus Chimie 8:441
223. Meloni D, Laforge S, Martin D, Guisnet M, Rombi E, Solinas V (2001) Appl Catal A-Gen 215:55
224. Corma A, Corell C, Pérez-Pariente J, Guil JM, Guil-López R, Nicolopoulos S, Gonzalez Calbet J, Vallet-Regi M (1996) Zeolites 16:7
225. Eder F, He Y, Mivarthy G, Lercher JA (1996) Recl Trav Chim Pays-Bas 115:531
226. He YJ, Nivarthy GS, Eder F, Seshan K, Lercher JA (1998) Micropor Mesopor Mat 25:207
227. Tsutsumi K, Shiraishi A, Nishimiya K, Kato M, Takaishi T (1991) In: Inui T, Namba S, Tatsumi T (eds) Chemistry of microporous crystals; Proc Int Symp Chemistry of Microporous Crystals, Tokyo, Japan, June 26–29, 1990. Elsevier, Amsterdam, p 141; Stud Surf Sci Catal 60:141
228. Vasil'eva EA, Khvoshchev SS (1983) Izvest Akad Nauk SSSR Ser Khim 1:15
229. Jänchen J, van Wolput JHMC, van Well WJM, Stach H (2001) Thermochim Acta 379:213
230. Klyachko AL, Kapustin GI, Glonti GO, Brueva TR, Rubinshtein AM (1985) Kinet Catal 26:613
231. Ferino I, Monaci R, Rombi E, Solinas V, Magnoux P, Guisnet M (1998) Appl Catal A-Gen 183:303
232. Diaz-Mendoza FA, Pernett-Bolano L, Cardona-Martinez N (1998) Thermochim Acta 312:47
233. Sayed M, Auroux A, Védrine JC (1989) J Catal 116:1
234. Coudurier G, Auroux A, Védrine JC, Farlee RD, Abrams L, Shannon RD (1987) J Catal 108:1
235. Occelli ML, Eckert H, Wölker A, Auroux A (1999) Micropor Mesopor Mat 30:219

236. Occelli ML, Eckert H, Hudalla C, Auroux A, Ritz P, Iyer PS (1997) Stud Surf Sci Catal 105:1981
237. Occelli ML, Schwering G, Fild C, Eckert H, Auroux A, Iyer PS (2000) Micropor Mesopor Mat 34:15
238. Eckert H, Hudalla C, Wölker A, Auroux A, Occelli ML (1997) Solid State NMR 9:143
239. Occelli ML, Schweizer AE, Fild C, Schwering G, Eckert H, Auroux A (2000) J Catal 192:119
240. Ducourty B, Occelli ML, Auroux A (1998) Thermochim Acta 312:27
241. Dumitriu E, Hulea V, Fechete I, Catrinescu C, Auroux A, Lacaze JF, Guimon C (1999) Appl Catal A-Gen 181:15
242. Parrillo DJ, Lee C, Gorte RJ, White D, Farneth WE (1995) J Phys Chem 99:8745
243. Dumitriu E, Hulea V, Fechete I, Auroux A, Lacaze J-F, Guimon C (2001) Micropor Mesopor Mat 43:341
244. Auroux A, Tuel A, Bandiera J, Ben Taarit Y, Guil JM (1993) Appl Catal 2:181–190
245. Jänchen J, Vorbeck G, Stach H, Parlitz B, van Hooff JHC (1995) In: Beyer HK, Karge HG, Kiricsi I, Nagy JB (eds) Catalysis by microporous materials; Proc ZEOCAT '95, Szombathely, Hungary, July 9–13, 1995. Elsevier, Amsterdam, p 108; Stud Surf Sci Catal 94:108
246. Vorbeck G, Jänchen J, Parlitz B, Schneider M, Fricke R (1994) J Chem Soc Chem Com p 123
247. Muscas M, Solinas V, Gontier S, Tuel A, Auroux A (1995) Stud Surf Sci Catal 94:101
248. Auroux A, Gervasini A, Jorda E, Tuel A (1994) In: Weitkamp J, Karge HG, Pfeifer H, Hölderich W (eds) Zeolites and related microporous materials: State of the art 1994; Proc 10th Int Zeolite Conf, Garmisch-Partenkirchen, July 17–22, 1994. Elsevier, Amsterdam, p 653; Stud Surf Sci Catal 84:653
249. Bolis V, Bordiga S, Lamberti C, Zecchina A, Carati A, Rivetti F, Spano G, Petrini G (1999) Micropor Mesopor Mat 30:67
250. Bolis V, Bordiga S, Lamberti C, Zecchina A, Carati A, Rivetti F, Spano G, Petrini G (1999) Langmuir 15:5753
251. Gervasini A, Picciau C, Auroux A (2000) Micropor Mesopor Mat 35–36:457
252. Doskocil EJ (2004) Micropor Mesopor Mat 76:177
253. Doskocil EJ (2005) J Phys Chem B 109:2315
254. Blasco T, Camblor MA, Corma A, Esteve P, Guil JM, Martinez A, Perdigon-Melon JA, Valencia S (1998) J Phys Chem B 102:75
255. Védrine JC, Auroux A, Dejaifve P, Ducarme V, Hoser H, Zhou S (1982) J Catal 73:147
256. Sayed MB, Auroux A, Védrine JC (1986) Appl Catal 23:49
257. Becker KA, Kowalak S (1985) J Chem Soc Faraday Trans I 81:1161
258. Occelli ML, Olivier JP, Auroux A (2002) J Catal 209:385
259. Auroux A, Ben Taarit Y, Lokolo M, Mériaudeau P, Naccache C (1997) In: Chon H, Ihm S-K, Uh YS (eds) Progress in zeolite and microporous materials; Proc 11th Int Zeolite Conf, Seoul, Korea, August 12–17, 1996. Elsevier, Amsterdam, p 1405; Stud Surf Sci Catal 105:1405
260. Auroux A, Gervasini A, Guimon C (1999) J Phys Chem B 103:7195
261. Sachtler WMH, Zhang Z (1993) Adv Catal 39:129
262. Silvestre-Albero J, Sanchez-Castillo MA, He R, Sepulveda-Escribano A, Rodriguez-Reinoso F, Dumesic JA (2001) Catal Lett 74:17
263. Chen JD, Haanepen MJ, van Hooff JHC, Sheldon RA (1994) In: Weitkamp J, Karge HG, Pfeifer H, Hölderich W (eds) Zeolites and related microporous materials: State of the art 1994; Proc 10th Int Zeolite Conf, Garmisch-Partenkirchen, July 17–22, 1994. Elsevier, Amsterdam, p 973; Stud Surf Sci Catal 84:973

264. Jänchen J, Stach H, Grobet PJ, Martens JA, Jacobs PA (1992) Zeolites 12:9
265. Jänchen J, Stach H, Uytterhoeven L, Mortier WJ (1996) J Phys Chem 100:12489
266. Jänchen J, Jahn E, Stach H (1991) In: Öhlmann G, Pfeifer H, Fricke R (eds) Catalysis and adsorption by zeolites; Proc of Zeocat '90, Leipzig, Germany, August 20–23, 1990. Elsevier, Amsterdam, p 128; Stud Surf Sci Catal 65:128; Or: Zeolites 12:9
267. Eder F, Lercher JA (1996) J Phys Chem 100 41:16460
268. Jänchen J, Stach H, Grobet PJ, Martens JA, Jacobs PA (1993) In: von Ballmoos R, Higgins JB, Treacy MMJ (eds) Proc 9th Int Zeolite Conf, Montreal, Canada, July 5–10, 1992. Butterworth-Heinemann, Boston, Vol II, p 21
269. d'Arbonneau S, Tuel A, Auroux A (1999) J Therm Anal Cal 56:287
270. Franco Garrido MJ (1992) PhD memoria, Universidad Complutense de Madrid, Spain
271. Stach H, Girnus I, Jänchen J, Loffler E, Lohse U, Parlitz B, Zibrowius B (1993) In: von Ballmoos R, Higgins JB, Treacy MMJ (eds) Proc 9th Int Zeolite Conf, Montreal, Canada, July 5–10, 1992. Butterworth-Heinemann, Boston
272. Lohse U, Parlitz B, Altrichter B, Jancke K, Löffer E, Schreier E, Vogt F (1995) J Chem Soc Faraday Trans 91:1155
273. Jänchen J, Haanepen MJ, Peeters MPJ, van Wolput JHMC, Wolthuizen JP, van Hooff JHC (1994) In: Weitkamp J, Karge HG, Pfeifer H, Hölderich W (eds) Zeolites and related microporous materials: State of the art 1994; Proc 10th Int Zeolite Conf, Garmisch-Partenkirchen, July 17–22, 1994. Elsevier, Amsterdam, p 373; Stud Surf Sci Catal 84:373
274. Lohse U, Parlitz B, Müller D, Schreier E, Bertram R, Fricke R (1997) Micropor Mat 12:39
275. Roque-Malherbe R (2000) Micropor Mesopor Mat 41:227
276. Jänchen J, Peeters MPJ, Wolthuizen JP, van Hooff JHC (1993) Europacat I, Book of Abstracts, Montpellier, France, September 12–17, 1993. ENSCM, Montpellier, vol 1, p 126
277. Yuen Lun-Teh, Zones SI, Harris TV, Gallegos EJ, Auroux A (1994) Micropor Mat 2:105
278. Zheng J, Song C, Xu X, Turaga UT, Zhao XS (2004) Ser Chem Eng 4:464
279. Jänchen J, Busio M, Hintze M, Stach H, van Hooff JHC (1997) In: Chon H, Ihm S-K, Uh YS (eds) Progress in zeolite and microporous materials; Proc 11th Int Zeolite Conf, Seoul, Korea, August 12–17, 1996. Elsevier, Amsterdam, p 1731; Stud Surf Sci Catal 105:1731
280. Occelli ML, Biz S, Auroux A, Ray GJ (1998) Micropor Mesopor Mat 26:193
281. Meziani MJ, Zajac J, Jones DJ, Partyka S, Roziere J, Auroux A (2000) Langmuir 16:2262
282. Meziani MJ, Benalla H (2001) Thermochim Acta 372:103
283. Llewellyn PL, Schüth F, Grillet Y, Rouquerol F, Rouquerol J, Unger KK (1995) Langmuir 11:574
284. Occelli ML, Biz S, Auroux A (1999) Appl Catal A-Gen 183:231
285. Kosslick H, Landmesser H, Fricke R (1997) J Chem Soc Faraday Trans 93:1849
286. Kosslick H, Lischke G, Landmesser H, Parlitz B, Storek W, Fricke R (1998) J Catal 176:102
287. He N, Li D, Tu M, Shen J, Bao S, Xu Q (1999) J Therm Anal Cal 58:455
288. Bonelli B, Onida B, Fubini B, Chen JD, Galarneau A, Di Renzo F, Garrone E (2003) In: Park S-E, Ryoo R, Ahn W-S, Lee CW, Chang (eds) Nanotechnology in Mesostructured Materials, Proc 3rd Int Symp Mesostructured Materials, Jeju, Korea, July 8–11, 2002. Elsevier, Amsterdam, p 319; Stud Surf Sci Catal 146:319
289. Chen DT, Zhang L, Kobe JM, Chen Yi, Dumesic JA (1994) J Mol Catal 93:337

290. Babitz SM, Kuehne MA, Kung HH, Miller JT (1997) Ind Eng Chem Res 36:3027
291. Borgard GD, Molvik S, Balaraman P, Root TW, Dumesic JA (1995) Langmuir 11:2065
292. Auroux A, Picciau C, Gervasini A (1999) In: Kiricsi I, Pál-Borbély G, Nagy JB, Karge HG (eds) Porous materials in environmentally friendly processes; Proc 1st Int FEZA Conf, Eger, Hungary, September 1–4, 1999. Elsevier, Amsterdam, p 555; Stud Surf Sci Catal 125:555
293. Gervasini A, Carniti P, Auroux A (2001) Thermochim Acta 379:95
294. Carniti P, Gervasini A, Auroux A (2001) Langmuir 17:6938
295. Bolis V, Bordiga S, Graneris V, Lamberti C, Turnes Palomino G, Zecchina A (2000) In: Corma A, Melo FV, Mendioroz S, Fierro JLG (eds) Proc 12th Int Congress on Catalysis, Granada, Spain, July 9–14, 2000. Elsevier, Amsterdam, p 3261; Stud Surf Sci Catal 130:3261
296. Auroux A (2001) In: Proc 29th NATAS Annual Conf on Therm Anal and Appl, St. Louis, Mo., USA, September 24–26, 2001. Omnipress, Madison, p 53

Mol Sieves (2008) 6: 153–212
DOI 10.1007/3829_2007_017

Published online: 25 January 2008

Catalytic Test Reactions for Probing the Acidity and Basicity of Zeolites

Johannes A. Lercher[1] (✉) · Andreas Jentys[1] · Axel Brait[2]

[1]Department Chemie, Technische Universität München, Lichtenbergstr. 4, 85748 Garching, Germany
johannes.lercher@ch.tum.de

[2]Chevron Research & Technology Co., 100 Chevron Way, Richmond, CA 94802-0627, USA

1 Introduction 155
1.1 Nature of the Acid Sites 156
1.1.1 Brønsted Acidity 157
1.1.2 Acid Site Concentration 158
1.1.3 Lewis Acidity 159
1.2 Nature of the Basic Sites 161
1.2.1 Framework Basicity 161
1.2.2 Hydroxyl Groups as Basic Sites 161
1.2.3 Clusters in Zeolite Cages with Basic Properties 162
1.2.4 Influence of the Zeolite Structure 162

2 Catalytic Test Reactions 162
2.1 Probing Acid Sites in Zeolites 163
2.1.1 On the Acid Strength Necessary to Catalyze Various Reactions 165
2.1.2 Carbon–Carbon Bond Cleavage 168
2.1.3 Disproportionation Reactions 179
2.1.4 Isomerization 182
2.1.5 Alcohol Dehydration Reactions 185
2.1.6 Other Test Reactions 189
2.2 Specific Reactions for Probing Acid Site Density 189
2.2.1 Cyclohexene Reactions 189
2.2.2 Hydride Transfer Reactions 192
2.3 Tests for Probing Acid and Basic Bifunctional Properties 193
2.3.1 Butene Isomerization 193
2.3.2 Toluene Alkylation 194
2.3.3 Alcohol Conversion 195
2.3.4 Acetonylacetone Cyclization 196
2.4 Probing Basicity of Zeolites 197
2.4.1 Butene Isomerization 198
2.4.2 Alcohol Conversion 198
2.4.3 Toluene Alkylation 199
2.4.4 Acetone Condensation and Diacetone Alcohol Decomposition 200
2.4.5 Knoevenagel Condensation 201
2.4.6 Ring Exchange Reactions 202
2.4.7 Diketone Cyclization 203

2.4.8 Interconversion of Nitriles 203
2.4.9 Transformation of Alcohol/Ketone Mixtures 204

3 Concluding Remarks 204

References 205

Abstract Test reactions are one of the key methods to characterize the complex acid–base properties of zeolites. Although such reactions will not probe solely the acid or the base properties, observations in test reactions give a unique fingerprint of the catalytic properties of a material. They are best when the application of the zeolite requires similar conversion steps. The present review compiles currently used test reactions together with examples of their applications and also discusses the associated limitations.

Keywords Acid sites · Base sites · Characterization · Test reactions · Zeolites

Abbreviations

AcAc	Acetonylacetone
AHF	Ammonium hexafluorosilicate
AlPO-11	Aluminophosphate structure*
Beta	Zeolite structure, zeolite Beta*
CI	Constraint index
DMF	Dimethylfuran
EDTA	Ethylenediaminetetraacetic acid
EEM	Electronegativity equalization method
EFAL	Extra-framework alumina species
FAU	Zeolite structure, acronym for faujasite*
HF-OH	High-frequency hydroxyl band
H_0	Hammett acidity function
HMB	3-Hydroxy-3-methyl-2-butanone
IR	Infrared
K	Equilibrium constant
L	Linde-type L zeolite (LTL)*
LF-OH	Low-frequency hydroxyl band
LTL	Zeolite structure, acronym for Linde-type L zeolite*.
MBOH	2-Methyl-3-butyn-2-ol
MBYNE	3-Methyl-3-buten-1-yne
MCP	3-Methyl-2-cyclopentenone
MeSAPO	Microporous aluminophosphate with metal and silicon in the framework
MFI	Zeolite structure, acronym for ZSM-5*
MIPK	3-Methyl-3-butene-2-one
MOR	Zeolite structure, acronym for mordenite*
MR	Membered ring (indicating the pore aperture of the zeolite)
NMR	Nuclear magnetic resonance
OFF	Zeolite structure, acronym for offretite*
PRENAL	3-Methyl-2-butenal
RCI	Refined constraint index
SAPO-11	Microporous metal aluminophosphate with silicon in the framework*
SAPO-31	Microporous metal aluminophosphate with silicon in the framework*
SAPO-37	Microporous metal aluminophosphate with silicon in the framework*

SAPO-41	Microporous metal aluminophosphate with silicon in the framework*
SI	Spaciousness index
TOF	Turnover frequency
TOS	Time on stream
TPD	Temperature-programmed desorption
USY	Ultrastable zeolite Y
X zeolite	Structure, X-type zeolite*
Y zeolite	Structure, Y-type zeolite*
ZSM-5	Zeolite structure*
ZSM-8	Zeolite structure*
ZSM-11	Zeolite structure*
ZSM-22	Zeolite structure*
θ	Coverage of sites
*	See [1]

1 Introduction

Zeolites are highly crystalline tectosilicates possessing a well-defined one-, two-, or three-dimensional pore structure containing micropores with diameters in the range of 3 to 12 Å [2]. The materials are built up by SiO_4 tetrahedra, which are connected via their corner oxygen atoms [3, 4]. Therefore, two silicon atoms share one oxygen atom (see Scheme 1). From this primary building block more than 100 different types of zeolites are formed that contain one-, two-, or three-dimensional pore systems. In some structures, e.g., faujasite or erionite, cages are also present at the channel intersections [2].

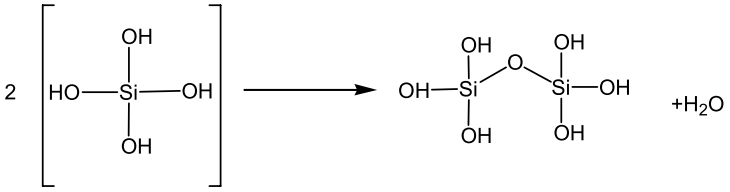

Scheme 1 Formation of SiO_4 tetrahedra by condensation

The unique properties of zeolites for application in ion exchange, sorption, and catalysis are related to the fact that (1) the diameters of the micropores are in the range of the kinetic diameters of potential reactants (see Fig. 1) and (2) the surface functional groups having acid–base or redox properties are an integral part of the crystal structure. Thus, the nonspecific interactions between these materials and the reactant molecules are typically very strong and, therefore, the sorption properties markedly influence the catalytic activity.

Model reactions are, in addition to spectroscopic characterization [5, 6], an effective tool for obtaining information on the acid–base properties, the size of the pore system, and the access of reactant molecules to the active sites in

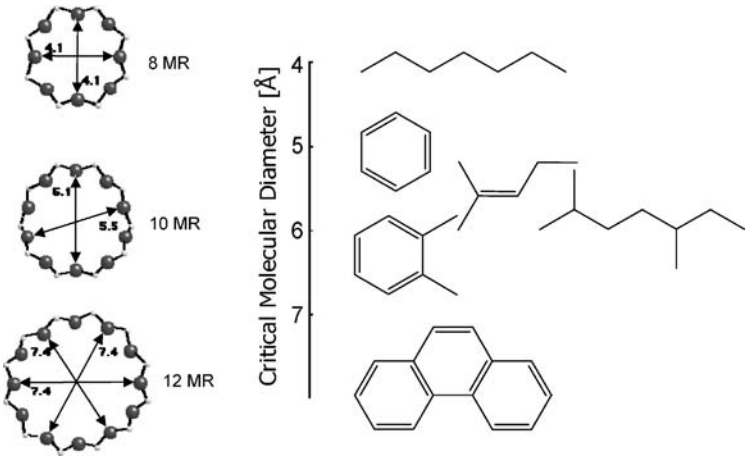

Fig. 1 Comparison between the diameters of the pore openings and the size of typical reactant molecules

catalysts. The main advantage over other methods is that the information is obtained under conditions that are typical of the application of the materials in the catalytic reactions.

In the following, we will briefly discuss the nature of the catalytically active sites in zeolites. A much deeper discussion of acidity and basicity is given in several reviews [7–18] and, therefore, we will restrict ourselves to the most important points.

1.1 Nature of the Acid Sites

Pure siliceous zeolites are electrically neutral. A negatively charged tetrahedron in the lattice is created by the substitution of a tetrahedrally coordinated silicon atom, having a formal charge of 4+, by an atom with a formal charge of 3+, such as aluminum (see Scheme 2).

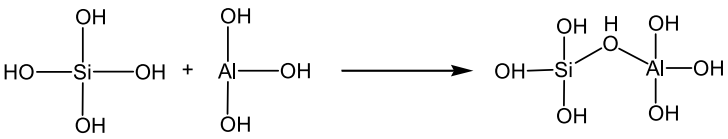

Scheme 2 Formation of Brønsted acid sites via linking of silicon–oxygen and aluminum–oxygen tetrahedra

The resulting negative charge of the lattice is balanced by protons, generating an acidic hydroxyl group or metal cations, which can balance one to three negatively charged AlO_4 tetrahedra depending on their charge. The way

these sites act and can be manipulated will be briefly discussed below. A more detailed discussion can be found in several reviews [2, 3, 7, 10, 18].

The cations required to compensate the negative charge generated by the isomorphous substitution of Si^{4+} by Al^{3+} can be exchanged in the aqueous phase, which is mostly done for the exchange with metal cations, or by solid-state ion exchange [19]. The direct ion exchange with protons is difficult as the low pH necessary for the ion exchange would lead to partial removal of Al^{3+} from the lattice, and thus to a potential destruction of the molecular sieves. It works, however, with zeolites having a high Si/Al ratio such as mordenite or clinoptilolite. Therefore, ion exchange is typically performed with ammonium ions (using, e.g., NH_4OH, NH_4NO_3, or NH_4Cl), followed by careful washing and subsequent thermal decomposition of the ammonium ions into protons and NH_3. The protons are bound covalently to the bridging oxygen atoms of Si – O – Al groups and form hydroxyl groups that may act as Brønsted acid sites [20].

Tectosilicates are metastable and transform at higher temperatures into dense silica phases. This is not a one-step process and it proceeds by breaking the most labile bonds, typically the Si – O – Al bonds, first leading to a partial dealumination of the zeolite structure [21, 22]. Steam greatly enhances the rate of this T – O – T bond cleavage (T=tetrahedral framework atom), which leads to the removal of tetrahedrally coordinated aluminum from the lattice and, thus, reduces the concentration of Brønsted acid sites [23]. These leached alumina species remain in the micropores and may affect the catalytic activity [24]. The possible influences range from (1) action as Lewis acids that activate alkanes [25, 26], (2) interactions with Brønsted acid sites enhancing their catalytic activity [27, 28], (3) replacement of the proton of Brønsted acid sites and neutralizing the acid sites [29], to (4) the formation of large clusters of amorphous alumina or alumina–silica species that block the access to certain micropores [29].

1.1.1 Brønsted Acidity

Brønsted acid sites have different acid strengths depending on their environment, i.e., the chemical composition and structure of the zeolite [30]. The simplest approach accounts for the chemical composition of the molecular sieve only, without considering structural aspects. The electronegativity equalization principle of Sanderson has been most successful in this respect [31]. Mortier [32] calculated on this basis the intermediate electronegativities of molecular sieves and the average partial charge of protons. Higher intermediate electronegativity corresponds to a lower concentration of aluminum in the lattice and a higher acid strength. Jacobs [33] showed that the variation in the acid strength of the proton forms of zeolites can be explained in these terms and that changes in acid strength are the results of changes in the overall chemical

composition. The inherent disadvantage of the Sanderson formalism is that it does not take into account that the same atoms can exist in different bonding situations, i.e., that the atoms can have different local environments.

To solve these shortcomings, the formalism was extended by Mortier et al. [34, 35] to include local environment effects. In this approach, a semiempirical formalism, based on density functional theory, is used to calculate the charge distribution in molecules and their perturbation by molecular interaction [36]. After calibration by ab initio calculations, this method allows precise predictions for large molecules, such as zeolites. In [37], for example, the hydrogen exchange reactivity of methane was calculated in terms of hardness of the reaction (i.e., the difficulty in exchanging a hydrogen atom) and related to the amount of aluminum present in the zeolite lattice. It was found that the reactivity decreased with increasing Al content, and thus earlier observations were confirmed showing that the acid strength is lower with increasing Al content.

As noted above, the local environment of the acid site in a molecular sieve is determined by the structure, i.e., the coordination of the TO_4 tetrahedra in the framework topology. This leads to different amounts of topologically nonequivalent T sites for different zeolite structures. In this respect, LTL zeolites have two, MOR four, and MFI 12 nonequivalent T sites [1], while in the FAU structure all T sites are equivalent. These tetrahedral positions can differ in T – O – T bond angles and T – O bond lengths [31, 38]. Quantum chemical calculations indicate that the O – H bond length and the deprotonation energy depend on the lengths of Al – O and Si – O bonds and the corresponding Al – O – Si and Si – O – Si angles [31, 39]. Redondo and Hay [31] showed for H-ZSM-5 using semiempirical quantum chemical methods that for the 12 acid site positions in the MFI structure different T – O – T angles are present, which results in different deprotonation energies and leads to differences in the acid strengths of the corresponding sites. These results are supported by the ab initio calculations of Kramer and van Santen [40] as well as by Brändle and Sauer [41], who calculated proton affinities for FAU, MOR, and MFI structures and also found different protonation energies for topologically different sites.

All results discussed so far indicate that the Brønsted acidity depends on the zeolite structure and the chemical composition of the molecular sieves. Additionally, the concentration of aluminum in a molecular sieve will influence the acidity of a catalytic site due to a different distribution in the framework, resulting in different acid site concentrations and strengths.

1.1.2 Acid Site Concentration

Due to the high charge density of the exchanged cations or protons and the resulting lability of the Al – O – Al bonds, the formation of Al – O – Al pairs does not occur in zeolites (Loewenstein's rule [42]). Thus, only half of all sil-

icon atoms can be replaced by aluminum in a molecular sieve material, i.e., the lowest Si/Al ratio possible is unity. In this configuration, zeolite structures have one Al site surrounded by four Si atoms as nearest neighbors and various numbers of Al atoms as next-nearest neighbors (NNN) depending on the zeolite, such as nine in the FAU or 12 in the MFI structure [1, 43]. Various models, as reviewed by Barthomeuf [30], relate the acid strength of a bridging hydroxy group to the number of Al atoms in the NNN layer. The strongest acid hydroxy groups are connected to sites with no Al atoms in the second layer. The limit m_{NNN} (m = Al/[Al + Si]), which defines the maximum Al content without the (statistical) possibility of forming AlO_4^- in NNN positions, depends on the framework structure. It determines the maximum Al content for achieving Brønsted acid sites with the highest acid strength. Below this limit, the acid strength remains constant. At higher Al concentrations the strength of the Brønsted acid sites decreases due to the formation of Al pairs in NNN positions. This model was shown to correlate well with theoretical calculations performed by Mortier's group [37]. Another model considers also the second to fifth layers around the Al site to include overall effects in a zeolite structure [43]. Both models suggest that acid strength is highest for isolated Al atoms. The limiting concentration of Al atoms lies between 23 and 40 Al atoms per unit cell (corresponding to the Si/Al ratios for some zeolites, as indicated in brackets: MFI (9.5) > MOR (9.4) > OFF (8.3) > FAU (6.8)), depending on the topological density of the zeolite and the model applied.

These results clearly show that the (local) acid site concentration, which depends on the concentration of aluminum in the zeolite, strongly influences the strength. The acid strength of a Brønsted site depends, thus, on its local geometry, i.e., the length of the T – O bonds and T – O – T angles and the concentration of aluminum in the zeolite.

In the following, the Brønsted acid sites will be classified into strong, medium, and weak acid sites. As will be seen, this classification can be verified by poisoning experiments with basic molecules, or by the use of test reactions requiring varying strengths of acid sites, while measurements with Hammett acidity indicators are frequently strongly limited (see [44]).

1.1.3 Lewis Acidity

Positively charged oxide clusters or ions act as Lewis acid sites, i.e., electron pair acceptor sites, within the pores of zeolites. These species are typically alumina or silica/alumina, generated by the extraction of aluminum from the lattice, or metal cations balancing the negative charge of the framework. Depending on the nature of the metal cations these oxide clusters may also contain hydroxyl groups formed by a partial hydrolysis of water.

The former type of Lewis acidity, i.e., aluminum oxide clusters containing alumina in octahedral and tetrahedral coordination, are usually stronger Lewis acids than exchangeable metal cations [45]. The oxide clusters are typically extracted out of the zeolite framework by steam treatment (as shown in Scheme 3) at higher temperatures and form oxohydroxides or oligomeric species [23], which can be charged or neutral. Extra-framework alumina species (EFAL) can either block an active site by exchanging for a proton, enhance the acidity by interacting with a Brønsted acid site [28], or block the access to micropores when forming voluminous oligomeric species. Due to the formation of such different species the influence on the catalytic behavior of a zeolite is very diverse, varying from enhancing to weakening the strength of Brønsted acid sites; examples are well documented in the literature [46–50]. Note in this context that ion exchange with rare earth cations, such as La^{3+}, is also claimed to enhance the acid strength of a nearby Brønsted acid site by inductive effects [27].

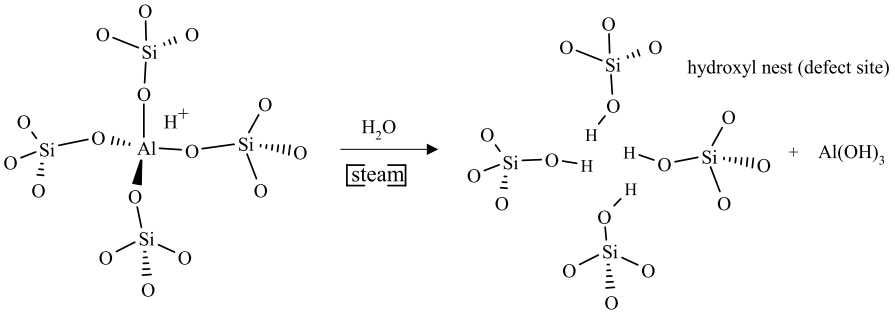

Scheme 3 Hydrothermal extraction of aluminum from the zeolite lattice

However, Lewis acid sites not only modify the Brønsted acid sites. These species will also act themselves in various ways in molecular sieve catalysis. Together with the adjacent framework oxygen atoms, Lewis acid sites will act as Lewis acid–base pairs, and may polarize bonds in reacting molecules, possibly enhancing their chemical reactivity [27, 28]. For molecules that are already polar, this polarization could also be sufficient to catalyze a chemical transformation, e.g., in the reaction of alcohols [51]. Lewis acid sites also act as hydride or anion receptors in a variety of reactions. Thus, in most cases the character of an acid–base pair site will be more pronounced in the case of Lewis than in the case of Brønsted acid sites [52, 53].

1.2 Nature of the Basic Sites

Oxygen atoms in a zeolite lattice have an intrinsic Lewis base character due to the electron pairs they can donate and to the partial negative charges they bear. Silicon or aluminum atoms provide partial positive charges, which reduce the strength of such a donation [8, 54]. However, every zeolite framework possesses an intrinsic Lewis base character. Additional basic sites can be created by metal or metal oxide clusters within the micropores of the zeolite [54]. The different basic sites will be discussed in the following paragraphs.

1.2.1 Framework Basicity

In a zeolite framework oxygen atoms of the SiO_4 and AlO_4 tetrahedra are negatively charged and, in principle, are Lewis basic sites (electron pair donors) [55–57]. As acid-catalyzed reactions (proton donation) are in general much faster than base-catalyzed reactions, the activity of Brønsted acid sites will be much higher than any activity of basic sites [58]. By exchanging the protons with cations, the proton-catalyzed reactions are eliminated and the basic character of the zeolite structure will become more dominant. The basicity of the oxygen atoms in the lattice depends on the angles between oxygen and T atoms and the nature of the tetrahedral atom (e.g., oxygen atoms in AlO_4 tetrahedra are more basic than in SiO_4 tetrahedra) [54, 55, 59]. During adsorption and catalysis, the reactant potentially interacts with oxygen atoms of different base strengths, which result from their charge and neighborhood. The extra-framework cations are, to a certain extent, mobile and thus their position in the pores can also depend on the type and concentration of the reactant. This can cause lattice relaxations and changes in the framework angles and, therefore, might influence the charge distribution and basicity of the oxygen atoms. This interactive behavior is an important factor in dynamic adsorption/desorption processes on the zeolite structures [54].

Basicity can be estimated by the intermediate electronegativity using the Sanderson electronegativity principle [60] and the electronegativity equalization method (EEM) introduced by Mortier et al. [32]. The negative charge at the oxygen, i.e., the basic strength, is inversely proportional to the intermediate electronegativity [8, 61].

1.2.2 Hydroxyl Groups as Basic Sites

Because of the negatively charged framework of zeolites, basic framework hydroxyl groups do not exist [55]. Moreover, positively charged frameworks have not been reported for molecular sieve structures so far. Basic hydroxyl

groups are, therefore, linked to extra-framework species in the zeolite pores, such as small clusters of MgO or CaO, or to metal cations, which generate basic hydroxyl groups by the following reaction:

$$Me^{2+}(H_2O) \rightleftharpoons Me^{2+}OH^- + H^+ . \quad (1)$$

In this case, it is important to notice that by hydrolyzing the hydrated metal cation a basic OH^- and an acid H^+ are created. The latter will form a Brønsted acid site. Therefore, Mg and Ca ion-exchanged zeolites still show acid behavior.

1.2.3
Clusters in Zeolite Cages with Basic Properties

The overall basicity of a zeolite can be enhanced by the introduction of alkaline or alkaline earth oxide–hydroxide clusters into the micropores [62, 63]. For the divalent cations of alkaline earth metals, hydrolysis takes place and subsequent heating forms metal oxide species in the micropores [54, 64–66]. Such materials showed high activity in base-catalyzed reactions, for example, alcohol dehydrogenation or toluene side chain alkylation [67]. The introduction of metals by vapor treatment or decomposition of organo-alkali metal compounds or alkali metal azides results in ionic alkali metal clusters [56]. These clusters interact with framework oxygen atoms and increase the charge of the oxygen in the framework, thus enhancing the base strength.

1.2.4
Influence of the Zeolite Structure

Adsorption and diffusion in the micropores plays an important role in the activity of a zeolite. The adsorption of a base molecule is not only influenced by the strength and number of acid sites present in the molecular sieve, but also by the geometry of the micropores [68]. As the reaction rate of a test molecule is dependent on its adsorption properties, a measured rate will inherently depend on acidity and pore geometry factors.

2
Catalytic Test Reactions

Different methods exist to characterize acid and basic sites including titration with various probe molecules, spectroscopic methods, adsorption of probe molecules, and observation with spectroscopic and thermoanalytical methods [5, 6, 69–71]. Most approaches of characterization, however, face the problem that the measurement and description of the acid sites are done under conditions remote from those applied in catalytic reactions. Therefore,

it remains in question whether or not the sites characterized exist under reaction conditions and have the same properties as when probed near ambient conditions.

One possibility to solve this ambiguity is to use test reactions that allow the nature, strength, and number of active sites to be distinguished [7, 72]. Two points are important when choosing an appropriate test reaction: (1) the reaction should proceed along one pathway, i.e., extensive side reactions should not occur, and (2) a low conversion should be maintained to directly measure intrinsic (differential) reaction rates and exclude the influence of product inhibition. However, even when all criteria are fulfilled, one should not forget that the information obtained is complex and can only be fully utilized if the adsorption/desorption and diffusion of the reactants and products and the reaction steps can be differentiated. Thus, it is insufficient to report only activity or the activity/selectivity pattern to deduce the acid–base properties. The reaction orders should be given in addition, with at least the rate of reaction normalized to the specific surface area of the catalytic material under study. Ideally, a microkinetic model describes the reaction studied.

An important problem to be taken into account when comparing the catalytic activity is the deactivation of the catalysts. Many reactions over zeolites or zeolite-containing catalysts show a decreasing activity with time on stream (TOS), due to poisoning or blocking of the catalytically active sites. If deactivation is observed, the analysis requires the application of catalyst decay functions in order to obtain activity values at initial TOS. Wojciechowski [73, 74] was one of the first to treat catalyst decay rigorously and to describe the kinetics of catalyst decay with TOS. Reviews concerning deactivation have been published by Wolf and Alfani [75], Bhatia et al. [76], Guisnet and Magnoux [77], Butt and Petersen [78], and Bauer and Karge [79]. In this review, however, we will only deal with deactivation in close connection with its influence on the activity of catalytic test reactions.

In the following, we will first discuss catalytic test reactions sensitive to probe acid sites in zeolites, which is by far the most studied type of reaction due to widespread use of zeolites as solid acids. Then, we will address bimolecular reactions, which require adjacent acid and base sites to proceed. Test reactions for probing the acid and basic properties of zeolites via product selectivity will be discussed subsequently. The last part will deal with reactions probing basic sites in zeolites, which is still not as well explored as probing acidity.

2.1 Probing Acid Sites in Zeolites

Test reactions have to be applied to evaluate the acid sites in zeolites with respect to (1) the type of site catalyzing the reaction (Brønsted, Lewis), (2) the extensive factor of acidity, i.e., the concentration of the active sites in the zeolites, and (3) the intensive factor of acidity, i.e., the strengths of the active sites

involved in the test reaction. However, the activation energies of catalyzed reactions tend to average the contributions by various acid sites present.

The concentration of the active sites is always positively related to the reaction rate. In most cases, this is implicitly assumed to be a first-order reaction, and the reaction rate is normalized to the concentration of the active sites. This rate is usually called turnover frequency (TOF) or turnover rate. While this is conceptually straightforward, in practice one does not know which acid sites are catalytically active and, therefore, providing a good basis for this normalization is often difficult. The best approach is to gradually eliminate the potential basis for the normalization by at least (arbitrarily and experimentally) differentiating between acid sites, as has been outlined above, and then searching for positive correlations. Strongly negative correlations with the target reaction would suggest the presence of competing side reactions.

Related to the concentration of the active sites, the concentration of the reactant at the catalyst is part of the reaction rate equation. In order to be able to differentiate between extensive (concentration of adsorbed reactant species) and intensive (impact of the catalytically active site on the reactant molecule) factors, the reaction kinetic equation has to be known in detail and to be carefully analyzed or valuable information would be wasted.

Let us outline this with a monomolecular reaction (such as the protolytic cracking of alkanes). Assuming a Langmuir-type adsorption, the rate normalized to the total concentration of active sites can be expressed as:

$$r = k \cdot \theta_{\text{reactant}} = k \cdot \frac{K \cdot p_{\text{reactant}}}{1 + K \cdot p_{\text{reactant}}} \tag{2}$$

θ_{reactant} = [molecules adsorbed on active sites]/[active sites] .

The equilibrium constant K is related to the concentration of adsorbed species at the active sites. In many cases, a direct correlation between the acid strength and the adsorption constant exists, i.e., the higher the acid strength of a particular site, the higher the constant K will be. If sites with different acid strengths are present in the sample, different equilibrium constants K have to be assumed for each type of site and, consequently, the measured rate will represent a combination of the acid strength and the acid site concentration [39]. As a result, one obtains a concentration of active sites with an average value of K for the test reaction studied. Therefore, it would be possible that a zeolite with a smaller concentration of strong acid sites shows the same activity as a zeolite with a higher concentration of weak acid sites. However, this will only be important if the apparent energies of activation and the specific reaction rate constants are rather similar in the temperature range studied. Differences of 20 kJ mol^{-1} will leave the site with the higher apparent energy of activation completely inactive for the test reaction. This leaves the description of the kinetics of these probe reactions surprisingly straightforward and, despite the

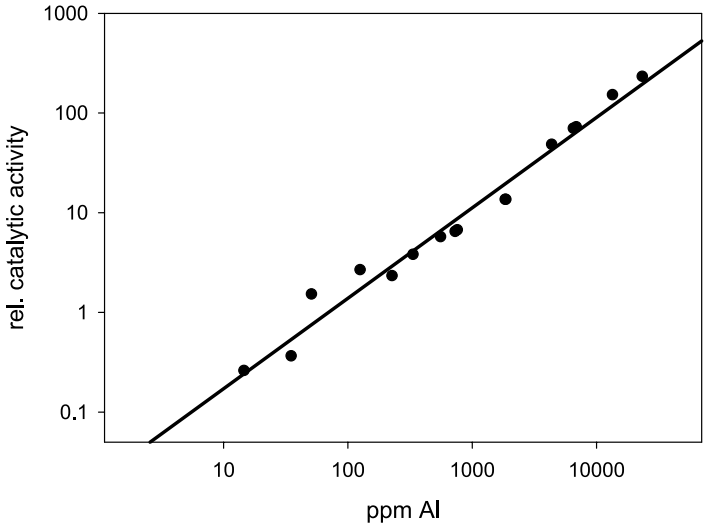

Fig. 2 *n*-Hexane cracking activity vs the concentration of aluminum in H-ZSM-5

wide distribution of site strengths seen by physicochemical methods, the use of Langmuir models is justified in most cases.

In an elegant example Haag et al. [80, 81] used the cracking of *n*-hexane over H-ZSM-5 zeolites with Al concentrations ranging from 20 up to 50 000 ppm (Si/Al = 10 to 100 000) to show that all acid sites had the same TOF, by demonstrating a linear relationship between concentration of Al (acid site concentration) and the reaction rate (see Fig. 2).

In contrast, it was shown by De Canio et al. [82] for the conversion of methanol that an H-Y zeolite with 12 Al atoms per unit cell had the same activity as one with 54 Al atoms per unit cell, which had a four times higher concentration of Brønsted acid sites. Acid sites in the zeolite with a lower concentration of Al atoms have a higher acid strength, and thus the TOF is higher compared to that of the zeolite with the higher Al concentration in the lattice.

These two examples emphasize the importance of measuring the concentration and strength of all potentially active sites and then looking for relations between quantitative properties. However, for cases where this would not be possible, the use of test reactions requiring a particular strength of acid sites has been proposed. The feasibility of this approach will be discussed below.

2.1.1
On the Acid Strength Necessary to Catalyze Various Reactions

The initiating landmark paper is probably the thermodynamic study of Fabre et al. [83], who investigated the reactivity of alkanes in superacid medium

(HF). The alkane concentrations were determined in situ using electrochemical methods, which allowed a quantitative analysis of the hydrocarbon reactions. The reactivity of methane up to hexane (and isohexane) was studied as a function of the acid strength (expressed as H_0, the Hammett acidity function) of the medium by treating the reactions as redox pairs with corresponding electrochemical potentials. The reactions studied included the formation of carbenium ions from alkanes via protolytic dehydrogenation (i.e., $RH + H^+ \rightleftharpoons R^+ + H_2$) or protolytic cracking (i.e., $R_1R_2 + H^+ \rightleftharpoons R_1H + R_2^+$), the conversion of carbenium ions by β scission (i.e., $R_1R_2^+ \rightleftharpoons R_1^+ + R_2^=$), the isomerization of carbenium ions, and the alkylation of carbenium ions.

Guisnet et al. [84, 85] used test reactions to estimate the acid strength necessary to catalyze isomerization and cracking reactions. To estimate the minimum acid strength necessary to catalyze these reactions, the catalysts were poisoned with pyridine, which was subsequently thermally desorbed in order to generate a series of catalysts with identical structure (zeolite H-Y) but increasing strength of the available acid sites. The reactions studied included isomerization of 3,3-dimethyl-1-butene, isomerization and cracking of 2,2,4-trimethylpentane and 2,4-dimethylpentane, isomerization and cracking of 2-methylpentane and *n*-hexane, and isomerization and disproportionation of *o*-xylene and 1,2,4-trimethylbenzene. Isomerization reactions were observed after removing pyridine at 220 °C, while cracking did not occur on the poisoned catalysts until pyridine was removed at 520 °C. This shows that it is possible to estimate the acid strength distribution of the active acid sites in a zeolite by using test reactions that require sites of different acid strength. However, it was also shown that in some cases the catalysts regained their full activity, although the strongest acidic sites were still covered by pyridine. This could lead to the conclusion that either an upper limit of acid strength required for a certain test reaction exists or that the activity on the nonpoisoned catalyst was studied after the deactivation of the strongest acidic sites, e.g., by coke formation. However, it is also necessary to carefully check possible steric constraints when using a bulky base such as pyridine.

In a related experiment Lombardo et al. [86] compared the cracking of neopentane on selectively ammonia-poisoned H-ZSM-5, H-mordenite, and H-Y zeolites. They could show that the conversion declined to zero after poisoning 3 to 15% of all framework aluminum sites, which indicates that only the acid sites with the highest acid strength, i.e., only a small fraction of all Brønsted acid sites, are able to catalyze the reaction. Differences in the distribution of the acid sites of the catalysts studied were shown by comparing the initial activity to the activity observed after ammonia poisoning and subsequent desorption at 500 °C. In all cases, the catalysts regained their activity for neopentane cracking only after desorbing ammonia above 400 to 450 °C.

Yushchenko et al. [87] studied the isomerization of *o*-xylene as a function of the acidity of H-ZSM-5 and H-ZSM-11. By poisoning acid sites with ammonia, the lower threshold of acid strength for the sites required for

the isomerization reaction was estimated. After desorbing ammonia above 200 °C, the catalysts regained their full activity for *o*-xylene isomerization.

These two studies show that different reactions, i.e., neopentane cracking and *o*-xylene isomerization, require sites of different acid strength to proceed. At first sight this seems to contradict the observations of Haag et al. [80, 81], who concluded that all active sites in H-ZSM-5 are of the same acid strength over a large range of Al concentrations in the lattice. However, the ZSM-5 structure has 12 topologically different T sites, which are typically surrounded by various numbers of neighboring Al sites. Thus, alkane cracking (chosen by Haag) uses only the strongest sites, i.e., those also active for neopentane cracking. These sites seem to be only a function of the aluminum concentration in H-ZSM-5. *o*-Xylene, on the other hand, appears to be also catalyzed by other acid sites, much weaker in strength, which are speculated to be formed, e.g., by dealumination.

A clear relationship between the acid strength of amorphous silica–alumina catalysts and the activity for the methyl shift versus double bond shift reaction in the isomerization of 2-methyl-2-pentene was found by Lin and Haller [88]. 4-Methyl-2-pentene (4M2P) is formed by double-bond isomerization essentially on all acid sites, while the formation of 3-methyl-2-pentene (3M2P) requires sites of higher acid strength. Consequently, the ratio between 3M2P and 4M2P formation correlates well with the average partial charge on Si (measured by ^{29}Si NMR chemical shifts), which in turn controls the charge distributions and acid strength of the bridging hydroxyl groups.

Wang et al. [89] defined the acidity and acid strength of H-ZSM-5 using the activity and selectivity in the conversion of various α-olefins and paraffins on H-ZSM-5 partially poisoned with pyridine. The conversion of olefins required weaker acid sites than the conversion of paraffins. Furthermore, sites with a higher acid strength favor the formation of aromatics, which indicates that dehydrocyclization requires very strong acid sites to proceed.

Choudhary and Akolekar [90] studied the conversion of cumene, isooctane, and *o*-xylene over various low-silica and high-silica zeolites. They defined strong acid sites as sites from which pyridine desorbs above 400 °C and found that isooctane cracking required essentially these very strong acid sites, while *o*-xylene isomerization and cumene cracking were also catalyzed by weaker acid sites.

Zi et al. [91] measured the acidity of chemically dealuminated Y zeolites by titration with *n*-butylamine using various indicators. The strengths of the acid sites were compared to the activity of the catalysts for cumene cracking and *n*-propanol dehydration. Cumene cracking was only observed on strongly acidic sites (Hammett acidity function $H_0 < -3$), while the dehydration of *n*-propanol was catalyzed by (nearly) all acid sites on the catalyst surface.

Thus, all results discussed so far show that typically a lower limit for the acid strength required for a particular catalytic reaction exists. In general, the highest acid strength is required to catalyze the cracking of paraffins, fol-

lowed by the cracking of cumene and the isomerization of *o*-xylene, while the dehydration of alcohols is catalyzed by almost all acid sites present on the catalyst surface.

Humphries et al. [92, 93] gave an overview of different test reactions used to characterize the acidity of zeolites. The reactions included cracking, isomerization, disproportionation, and alcohol dehydration as well as hydride transfer reactions involving cyclohexene conversion. In the following sections, we will discuss each class of these test reactions for their ability to give information about the nature, concentration, and strength of the active sites involved in acid-catalyzed reactions.

2.1.2 Carbon–Carbon Bond Cleavage

The catalytic cracking of alkanes and alkenes requires acid sites with a high acid strength and reaction temperatures of approximately 400–500 °C. The high stability of the C – C bond makes the reaction ideal to probe strong Brønsted acid sites. Substantial complications with the interpretation are, however, involved, as the reactions tend to be complex and to involve various reaction pathways subtly depending on the reaction conditions and the molecules converted. In general, three groups of mechanistic pathways can be distinguished for catalytic alkane and alkene cracking on zeolites, i.e., protolytic cracking via carbonium ions, β cracking via carbenium ions, and cracking that is preceded by oligomerization of reactants and/or followed by oligomerization of products. The importance of a particular reaction route depends upon the reaction conditions and the zeolite used. However, because of the higher reactivity of alkenes usually alkanes are used for test reactions, as catalyst deactivation can be kept relatively low.

The activation of an alkene is a rather facile reaction. Upon contact with a zeolite at ambient temperature an alkoxy group is immediately formed. These alkoxy groups, however, tend to be rather susceptible to alkylation by another olefin resulting in a rapidly growing alkoxy chain [94]. In the transition state, the alkoxy group forms a carbenium ion, which cleaves forming an alkene and a smaller carbenium ion. The carbon–carbon bond cleaved is located in a β position to the carbon atom bearing the positive charge (β cracking; see Scheme 4). When the smaller carbenium ion donates the proton back to the zeolite, an olefin is formed. Alternatively, the carbenium ion can abstract a hydride ion from an alkane, leading to desorption of an alkane and the formation of a new carbenium ion.

Thus, for alkanes this cracking route proceeds via a chain mechanism [95, 96]. The overall process is governed by the stability of the carbenium ions in the initial and final states of the reaction. As shown also by theoretical calculations, the difference in the stability of the carbenium ions determines the true energies of activation for the elementary step of carbon–carbon bond

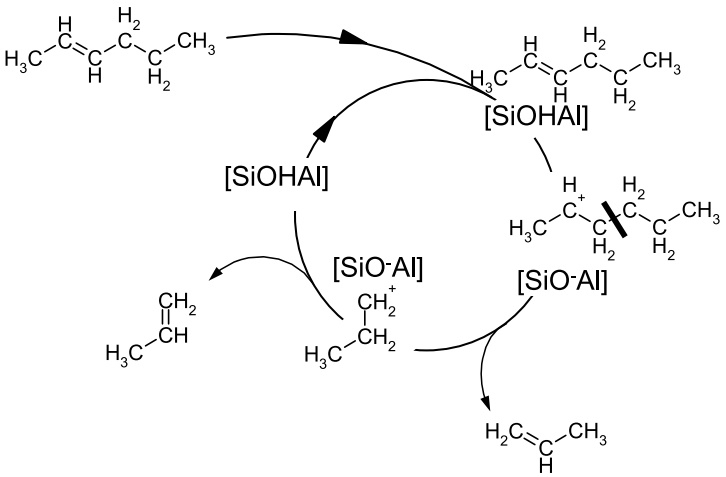

Scheme 4 Cracking of 2-hexene via carbenium ions (β cracking)

cleavage. Thus, when only considering the initial state, cracking of a carbenium ion with the positive charge at a tertiary carbon will be more probable than cracking of a carbenium ion with the positive charge at a secondary or primary carbon atom. Similarly, the ease of reaction decreases in the sequence tertiary > secondary > primary carbenium ion formed. Note that this is related to the influence of the Polyani relationship between the initial and final state upon the true energy of activation [97]. The energy of activation usually increases with increasing energy level of the final state. Therefore, the rate for reactions starting from a tertiary carbenium ion and ending with a tertiary carbenium ion (type A) is faster than the reaction starting from and ending with a secondary carbenium ion (type C). The possible pathways for the reaction are depicted in Scheme 5 [98]. Note that these rather simple assumptions for the mechanism lead to a surprisingly good prediction of the cracking selectivity observed [95].

The activation of alkanes is, however, significantly more demanding and usually requires one of three reaction routes. The easiest is the one that is described above implicitly, i.e., hydride abstraction from a carbenium ion, e.g., formed by protonation of an olefin present as impurity.

In the absence of olefins, strong Lewis acid sites can initiate a polarization of the C – H bond of alkanes and the elimination of H_2 forming an olefin that is readily protonated. In the presence of traces of oxygen, this can also lead to oxidative dehydrogenation of the alkane. Variants of this route were described by McVicker et al. [99, 100], who assumed that radicals are formed at the initial stage by the interaction of the alkane with an electron acceptor site to form subsequently H_2 and an alkene or, alternatively, methane and an alkene (with one carbon less than the feed molecules). In contrast, Kazansky et al. proposed this step to be initiated by Lewis acids (extra-framework alu-

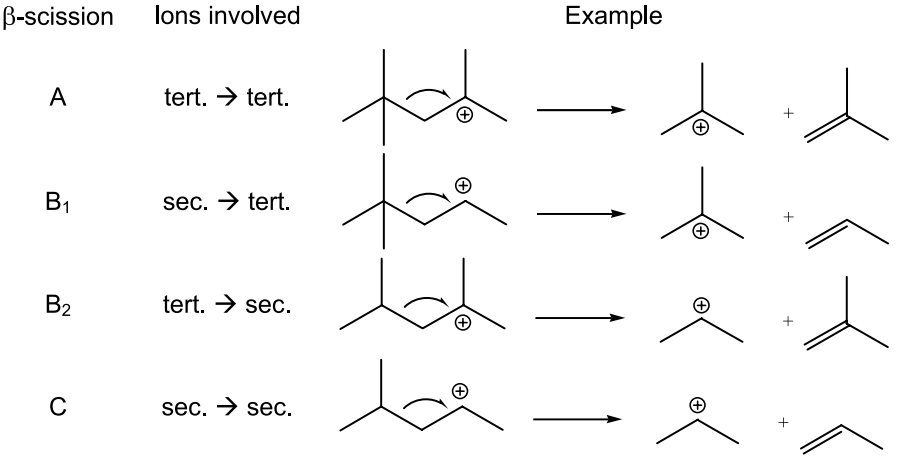

Scheme 5 Classification of β scissions of alkylcarbenium ions [98]

minum cations) via an ionic pathway also forming hydrogen, methane, some ethane, and the corresponding carbenium ions [24, 25].

The third possibility, the direct protonation of an alkane by a proton in liquid superacids at low temperatures, has been known from the work of Olah for some time, before Haag and Dessau [101] postulated in a landmark paper that alkanes may be directly protonated to form "surface stabilized" carbonium ions in zeolites (see also [102]). Because the reactive decay of the carbonium ion leads to breaking of the C – C or C – H bonds at the insertion point of the proton, the reaction has been named protolytic cracking. These products correspond to those observed from the collapse of a $C_6H_{15}^+$ ion in a mass spectrometer [103].

Monomolecular (protolytic) cracking dominates at low conversions, high reaction temperatures, low reactant pressures, and with medium and small pore zeolites that have a low concentration of Brønsted acid sites (see Scheme 6). All these conditions favor a low concentration of reactants in the pores and impede hydride transfer. The decay of the carbonium ion into an alkane and a smaller carbonium ion, which is the core elementary step in protolytic cracking, depends on the concentration of such ions in the pores. Thus, protolytic cracking depends subtly upon physisorption, the presence of polarizing oxide species in the pores, and the concentration of strong Brønsted acid sites. Results with *n*-alkanes in various zeolites suggest that the true energy of activation of cleaving the carbon–carbon bond is equal for all bonds in the molecule and that the selectivity of the cleavage is primarily related to entropic effects [104].

In contrast, at higher reactant partial pressures, higher conversion, and lower temperatures the monomolecular carbonium ion cracking is gradually replaced by the bimolecular carbenium ion cracking described above for

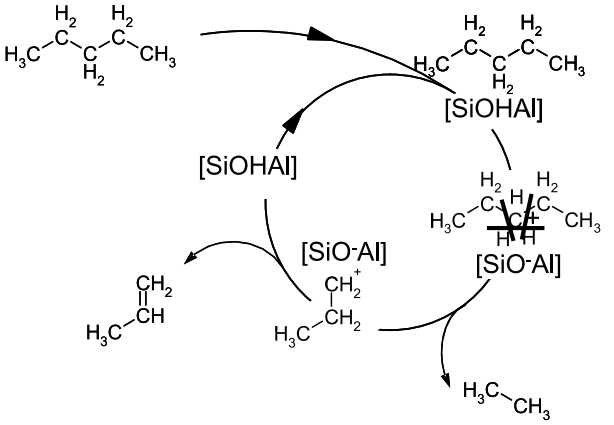

Scheme 6 Protolytic cracking of *n*-pentane

cracking of olefins. Under such conditions, the alkane is activated by hydride abstraction from a carbenium ion and forms a carbenium ion. The cracking pathway for carbenium ions proceeds according to Scheme 4.

At even higher pressures or conversions, these pathways are gradually replaced by a cracking mechanism that has substantial oligomerization preceding the cracking process. Clear evidence for such a route comes from labeling studies that show complete scrambling of carbon-labeled olefinic products of cracking [105]. While that route is important for accounting for the product distribution in some cases, the basic chemistry related to cracking is identical with that observed in β cracking. Therefore, the use of alkane cracking as a test reaction for acidity requires a careful choice of operating conditions and data treatment. Kinetic rates should be measured in a regime where one of the two first mechanisms prevails and cracking via oligomerization is minimized.

2.1.2.1 Butanes and Pentanes

Umansky et al. [106] showed that the intensive factor (acid site strengths) dominates over the extensive factor (concentration of the active sites) in controlling acid–base properties and the catalytic activity. The conclusion was reached by comparing the activity to convert isobutane of silica–aluminas, Y, ZSM-5, MOR, and β-zeolites, as well as sulfated zirconia and SbF_5-promoted silica–alumina to the acidity expressed as H_0 values of the strongest acid sites, which were determined from the spectral shift of adsorbed 4-nitrotoluene and 4-nitrofluorobenzene.

Union Carbide introduced the cracking of *n*-butane [107] to probe the acidity of various zeolites. *n*-Butane (2 mol % in He) has been used for the following reasons: (1) *n*-butane is a light gas and therefore easy to maintain

at a constant concentration; (2) the cracked products are light hydrocarbons and therefore easy to separate and analyze; (3) *n*-butane compared to, e.g., *n*-hexane, is more suitable to test strongly acid zeolites because of its lower reactivity; and (4) the use of 2 mol % *n*-butane avoids extensive deactivation of the catalyst. Seven different zeolite structures were studied and compared to quartz and silica–alumina. Acidity was found to depend on the Si/Al ratio of the zeolite and on the level of the alkaline ions present. The authors, however, did not distinguish between the acid strength and the concentration of acid sites on the catalyst surface and, therefore, a broad maximum in the correlation of the activity as a function of the acid site concentration was observed.

A more in-depth study on FAU-structure zeolites with high silica content by Beyerlein et al. [108] addresses the influence of extra-framework species (EFAL) on the catalytic activity for the isobutane conversion. Overall, the cracking activity increased linearly with the concentration of framework aluminum sites for all catalysts. However, FAU samples dealuminated with ammonium hexafluorosilicate (AHF) showed a lower activity compared to conventionally hydrothermally treated catalysts. Steaming of the chemically dealuminated catalysts led to an increased activity in cracking isobutane compared to the parent FAU. This is interpreted as an indication that extra-framework aluminum species, typically acting as Lewis acid sites, are interacting with Brønsted acid sites to form new and stronger acidic sites.

Auroux et al. [109] compared the activity of substituted ZSM-5 zeolites for the cracking of propane, *n*-butane, and isobutane with the reactivity of the C – C and C – H bonds. The heats of adsorption of the alkanes on the H-ZSM-5 samples, measured by microcalorimetry, decreased with the size of the alkane, which was related to the electron density at the C – C or C – H bonds. A trend to a lower overall cracking activity with increasing basicity of the alkane C – C bond was observed. Less acidic hydroxyl groups tend to interact selectively with the C – H bonds rather than the C – C bonds of the alkane and, therefore, increase the selectivity of the catalysts to dehydrogenation.

The cracking of neopentane over various solid acids (silica–alumina, $AlCl_3$/alumina, H-ZSM-5, H-Y and H-MOR) was investigated by Lombardo et al. [110], identifying two properties related to the acid strength of the active sites. One was the apparent activation energy for the formation of methane, which reflects the interaction between the Brønsted acid site and neopentane forming a carbonium ion that can only produce methane and a *t*-butyl carbenium ion. It is, therefore, directly related to the strength of the acid site provided that the heat of adsorption of neopentane is identical on all materials. The other is the equilibrium in the isobutene adsorption on an acid site ($Z^- - H^+$) forming the *t*-butyl alkoxy group (carbenium ion).

$$Z^- - H^+ + (CH_3)_2C = CH_2 \rightleftharpoons (CH_3)_3C - Z \rightleftharpoons (CH_3)_3C^+Z^- \,. \qquad (3)$$

The position of the equilibrium depends on the acid strength. Higher acid strengths will shift the equilibrium to the right. Thus, the higher the strength

of the Brønsted acid sites the longer will be the lifetime of the carbenium ion. This, in turn, leads to a more pronounced selectivity to secondary reactions.

However, the acid strength of the sites depends not only on the proton-donating ability of the active site toward a base (a reacting molecule), but also on the stabilization of the resulting alkoxy group or carbenium ions [111, 112]. Engelhardt and Hall [111] studied the effect of residual Na^+ in Y zeolites and concluded that by removing Na^+, the concentrations of acid sites and also the strength of the acid sites must have increased, which was explained either by a strength increase of all sites or creation of a small fraction of very active sites. The experiments of Lombardo et al. [110] indicated that the acidity of the solid acids investigated is not sufficiently strong to protonate the primary C – H bonds of neopentane, because hydrogen formation was not detected. In slight contrast Shigeishi et al. [113] showed for the cracking of *n*-butane and isobutane that H-ZSM-5 has sufficient acid strength to protonate the secondary and primary C – H bonds of alkanes.

Short chain alkanes (C_4 and C_5), especially isobutane and neopentane, were frequently used to elucidate the reaction mechanism of catalytic cracking, e.g., in papers by Hall et al. [110, 114] and Kranilla et al. [115]. In these publications, however, few comparisons were made to distinguish the intensive and extensive factors of the zeolite acidity.

2.1.2.2 Hexanes

The catalytic conversion of *n*-hexane was proposed in 1966 and 1980 as a test reaction for zeolite catalysts by Mobil [80, 116] and is nowadays used in the form of the so-called α test. The α activity is the ratio of the cracking rate constant for a given catalyst and the rate constant of an equal volume of a standard amorphous silica–alumina cracking catalyst.

Zholobenko et al. [117] investigated the conversion of *n*-hexane over mildly and severely steamed H-ZSM-5 zeolites and found, in agreement with Lago et al. [118, 119], an increase in the activity for *n*-hexane cracking over the mildly steamed zeolites. Lago et al. [118, 119] explained this by the presence of Al pairs, in which one Al^{3+} is removed from the framework under formation of a Lewis acid site that withdraws electron density from the neighboring Brønsted acid site and, thus, enhances its acidity. Zholobenko et al. [25], however, concluded that the presence of Lewis acid sites, formed during mild steaming, enhances the activity in *n*-hexane cracking due to their ability to strongly polarize C – H bonds. These Lewis acid sites initiate *n*-hexane cracking by H_2 or CH_4 abstraction and formation of a reactive olefin that is subsequently transformed via the classical carbenium ion mechanism on Brønsted acid sites. Additional experiments by Zholobenko et al. [24], where they cofed 1-hexene to their reactant, supported the con-

clusion of catalytically active Lewis sites. Thus, for achieving the maximum activity an optimal ratio of Brønsted to Lewis acid sites seems to exist.

In contrast to H-ZSM-5, severe steaming of H-Y zeolites leads to catalysts with stronger acidic sites. H-Y in the as-synthesized form has typically an Si/Al ratio between 2.5 and 3, while ZSM-5 can be synthesized with Si/Al ratios above 30. Therefore, in ZSM-5 all aluminum atoms are rather isolated within the zeolite framework (i.e., without other aluminum atoms as next-nearest neighbors). Partial deactivation of H-Y with 2,6-dimethylpyridine [120] and sodium [28] indicated that only a fraction of the Brønsted acid sites is active in the conversion of *n*-hexane. In both studies, IR spectroscopy was used to study the type and concentration of surface hydroxyl groups. The IR spectra revealed that, besides the typically observed HF- and LF-OH groups of H-Y at 3630 and 3550 cm^{-1}, respectively, an additional IR band at 3600 cm^{-1} is present, which can be correlated to the catalytic activity of the zeolites. This band was assigned to an OH group, which is pointing into the supercage, but is further perturbed by the interaction with cationic tetrahedral aluminum present in the β cages as $AlOH^{2+}$ species, as described by Lonyi and Lunsford [27, 28].

A good example of the advantage of using catalytic test reactions over other methods to probe acidity was shown by Parillo et al. [121], who studied different ZSM-5 zeolites by measuring the heat of adsorption of ammonia and pyridine and comparing the results to the reactivity in *n*-hexane cracking, propene oligomerization, and 2-methyl-2-propanol decomposition. Marked differences in the activities of these zeolites were observed, while the heat of adsorption was the same suggesting that the heat of adsorption for strong bases is not related to catalytic activity in a simple way.

In order to differentiate the available reaction space, Frillette et al. [122] introduced the constraint index (CI), which is determined from the ratio between the relative rates of *n*-hexane and 3-methylpentane cracking:

$$\mathrm{CI} = \frac{k_{n\text{-hexane cracking}}}{k_{3\text{-methylpentane cracking}}}. \tag{4}$$

For amorphous silica–alumina and for faujasite structures, a CI of 0.6 was observed, while for zeolites with ten-membered-ring (10-MR) channels (ZSM-5) values of ~8 and for zeolites with 8 MR (erionite) a CI of 38 were reported. This shows that the CI can be used to differentiate between zeolites with medium ($1 < \mathrm{CI} < 12$) to small pore sizes ($\mathrm{CI} > 12$), while it is not sensitive enough to classify zeolites with pores consisting of 12 or more oxygen atoms ($\mathrm{CI} < 1$).

2.1.2.3 Heptanes and Octanes

Lopes et al. [123, 124] compared the activity of SAPO-37 and H-Y zeolites in the conversion of *n*-heptane and 2,2,4-trimethylpentane. Because of the dif-

ferent reactivity of hydrogen atoms at secondary and tertiary carbon atoms and the different potential cracking routes, *n*-heptane requires stronger acid sites than 2,2,4-trimethylpentane. The higher concentration of acid sites in H-Y compared to SAPO-37 led to higher initial rates for both reactions with H-Y. The ratio between the initial rates of 2,2,4-trimethylpentane and *n*-heptane cracking was significantly higher with SAPO-37 than with H-Y. As this ratio should reflect the relative contribution of stronger and weaker acid sites, the results indicate that SAPO-37 had weaker acid sites than the H-Y sample.

In a further example, Lopes et al. [125] compared the acid strength of H-ZSM-20, H-Y, and USH-Y determined by ammonia temperature-programmed desorption (TPD) to the activity for *n*-heptane conversion. While hardly any differences were seen in the ammonia TPD, the initial activities observed for *n*-heptane cracking were clearly different and allowed a subtle discussion of the effects controlling the activity. It is impressive that the higher activity of H-ZSM-20 could be traced to the better distribution of aluminum throughout the framework. In a similar study the authors applied the probe reaction to a subtle comparison of the role of ion exchange degrees in the structurally related zeolites Y and ZSM-20 [126].

Kumar et al. [127] studied the influence of cation exchange on the strength and distribution of acid sites in ultrastable zeolite Y for *n*-heptane and gas oil cracking. Exchange with Li^+, Na^+, K^+, and Mg^{2+} leads to a decrease in the intrinsic activity per Brønsted acid site for protolytic *n*-heptane cracking. In contrast, the activity for gas oil cracking was hardly affected. This indicates that weaker sites are generated in the steaming process to generate ultrastable zeolite Y, which catalyzes cracking of the more complex reactant mixture. However, the selectivity changed subtly indicating that the secondary cracking of the smaller hydrocarbons was suppressed after ion exchange. This indicates that great care has to be taken when extrapolating catalyst evaluations with test reactions to more or less reactive molecules.

Like for the smaller molecules, also for heptanes and octanes a large number of researchers report direct correlations between the catalytic activity and the concentration of aluminum in the zeolite framework or the concentration of strong Brønsted acid sites. Lischke et al. [29] compared the activity of the cubic and the hexagonal forms of Y zeolite for the *n*-heptane conversion. The acid sites were modified by steam dealumination at various temperatures and by acid leaching with 0.5M HCl. For the dealuminated samples, a linear relationship between the concentration of acid sites and the initial rate of *n*-heptane cracking was observed. Similarly, Rustamov et al. [128] demonstrated for catalysts based on zeolite Y that the catalytic conversion of *n*-heptane was proportional to the concentration of strong Brønsted acid sites. Derewinski and Fajula [129] showed the same trend for [B]- and [Al]-beta zeolites and Klyachko et al. [130] for mordenite and ZSM-5 zeolites. It is important to note that in all these examples only the concentration of strong

Brønsted acid sites, but not the concentration of all Brønsted acid sites, correlated well with the catalytic activity.

In a more complex study, Yamagishi et al. [131] found a linear relationship between the concentration of framework aluminum of the parent ZSM-5 and the activity for *n*-octane cracking. For a given Brønsted acid site concentration, ZSM-5 aluminated with $AlCl_3$ had a higher activity than the parent sample. This suggests that the presence of alumina species in the pores enhances the reaction rate. While not being discussed explicitly in the paper, the potential reaction routes could include additional dehydrogenation, stronger adsorption, or an enhancement of the Brønsted acid site itself.

Corma et al. [132] measured the initial selectivities for cracking of *n*-heptane on rare-earth-containing H-Y zeolites. From a combination with molecular orbital calculations, it was shown that cracking can initially take place on Brønsted acid sites via protolytic cracking, or on Lewis acid sites via a classical β-scission mechanism. Note that this paper appeared simultaneously with the paper by Haag and Dessau. The suggestion that the activation energy for protolytic cracking is lower than that for the β scission of *n*-heptane appears, however, to be an artifact of the quantum chemical calculations.

Chauvin et al. [133] studied the conversion of isooctane over chemically dealuminated faujasite, offretite, and mazzite. Stepwise thermal desorption of ammonia showed the presence of stronger acid sites on offretite and mazzite compared to faujasite, which was, however, not reflected in the initial activities for isooctane conversion. The comparison of the acidity and the activity points to possible limitations when comparing catalysts with different zeolite structures. The conversion over offretite (channel diameter 6.8×6.7 Å [1]) has strong diffusional constraints and is, therefore, not controlled by the number and strength of the acid sites involved. The mazzite sample (channel diameter 7.4×7.4 Å) showed a higher conversion, but the very high deactivation of this catalyst due to the presence of strongly acidic sites makes the estimation of initial rates very inaccurate. Choudhary and Akolekar [90] studied isooctane conversion over ZSM-5, ZSM-8, ZSM-11, MOR, and L-, X-, and Y-type zeolites. They also found the conversion over ZSM-type zeolites to be strongly diffusion-limited showing that even when test reactions are used, diffusion limitations need to be checked.

The results show that the activity of a catalyst toward a test reaction depends on the number and strength of the acid sites, the ratio of Lewis to Brønsted acid sites and, when different zeolite structures are compared, additionally on geometrical factors. Therefore, catalytic test reactions are only of a very limited value for the comparison of different zeolites without an in-depth analysis of the reaction pathways involved. Thus, it is obvious that branched isomers are not an appropriate choice for probing small and medium pore zeolites due to the diffusion limitations of the test molecules. The diffusional constraints can even be present in deeply dealuminated large

pore zeolites due to the formation of extra-framework alumina–silica species that can block the access into pores and to the active sites for bulky reactant molecules.

2.1.2.4 Long Chain Alkanes

Long chain alkanes are used in testing the acid properties of microporous catalysts [134–136]. One of the most often used reactant molecules is *n*-hexadecane [137–139], due to its relevance for determining the cetane number of diesel fuel for quality evaluation [140]. Frequently, zeolites with large pores or mesopores [138, 141] and bifunctional catalysts (e.g., Pt containing zeolites) [142] are studied. Due to the easy access of small molecules to the zeolite pores, only larger or highly branched hydrocarbons can be used to study the contributions of acid sites on the outer surface. Based on a comparison between measured and simulated adsorption properties, Schenk et al. [143] showed that the pores of zeolites are saturated with the long chain reactants, which leads to the selective production and adsorption of the most compact, branched paraffins in *n*-hexadecane hydroconversion in molecular sieves.

2.1.2.5 Cumene

A reaction already used for a long time to test acid catalysts is the cracking of cumene (isopropylbenzene). This molecule has a very simple cracking scheme due to the fact that the benzene ring is not attacked under these conditions. Therefore, the primary products in cumene cracking are propene and benzene. Additional products of this reaction are diisopropylbenzene, toluene, ethyltoluene, ethylene, ethane, butenes, ethyl- and propylbenzenes, cymene (*p*-methylcumene), methane, and isobutane. Thus, a thorough kinetic analysis is needed to distinguish between all possible products and to obtain the correct activity, which can be related to the number and/or strength of the acid sites. A review by Corma and Wojciechowski [144] addresses all aspects of the reaction mechanism of cumene cracking. Only a part of the Brønsted acid sites is claimed to be active in cumene conversion, and some by-products are formed on Lewis acid sites. Therefore, this reaction can also be used to differentiate between Lewis and Brønsted acid sites.

The deactivation of the catalysts in this reaction was studied by Bellare and Dadyburjor [145], Corma et al. [48], Al-Khattaf et al. [146], and Choudhary and Akokelar [90]. Especially the latter authors showed the differences in the deactivation over a variety of zeolite structures. Thus, we wish to emphasize that in this reaction (or more generally for every reaction that strongly suffers from deactivation), activity measurements that are not taken from initial

conversion values seem to be useless for a ranking of acidity, if the deactivation behavior is not the same for all catalysts studied. Even for the same zeolite structures, differences in the ion-exchange level, the dealumination level, and the site density can exhibit different deactivation trends. Dadyburjor and Bellare [147] as well as Fukase and Wojciechowski [148] studied the conversion of cumene over Y and ZSM-5 zeolites and concluded that this reaction strongly depends on the pore dimensions of the zeolite, especially when shape selectivity plays an important role such as in the case of ZSM-5. Therefore, erroneous results regarding acid strength or number of acid sites might be obtained.

Despite all the limitations mentioned many studies of cumene cracking over zeolites exist, which show good correlations between the acidic properties and catalytic activity. Yamagishi et al. [131] studied the alumination of ZSM-5-type zeolites by treatment with $AlCl_3$ and found that the first-order rate constant of cumene cracking is a linear function of the concentration of framework aluminum. Their results indicated that, although the ratio between Brønsted and Lewis acid sites was different if the catalyst was aluminated, the total activity was the same. This seems to suggest that an interaction between Lewis and Brønsted acid sites exists and, therefore, the same activity can be reached for catalysts with different concentrations of Lewis and Brønsted acid sites. DeCanio et al. [82] studied cumene cracking over a series of Y zeolites, dealuminated with $SiCl_4$ and steam treatment, and one ZSM-5 catalyst. For the catalysts dealuminated with $SiCl_4$ they found the same TOFs over a range of framework aluminum atoms from 0 up to 15 aluminum atoms per unit cell. This suggests that the acid strength of the $SiCl_4$-dealuminated zeolites is not a function of the framework aluminum content and that, therefore, the activity can be directly related to the concentration of acid sites. In contrast, the TOF of the steam-dealuminated sample was significantly lower compared to the other Y zeolite samples. For ZSM-5, a higher TOF in cumene cracking was reported after steaming. These results show that within a class of dealuminated zeolites, the TOFs are constant and cumene cracking can be used as a measure of the concentration of acid sites. If other zeolites are compared, acid site strength also has to be taken into account.

Zi et al. [91] studied Y zeolites dealuminated with H_4EDTA and $(NH_4)_2SiF_6$. The surface acidity of the zeolites was determined by *n*-butylamine titration, and the amount of strong ($H_0 < -3.0$) acid sites was correlated with the cumene conversion. Both values showed a volcano-type curve if plotted against the amount of Al in the framework. The maximum in these plots was found to be around 30 aluminums per unit cell, which agrees with the results published by DeCanio et al. [82].

Nayak and Choudhary [149] studied hydrothermally dealuminated ZSM-5 zeolites and found that the decrease in catalytic activity of cumene conversion and the decrease in the amount of strong acid sites (which adsorb pyridine irreversibly at 400 °C) followed the same trend. They reported a linear relation between cumene conversion and the concentration of strong acid sites,

which deviates at conversions higher than 50%, which might possibly be caused by the fact that less acidic sites active in cumene cracking were present (adsorbing pyridine at somewhat lower temperatures). This is supported by the results of Choudhary [150], who selectively poisoned sites by adsorbing pyridine at different temperatures and estimated the retained activity of the catalyst. With 55% conversion in the nonpoisoned state, he found an activity of around 2% when pyridine was adsorbed at 325 °C and of around 8% when it was adsorbed at 400 °C. Also, in this case, the results have to be used with caution, because the sorption of pyridine is expected to generate steric constraints for the reacting molecules.

Akolekar [151] found a linear relation between the number of strong acid sites (determined by adsorption of pyridine at 400 °C) and the conversion of cumene over metal-substituted AlPO-11 with the exception of Mg-AlPO-11. A closer look at the acid site distribution, however, showed that this catalyst has the largest concentration of sites with lower acid strength (pyridine desorption between 300 and 400 °C). As described above, the activity of these sites must be included. Tian et al. [152] studied SAPO-11 molecular sieves, which were dealuminated by EDTA to achieve different Al contents. After dealumination the activity for cumene cracking improved, which was attributed to the formation of strong Brønsted acid sites around Si domains and to a reduction of the Lewis acidity.

Narayanan et al. [153] compared two ZSM-5 zeolites, one synthesized with and the other without a template. Although these catalysts were different in the amounts of Lewis and Brønsted acid sites, the conversion of cumene was found to be in the same range, which indicates that Lewis acid sites did not strongly influence the cracking of cumene. More conclusions cannot be drawn from this study because of the lack of acid site distributions.

2.1.3 Disproportionation Reactions

2.1.3.1 Toluene

In toluene disproportionation, two toluene molecules react to yield benzene and xylenes by transferring a methyl group from one toluene to the other. This reaction has to be done at moderate temperatures to avoid cracking and dealkylation of toluene. Therefore, reactions are mostly carried out at around 400 °C. Rhodes and Rudham [154] studied this reaction over steam- and EDTA-dealuminated Y zeolites and found initially an increase of conversion with time, followed by a maximum after 5 to 20 min. Subsequently a complete deactivation of the catalysts occurred after 10 to 25 minutes. This behavior resulted from the formation of catalytically active coke during the reaction. The maximum activity over all catalysts was linearly related

to concentration of acid sites. The initial activities, however, were different for steam-dealuminated and EDTA-dealuminated catalysts. This suggests that toluene disproportionation is initially catalyzed by strong Brønsted acid sites associated with extra-framework aluminum species. At the initial stage of conversion, steam-dealuminated catalysts show a much higher activity than EDTA-dealuminated catalysts with the same concentration of acid sites. Due to coking, this effect is leveled and both catalysts show the same conversion. The paper proposes that better correlations of acidity and activity are reached by comparing the maximum activities rather than the initial ones.

Meshram [155] investigated the influence of acidity of ZSM-5 zeolites modified with Ni, Mg, P, and B on the activity in toluene disproportionation. The order of activity was: H-ZSM-5 > Ni,H-ZSM-5 > P,Mg,H-ZSM-5 > B,H-ZSM-5. The acidity of these zeolites, measured by TPD of NH_3, followed the same trend. H-ZSM-5 showed a benzene/xylene molar ratio of more than one, which is a sign that some cracking is catalyzed by this catalyst to yield benzene and gaseous products. Note that while H-ZSM-5 seems to have sites able to catalyze cracking, the Ni-exchanged sample has a benzene/xylene ratio of around one indicating that the sites are too weak to catalyze cracking under the chosen reaction conditions.

Ej-Jennane et al. [156] compared H-ZSM-5, H-MOR, and H-Y zeolites in the disproportionation of toluene at long TOS. They found that the catalytic activity was related to the number of acid sites for the H-ZSM-5 structure which did not show much deactivation, that there was a strong diffusional limitation with H-MOR due to pore blocking, and that the reactions over H-Y were limited by site poisoning. These results show that measurements after a long stabilization period are very hard to compare to acidity values which are measured on the fresh catalysts. If no initial activity is taken for comparison, different modes of deactivation over various catalysts will make it nearly impossible to evaluate the acidity of zeolites with different structures by means of this test reaction.

2.1.3.2 Ethylbenzene

Two potential pathways exist for ethylbenzene disproportionation. One proceeds via dealkylation/alkylation, for which a first ethylbenzene is dealkylated to benzene and an ethylcarbenium ion, which subsequently alkylates a second ethylbenzene molecule to yield diethylbenzenes. The other pathway is the reaction via a diphenylethane intermediate, which would prevent the formation of alkenes and subsequent deactivation reactions. As already noted for toluene disproportionation, cracking can become the main reaction at higher reaction temperatures.

Karge et al. studied this reaction in a series of papers [157–161], investigating various ion-exchanged mordenites (e.g., with H, Na, Be, Mg, Ca, Sr,

Ba, La) and their dealuminated forms (1N HNO_3 leaching) [157]. By comparing the OH stretching vibration of MOR at 3600 cm^{-1}, the pyridinium band at 1542 cm^{-1} (both measured by IR spectroscopy), and the catalytic activity, a linear relationship between the activity and the concentration of acid sites was established for all catalysts. The results suggest that Lewis acid sites are not relevant for the reaction. Moreover, the Ba-exchanged mordenite was inactive for ethylbenzene conversion, although it had Brønsted acid sites. This indicates that the acid sites in Ba-MOR are too weak to catalyze ethylbenzene disproportionation. In the temperature range from 200 to 300 °C only transalkylation was observed, i.e., a benzene to diethylbenzene ratio of 1. As cracking reactions were not observed in this temperature range, deactivation was not observed over these catalysts. These results were confirmed and extended to pentasil-type zeolites (H-ZSM-5 and H-ZSM-11). In this case, a linear relation between the intensity of the pyridinium band (measured by IR spectroscopy) and the catalytic activity was not observed, which was explained by the additional influence of the acid site strength. Additionally, the formation of *o*-diethylbenzene was not observed for H-ZSM-5 and H-ZSM-11, while the ratio between the three isomers was close to equilibrium over mordenite. This suggests that different mechanistic routes can be present with the different zeolite types and that shape selectivity plays a role for 10-MR zeolites, such as H-ZSM-5 and H-ZSM-11. Note that a reaction temperature of 350 °C was required for ethylbenzene conversion over H-ZSM-5 and H-ZSM-11. At this temperature mordenite had already started to deactivate by coke formation.

Again, this clearly points out possible limitations when rates of test reactions are compared for different zeolite types, especially when comparing large pore to small pore zeolites. Conversion of ethylbenzene over Na-, NH_4-, Be-, Mg-, Ca-, Sr-, Ba-, and La-X and Y zeolites and H,K-L, NH_4,K-L, Na-ZSM-5, and NH_4,Na-ZSM-5 was studied in [158]. The Sr- and Ba-exchanged forms of Y and nearly all ion-exchanged forms of the X zeolites showed no or only a very low conversion.

It is interesting to note that La,Na-X showed a 1.6 times higher conversion than the La,Na-Y zeolite, yielding benzene to diethylbenzene ratios of unity. The ranking of the catalysts with respect to their total acidity did not correlate with the activity in ethylbenzene disproportionation, while the concentration of very strong acid sites ($H_0 < -8.2$) correlated very well with the catalytic activity of the faujasite-type materials. Sr- and Ba-Y samples, which do not possess strongly acidic sites, were not active in this test reaction.

Rhodes and Rudham [162] studied the conversion of ethylbenzene over a series of hydrothermally dealuminated Y zeolites, which were subsequently treated with Na_2H_2EDTA to extract the extra-framework Al oxide species. Catalyst characterization by TPD of NH_3 showed a correlation between the activity for ethylbenzene disproportionation and the acidity. The linear relation indicates that (strong) Brønsted acid sites are active sites for the ethyl-

benzene conversion. Interestingly, a synergistic effect of extra-framework aluminum species and Brønsted acid sites, led to an increased activity of the catalysts before EDTA leaching. In contrast, Sobrinho et al. [163] did not find evidence that extra-framework aluminum species play a role in ethylbenzene conversion by comparing steamed and acid-leached Y zeolite samples.

These latter results illustrate the controversy on the influence of extra-framework species in zeolites for catalytic reactions. Note that on the one hand the extra-framework aluminum includes synergistic effects and, hence, increases the activity. On the other hand, the introduction of diffusional constraints resulting from a partial blockage of the pores or acid sites leads to a decrease of the reaction rates. Therefore, the evaluation of acid–base properties using the rates of test reactions over various catalysts might be restricted to a certain degree, and without a detailed analysis of the acid site and strength distribution only zeolites of one structural type, or even with the same preparation history, can be reliably compared.

Niu and Hofmann [164] related the activity of USY, H-ZSM-5, and H-MOR zeolite catalysts in ethylbenzene conversion to the acidity measured by IR spectroscopy using pyridine adsorption and TPD of NH_3. Catalytic measurements at 300 °C did not show deactivation over all three catalysts, while increasing the reaction temperature to 400 °C led to a strong deactivation for H-MOR and some deactivation of USY. The conversion over H-ZSM-5 was not affected by deactivation. At 300 °C only disproportionation reactions were observed, while at 400 °C large contributions of cracking were found (i.e., benzene to diethylbenzene ratios above 1) over all three catalysts.

2.1.4 Isomerization

2.1.4.1 Alkanes

The hydroconversion of *n*-alkanes over noble metal-loaded zeolites follows a bifunctional mechanism, in which the reactant is dehydrogenated on the metal particles and the formed alkene is isomerized and/or cracked over the acid sites of the zeolite, followed by a subsequent hydrogenation of all unsaturated products on the metallic sites (see reaction Scheme 7).

According to Jacobs [33], the rearrangement of the carbenium ions is rate determining in this reaction, when the metal loading of the catalysts is sufficiently high. In this case, the selectivities for cracking or isomerization depend on the lifetime of the carbenium ion on the acid site. The stronger the acid sites the longer the lifetime and, thus, the more cracking is expected compared to isomerization. Additionally, the rate of hydroconversion will depend on the concentration of acid sites present in the zeolite. Therefore, these reactions should be able to probe acid site concentration using the reaction

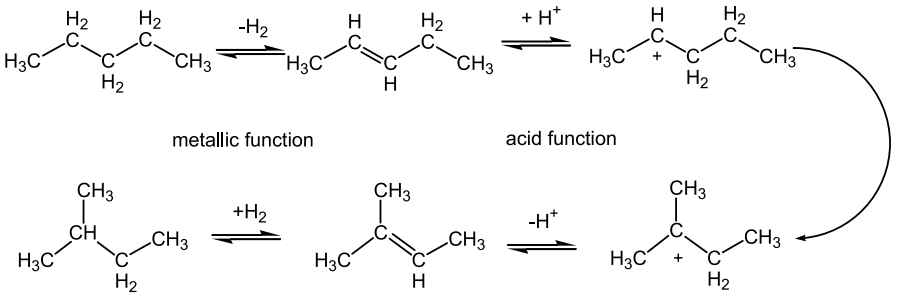

Scheme 7 Bifunctional hydroisomerization of *n*-pentane

rate as well as the acid strength of the sites by the ratio of cracking to isomerization. The nearly complete absence of catalyst deactivation is a further advantage in comparison to conventional cracking and isomerization.

For the hydroconversion of *n*-heptane and *n*-decane, the group of Jacobs [96, 165–169] reported a linear relation between the rates of hydroisomerization normalized to the concentration of tetrahedral Al and the concentration of pentacoordinated and tetrahedrally distorted Al (analyzed by ^{27}Al MAS NMR) [166]. This emphasizes that the interaction of extraframework aluminum species with Brønsted acid sites creates more active sites. The work by Blomsma et al. [96, 165, 167] shows that hydroconversion of *n*-heptane over Pd/H-Beta zeolites is a combination of classic bifunctional hydrocracking and cracking of dimerized C_7 species.

From these studies, it is clear that hydroconversion can be used to probe the acidity of zeolite catalysts, but there will be difficulties in establishing a scale when comparing different zeolite structures due to restraints for bulkier intermediates or transition states to fit into smaller pores. For small pore zeolites such as ZSM-22, the high yields of skeletal isomerization of heptadecane (90%) obtained are explained by the limited penetration of these molecules into the micropore openings of the zeolite and the conversion in the pore mouth region, preventing their cracking via the β-scission reaction mechanisms [168]. In fact, *n*-decane hydroconversion [136, 141, 170] and the hydrocracking of *n*-butylcyclohexane have been developed into a successful test method to probe the void space of molecular sieves by comparing product distributions. The refined constraint index (RCI) is calculated from the ratio of 2-methylnonane and 5-methylnonane formed in *n*-decane hydroconversion [141, 170]. The space requirement for the formation of 5-methylnonane is larger than that for 2-methylnonane and, therefore, the RCI will increase with decreasing pore diameter. Due to the size of the reactant and probe molecules, this method is especially well suited for the characterization of zeolites with 10-MR pore systems.

Zeolites with 12-MR pore systems can be characterized with the spaciousness index (SI), which is determined from the ratio between isobutane and

n-butane formed during hydrocracking of *n*-butylcyclohexane [171]. Isobutane is formed via a smaller transition state than *n*-butane, therefore the SI decreases with increasing pore size.

2.1.4.2 Xylenes

Xylene isomerization is a test reaction which is claimed to require moderately strong Brønsted acid sites to proceed. One reason for this is the very good stabilization of the formed carbenium ions over the benzene ring. The reaction proceeds via a benzenium ion and the rate-limiting step in this reaction is the intramolecular methyl transfer. Besides the monomolecular mechanism, xylene isomerization can also proceed via a bimolecular reaction pathway as outlined by Morin et al. [172]. They determined the contributions of both pathways and determined the contribution of the monomolecular reaction, which they propose to compare activity and acidity in zeolites. These findings emphasize that the reaction pathway should be known in order to properly estimate acidity. Especially for large pore zeolites, this may be a problem.

Bourdillon et al. [84] studied the activity of Y zeolites, which have a very broad acid strength distribution, in *o*-xylene isomerization. After blocking the acid sites by adsorption of pyridine and desorption at 300 °C, the catalysts did not regain activity, while after desorption at 500 °C the complete activity was restored. However, this also indicates the strength of acid sites necessary to convert alkanes. Yushchenko et al. [87] blocked the acid sites of ZSM-5 and ZSM-11 type zeolites with ammonia and pyridine and found that a desorption temperature of 200 and 300 °C for ammonia and pyridine, respectively, was necessary for regaining the activity for *o*-xylene conversion. Pyridine has a stronger interaction and exhibits additional diffusion constraints compared to ammonia. Therefore, caution is needed if certain absolute values are compared. Choudhary [149] studied hydrothermally treated ZSM-5 samples and found a close relationship between the concentrations of strong Brønsted acid sites (desorption of pyridine at 400 °C) and the activity in *o*-xylene isomerization. In [90], Choudhary compared different zeolites including MOR, X, Y, L, ZSM-8, ZSM-5, and ZSM-11, and found that xylene isomerization was also catalyzed by sites from which pyridine desorbs at temperatures below 400 °C, especially for the X, Y, and L zeolites. The catalytic activities per strong acid site were not the same for the different zeolites studied and depended also on the structure and topology of the zeolite. These results suggest that only one probe reaction may not suffice for a comparison of different zeolite structures. It is unclear if this is related to steric reasons for stabilizing the carbenium ion intermediates, restrictions of access to acid sites, or different acid site distributions in the zeolites. Similar to this, Akolekar [151] compared a series of metal-substituted aluminophosphates

with AlPO-11 structure and also found limitations when applying only one test reaction for zeolites identical in structure, but having framework atoms substituted by different elements.

Hong et al. [173] could provide evidence for a synergistic effect of Lewis acid sites in the conversion of *o*-xylene over dealuminated MOR zeolite. These authors correlated the turnover numbers, normalized to the Brønsted site concentrations, against the concentration of Lewis acid sites and a linear relationship was found. It should be emphasized that most of these studies do not differentiate between a higher surface concentration of *o*-xylene induced by the presence of Lewis acid sites and a higher intrinsic activity of the Brønsted acid sites.

2.1.5
Alcohol Dehydration Reactions

The dehydration of alcohols over zeolites proceeds via the interaction of the alcohol molecule with Brønsted or Lewis acid sites. When both sites are present, the reaction pathway involving Brønsted acid sites dominates. In principle, two products can be formed: ethers and olefins. A detailed study of the reactivity of alcohols on zeolites and other molecular sieves can be found, e.g., in [174].

The first step in the alcohol conversion is adsorption on a Brønsted or Lewis acid site, followed by the cleavage of the OH group and the formation of an alkoxy species (carbenium ion in the excited state). When Brønsted acid sites are catalytically active, water is eliminated in this step. The resulting alkoxy group subsequently decomposes into an alkene and the proton. In the case of the Brønsted acid site, this regenerates the catalytically active center. With Lewis acid sites being catalytically active, the OH group cleaved in the first step and the proton generated by the decomposition of the carbenium ion recombine and desorb as water, thus regenerating the Lewis acid site. Note that the olefins can react further by isomerization and oligomerization eventually leading to catalyst deactivation. Of all the reactions discussed so far for the characterization of acid sites, alcohol dehydration requires the lowest acid site strength to proceed.

2.1.5.1
Methanol, Ethanol, Propanol, and Butanol

Methanol conversion is a special case, because it cannot form unsaturated species by dehydration. Therefore, the primary product of methanol conversion is dimethyl ether, which is produced by an intermolecular dehydration reaction [174]. For this reaction a contribution of the lattice oxygen atoms (basic sites) is also proposed [175], which would rule out the application of methanol conversion as a probe reaction for acid sites.

However, very little information can be found in the literature regarding the reaction of methanol to dimethyl ether and the correlation to the strength and concentration of acid sites, while most of the recent literature deals with the conversion of methanol to hydrocarbons (MTG reaction) [176, 177]. In this reaction many possible products, i.e., alkenes, alkanes, and aromatics, can be formed, which limits the application of the reaction as a test reaction for acid sites. Nevertheless, Lietz et al. [178] observed that active sites with a higher acid strength, which are formed by the synergistic interaction between framework Al and extra-framework sites, increase the aromatization of methanol. The same conclusion was drawn by Lukyanov [179], who showed that the sites with enhanced activity are not active in the initial stages of the formation of alkenes or dimethyl ether from methanol. Gayubo et al. [180] reported that with increasing acid site strength, the selectivity to higher hydrocarbons increased due to the higher coverage on these acid sites, which increases the sequential reaction to form higher hydrocarbons. In a study of methanol conversion over SAPO-34 molecular sieves, van Niekerk et al. [181] found a direct relationship between the conversion of methanol and the strong acidity measured by TPD of NH_3.

The conversion of ethanol to primary products, such as ethene and diethyl ether, is even less studied. Akolekar [151] compared different AlPO molecular sieves in the conversion of ethanol to hydrocarbons, and could not find a direct relationship between the concentration of acid sites with different acid strength and the activity of the catalysts. The catalysts investigated, however, had different acid site strength distributions and, as shown by DeCanio et al. [82], in this case the activity for a certain reaction is determined by the concentration of acid sites with highest strength.

The dehydration of isopropanol to propene, diisopropyl ether, and water was studied by Korah and Viswanathan [182] to evaluate the acidity of H-Y zeolites. They progressively poisoned the catalysts in situ with organic amines (i.e., *n*-butylamine, pyridine, and piperidine) and determined the activity in isopropanol dehydration with increasing degree of poisoning. In this way, the acid strength distribution of the various catalysts was determined. They found that the concentration of acid sites of these catalysts did not change with differences in the reaction temperature, while the acid site strength distribution, i.e., the intrinsic acidity factor, varied. These results show that it is possible to determine the acid strength distributions as a function of the reaction temperature using different test reactions. Isopropanol elimination reactions are frequently used to probe the acid–base bifunctionality of zeolites and will be addressed in detail below.

The dehydration of isobutanol was studied by Singh et al. [183] over a series of SAPO-11 samples. The concentration of acid sites was related to the activity in isobutanol conversion, and the selectivity in the subsequent isomerization to butenes was related to the acid strength distribution of these catalysts. The authors, however, made a rather qualitative evaluation

of acidity and did not explore acid site strength and acid site concentration in detail.

All test reactions of the linear alcohols discussed here face the major problem of deactivation of acid sites due to the high activity of the formed linear alkenes to polymerize and, thus, to deactivate the catalyst surface by coke species. In this case, measuring the initial activity in alcohol conversion is necessary to achieve a meaningful rating of the catalyst. Another possibility is the usage of alcohols, which react to a rather inert alkene and, therefore, show less deactivation (see Sect. 2.1.5.2).

2.1.5.2 Cyclohexanol

Using cyclohexanol as a test molecule to estimate acid sites in zeolites has an advantage over linear molecules, because the dehydration yields cyclohexene, which has a lower affinity to oligomerize compared to linear or branched alkenes. Therefore, deactivation of the catalysts may be significantly lower or even absent.

The dehydration of cyclohexanol requires relatively weak acid sites as shown by Datka et al. [184–187], who studied Al-free boralite (i.e., boron-substituted ZSM-5), H-boralite with small amounts of aluminum, and H-ZSM-5. Activity for dehydration was found on all three catalysts, while further reactions of cyclohexene, such as isomerization to methylcyclopentenes or disproportionation to yield methylcyclopentane and cyclohexane, occurred only on zeolites containing bridging Si – OH – Al groups (strong Brønsted acid sites). Poisoning with pyridine showed that the dehydration activity is fully regained after desorption of pyridine at 200 °C. The rate of dehydration did not increase when more and stronger sites became available by increasing the pyridine desorption temperature. This may evidence that the dehydration does not occur on the strong acid sites, possibly due to the competitive adsorption of cyclohexene on these sites. The consecutive reactions increase strongly as the strong acid sites become available. Therefore, by comparing the rate of dehydration to those of consecutive reactions, cyclohexanol conversion is a convenient test reaction to study weak and strong Brønsted acid sites.

Cyclohexanol conversion over H-ZSM-5 and H-boralite was also studied by Brabec et al. [188], who addressed the effects of concentration and strength of acid sites on catalytic activity. They found the number of acid sites needed increases in the order of dehydrogenation (formation of cyclohexene) < isomerization (formation of methylcyclopentene) < intermolecular reactions (formation of cyclohexane and methylcyclopentane). Even at reaction temperatures around 180 °C all products were observed. The intermolecular reaction pathway decreased in importance with TOS and practically vanished after 30 min. Deactivation, which is in general only slight on these catalysts,

strongly influenced this pathway. These results strongly suggest that adjacent sites are responsible for the formation of methylcyclopentane and the subsequent coking reaction.

Karge et al. [189] studied cyclohexanol conversion over mordenite, clinoptilolite, and faujasite in the hydrogen and alkaline earth-exchanged forms. They found a slight, but reversible, deactivation during reaction resulting from adsorbed water, which was produced in the dehydration reaction. With mordenite a ranking in catalytic activity was observed ranging from the H-form to La-, Be-, Mg-, Ca-, Sr-, and Ba-exchanged forms, which was in clear relation to the tendency to form OH groups.

Clinoptilolite catalysts converted cyclohexanol only on the outer surface, which was found by the linear relationship between the amount of 2,6-di-*tert*-butylpyridine adsorbed on the catalyst and the rate of cyclohexanol dehydration. Note that the 2,6-di-*tert*-butylpyridine molecule is too large to enter the zeolite structure and, therefore, only probes acid sites on the outer surface of the zeolite crystals [190]. For mordenite, a nearly linear relationship between the concentration of adsorbed pyridinium ions and the catalytic activity was observed. Note that this relation was the same if plotted against the concentration of acid sites determined by the adsorption of 2,6-di-*tert*-butylpyridine. Therefore, Karge et al. [189] concluded that cyclohexanol is only converted in the outer shell of the zeolite crystals and that the acid sites are distributed homogeneously over the particles.

The correlation to Brønsted acid sites of faujasite-type zeolites was less obvious, as for Ba- and Mg-exchanged samples a linear relation between Brønsted acid site concentration and catalytic activity was not observed. This could be related to the higher concentrations of Na ions present after the ion exchange, as the Ba- and Mg-Y samples had residual Na_2O concentrations of 4 mol %, while the others had only 2–2.5 mol %. Small changes of these cations can strongly influence the activity of the zeolite. Note that it is unclear what the reason is for this strong influence. It is also important to note the ambiguities that can be introduced through a more complex steric surface chemistry. Cyclohexanol cannot enter the pores of clinoptilolite, while the cyclohexene formed on strongly acidic sites blocks the access into the pores of mordenite very fast. Therefore, catalysis occurred on both catalysts on the outer surface only, although the reason for this behavior was conceptually different.

Also, Murthy et al. [191] used cyclohexanol conversion as a test reaction to probe the acidity of H-ZSM-5, H-Y, SAPO, and MeSAPO catalysts. All these catalysts showed high activity indicating the presence of acidic sites.

The results reported indicate that cyclohexanol appears to be a good test molecule for probing acidity, due to the relatively low deactivation and the possibility of tracing acid sites with different strength. Unfortunately, the molecule seems to be too large to enter the pores of small and maybe even medium pore size zeolites and, therefore, diffusional limitations might affect the kinetic rates measured.

2.1.6
Other Test Reactions

Algarra et al. [192, 193] described the rearrangement of dimethyl or cyclic ethylene acetals of 2-bromopropiophenone to 2-phenylpropanoates in the liquid phase to characterize different sites in metal-ion-exchanged large pore zeolites. The hydrolysis of the acetal was a major side reaction. A direct correlation was found between the ratio of the rates of hydrolysis and rearrangement and the ratio of the concentration of Brønsted and Lewis acid sites, determined from the intensities of the peaks at 1540 and 1450 cm^{-1} from IR pyridine adsorption experiments. They concluded that Brønsted acid sites and hard Lewis acid sites, e.g., in La^{3+}-exchanged zeolites, catalyze the hydrolysis reactions, while zeolites with soft Lewis acid sites, i.e., Zn-, Hg-, and Ag-exchanged zeolites, catalyze the rearrangement reactions. Depending on the softness/hardness of the catalytic sites, different ratios of the phenyl migration product to the alkoxy migration product are observed. This test reaction can, therefore, be used to evaluate Lewis acid sites present in a zeolite structure. Disadvantages of this method are the restriction to large pore zeolites due to the reactant size and possible radical side reactions, which were also described by the authors.

2.2
Specific Reactions for Probing Acid Site Density

In this section reactions are addressed that require (or are assumed to require) active sites which are in close vicinity to each other and, thus, probe the actual acid site density. We would like to use the term site density to distinguish it from site concentration. The distribution of Al atoms within the framework of the zeolite determines, for a given overall concentration of aluminum, the site density. Thus, for a given structure and concentration of aluminum the density of acid sites will be lower the more homogeneously the aluminum is distributed. Moreover, the site density will be determined by the connectivity of a zeolite structure, e.g., MOR has 12 next-nearest neighbors, while FAU structures have only nine. Thus, the same concentration of acid sites may lead to varying concentrations of sites with next-nearest neighbors. It should be noted that in most cases the vicinity of a second site is needed for locally increasing the concentration of the reactants or products.

2.2.1
Cyclohexene Reactions

The reaction of cyclohexene has two different possible reaction pathways (see Scheme 8 [184–187]). The first is the (monomolecular) isomerization to yield methylcyclopentenes. The second pathway is the (bimolecular) forma-

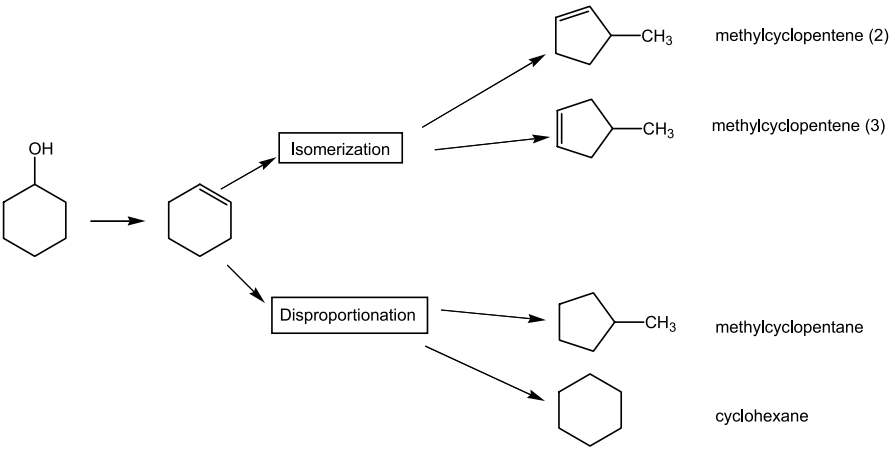

Scheme 8 Reaction pathways of cyclohexanol [184, 185]

tion of cyclohexane by hydride transfer from a feed molecule. The formation of methylcyclopentane is a secondary reaction of methylcyclopentenes with a feed molecule. By-products in this test reaction are C_{12} components formed by dimerization (saturated and unsaturated) and coke.

Cheng and Rajagopalan [194] investigated this reaction over Y zeolites with unit cell sizes from 24.23 up to 24.48 Å, corresponding to aluminum contents of up to 30 Al atoms per unit cell. The hydride transfer (formation of cyclohexane) decreased with decreasing unit cell size. Contrarily, the isomerization (formation of methylcyclopentenes) was the same for the catalysts with the higher unit cell sizes, and only for the catalyst with the lowest amount of aluminum in the framework was an increased isomerization activity observed. The results suggest that the hydride transfer reaction requires active sites with next-nearest Al neighbors and, therefore, a decrease in its rate with decreasing Al content due to the smaller number of adjacent sites was observed. On the contrary, the isomerization proceeds on a single site and, therefore, a comparison between hydride transfer and isomerization (i.e., cyclohexane vs methylcyclopentene formation) can be used for the evaluation of the density and the strength of the acid sites in a zeolite.

Macedo et al. [195] studied hydrothermally dealuminated, acid leached and chemically dealuminated Y zeolites and correlated the heat of adsorption of ammonia to the activity in the conversion of cyclohexene. After mild, selective acid leaching (with 1.5N HCl), Brønsted acid sites, which were blocked by extra-framework alumina species after steaming, became available and, therefore, the conversion of cyclohexene was enhanced. Severe acid leaching (with 4N HCl), on the other hand, also attacked the framework aluminum atoms, partially destroyed the zeolite structure, and hence had a negative effect on the conversion. For chemically dealuminated zeolites an increase in

cyclohexene conversion, attributed to an increase in acid site strength with decreasing unit cell size, was observed. These results exemplify that, for the concentration range of aluminum studied, the negative effect of decreasing the Brønsted acid site concentration by dealumination is overcompensated by the increase in acid strength (seen in higher adsorption enthalpies for ammonia). The example also demonstrates that the cyclohexene conversion is strongly affected by deactivation with TOS, and thus also in this case initial activities have to be determined.

The group of Lavalley studied the conversion of cyclohexene over dealuminated Y zeolites and followed the reaction by in situ IR spectroscopy [196–198] in order to explore the role of the different acid sites in the reaction. The zeolite Y samples used were either steam-dealuminated or chemically dealuminated with $(NH_4)_2SiF_6$. In [198], the adsorption of 2,6-dimethylpyridine, pyridine, and deuterated acetonitrile was studied to obtain a detailed picture of the acid sites on the surface of the zeolites. The chemically dealuminated sample showed silanol groups and Si – OH – Al groups pointing into the supercages (HF – OH) or pointing into the sodalite cages (LF – OH). HF – OH groups are claimed to be stronger acid sites than the LF – OH groups. In the steam-dealuminated sample, an additional OH group with a frequency of 3600 cm^{-1} was observed, which is between the frequencies of the HF and LF – OH groups. All three groups were more strongly acidic than those in the chemically dealuminated sample, with the newly formed OH groups being the strongest acidic ones. Additionally, Lewis acid sites, indicated by coordinatively bound pyridine, were only found in the steam-dealuminated zeolites.

During cyclohexene conversion, differentiation between hydrogen transfer, isomerization, cracking, and coking reactions was achieved. In the chemically dealuminated zeolite only the HF – OH groups participated in the reaction. In parallel to their decrease in concentration, cracking and hydride transfer decreased, while coking increased. Isomerization was not strongly affected by the presence of coke, which led to the conclusion that acid sites with medium strength are the active sites for this reaction path. After adsorption of 2,6-dimethylpyridine followed by desorption at various temperatures (150, 350, and 400 °C) [196], H-Y zeolites with a different distribution of acid sites were obtained (percentages of sites blocked: 100, 50, and 35%). It was found that cyclohexene isomerization occurred even on those catalysts which did not show Brønsted acid sites. This suggests that isomerization requires only a very small number of acid sites. Hydrogen transfer remained constant up to a poisoning level of 50%. These results appear to be in contrast to the assumption that adjacent Brønsted acid sites are necessary for hydride transfer. It should be noted, however, that Lewis acid sites are not affected by the adsorption of 2,6-dimethylpyridine, and the results point to an important role of these sites in providing a sorption site for molecules involved in hydride transfer [198]. An alternative explanation would be that isomerization is not proceeding on very strong acid sites due to the very fast deactivation

of these sites. Weaker sites are the last ones being covered by the substituted pyridine and might be, therefore, still active for isomerization. The steam-dealuminated sample, which shows the strongest acid sites, is most active in the cracking of cyclohexene. For this catalyst blocking of 35% of the zeolite sites by adsorption of 2,6-dimethylpyridine decreases the initial activity by 50%. The coking reactions [197] significantly decrease the number of sites active for cracking, which suggests that coking reactions occur mainly on strong acid sites.

Jaquinot et al. [199, 200] used cyclohexene for evaluating the catalytic performance of H-Y, H-Beta, and H-Omega zeolites. All catalysts were steam-dealuminated and acid-leached. As expected, steaming reduced the concentration of catalytically active sites and led to a decrease in cyclohexene conversion with H-Beta and H-Omega. With H-Y a plateau or maximum of catalytic activity was observed with progressive leaching. In this case, the decrease of the concentration of acid sites was compensated by the increase of their strength. The activity in cyclohexene conversion (H-Beta > H-Y > H-Omega) also reflected well the acid site distribution and concentration in this case.

2.2.2 Hydride Transfer Reactions

Hydride transfer in zeolites plays an important role in many complex reactions, such as cracking, aromatization, and alkylation. Very often, hydride transfer is connected with the formation of coke, as it typically leads to a redistribution of hydrogen and to the formation of highly unsaturated, polynuclear coke precursor components. A suitable test reaction for estimating the hydrogen transfer properties of a certain catalyst has therefore high importance. In principle, hydrogen transfer reactions can be followed by any test reaction that leads to the formation of unsaturated hydrocarbons. One of the frequently used reactions, cyclohexene conversion, has already been discussed in the previous paragraphs. Here we will discuss other options reported.

Lukyanov [201] proposed a simple method to quantitatively characterize the hydrogen transfer activity, by measuring the rate of isobutane formation in the cracking reaction of *n*-hexane at low conversions (<4%). Under these conditions, the ratio between the rate of isobutane and isobutene formation is directly proportional to the hydride transfer activity. In [202] Lukyanov compared a series of steamed H-ZSM-5 catalysts and concluded that the enhanced active sites found after mild steaming also increase hydride transfer reactions. By comparing the formation of different hydride transfer products during *n*-hexane conversion, i.e., propane, *n*-butane, and isobutene, Lukyanov [203] found that the hydrogen transfer to propane mainly correlates to the acid properties, while the production of isobutane relates (to a large part) to the structural properties. A comparison of H-ZSM-5, H-Y, and H-MOR shows

a ratio of hydride transfer of 1 : 1.17 : 1.84 in the case of propane and of 1 : 6.15 : 10.5 in the case of isobutane formation. This clearly shows the strong influence of the smaller pore structure of H-ZSM-5 compared to the others in isobutane formation.

Corma et al. [204] studied the conversion of *n*-heptane over a series of dealuminated Y zeolites. They did not correlate the hydride transfer activity to the presence of adjacent sites, as often done in the literature, but to the more hydrophobic nature of a more severely dealuminated zeolite. The tendency to adsorb a more polar molecule (i.e., an olefin) decreases compared to the less polar molecule (i.e., a paraffin) and, therefore, the conversion of adsorbed olefins to paraffins will decrease. By a change in adsorption properties hydride transfer, which is a bimolecular mechanism, will be much more influenced than cracking, which proceeds via a monomolecular mechanism. This explains the stronger decrease of hydride transfer compared to cracking.

Another possibility has been proposed by des Rochettes et al. [205]. In studying the kinetics of hydride transfer and isomerization of cyclopentene and cyclohexene over two Y-type zeolites, it was concluded that two neighboring acid sites are involved. The feed molecule is sufficiently long to be immobilized between two acid sites (one being free and one with an adsorbed carbenium ion) to undergo hydride transfer. This mechanism does require a second site, but it is not a dual-site mechanism from a kinetic point of view.

The last two contributions show the controversy about the mechanism and involvement of acid sites in the hydride transfer reactions over zeolites. If the hydride transfer activity depends on the hydrophobicity, the rate should correlate to the acid strength of the sites, but not to the acid site density, i.e., the concentration of adjacent active sites. If the reaction is expected to proceed via two carbenium ions adsorbed on adjacent sites or one adsorbed carbenium ion on one site and a feed molecule influenced by the second adjacent site, the acid site density would be probed, but the information about the acid strength would be less obvious. However, in both cases it does not seem that these test reactions can be applied to compare large, medium, and small pore zeolite structures, due to the large (bimolecular) transition state proposed for hydride transfer reactions (unless very small molecules are used [203]).

2.3
Tests for Probing Acid and Basic Bifunctional Properties

2.3.1
Butene Isomerization

A test reaction already in use for many years is the isomerization of 1-butene to yield *cis*/*trans*-2-butene (see Scheme 9). This reaction does not require very strong sites and, therefore, can be used to characterize a large number of catalysts with acid–base properties. The *cis*/*trans* ratio of the 2-butene

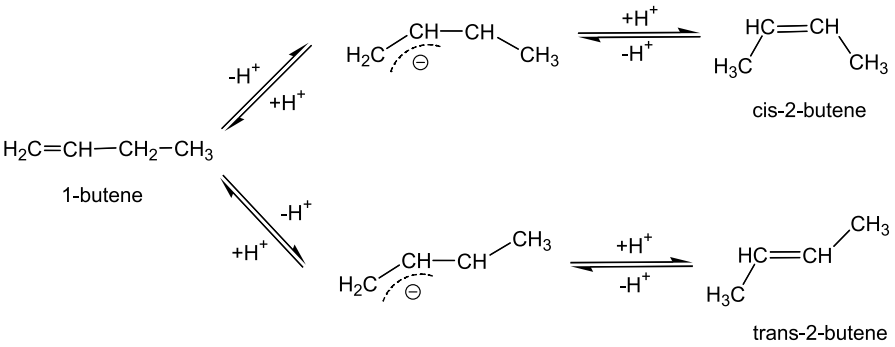

Scheme 9 Base catalyzed 1-butene double bond isomerization

formed allows one to distinguish between acid and basic sites in the catalysts [56, 206–208]. Over acid sites, the reaction proceeds via carbenium ions and the *cis*/*trans* ratio is close to unity. Over basic sites, the reaction proceeds via allylic carbanions, and in this case the *cis*/*trans* ratio is significantly higher than unity. This reaction was investigated for different Y zeolites and pillared clays by Beres et al. [209] and for Y zeolites and metal oxides by Tsuchiya [210]. While in [209] only the *cis*/*trans* ratio was reported, a triangular diagram method was employed in [210], where the concentrations of 1-butene, *cis*-2-butene, and *trans*-2-butene were included in a triangular diagram and the reaction was started at various concentrations of all three components. The shape of the curves in the diagrams depends on the character of the active sites. *Cis*-convex, *trans*-convex, and rake-type diagrams are distinguished, which indicate basic, acid, or a majority of acid catalytic sites on the surface. Tsuji et al. [211] and Bordawekar and Davis [66, 212] investigated X-type zeolites exchanged with Na, K, Rb, and Cs using alkali acetates for the impregnation. They reported strong basicity measured by TPD of CO_2, which led to active sites for 1-butene isomerization at 273 K. Alkali-modified X and Y zeolites, containing cesium oxides and alkali metals (Na, Cs), showed a direct relation between the CO_2 sorption capacity (used to evaluate the concentration of basic metals) and the catalytic activity for 1-butene isomerization.

2.3.2 Toluene Alkylation

The alkylation of toluene with methanol is another test reaction to characterize acid and basic sites in zeolites. The acid-catalyzed route will lead to the formation of ring alkylated products, i.e., the xylenes. Through the base-catalyzed route, side chain alkylated products, i.e., ethylbenzene and styrene, will be formed (see Sect. 2.4.3, Scheme 10). Giordano et al. [213] showed that with increasing intermediate zeolite electronegativity, i.e., increasing acidity,

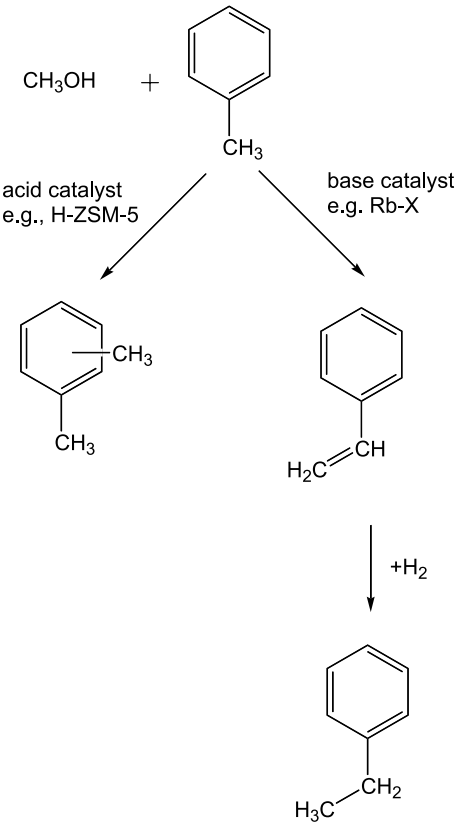

Scheme 10 Alkylation of toluene with methanol over acid and base catalysts

the amount of ethylbenzene/styrene formed approaches zero while the formation of xylenes increases. This different behavior is due to a completely different sorption behavior of toluene and methanol in the zeolite pores, as pointed out by Eder-Mirth et al. [214–216].

Prakash et al. [217] compared the activity of SAPO-11, SAPO-31, and SAPO-41 for toluene alkylation. TPD of ammonia showed a decrease in acidity in the order of SAPO-41 > SAPO-31 > SAPO-11, which was the same order as that observed in the activity for toluene alkylation. Ethylbenzene and styrene were not formed over these catalysts, which confirmed that basic sites do not exist on these molecular sieves.

2.3.3 Alcohol Conversion

One of the test reactions proposed to estimate the acid–base properties of solids is the conversion of 2-methyl-3-butyn-2-ol (MBOH), studied first by

Lauron-Pernot et al. [218]. This reaction will produce 3-methyl-3-buten-1-yne (MBYNE) by dehydration and 3-methyl-2-butenal (PRENAL) by an intermolecular rearrangement over zeolites with acid sites and acetone and acetylene by C – C cleavage reactions over basic sites. Amphoteric sites will form 3-hydroxy-3-methyl-2-butanone (HMB) and 3-methyl-3-butene-2-one (MIPK), which is the corresponding dehydrated product (see Scheme 11).

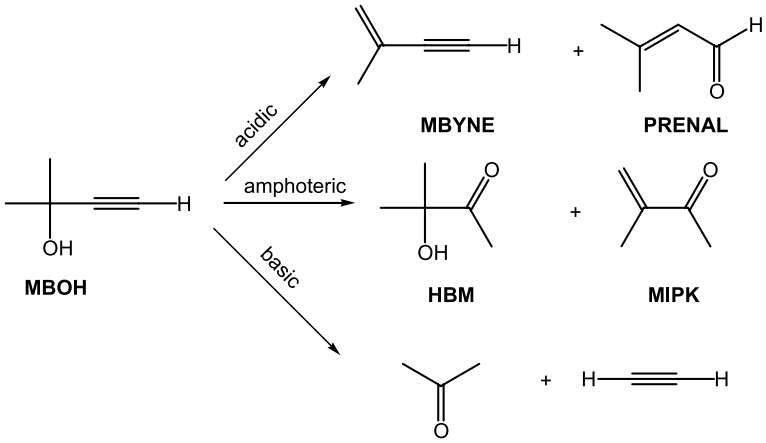

Scheme 11 Conversion of 2-methyl-3-butyn-2-ol over acid, basic, and amphoteric catalysts

Huang and Kaliaguine [51–53] applied this test reaction to a series of alkali-exchanged zeolites including zeolites X, Y, A, L, MOR, and ZSM-5. The Li-, Na-, K-, Rb-, and Cs-exchanged forms of zeolite X and the Na-exchanged forms of all other zeolites were explored. In [51] the study was expanded to Li-, K-, Rb-, and Cs-exchanged ZSM-5. The charges on oxygen calculated according to the Sanderson electronegativity equalization method [34, 219] have been found to be a good measure for the Lewis basicity, while the charge on the metal cations divided by the squared ion radius can be used as a measure for the Lewis acidity. The formation of acetylene and acetone increased monotonously with the Lewis base strength, while the formation of PRENAL and MBYNE increased monotonously with the Lewis acid strength. The catalytic conversion of MBOH to yield MIPK was found to be catalyzed by strong Brønsted acid sites. It should be noted that this reaction is one of the few test reactions able to differentiate between Brønsted acid, Lewis acid, and Lewis basic sites.

2.3.4 Acetonylacetone Cyclization

The cyclization of acetonylacetone (AcAc) was introduced as a test reaction for the acid–base properties of modified H-ZSM-5 [220]. On acid sites the

reaction product 2,5-dimethylfuran (DMF) is formed, while in the presence of basic sites 3-methyl-2-cyclopentenone (MCP) is the main product [221] (see Scheme 12). The ratio between the two products is thus related to the acid–base properties. If the ratio between MCP and DMF is larger than one, the material shows predominantly basic character, whereas the acid character dominates when the ratio is smaller than one [221]. The reaction was tested for several alumina, silica, and niobia oxides. Compared with the isopropanol conversion (see Sect. 2.3.3) the ranking of the catalysts with respect to basicity was different, which was attributed to different reaction mechanisms and to the higher conversion over silica and alumina enhancing the selectivity to side reaction products [221].

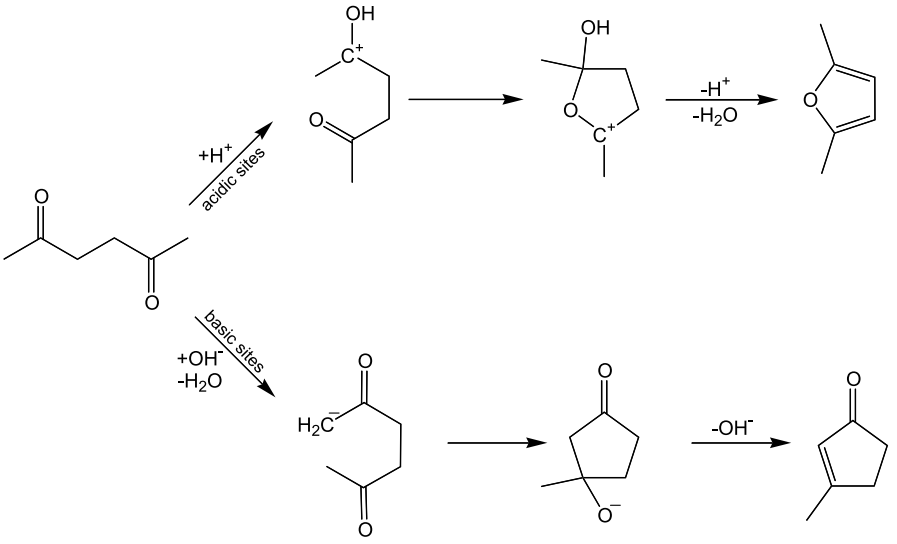

Scheme 12 Cyclization of acetonylacetone to 2,5-dimethylfuran (acid sites) and 3-methyl-2-cyclopentenone (basic sites)

2.4 Probing Basicity of Zeolites

Contrary to the determination of acidity, the characterization of sites with basic character in zeolites is less developed. One of the reasons is that most of the zeolites are used in catalytic reactions that require sites with acidic character, while basic zeolites (i.e., non-Brønsted acidic zeolites) are more often used in adsorption processes.

To be able to probe sites with basic character in a zeolite it is necessary to completely avoid the presence of Brønsted acid sites. For most reactions with organic molecules a basic and an acidic reaction pathway is possible and,

typically, the rates of the base-catalyzed routes are lower compared to those of the acid-catalyzed routes. Therefore, the presence of Brønsted acid sites in a zeolite will mask the basic features one would like to study.

The polarization of individual bonds is the dominant effect in catalytic reactions over molecular sieves, while complete charge transfer and, therefore, cation/anion chemistry is less important. Thus, the polarization will always be a cooperative acid–base effect. The following examples will also focus on the question of whether it is possible to distinguish between Lewis acid and base sites in a molecular sieve with moderate acid–base strength.

Base-catalyzed reactions were reviewed in general by Hattori [208, 222], and from the reactions described butene isomerization, alcohol conversion, toluene alkylation, acetone condensation/diacetone alcohol decomposition, Knoevenagel condensations, diketone cyclization, ring transformation reactions, and dimerization of aldehydes to the corresponding esters were used to evaluate the acid–base properties in molecular sieves.

2.4.1 Butene Isomerization

Butene isomerization has already been discussed in Sect. 2.3.1 and the limitations for the characterization of acidity and basicity with this test reaction were outlined. As the products of the acid- and base-catalyzed reactions are the same (see Scheme 9), the combined presence of both types of sites would make the determination of acidity or basicity very difficult, if possible at all.

2.4.2 Alcohol Conversion

The conversion of alcohols is a frequently used test reaction to study the acid–base properties of zeolites (see Sects. 2.1.5 and 2.3.3). On acid sites alcohols are dehydrated to alkenes, while they dehydrogenate on basic sites to produce aldehydes or ketones (Scheme 13).

With acid sites, the conversion of methanol yields dimethyl ether or, subsequently, hydrocarbons (see Sect. 2.1.5.1). Over basic sites, CO and hydrogen are formed by decomposition of formaldehyde which is a primary product. However, for the acid-catalyzed route it was already found that the interaction of acid–base pairs is required to proceed [175], and there was no clear tendency of the influence of zeolites with different basicity (Na-, K-, Rb-, and Cs-exchanged zeolites) on the methanol reaction.

From propan-2-ol, propene is formed with zeolites of predominantly acid character, while it is converted to acetone over predominantly basic materials. Hathaway and Davis [223] used it to explore alkali metal-exchanged X and Y zeolites. The study shows unequivocally that propene is formed with Brønsted and Lewis acid sites. It is also formed via alkoxide intermediates

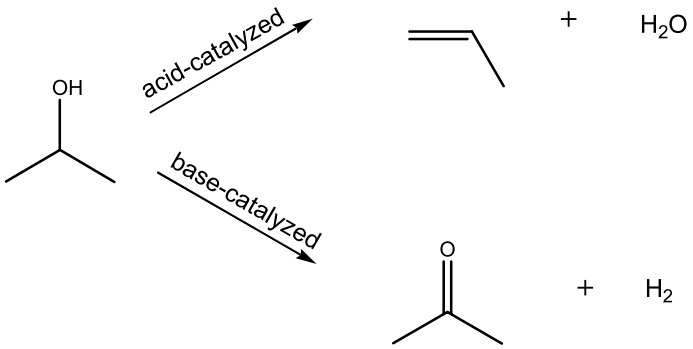

Scheme 13 Conversion of alcohols over acid and basic sites

over metal oxide inclusions in the pores (extra-lattice alumina, mixed alkali metal/aluminum oxide particles). However, acetone formation only increased significantly for samples with an exchange degree above 100%, indicating that the active sites for dehydrogenation are alkali metal oxide clusters.

2.4.3 Toluene Alkylation

In a zeolite with basic character, toluene and methanol are independently adsorbed. The toluene ring strongly interacts with metal cations (i.e., Lewis acid sites), while the methyl group strongly interacts with the framework oxygen atoms, i.e., the Lewis basic sites. This polarizes the toluene molecule to the extent that a side chain alkylation with methanol or formaldehyde is possible. In a zeolite with acidic character methanol is preferentially adsorbed over toluene and, thus, toluene is hydrogen bonded to the chemisorbed methanol (see Sect. 2.3.2 and Scheme 10). This sorption structure is a precursor for the transition state of the reaction to form a C – C bond between the methyl group and the aromatic ring. However, for a successful side chain alkylation the materials must not only be able to sorb toluene and methanol in a 1 : 1 ratio, but also the zeolite must be able to eventually convert methanol into formaldehyde or a surface formaldehyde precursor. The abundance of both sorbed species varies strongly with the acid–base nature of the zeolite.

Vasiliev and Galinsky [224] and Palomares et al. [225] studied X-type zeolites exchanged with K, Rb, and Cs and found that the Cs-exchanged X zeolite was the most active for side chain alkylation, producing nearly no xylene isomers. On the other hand, toluene alkylation over Na-X mainly led to the formation of xylenes. An IR-spectroscopic study in [225] revealed that on Na-X, methanol was by far the most abundant species on the catalyst surface, while on the more basic Cs,Na-X it was toluene. Miyamoto et al. [226] visualized the acid–base cooperative catalysis in the side chain alkylation of toluene by computer graphics and also used it to explore geometrical factors.

Archier et al. [227] noted that the side chain alkylation of toluene required the simultaneous presence of Cs_2O bulk oxide and dispersed Cs^+ cations. Addition of boron was found to attenuate the basicity of Cs_2O. However, too strong basic sites would enhance the decomposition of formaldehyde, formed by dehydrogenation of methanol on the basic sites. This exemplifies the fact that not only the surface species have to be present in the ratios outlined above. It is also important that the reaction partners are both activated in the same temperature interval around 400 °C. Because the boron-modified zeolites had sites with lower basic strength, decomposition of formaldehyde/methanol was more retarded and formaldehyde was available for the side chain alkylation, enhancing the activity of these catalysts for side chain alkylation.

Thus, overall toluene side chain alkylation is a very special probe reaction, which should only be used for probing a typical environment for this reaction as outlined in the papers mentioned. It is not recommended to be used for a more general characterization of the basic properties of the material.

2.4.4 Acetone Condensation and Diacetone Alcohol Decomposition

The base-catalyzed reaction of acetone to form diacetone alcohol and the reverse decomposition can be used as a test reaction to probe the basicity of molecular sieves (see Scheme 14). Fundamental studies on this reaction by Zhang et al. [228] using a series of alkaline earth oxides as well as La_2O_3, ZrO_2, SiO_2–Al_2O_3, and Nb_2O_5 showed that the oxides with stronger basic sites promoted the reaction more effectively. The rate-determining step in this reaction was found to be the addition of an acetone molecule to the carbanion formed from a second acetone molecule. The reaction rate depends on the concentration of the carbanions formed and hence their stability. It is important to note that this does not necessarily correlate with the highest negative charge at the lattice oxygen. The potential subsequent dehydrogenation to mesityl oxide is catalyzed by Lewis acid sites, which allows the presence of both types of sites to be probed [229, 230].

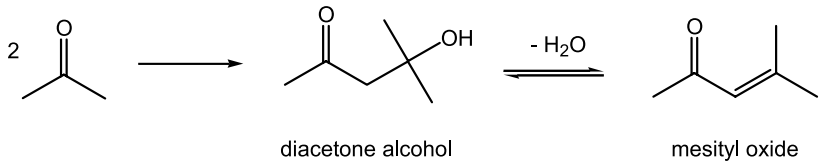

Scheme 14 Base-catalyzed reaction of acetone to diacetone alcohol

Huang and Kaliaguine [51–53] studied this reaction over Na-exchanged X, Y, A, L, MOR, and ZSM-5 and Li-, K-, Rb-, and Cs-exchanged X zeolite. The

condensation reaction did not occur over zeolite A and MOR and became less important over zeolites Y and L. The comparison of various exchanged X zeolites showed that not only the basic oxygen but also the presence of Lewis acid sites, i.e., the alkali cation, is necessary for condensation. The paper emphasizes that the Lewis basic sites and Lewis acid sites should be treated as acid–base pairs rather than distinct acid and basic sites. If the reaction is carried out over zeolites loaded with sodium metal clusters, which induce strongly basic sites, the results indicated that not only the strength of the basic sites but also the structure of the molecular sieve (i.e., effects of shape selectivity) play an important role [231, 232].

The reverse reaction, i.e., the decomposition of diacetone alcohol to acetone, was used by Jurczyk and Kania [233]. They explored Fe-, Cr-, Ni-, Mo-, and Mg-modified aluminas as catalysts. Similarly, Na-X, Na-Y, H,Na-X, and H,Na-Y were employed by Przystaiko et al. [234] as a test reaction for sites with basic character. As the critical ability of the catalyst is to polarize bonds, acidic and basic sites play a role in the catalysis. However, the strength of the basic site will determine the effectiveness of the catalyst.

The fact that both reactions are catalyzed by the polarizing action of an acid–base pair emphasizes this property as the main characterization feature. The reaction will not be probing properties such as the ability to abstract protons from reacting molecules [235]. The probe reaction also exemplifies that catalysis is seldom an action of a single monofunctional site, but requires a multitude (of sites) to facilitate the complex rearrangement of bonds during reactions.

2.4.5
Knoevenagel Condensation

Another frequently used reaction to estimate the number and strength of basic sites in zeolites is the Knoevenagel condensation. As an example, the Knoevenagel condensation of acetophenone and malononitrile is shown in Scheme 15. The reactions were studied, e.g., by Corma et al. [236–238] and Rodriguez et al. [239–241]. In this reaction, the basic sites in the zeolite abstract a proton from the methylenic compound, e.g., a nitrile or ester. The

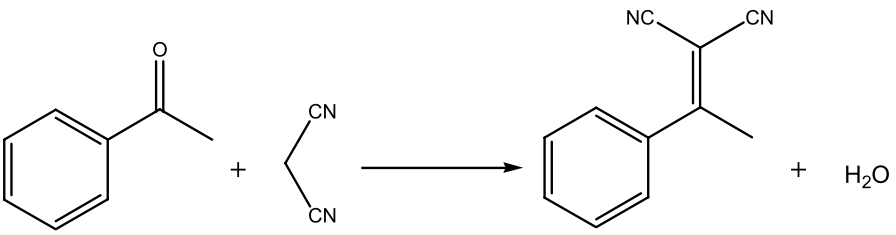

Scheme 15 Knoevenagel condensation of acetophenone and malononitrile

formed carbanions subsequently react with the carbon atom of the carbonyl groups to form a C – C bond and the corresponding enols. These enols dehydrate to form a double bond and restore the active site on the catalyst surface. The catalysts investigated were Li-, Na-, K-, and Cs-exchanged X and Y, Na-X, an Na-X in which Si was substituted by Ge, and zeolite Beta with Ga and Ge substituted for Si in the framework. A comparison between X and Y zeolites showed that X zeolites were more active, which results from the higher Al content in X-type zeolites. The average charge on the framework oxygen atoms increases with increasing aluminum content and, therefore, the basicity of the zeolites becomes higher. Additionally, the average oxygen charge also increases with the ionic radius of the (exchanged) counter ions and, therefore, the order of reactivity observed was Li < Na < K < Cs. To compare the basicity of the zeolites to other basic media, the reactions were also performed in pyridine ($pK_b = 8.8$) and piperidine ($pK_b = 11.1$). Piperidine was more active than the zeolites, while pyridine was less active than the Na-, K-, and Cs-exchanged form of zeolite X. Additional experiments using esters with different pK_a values (ethyl cyanoacetate <9, ethyl malonate 13.3, ethyl acetoacetate 10.7) suggested that most of the basic sites in X and Y zeolites would correspond to pK_b values < 10.3, while only few sites correspond to $pK_b > 13$ in the more basic Cs-X zeolite. It should pointed out that the pK_a and pK_b values are given only as an indication of the acidic and basic properties, as all values only refer to the aqueous phase.

Rodriguez et al. [240] showed that for up to six Cs atoms per unit cell, the initial rate of the benzaldehyde–ethyl cyanoacetate condensation depends linearly on the concentration of Cs atoms. Therefore, the TOF is constant, which suggests that the active sites have the same basic strength. At higher Cs loadings, external (non ion-exchanged) Cs compounds (i.e., carbonates) will be formed, which explains the additional activity the authors observed.

2.4.6 Ring Exchange Reactions

Base-catalyzed ring exchange reactions, for example the conversion of tetrahydrofuran to tetrahydrothiophene or butyrolactones to thiobutyrolactones, are described by Hölderich [235], Hattori [222], and Barthomeuf et al. [8]. The reaction of butyrolactone with hydrogen sulfide to give thiobutyrolactone and water shows a much higher rate over alkali ion-exchanged Y and X zeolites compared to the acid forms [8, 235]. The addition of HCl inhibited the catalytic reaction, while addition of pyridine enhanced it, which indicates that basic sites are associated with the active centers. The order of the catalytic activity, which was found to be Li-Y < Na-Y < K-Y < Rb-Y < Cs-Y and Na-Y < Na-X, was correlated to an increasing basic strength of the oxygen anions in an AlO_4^- tetrahedron.

The ring exchange of tetrahydrofuran to tetrahydrothiophene is also catalyzed by basic sites and showed a decrease in activity with addition of HCl [8, 235]. However, pyridine adsorption also decreased the catalytic activity of the reaction on alkali-exchanged zeolites. In this case, acid and basic sites seem to be necessary for catalysis.

Ferino et al. [242], exploring the reaction of 2-methylfuran to 2-methylthiophene on Me-Y zeolites (Me = Li, Na, K, Rb, Cs), proposed ionic and radical reaction pathways. The ratio of these two pathways was found to be directly correlated to the partial charge on the oxygen as calculated by the Sanderson electronegativity equalization principle. The selectivity to form 2-methylthiophene increased in the order Li,Na-Y < Na-Y < K,Na-Y < Rb,Na-Y = Cs,Na-Y, which is in line with the increasing basicity of these zeolites. As the catalytic activity exhibited a rather complex behavior due to the contribution of the two reaction pathways, more work seems necessary to allow use of this reaction on a broader basis.

2.4.7
Diketone Cyclization

Dessau [220] introduced the cyclization of diketones as a possible test reaction for distinguishing between the acid and base sites of alkali-exchanged ZSM-5. 2,5-Hexanedione (acetonylacetone) is converted to dimethylfuran via the acid-catalyzed pathway and to methylcyclopentenone via the base-catalyzed route (see Scheme 12).

While the acid forms of ZSM-5 produced dimethylfuran with nearly 100% selectivity, sodium-exchanged forms of ZSM-5 led to the formation of methycyclopentenone with more than 90% selectivity. However, further investigations into this reaction are needed, as there was no report about correlations of the rate of reaction with different basic strengths or basic site concentrations.

2.4.8
Interconversion of Nitriles

Kiricsi et al. [243, 244] investigated the interconversion of unsaturated C_4 nitriles (allyl cyanide, crotononitrile, and methacrylonitrile) under basic conditions. IR-spectroscopic studies of this reaction in butyl-lithium in the liquid phase [243] revealed the existence of resonance stabilized carbanionic intermediates. The investigation of this reaction over zeolite catalysts (Na-Y and Na-Y impregnated with NaN_3 to obtain strong basic sites) [244] suggests the presence of a common anionic intermediate, as in the case of the liquid phase reaction. The strongly basic Na/Na-Y was able to interconvert all nitriles, while the Na-Y catalyzed only double bond migration, i.e., interconversion of allyl cyanide and crotononitrile.

2.4.9
Transformation of Alcohol/Ketone Mixtures

The transformation of a mixture of cyclopentanol and cyclohexanone over several solid catalysts (MgO, Cs-exchanged Na-X, alumina, and K-impregnated alumina) was studied by Berkani et al. [245] to evaluate the acid–base properties. The formation of cyclopentene was attributed to an acid mechanism, while the formation of cyclopentanone and cyclohexanol (hydrogen transfer reaction) is catalyzed by basic sites in the catalyst. MgO showed the highest activity for the hydrogen transfer reaction, followed by the K-impregnated alumina, alumina, and Cs,Na-X. With decreasing Cs content in Cs,Na-X, the hydrogen transfer reaction decreased, while the dehydrogenation reaction increased. These results are in line with the higher basicity and/or a higher basic site concentration, which makes this reaction a possible tool to estimate acid and basic properties at the same time.

3
Concluding Remarks

Over the years, a sizeable number of test reactions have been proposed for evaluating the acid and base properties of zeolites. Most of these reactions are suitable and more than one will be needed to appraise the complex properties of microporous materials. So, at first sight a ready toolbox for evaluation is available to the practitioner. Despite this apparent maturity of the subject, it is somewhat surprising that problems in the usage of the reactions still exist. Let us address at this point only the most severe challenges.

Utilizing a test reaction is a subtle exercise and in many cases, important reaction engineering aspects are neglected. In principle, it starts with the lack of common standards with known distribution of properties that can be used as benchmarks for the practitioner. The availability of such a standard would be an invaluable service to the community.

However, the direct reactor-engineering related questions are not less important. These range from using the right sieve fraction of the catalyst to the isothermicity of the reactor and the constancy of the feed (especially in the case of liquid feeds that need to be vaporized). This requires constant reevaluation of results and a much better control of these parameters to be comparable between laboratories. The reader is referred to textbooks on reactor engineering and the good laboratory practice outlined. A taste of the potential problem can be found in [246].

It should also be emphasized that all reactions used have to be tested with respect to external and internal transport limitations, and the results should be documented in the additional material accompanying the paper. The problem is even more severe if molecular sieves with different pore sizes and

channel structures are compared. Intrinsic steric constraints can be present that have to be evaluated by a large number of test reactions that also probe the access to the pore system and potential limitations to reaching certain transition states.

However, even after considering all these external effects, exploring a reaction rate at a given temperature is insufficient. In order to derive meaningful relations the temperature dependence (the measured energy of activation), the reaction order, and the heat of adsorption of the reactants should be measured and reported. Doing so would allow differentiation between effects related to catalysis and effects related to sorption. However, using only two or three reactants for zeolite evaluation will make this a formidable exercise.

Therefore, at the end the question arises of whether it is better to study the target reaction itself. The answer is complex. If the target reaction is a well-defined reaction, directly exploring the kinetics is indeed a better approach. However, if the target reaction is highly complex, such as cracking of a distillate fraction, test reactions clearly have an advantage in terms of throughput. For such applications, it is then mandatory that the test reaction mirrors all properties that a successful catalyst must have. Examples of this have been discussed at various points throughout the paper, but they need to be critically evaluated case by case.

Acknowledgements The help and discussions in the framework of the Network of Excellence IDECAT are gratefully acknowledged.

References

1. Baerlocher C, Meier WM, Olson DH (2001) Atlas of zeolite framework types, 5th edn. Elsevier, Amsterdam
2. Thomas JM, Bell RG, Catlow CRA (1997) Zeolites and related molecular sieves. In: Ertl G, Knözinger H, Weitkamp J (eds) Handbook of heterogeneous catalysis, vol 1. Wiley, Weinheim, p 286
3. Weitkamp J (2000) Solid State Ionics 131:175
4. Lercher JA, Jentys A (2004) Catalytic properties of micro- and mesoporous nanomaterials. In: Schwarz JA, Contescu CI, Putyera K (eds) Dekker encyclopedia of nanoscience. Marcel Dekker, New York, p 633
5. Karge HG, Weitkamp J (eds) (2004) Molecular Sieves: Science and Technology, vol 4. Characterization I. Springer, Berlin, Heidelberg
6. Karge HG, Weitkamp J (eds) (2007) Molecular Sieves: Science and Technology, vol 5. Characterization II. Springer, Berlin, Heidelberg
7. Benesi HA, Winquist BHC (1978) Adv Catal 27:97
8. Barthomeuf D, Coudurier G, Vedrine JC (1988) Mater Chem Phys 18:553
9. Rabo JA (1981) Catal Rev Sci Eng 23:293
10. Corma A (1997) Curr Opin Solid State Mater Sci 2:63
11. de Jong KP (1996) Catal Today 39:171
12. Chen NY, Degnan TF (1988) Chem Eng Prog 84:32
13. Degnan TF (2000) Top Catal 13:349

14. Hölderich WF, Röseler J, Heitmann G, Liebens AT (1997) Catal Today 37:353
15. Venuto PB (1971) Adv Chem Ser 102:260
16. Haw JF (2002) Phys Chem Chem Phys 4:5431
17. van Santen RA (1997) Catal Today 38:377
18. Gorte RJ (2002) Surface acidity. In: Schüth F, Sing KS, Weitkamp J (eds) Handbook of porous solids, vol 1. Wiley, Weinheim, p 432
19. Karge HG, Beyer HK (2002) In: Karge HG, Weitkamp J (eds) Molecular Sieves: Science and Technology, vol 3. Post-Synthesis Modification I. Springer, Berlin, Heidelberg, p 43
20. Breck DW (1974) Zeolite molecular sieves: structure, chemistry and use. Wiley, New York
21. Beyer HK (2002) In: Karge HG, Weitkamp J (eds) Molecular Sieves: Science and Technology, vol 3. Post-Synthesis Modification I. Springer, Berlin, Heidelberg, p 203
22. Hunger M, Brunner E (2004) In: Karge HG, Weitkamp J (eds) Molecular Sieves: Science and Technology, vol 4. Characterization I. Springer, Berlin, Heidelberg, p 201
23. Scherzer J (1984) ACS Symp Ser 248:157
24. Zholobenko VL, Kustov LM, Kazansky VB, Löffler E, Lohse U, Oehlmann G (1991) Zeolites 11:132
25. Zholobenko VL, Kustov LM, Borovkov VY, Kazanskii VB (1987) Kinet Catal 28:847
26. Chen FR, Fripiat JJ (1993) J Phys Chem 97:5796
27. Carvajal R, Chu P-J, Lunsford JH (1990) J Catal 125:123
28. Lonyi F, Lunsford JH (1992) J Catal 136:566
29. Lischke G, Schreier E, Parlitz B, Pitsch I, Lohse U, Wöttke M (1995) Appl Catal A 129:57
30. Barthomeuf D (1987) Mater Chem Phys 17:49
31. Redondo A, Hay PJ (1993) J Phys Chem 97:11754
32. Mortier WJ (1978) J Catal 55:138
33. Jacobs PA (1982) Catal Rev Sci Eng 24:415
34. Mortier WJ, Ghosh SK, Shankar S (1986) J Am Chem Soc 108:4315
35. Mortier WJ, van Gnechten K, Gasteiger J (1985) J Am Chem Soc 107:829
36. Uytterhoeven L, Mortier WJ (1992) J Chem Soc Faraday Trans 88:2747
37. Janssens GOA, Toufar H, Baekelandt BG, Mortier WJ, Schoonheydt RA (1996) J Phys Chem 100:14443
38. de Vries AH, Sherwood P, Collins SJ, Rigby AM, Rigutto M, Kramer GJ (1999) J Phys Chem B 103:6133
39. Rabo JA, Gajda GJ (1989) Catal Rev Sci Eng 31:385
40. Kramer GJ, van Santen RA (1993) J Am Chem Soc 115:2887
41. Brändle M, Sauer J (1998) J Am Chem Soc 120:1556
42. Loewenstein W (1954) Am Mineral 39:92
43. Barthomeuf D (1993) J Phys Chem 97:10092
44. Deeba M, Hall WK (1979) J Catal 60:417
45. Karge HG, Dondur V, Weitkamp J (1991) J Phys Chem 95:283
46. Evanics F, Kiricsi I, Tasi G, Förster H, Fejes P (1995) J Mol Catal A 95:269
47. Lombardo EA, Hall WK (1988) J Catal 565
48. Corma A, Faraq H, Wojciechowski BW (1981) Int J Chem Kinet 13:883
49. Abbot J, Guerzoni FN (1992) Appl Catal A 85:173
50. Narbeshuber TF, Brait A, Seshan K, Lercher JA (1996) Appl Catal A 146:119
51. Huang M, Kaliaguine S (1993) Catal Lett 18:373

52. Huang M, Kaliaguine S (1993) In: Guisnet M, Barbier J, Barrault J, Bouchoule C, Duprez D, Pérot G, Montassier C (eds) Proceedings of the 3rd international symposium on fine chemicals and catalysis, Poitiers, France, 5–8 April 1993. Elsevier, Amsterdam, p 559
53. Huang M, Kaliaguine S (1993) Stud Surf Sci Catal 78:559
54. Barthomeuf D (1996) Catal Rev Sci Eng 38:521
55. Barthomeuf D (2003) Microporous Mesoporous Mater 66:1
56. Weitkamp J, Hunger M, Rymsa U (2001) Microporous Mesoporous Mater 48:255
57. Barthomeuf D (2005) J Phys Chem B 109:2047
58. Tanabe K, Hölderich WF (1999) Appl Catal A 181:399
59. Kramer GJ, Deman AJM, van Santen RA (1991) J Am Chem Soc 113:6435
60. Sanderson RT (1976) Chemical bonds and bond energy. Academic, New York
61. Barthomeuf D (1984) J Phys Chem 88:42
62. Weitkamp J, Rymsa U, Wark M, Schulz-Ekloff G (2002) In: Karge HG, Weitkamp J (eds) Molecular Sieves: Science and Technology, vol 3. Post-Synthesis Modification I. Springer, Berlin, Heidelberg, p 333
63. Davis RJ (2003) J Catal 216:396
64. Yamaguchi T, Zhu JH, Wang Y, Komatsu M, Ookawa M (1997) Chem Lett 10:989
65. Wang Y, Zhu JH, Cao JM, Chun Y, Xu QH (1998) Microporous Mesoporous Mater 26:175
66. Davis RJ, Doskocil EJ, Bordawekar S (2000) Catal Today 62:241
67. Kovacheva P, Arishtirova K, Vassilev S (2001) Appl Catal A 210:391
68. Eder F, Lercher JA (1997) J Phys Chem B 101:1273
69. Chen DT, Sharma SB, Filimonov I, Dumesic JA (1992) Catal Lett 12:201
70. Stöcker M (1996) Microporous Materials 6:235
71. Jentys A, Lercher JA (2001) Techniques of zeolite characterization. In: van Bekkum H, Flanigen EM, Jacobs PA, Jansen JC (eds) Introduction to zeolite science and practice. Elsevier, Amsterdam, p 345
72. Forni L (1998) Catal Today 41:221
73. Wojciechowski BW (1974) Catal Rev Sci Eng 9:79
74. Wojciechowski BW (1968) Can J Chem Eng 46:48
75. Wolf EE, Alfani F (1982) Catal Rev Sci Eng 24:329
76. Bhatia S, Beltramini J, Do DD (1989) Catal Rev Sci Eng 31:431
77. Guisnet M, Magnoux P (1997) Catal Today 36:477
78. Butt JB, Petersen EE (1988) Activation, deactivation and poisoning of catalysts. Academic, San Diego
79. Bauer F, Karge HG (2007) In: Karge HG, Weitkamp J (eds) Molecular Sieves: Science and Technology, vol 5. Characterization II. Springer, Berlin, Heidelberg, p 249
80. Olson DH, Haag WO, Lago RM (1980) J Catal 61:390
81. Haag WO, Lago RM, Weisz PB (1984) Nature 309:589
82. De Canio SJ, Sohn JR, Fritz PO, Lunsford JH (1986) J Catal 101:132
83. Fabre PL, Devynck J, Tremillon JM (1982) Chem Rev 82:591
84. Bourdillon G, Gueguen C, Guisnet MR (1990) Appl Catal 61:123
85. Guisnet MR (1990) Acc Chem Res 23:392
86. Lombardo EA, Sill GA, Hall WK (1989) J Catal 119:426
87. Yushchenko VV, Vanegas KF, Romanovskii BV, Meged NF (1989) Kinet Catal 30:440
88. Lin CY, Haller GL (1995) Science and technology in catalysis 1994, Stud Surf Sci Catal 92:173
89. Wang DZ, Lu XD, Dou XY, Li WB, Yang CH (1990) Appl Catal 59:75
90. Choudhary VR, Akolekar DB (1990) J Catal 125:143

91. Zi G, Yi T, Yugin Z (1989) Appl Catal 56:83
92. Humphries A, Harris DH, O'Connor P (1993) In: Magee JS, Mitchell MM Jr (eds) Fluid catalytic cracking: science and technology. Elsevier, Amsterdam, p 41
93. Humphries A, Harris DH, O'Connor P (1993) Stud Surf Sci Catal 76:41
94. Nivarthy GS, He YJ, Seshan K, Lercher JA (1998) J Catal 176:192
95. Gates BC, Katzer JR, Schuit GCA (1979) Chemistry of catalytic processes. McGraw-Hill, New York
96. Blomsma E, Martens JA, Jacobs PA (1995) J Catal 155:141
97. Dixit L, Rao T (1999) J Chem Inf Comput Sci 39:218
98. Weitkamp J, Traa Y (1997) Alkylation of isobutane with alkenes on solid catalysts. In: Ertl G, Knözinger H, Weitkamp J (eds) Handbook of heterogeneous catalysis, vol 4. Wiley-VCH, Weinheim, p 2039
99. McVicker GB, Kramer GJ, Ziemiak JJ (1983) J Catal 83:286
100. Kramer GJ, McVicker GB (1989) J Catal 115:608
101. Haag WO, Dessau RM (1984) Duality of mechanism for acid-catalyzed paraffin cracking. In: Proceedings of the 8th international congress on catalysis, Berlin, 1984, vol 2. Verlag Chemie-Dechema, Heidelberg, p 305
102. Kotrel S, Knözinger H, Gates BC (2000) Microporous Mesoporous Mater 6:11
103. Houriet R, Parisod G, Gaumann T (1997) J Am Chem Soc 99:3599
104. Narbeshuber T, Vinek H, Lercher JA (1997) J Catal 157:338
105. Werst DW, Han P, Choure SC, Vinokur EI, Xu L, Trifunac AD, Eriksson LA (1999) J Phys Chem B 103:9219
106. Umansky B, Engelhardt J, Hall WK (1991) J Catal 127:128
107. Rastelli H, Lok BM, Duisman JA, Earls DE, Mullhaupt JT (1982) Can J Chem Eng 60:44
108. Beyerlein RA, McVicker GB, Yacullo LN, Ziemiak JJ (1988) J Phys Chem 92:1967
109. Auroux A, Tuel A, Bandiera J, Ben Taarit Y, Guil JM (1993) Appl Catal A 93:181
110. Lombardo EA, Pierantozzi R, Hall WK (1988) J Catal 110:171
111. Engelhardt J, Hall WK (1990) J Catal 125:472
112. Shertukde PV, Marcelin G, Sill GA, Hall WK (1992) J Catal 136:446
113. Shigeishi R, Garforth A, Harris I, Dwyer J (1991) J Catal 130:423
114. Hall WK, Lombardo EA, Engelhardt J (1989) J Catal 115:611
115. Krannila H, Haag WO, Gates BC (1992) J Catal 135:115
116. Miale JN, Chen NY, Weisz PB (1966) J Catal 6:278
117. Zholobenko VL, Kustov LM, Kazansky VB, Loeffler E, Lohse U, Peuker C, Oehlmann G (1990) Zeolites 10:304
118. Lago RM, Haag WO, Mikowski RJ, Olson DH, Hellring SD, Schmidt KD, Kerr GT (1986) In: Murakami Y, Iijima A, Ward JW (eds) New developments in zeolite science and technology. Proceedings of the 7th international zeolite conference, Kodansha, Tokyo, 17–22 August 1986. Elsevier, Amsterdam, p 677
119. Lago RM, Haag WO, Mikowski RJ, Olson DH, Hellring SD, Schmidt KD, Kerr GT (1986) Stud Surf Sci Catal 28:677
120. Jolly S, Saussey J, Lavalley JC, Zanier N, Benazzi E, Joly JF (1993) Ber Bunsen Ges 97:313
121. Parillo DJ, Lee C, Gorte RJ, White D, Farneth WE (1995) J Phys Chem 99:8745
122. Frillette VJ, Haag WO, Lago RM (1981) J Catal 67:218
123. Lopes JM, Lemos F, Ribeiro FR, Derouane EG (1991) In: Jacobs PA, Jaeger NI, Kubelkova L, Wichterlova B (eds) Zeolite chemistry and catalysis. Proceedings of an international symposium, Prague, 8–13 Sept 1991. Elsevier, Amsterdam, p 365
124. Lopes JM, Lemos F, Ribeiro FR, Derouane EG (1991) Stud Surf Sci Catal 69:365

125. Lopes JM, Lemos F, Ribeiro FR, Derouane EG (1994) Appl Catal A 119:139
126. Lopes JM, Lemos F, Derouane EG, Ribeiro FR (1996) React Kinet Catal Lett 58:33
127. Kumar R, Cheng WC, Rajagopalan K, Peters AW, Basu P (1993) J Catal 143:594
128. Rustamov MI, Shakhtakhtinskaya AT, Farkhadova GT, Guseinova SB, Mamedova EM, Agaeva RR, Saprykina LI (1991) Kinet Catal 32:442
129. Derewinski M, Fajula F (1994) Appl Catal A 108:53
130. Klyachko AL, Kapustin GI, Brueva TR, Rubinstein AM (1987) Zeolites 7:119
131. Yamagishi K, Namba S, Yashima T (1990) J Catal 121:47
132. Corma A, Planelles J, Sanchezmarin J, Tomas F (1985) J Catal 93:30
133. Chauvin B, Boulet M, Massiani P, Fajula F, Figueras F, Descourieres T (1990) J Catal 126:532
134. Weitkamp J (1976) Erdöl Kohle Erdgas Petrochem 29:213
135. Steijns M, Froment G, Jacobs P, Uytterhoeven J, Weitkamp J (1981) Ind Eng Chem Prod Res Dev 20:654
136. Weitkamp J, Jacobs PA, Martens JA (1983) Appl Catal 8:123
137. Corma A, Chica A, Guil JM, Llopis FJ, Mabilon G, Perdigon-Melon JA, Valencia S (2000) J Catal 189:382
138. Bhave AN, Klemt A, Patwardhan SR, Reschetilowski W (2001) Petrol Chem 41:401
139. Kustova MY, Hasselriis P, Christensen CH (2004) Catal Lett 96:205
140. Sastre G, Chica A, Corma A (2000) J Catal 195:227
141. Martens JA, Tielen M, Jacobs PA, Weitkamp J (1984) Zeolites 4:98
142. Park KC, Ihm SK (2000) Appl Catal A 203:201
143. Schenk M, Calero S, Maesen TLM, Vlugt TJH, van Benthem LL, Verbeek MG, Schnell B, Smit B (2003) J Catal 214:88
144. Corma A, Wojciechowski BW (1982) Catal Rev Sci Eng 24:1
145. Bellare A, Dadyburjor DB (1993) J Catal 140:510
146. Al-Khattaf S, de Lasa H (2001) Ind Eng Chem Res 40:5398
147. Dadyburjor DB, Bellare A (1990) J Catal 126:261
148. Fukase S, Wojciechowski BW (1988) J Catal 109:180
149. Nayak VS, Choudhary VR (1984) Appl Catal 10:137
150. Choudhary VR (1987) Zeolites 7:272
151. Akolekar DB (1995) J Mol Catal A 104:95
152. Tian HP, Li CL (1999) J Mol Catal A 149:205
153. Narayanan S, Sultana A, Meriaudeau P, Naccache C, Auroux A, Viornery C (1996) Appl Catal A 143:337
154. Rhodes NP, Rudham R (1994) J Chem Soc Faraday Trans 90:809
155. Meshram NR (1987) J Chem Technol Biotechnol 37:111
156. Ej-Jennane K, Marcilly C, Travers C, Joly JF, Benazzi E (1992) In: von Ballmoos R, Higgins JB, Treacy MMJ (eds) Proceedings of the 9th international zeolite conference, Montreal, 5–10 July 1992, vol II. Butterworth-Heinemann, Boston, 1993, p 517
157. Karge HG, Ladebeck J, Sarbak Z, Hatada K (1982) Zeolites 2:94
158. Karge HG, Hatada K, Zhang Y, Fiedorow R (1983) Zeolites 3:13
159. Karge HG, Sarbak Z, Hatada K, Weitkamp J, Jacobs PA (1983) J Catal 82:236
160. Arsenova N, Haag WO, Karge HG (1995) In: Beyer HK, Karge HG, Kiricsi I, Nagy JB (eds) Catalysis by microporous materials. Proceedings of ZEOCAT '95, Szombathely, 9–13 July 1995. Elsevier, Amsterdam, p 441
161. Arsenova N, Haag WO, Karge HG (1995) Stud Surf Sci Catal 94:441
162. Rhodes NP, Rudham R (1993) J Chem Soc Faraday Trans 89:2551
163. Sobrinho EV, Cardoso D, Saguiar EF, Silva JG (1995) Appl Catal A 127:157
164. Niu FH, Hofmann H (1995) Appl Catal A 128:107

165. Blomsma E, Martens JA, Jacobs PA (1996) J Catal 159:323
166. Remy MJ, Stanica D, Poncelet G, Feijen EJP, Grobet PJ, Martens JA, Jacobs PA (1996) J Phys Chem 100:12440
167. Blomsma E, Martens JA, Jacobs PA (1997) J Catal 165:241
168. Souverijns W, Martens JA, Froment GF, Jacobs PA (1998) J Catal 174:177
169. Arroyo JAM, Martens GG, Froment GF, Marin GB, Jacobs PA, Martens JA (2000) Appl Catal A 192:9
170. Martens JA, Jacobs PA (1986) Zeolites 6:334
171. Weitkamp J, Ernst S, Kumar R (1986) Appl Catal 27:207
172. Morin S, Gnep NS, Guisnet M (1996) J Catal 159:296
173. Hong Y, Gruver V, Fripiat JJ (1994) J Catal 150:421
174. Bezoukhanova CP, Kalvachev YA (1994) Catal Rev Sci Eng 36:125
175. Santacesaria E, Gelosa D, Giorgi E, Carra S (1984) J Catal 90:1
176. Benito PL, Gayubo AG, Aguayo AT, Olazar M, Bilbao J (1996) J Chem Technol Biotechnol 66:183
177. Stöcker M (1999) Microporous Mesoporous Mater 29:3
178. Lietz G, Schnabel KH, Peuker C, Gross T, Storek W, Volter J (1994) J Catal 148:562
179. Lukyanov DB (1991) Appl Catal 68:L9
180. Gayubo AG, Benito PL, Aguayo AT, Olazar M, Bilbao J (1996) J Chem Technol Biotechnol 65:186
181. van Niekerk MJ, Fletcher JCQ, O'Connor CT (1996) Appl Catal A 138:135
182. Korah PC, Viswanathan B (1994) Ind J Chem A 33:380
183. Singh P, Bandyopadhyay R, Rao B (1996) J Chem Soc Faraday Trans 92:2017
184. Datka J, Vogt O, Rakoczy J, Kubacka A (1995) In: Beyer HK, Karge HG, Kiricsi I, Nagy JB (eds) Catalysis by microporous materials. Proceedings of ZEOCAT '95, Szombathely, 9–13 July 1995. Elsevier, Amsterdam, p 240
185. Datka J, Vogt O, Rakoczy J, Kubacka A (1995) Stud Surf Sci Catal 94:240
186. Datka J, Gil B, Vogt O, Rakoczy J (1999) In: Kiricsi I, Pál-Borbély G, Nagy JB, Karge HG (eds) Porous materials in environmentally friendly processes. Proceedings of the 1st international FEZA conference, Eger, 1–4 Sept 1999. Elsevier, Amsterdam, p 409
187. Datka J, Gil B, Vogt O, Rakoczy J (1999) Stud Surf Sci Catal 125:409
188. Brabec L, Novakova J, Kubelkova L (1994) J Mol Catal 94:117
189. Karge HG, Kösters H, Wada H (1984) In: Olson DH, Bisio A (eds) Proceedings of the 6th international zeolite conference, Reno, 10–15 July 1983. Butterworth, Guildford, p 308
190. Corma A, Fornes V, Forni L, Marquez F, Martinez-Triguero J, Moscotti D (1998) J Catal 179:451
191. Murthy K, Srinivas B, Kulkarni SJ, Kaushik VK, Subrahmanyam M, Rao PK (1996) Ind J Chem A 35:649
192. Algarra F, Corma A, Fornes V, Garcia H, Martinez A, Primo J (1993) In: Guisnet M, Barbier J, Barrault J, Bouchoule C, Duprez D, Pérot G, Montassier C (eds) Proceedings of the 3rd international symposium on fine chemicals and catalysis, Poitiers, 5–8 April 1993. Elsevier, Amsterdam, p 653
193. Algarra F, Corma A, Fornes V, Garcia H, Martinez A, Primo J (1993) Stud Surf Sci Catal 78:653
194. Cheng WC, Rajagopalan K (1989) J Catal 119:354
195. Macedo A, Auroux A, Raatz F, Jacquinot E, Boulet M (1988) ACS Symp Ser 368:98
196. Jolly S, Saussey J, Lavalley JC, Zanier N, Benazzi E, Joly JF (1993) In: von Ballmoos R, Higgins JB, Treacy MMJ (eds) Proceedings of the 9th international zeolite conference, Montreal, 5–10 July 1992, vol II. Butterworth-Heinemann, Boston, p 319

197. Jolly S, Zanierszydlowski N, Colin S, Raatz F, Saussey J, Lavalley JC (1991) Catal Today 9:31
198. Jolly S, Saussey J, Lavalley JC (1994) J Mol Catal 86:401
199. Jacquinot E, Raatz F, Macedo A, Marcilly C (1988) In: Karge HG, Weitkamp J (eds) Zeolite as catalysts, sorbents and detergent builders: applications and innovations. Proceedings of an international symposium, Würzburg, 4–8 September 1988. Elsevier, Amsterdam, p 115
200. Jacquinot E, Raatz F, Macedo A, Marcilly C (1988) Stud Surf Sci Catal 46:115
201. Lukyanov DB (1994) J Catal 145:54
202. Lukyanov DB (1991) Zeolites 11:325
203. Lukyanov DB (1994) J Catal 147:494
204. Corma A, Faraldos M, Mifsud A (1989) Appl Catal 47:125
205. Des Rochettes BM, Marcilly C, Gueguen C, Bousquet J (1990) Appl Catal 58:35
206. Martens LRM, Grobet PJ, Vermieren WJM, Jacobs PA (1986) In: Murakami Y, Iijima A, Ward JW (eds) New developments in zeolite science and technology. Proceedings of the 7th international zeolite conference, Kodansha, Tokyo, 17–22 August 1986. Elsevier, Amsterdam, p 935
207. Martens LRM, Grobet PJ, Vermieren WJM, Jacobs PA (1986) Stud Surf Sci Catal 28:935
208. Hattori H (2001) Appl Catal A 222:247
209. Beres A, Hannus I, Kiricsi I (1995) React Kinet Catal Lett 56:55
210. Tsuchiya S (1989) Acid–base catalysis. In: Tanabe K, Hattori H, Yamaguchi T, Tanaka T (eds) Acid–base catalysis. VCH, Weinheim, p 169
211. Tsuji H, Yagi F, Hattori H (1991) Chem Lett Chem Soc Jpn 11:1881
212. Bordawekar SV, Davis RJ (2000) J Catal 189:79
213. Giordano N, Pino L, Cavallaro S, Vitarelli P, Rao BS (1987) Zeolites 7:131
214. Eder-Mirth G, Wanzenböck HD, Lercher JA (1995) In: Beyer HK, Karge HG, Kiricsi I, Nagy JB (eds) Catalysis by microporous materials. Proceedings of ZEOCAT '95, Szombathely, 9–13 July 1995. Elsevier, Amsterdam, p 449
215. Eder-Mirth G, Wanzenböck HD, Lercher JA (1995) Stud Surf Sci Catal 94:449
216. Eder-Mirth G, Lercher JA (1996) Recl Trav Chim Pays-Bas 115:3
217. Prakash AM, Chilukuri SVV, Bagwe RP, Ashtekar S, Chakrabarty DK (1996) Microporous Mater 6:89
218. Lauron-Pernot H, Luck F, Popa JM (1991) Appl Catal 78:213
219. Uytterhoeven L, Mortier WJ, Geerlings P (1989) J Phys Chem Solids 50:479
220. Dessau RM (1990) Zeolites 10:205
221. Calvino-Casilda V, Martin-Aranda R, Sobczak I, Ziołek M (2006) Appl Catal A 303:121
222. Hattori H (1995) Chem Rev 95:537
223. Hathaway PE, Davis ME (1989) J Catal 116:263
224. Vasiliev AN, Galinsky AA (1993) React Kinet Catal Lett 51:253
225. Palomares AE, Eder-Mirth G, Lercher JA (1997) J Catal 168:442
226. Miyamoto A, Iwamoto S, Agusa K, Inui T (1989) Catalysts in the side chain alkylation of toluene. In: Tanabe K, Hattori H, Yamaguchi T (eds) Acid–base catalysis. Kodansha/VCH, Tokyo/Weinheim, p 497
227. Archier D, Coudurier G, Naccache C (1993) In: von Ballmoos R, Higgins JB, Treacy MMJ (eds) Proceedings of the 9th international zeolite conference, Montreal, 5–10 July 1992, vol II. Butterworth-Heinemann, Boston, p 525
228. Zhang G, Hattori H, Tanabe K (1988) Appl Catal 49:183
229. Lercher JA, Noller H, Ritter G (1981) J Chem Soc Faraday Trans 77:621

230. Abello S, Medina F, Tichit D, Perez-Ramirez J, Groen JC, Sueiras JE, Salagre P, Cesteros Y (2005) Chem Eur J 11:728
231. Rodriguez I, Cambon H, Brunel D, Lasperas M, Geneste P (1993) In: Guisnet M, Barbier J, Barrault J, Bouchoule C, Duprez D, Pérot G, Montassier C (eds) Proceedings of the 3rd international symposium on fine chemicals and catalysis, Poitiers, 5–8 April 1993. Elsevier, Amsterdam, p 623
232. Rodriguez I, Cambon H, Brunel D, Lasperas M, Geneste P (1993) Stud Surf Sci Catal 78:623
233. Jurczyk K, Kania W (1989) Appl Catal 56:253
234. Przystajko W, Fiedorow R, Dalla Lana IG (1987) Zeolites 7:477
235. Hölderich WF (1989) In: Tanabe K, Hattori H, Yamaguchi T (eds) Acid–base catalysis. Kodansha, Tokyo, p 1
236. Corma A, Fornes V, Martin-Aranda RM, Garcia H, Primo J (1990) Appl Catal 59:237
237. Camblor MA, Corma A, Martin-Aranda RM, Perez-Pariente J (1993) In: von Ballmoos R, Higgins JB, Treacy MMJ (eds) Proceedings of the 9th international zeolite conference, Montreal, 5–10 July 1992, vol II. Butterworth-Heinemann, Boston, p 647
238. Climent MJ, Corma A, Iborra S, Velty A (2002) J Mol Catal A 182:327
239. Rodriguez I, Iborra S, Rey F, Corma A (2000) Appl Catal A 194:241
240. Rodriguez I, Cambon H, Brunel D, Lasperas M (1998) J Mol Catal A 130:195
241. Linares CF, Goldwasser MR, Machado FJ, Rivera A, Rodriguez-Fuentes G, Barrault J (2000) Microporous Mesoporous Mater 41:69
242. Ferino I, Monaci R, Solinas V, Oliva C, Pieri I, Forni L (1990) J Chem Soc Faraday Trans 86:193
243. Konya Z, Hannus I, Molnar A, Kiricsi I (1996) Appl Catal A 146:323
244. Beres A, Konya Z, Hannus I, Molnar A, Kiricsi I (1996) Appl Catal A 146:331
245. Berkani M, Lemberton JL, Marczewski M, Perot G (1995) Catal Lett 31:405
246. De Vos DE, Ernst S, Perego C, O'Connor CT, Stöcker M (2002) Microporous Mesoporous Mater 56:185

Mol Sieves (2008) 6: 213–267
DOI 10.1007/3829_2007_015

Published online: 11 October 2007

Acidity and Basicity of Ordered Silica-based Mesoporous Materials

Edoardo Garrone[1] (✉) · François Fajula[2]

[1]Dipartimento di Scienza dei Materiali e Ingegneria Chimica,
Corso Duca degli Abruzzi 24, 10129 Torino, Italy
edoardo.garrone@polito.it

[2]Institut Charles Gerhardt Montpellier,
UMR 5253 CNRS-ENSCM-UM2-UM1,
Ecole National Supérieur de Chimie,
8 rue de l'Ecole Normale, 34296 Montpellier, France

1 Introduction 216

2 Expected Basic Behavior in [Al]-MTS Systems: Ion-exchanged and Ion-impregnated Samples 220

3 Brønsted and Lewis Acidity of Protonic Forms H-[Al]-MTS 222
3.1 Non-spectroscopic Evidence Concerning Adsorption on Acidic Sites 223
3.2 NMR Spectroscopy 224
3.3 IR Spectroscopy 224
3.3.1 The Bare Samples 225
3.3.2 Proton Transfer to Strongly Basic Molecules 229
3.3.3 Propensity to Form H-bonded Adducts 229
3.3.4 Lewis Sites: Evidence Provided by CO Adsorption; Conversion into Brønsted Sites 237
3.4 Catalytic Evidence 239
3.4.1 Cracking of Hydrocarbons 239
3.4.2 Alkane Hydroconversion 240
3.5 Models for the Acidic Sites of H-Al-MTS (Brønsted and Lewis) 243
3.5.1 Literature Models for the Brønsted Acidic Sites 243
3.5.2 Discussion of the Models for Brønsted Acidity 246
3.5.3 Models for Lewis Sites 247
3.6 Comparison with Similar Systems 247
3.6.1 Outer Surfaces of Zeolites 247
3.6.2 Dealuminated Zeolites 249

4 Development of Acidity upon Cation Substitution 249

5 Considerations About Acidity/Basicity 253

6 Methods for Improving Acid Strength 255
6.1 Post-synthesis Alumination 255
6.2 Improved Synthesis Procedures 256

7 Trivalent T Atoms Other than Al 257
7.1 B as T Atom 258
7.2 Ga as T Atom 258
7.3 Fe as T Atom 259

8 Concluding Remarks 261

References 262

Abbreviations

A	Absorbance in the infrared, e.g., of OH groups
A_M	Maximum value of A
$Al(acac)_3$	Aluminum acetylacetonate
^{27}Al MAS NMR	Magic angle spinning nuclear magnetic resonance of the aluminum nucleus (spectroscopy)
^{27}Al NMR	Nuclear magnetic resonance of the aluminum nucleus (spectroscopy)
[Al]-MCM-41	Mesoporous material with hexagonal arrangement of the uniform mesopores (cf. Volume 1, Chapter 4 of this series) containing aluminum in the pore walls
[Al]-MTS	Micelle-templated silica material with uniform distribution of pore sizes containing aluminum in the framework
AlOH	Surface aluminol species
AlOH(I)	Slightly acidic aluminol species (shift with CO not exceeding 145 cm^{-1}), probably related to extra-framework debris
AlOH(II)	Acidic aluminol species (shift with CO ca. 200 cm^{-1}), absorbing, when visible at ca. 3660 cm^{-1}
AlOH(III)	Acidic aluminol species (shift with CO probably 230 cm^{-1}), probably with the same nature as $Al\cdots H_2O$
$Al\cdots H_2O$	Acidic species (shift with CO probably 230 cm^{-1}), constituted by a water molecule sitting on a strong Lewis acid site: documented on Na-bearing [Al]-MTS samples
ASA	amorphous silica alumina
B	Molecule with Brønsted basic character as in Scheme 4c
BEA	zeolite structure; beta (cf. [153])
BET	Brunauer Emmett Teller
Beta	zeolite-type (structure BEA, cf. [153])
Dim-Sil	Pair of silanols interacting via hydrogen bonding
EFAL	Extra-framework aluminium
EMT	Zeolite structure; cubic faujasite (cf. [153])
EMO	Zeolite structure; hexagonal faujasite (cf. [153])
FAU	Zeolite structure; hexagonal faujasite (cf. [153])
[Fe]-MCM-41	Mesoporous material with hexagonal arrangement of the uniform mesopores (cf. Volume 1, Chapter 4 of this series) containing iron in the pore walls
H-[Al]-MTS	Micelle-templated silica materials containing aluminum in the framework in which residual cations have been exchanged with protons (acidic form)
H-β	zeolite beta in protonic form
H-MOR	zeolite structure mordenite in protonic form (cf. [153])

H-FER	zeolite structure ferrierite in protonic form (cf. [153])
^{1}H MAS-NMR	Magic angle spinning nuclear magnetic resonance of the proton nucleus (spectroscopy)
H-MCM-41	mesoporous material with hexagonal arrangement of the uniform mesopores (cf. Volume 1, Chapter 4 of this series) in acidic form obtained by exchanging all cations by protons
H-MFI	zeolite structure ZSM-5 in protonic form (cf. [153])
H-MOR	Zeolite structure mordenite in protonic form (cf. [153])
H-Y	Zeolite faujasite in protonic form
I	Acid site with intermediate strength
iPr	isopropyl group
IR	Infrared (spectroscopy)
ITQ-2	zeolite-type, obtained by delamination of a MCM-22 (structure code MWW) zeolite precursor
K	Adsorption equilibrium constant in the Langmuir equation
L	Ligand with basic Lewis character as in Scheme 4a
MAS-5	Mesoporous aluminosilicate
MAS-NMR	Magic angle spinning nuclear magnetic resonance (spectroscopy)
MAT	Micro activity test (catalysis)
MCM-22	Zeolite-type (structure code MWW, (cf. [153]))
MCM-41	Mesoporous material with hexagonal arrangement of the uniform mesopores (cf. Volume 1, Chapter 4 of this series)
MCM-48	Mesoporous material with cubic arrangement of the uniform mesopores (cf. Volume 1, Chapter 4 of this series)
MCM-50	Mesoporous material with lamellar arrangement of the uniform mesopores (cf. Volume 1, Chapter 4 of this series)
MIX 60	Zeolite material consisting in an intergrowth 60/40 of EMT/EMO
MSU-S	Mesoporous material with worm-like arrangement of mesopores with uniform sizes ($S = 4–8$)
MTS	Micelle-templated silica with uniform distribution of mesopores
MTS-hex	Micelle-templated silica with hexagonal arrangement of the mesopores
MeAPOs	Microporous metal aluminophosphate zeolite-like structures with metal (Me) in the framework (cf. [153])
NMR	Nuclear magnetic resonance (spectroscopy)
Q^3	Silicon atom in a framework connected to three silicons (via siloxane bridges) and one OH
Q^4	Silicon atom in a framework connected to four silicons (via siloxane bridges)
p	Pressure
S	strong acid site
SAPOs	Microporous silicoaluminophosphate zeolite-like structures (cf. [153])
SAPO-11	Microporous silicoaluminophosphate zeolite-like structure (cf. [153])
SBA-*n*	Mesoporous material with narrow distribution of mesopore sizes (n = 3, 15)
Sil	Isolated silanol group
Si(OH)Al	bridging hydroxyl (Brønsted acidic site), typical of protonic zeolites, most probably absent on [Al]-MTS systems
[Si]-MCM-48	Mesoporous silica with cubic arrangement of the uniform mesopores (cf. Volume 1, Chapter 4 of this series)
^{29}Si NMR	Nuclear magnetic resonance of the silicon nucleus (spectroscopy)

T	(tetrahedrally coordinated) framework atom or cation such as Si, Al, Ti, Fe, V, B, Ge
TPD	Temperature-programmed desorption
USY	Ultra stable Y-type zeolite
W	Weak acid site
XANES	X-ray absorption near edge spectroscopy
XRD	X-ray diffraction
[Zn]-MCM-41	Mesoporous material with hexagonal arrangement of the uniform mesopores (cf. Volume 1, Chapter 4 of this series) containing zinc in the pore walls
ZSM-5	Zeolite-type (structure MFI, cf. [153])
ZSM-22	Zeolite-type (structure MTT, cf. [153])

Greek symbols

β	Zeolite beta (structure BEA, cf. [153])
δ	Chemical shift (in NMR spectroscopy) referenced to $Al(NO_3)$ in solution
θ	Fraction of the silanols interacting with probe molecules

1 Introduction

Making use of the self-assembling properties of long-chained surfactants in the sol-gel synthesis of silica-based solids, Mobil researchers [1] described the synthesis of ordered mesoporous aluminosilicates in 1990. This was indeed a major achievement. From the catalytic point of view, this new class of solids provided the possibility of exploiting a regular, tailored porosity much larger than that of zeolites and zeotypes, for carrying out reactions concerning molecules of sizeable dimensions.

On the other hand, these solids are the ideal hosts for a number of active species, comprising enzymes, nanoclusters, etc. [2, 3]. Functionalization of the inner surfaces is also possible, which allows grafting of active species, like dyes [4] and metal-containing complexes, e.g., for chiral synthesis [5]. A peculiar feature of these solids is that they provide systems with an a priori known porous structure: a side consequence of this has been the rebirth of studies, indeed out of fashion, concerning capillary condensation and hysteresis [6].

After the disclosure of silica-alumina-based mesostructures, workers tried to prepare by similar procedures other oxides in a mesoporous form [7]. The resulting solids, though interesting in principle, are usually not yet stable enough for practical catalytic usage: silica-based ordered mesoporous systems still dominate the subject.

A commonly accepted terminology for this type of materials has not yet been defined: we shall make use in the following of the denomination Micelle templated silica (MTS).

Order in the mesopores is revealed by low-angle XRD patterns, which also show that three structures are possible: a hexagonal one, MCM-41, a cubic

form, MCM-48, and a lamellar one, MCM-50. Other materials like, e.g., the Santa Barbara series, SBA-3, SBA-15, etc. also have similar structures, which are indeed dictated by the water/surfactant state diagram. Recent reviews are available on the subject [8].

XRD patterns also show that the walls are amorphous, because only long range order is revealed: this, a most remarkable feature, is a leitmotiv in the studies of MTS and will be invoked repeatedly in this chapter.

The most common solid, which can be assumed as a general reference, is the hexagonal form, MCM-41. An idealized model of these solids is shown in Fig. 1, which also illustrates the fact that such systems, when partially dehydrated, have hydrophilic and hydrophobic patches situated in the curved and the flat patches of the hexagons, respectively [9].

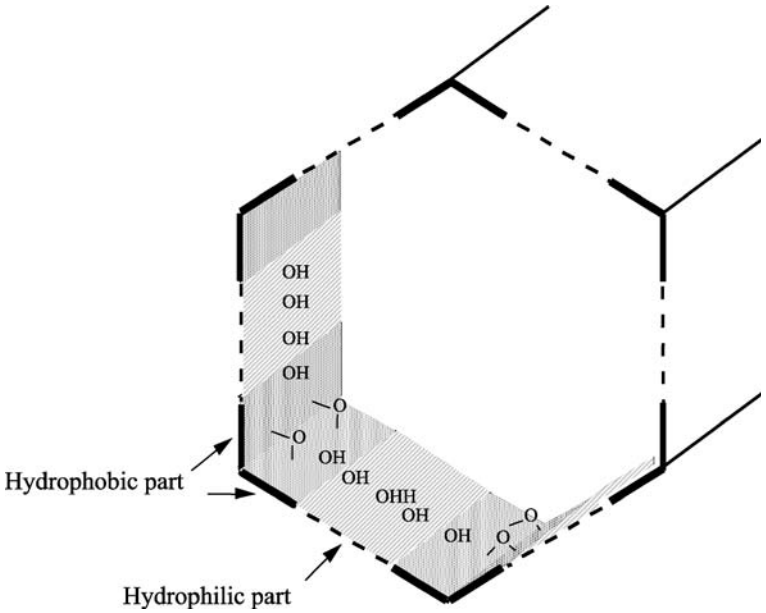

Fig. 1 Model of a pure-silica hexagonal MTS system showing hydrophilic and hydrophobic patches. After [9]

In this chapter, only silica-based systems are considered. We do not consider, however, pure silica or functionalized (grafted) samples. Acidity of the former type of solids is the same as that of other forms of silica. The latter constitute a field of growing importance and are giving rise to a new class of catalysts [5].

The main scope of this chapter is the study of the acidic and (possibly) basic properties of these systems arising from the presence of heteroatoms, i.e., atoms different from the constitutional Si species. By a mechanism similar to that operating in zeolites and zeotypes like SAPOs or MeAPOs, Brønsted

acidity/basicity may arise when the tetravalent Si atom is replaced with atoms M in tetrahedral position (referred to collectively as T atoms), bearing a lower oxidation number.

Compensation of charge, when a trivalent atom substitutes for the tetravalent Si, requires the presence either of exchangeable cations (as with zeolites) or of acidic protons. The former type of samples may in principle show basic behavior, the latter shows invariably acidity, either Lewis or Brønsted acidity. These acid/base properties, though much studied for their practical importance, are not well understood, and debate is going on. For this reason, a review on this subject is timely. We present here an account on the possible sources for acidic behavior of MTS, being aware that the interpretations proposed may be considered as subjective.

Research has mostly considered trivalent atoms, with a preference for tetrahedral coordination, i.e., M = Al, Ga, B, Fe (although substitution with divalent atoms has been attempted, e.g., Zn [10]). Of these, Al is particularly important, because as a whole, the main subject of this review is actually Al-substituted MTS.

Replacement of Si with other tetravalent species (Ti in particular) has been attempted, which does not bring about Brønsted acidity per se, but promotes catalytic behavior [11]. The same holds for pentavalent atoms like vanadium or niobium [11, 12].

The measure of acidity/basicity and discrimination between Lewis and Brønsted acidity is a delicate task. This topic is the subject of other chapters of this series "Molecular Sieves – Science and Technology" (cf. Volume 4, Chapter 1, Volume 5, Chapter 2, Volume 6, Chapters 3–6), to which the reader is referred for detailed information. We limit to note that means for measuring the acidity and basicity of MTS are the same as with other systems: titration, adsorption volumetry, gravimetry and microcalorimetry, temperature-programmed desorption (basically of ammonia), infrared and NMR spectroscopies and catalytic probe reactions.

Information on the topology/morphology of MTS mainly comes from XRD patterns, BET isotherms, ^{27}Al MAS-NMR results. As quoted above, XRD shows that MTS are amorphous in nature, with no short range (atomic) organization. This is elegantly confirmed by Raman spectroscopy [13], which shows the presence of a band at ca. 610 cm^{-1}, due to cyclic trisiloxane structures (three-membered rings), only found with amorphous silicas.

Contrary to zeolites, which are characterized by a rigid network of Si-O-Al(Si) linkages, with well-defined atomic positions and narrow distributions of bond angles and bond lengths, the walls of mesostructured silicoaluminates consist of a flexible and reactive framework lined with hydroxyl groups, leading to a broad distribution of Al environments and strong lateral interactions. Disorder in the structure arises from the extreme pliability of the Si-O-Si bond, as demonstrated by calculations on the model molecule siloxane $H_3Si-O-SiH_3$ [14]: a change in geometry from a Si-O-Si angle of 180°

to 120° is accomplished without energy expenditure, which comes into play for smaller angles.

Incorporation of Al as a T atom is readily checked by NMR spectroscopy. Figure 2 displays a typical NMR spectrum, showing how the possible coordinative states of Al atoms may be distinguished on the basis of their NMR shift: octahedral Al atoms have a small chemical shift with respect to the reference hexa-aquo-Al cation, tetrahedral Al atoms have a shift of ca. –60 ppm, and penta-coordinated species are characterized by an intermediate value.

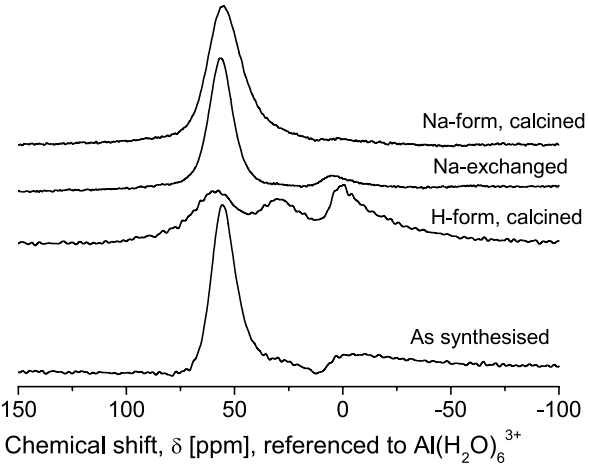

Fig. 2 ^{27}Al NMR of an [Al]-MCM-41(2.5) sample as synthesized in a Na-form, after further Na exchange, after calcination of this Na-form, and after calcination of the H-form. After [22]

Several factors affect the MTS behavior. These include type of heteroatom T, structure of the solid, T/Si ratio, thermal history and pretreatments. The source of Al also plays a role, e.g., it is known since long [15–17] that Al species can be incorporated as T atoms into the inorganic mesoporous framework, provided a monomeric alumina precursor is used in the synthesis.

Early work concerned mainly high Si/Al ratios, though already in the mid 90's a few papers appeared concerning samples with high Al content [18–20]. Hereafter, the Al content will be reported in parentheses after the acronym defining the material: e.g., H-[Al]-MCM-41 (38) indicates a MCM-41 system, containing Al as a T atom, in protonic form, with an Si/Al ratio of 38.

The structure of this chapter is as follows. As it concerns [Al]-MTS, first discussed are the cation-exchanged samples, potentially exhibiting basic behavior, then the H-forms, the acidic properties of which are, as a whole, the main subject, finally the development of acidity upon partial exchange of cations with protons. The last section is devoted to a brief description of MTS with heteroatoms other than Al.

In this review, we have considered as reference systems, on the one hand, pure silica and amorphous silica-aluminas (ASA), and zeolites on the other hand. Knowledge of MTS may help in understanding an old subject like the chemistry and structure of ASA, comparison with zeolites of similar composition may highlight the role of the amorphous structure.

2
Expected Basic Behavior in [Al]-MTS Systems: Ion-exchanged and Ion-impregnated Samples

As it concerns as-synthesized samples, i.e., still bearing template molecules, NMR spectra show, as depicted in Fig. 2, that Al atoms are all in tetrahedral coordination [21, 22]. No catalytic use of such systems is known (therefore no acidic or basic behavior), albeit the interior of micelles may be accessible. Indeed, when a MCM-41 silica is considered containing surfactant-embedded molecules of Congo red (a well-known dye and pH indicator) [23], contact with either ammonia or HCl in the gas phase leads to changes in color, so proving that the hybrid organic-inorganic material is permeable to gases.

After synthesis, the as-prepared MTS samples can undergo removal of the template (organic) phase either by destructive thermal treatment, or by washing with appropriate solvents. When the latter process is carried out with saline solutions, the replacement of the positive heads of the template molecule occurs with cations, e.g., alkaline or alkaline earth species [24]. If the synthesis was run in alkaline media, a substantial fraction of the template molecules may already be substituted by alkali cations [21].

Besides plain substitution, over-exchange may occur, depending on, for instance, whether the samples have been washed or not after treatment. Such post-synthesis treatment leads to potentially basic systems, as it is the case with zeolites [25]. Few studies are available about the basicity of MTS systems: evidence exists, however, that such systems show no basicity at all.

In [21], the basic properties were investigated of [Al]-MCM-41(25) systems bearing either Na or Cs cations ($M^+/Al = 0.96$). The expectation was that Cs-samples would show a basic behavior more marked than Na-samples (as coming from synthesis). Both washed and unwashed samples were considered. The basic behavior was studied by means of IR spectroscopic measurements concerning CO_2 adsorption and through catalytic studies of the isomerization of 1-butene. Complementary IR measurements, e.g., concerning CO adsorption, were also performed. The unexpected result was that unwashed (over-exchanged) Cs samples had no catalytic activity: a Cs-oxide phase was marginally present, though not active, but the majority of the Cs-oxide phase had reacted with the silica framework, to yield a Cs silicate, as well catalytically inactive. The interesting conclusion was also drawn that pure silica systems are more readily attacked by Cs oxide than Al-

rich silica systems, like faujasitic zeolites, which do seem indeed to resist attack.

Results with washed samples were puzzling: contrary to expectations, the Na form (as-synthesized) was definitely more active in the 1-butene reaction that the Cs-substituted form (Fig. 3).

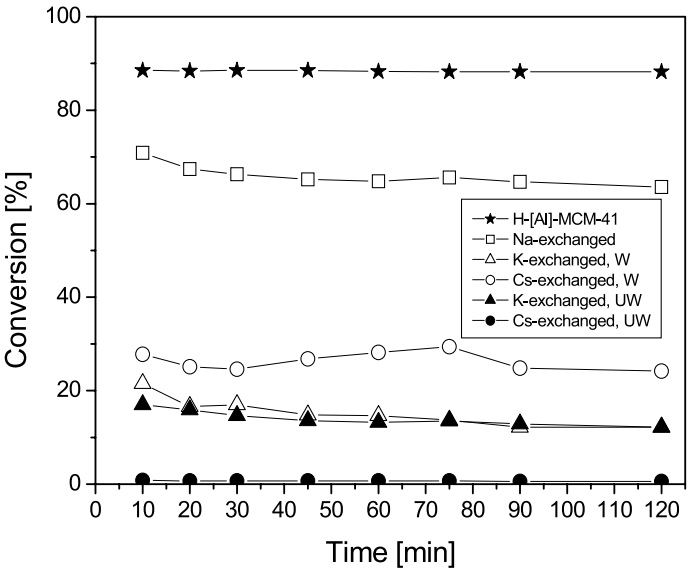

Fig. 3 Activity of alkali-cation exchanged [Al]-MCM-41(20) in the isomerization of 1-butene. Products are *cis*- and *trans*-2-butene in approximately 1 : 1 ratio; no isobutene formed. W and UW in the acronym stand for washed and unwashed after exchange, respectively. After [21]

The type of reaction products in the isomerization of 1-butene is very informative on the mechanism: formation of isobutene is related to the presence of strong Brønsted sites and the presence of 2-butenes with a strong prevalence of the cis-form is promoted by strong basic sites, whereas the presence in the reaction products of cis- and trans-butene-2 with a ratio about one is indicative of sites with moderate acidity. The result was a nearly 1 : 1 ratio in cis and trans -2-butene, with no isobutene formed.

The conclusion was, therefore, that basic sites are absent also on washed samples, and that the catalytic activity of the Na-sample was due to some residual acidic groups, not evident per se in the spectra. acidic sites, moreover, only show moderate acidity. Note that the Na/Al ratio was 0.96, and that the potential residual acidity is apparently limited to a few percent of the total Al content. These observations fit well into the general picture, developed below as it concerns acidic forms, that no really strong acidity is developed in [Al]-MTS systems. The question remains open as to the nature of the acidic species

promoting the isomerization reaction. A proposal is made in Sect. 4 of this chapter.

MTS systems with a high Al content are now being prepared [22, 26–30], showing an Al/Si ratio down to about one. Such samples may be prepared both in acidic form, the properties of which are discussed below, or in a cationic form, e.g., exchanged with either Na or Li cations. Interestingly, the ratio M^+/Al never reaches unity, i.e., there is always a fraction of H atoms balancing the charge of the overall system. For instance, when an Si/Al ratio of 2.5 is considered [30], the theoretical overall composition of the systems (under the assumptions that: i) protons compensate for the charge; ii) no dehydration has occurred) resulted to be $H_{0.17}Li_{0.12}Al_{0.29}Si_{0.71}O_2$ and $H_{0.05}Na_{0.24}Al_{0.29}Si_{0.71}O_2$.

The IR spectra of these samples have been studied, as well as the interaction with CO and CO_2, this latter with the purpose of obtaining evidence of any possible basic behavior. Carbon dioxide can indeed react with possibly occurring basic oxygen species to yield carbonates with characteristic IR features. No carbonate species was observed. Instead, a molecular interaction with cations, reversible at room temperature, was found, which was monitored both by IR and microcalorimetry. Besides showing the absence of basicity, interaction with carbon dioxide allowed to titrate the exposed M^+ cations, thus showing that only a fraction of cations are accessible. A dramatic decrease in the differential heats of adsorption, not accompanied by a concomitant shift in IR bands of the adsorbed species, indicated that interaction with CO_2 implies some "extraction" of cations from the surface, to which corresponds an endothermic step.

The fraction of accessible cations was only about 5% for the Li-sample and 3.6% for the Na-sample. The two figures being not far from each other, a comparable number of cationic sites are actually available on the two samples, notwithstanding the different cationic content. It thus appears that a remarkable fraction of cations are not readily reached by incoming molecules, as it happens with some zeolitic systems, e.g., cages of which are not readily accessed.

The presence of residual acidic sites was studied through interaction with CO, and is reported below in Sect. 4. The absence of any propensity for a basic behavior is worth noting: further considerations are made below in Sect. 5.

3
Brønsted and Lewis Acidity of Protonic Forms H-[Al]-MTS

When the proton is the charge-compensating species, Brønsted acidity may in principle develop. As reported repeatedly and depicted in Fig. 2, ^{27}Al NMR shows that the presence of the proton destabilizes the Al in tetrahedral positions [22, 24], so that octahedral and penta-coordinated Al species are formed.

Note that penta-coordinated Al species are not present in transition aluminas, so that they appear to be a feature of silica-aluminas and zeolitic systems. Simultaneously, Lewis acidity is expected. In what follows, a summary is reported on the available experimental evidence of the acidic forms of MTS.

3.1 Non-spectroscopic Evidence Concerning Adsorption on Acidic Sites

The overall acidic nature of Al-substituted MTS, expected on simple chemical grounds, may be proved by non-spectroscopic measurements, e.g., immersion calorimetry [31], or determination of the adsorption capacity for a base molecule (volumetric or gravimetric, e.g., [32]). Other overall methods employed to define acidity are also based on the interaction with strong bases, usually ammonia or pyridine. The interaction may be followed either by calorimetry (in the adsorption run) or through temperature-programmed desorption (TPD). Both techniques reveal the presence of sites, differing in one case by the differential heat of adsorption and in the second case by the temperature of the desorption peak.

Early reports [33, 34] on the acidity of MCM-41 materials, as evaluated by ammonia TPD, pointed to a moderate strength of the acid sites, comparable to that of traditional ASA and inferior to that of zeolites. Subsequent studies based on the TPD method do not provide, however, the same clear picture for the surface acidity of MTS. A typical TPD profile for a [Al]-MCM-41(20) is shown below in Fig. 14. Compared to zeolites, the MTS material does not feature the high-temperature desorption peak (in the range 350–450 °C), characteristic of strong acid sites, but rather a broad signal indicating a distribution of sites of moderate strength. On the contrary, Kosslick et al. [35] detected three well-defined desorption peaks, at 220 °C, 340–450 °C and 600 °C, attributed, respectively, to weak to medium acidic Brønsted sites, to strong Brønsted sites and to very strong Lewis sites. The intensity of the signal associated with the latter type of sites increased with the aluminum content of the samples, while that corresponding to the strong Brønsted sites was optimum for an Si/Al ratio around 5. These features are in line with an extensive dealumination of the framework at high Al contents.

The heterogeneity in strength of the acid sites of MCM-41 has been also evidenced by ammonia adsorption microcalorimetry experiments performed over a series of materials prepared with varying aluminum contents (Si/Al from 8 to 32) [36] or using different aluminum sources [37]. The authors concluded a low density of surface sites to exist with differential enthalpies of adsorption varying from –160 to –80 kJ mol^{-1}. Moreover, comparison of the acidity distributions showed that samples prepared from $Al(OH)_3$ contained a wide distribution of acid site strengths, while samples prepared with $Al(OiPr)_3$ or $NaAlO_2$ contained sites with a distinct strength around 130–150 kJ mol^{-1}.

It has to be noted, however, that both TPD and calorimetry methods are not able per se to discriminate between Lewis and Brønsted acidity, to which purpose IR measurements are required.

3.2 NMR Spectroscopy

Magic angle spinning-nuclear magnetic resonance (MAS NMR) spectroscopy has become in the last ten years or so one of the most powerful techniques for the investigation of solid acid catalysts [38, 39].

^{1}H MAS NMR provides evidence for an active site in silica-aluminas structurally different from that of zeolites. Proton NMR spectra of activated silica-aluminas usually show a single peak at $\delta = 1.7-1.8$ ppm assigned to terminal silanols, with a broader component located near 2.8 ppm attributed to Al – OH [38–41], in contrast to the typical bridging Si(OH)Al of zeolites which shows a sharp resonance near 4.2–4.4 ppm. According to Kuroda [40] a broad weak signal in the case of silica-alumina, which can be detected near 3.8 ppm, could be due to more acidic OH species.

Figure 2 shows that calcination induces a strong distortion of the Al environment. This is more pronounced at high Al contents and under hydrothermal conditions, and leads ultimately to dealumination and to an increase of the proportion of Lewis acidity. ^{27}Al NMR, as already reported, allows the discrimination of structural species into tetrahedral, octahedral and pentacoordinated forms. Unfortunately, the quadrupolar nature of the nucleus does not allow the observation of fine structures of the bands, thus limiting the amount of information achieved. One exception is the recently reported paper by Omegna et al. [42], according to which two kinds of octahedrally coordinated Al species in silica-aluminas occur. Part of these Al species are reported to change their coordination into tetrahedral when contacted with strong bases like ammonia. Section c of Scheme 4 reports the proposed interpretation, which is discussed together with other proposals in the appropriate section (Sect. 3.5.1).

3.3 IR Spectroscopy

Infrared spectroscopy may be used in several ways as it concerns the study of acidity (cf. also Volume IV, Chapter 1 of the series "Molecular Sieves Science and Technology"). In the first instance, Brønsted acidic species may show up in the spectrum in the appropriate O – H stretching region, the location and variety of bands providing information on them. This type of investigation has been classically carried out as it concerns all sorts of oxides: alkaline earth oxides, aluminas, zeolites, silicas, etc.

The second use of IR is the discrimination between Brønsted and Lewis acidity, mentioned above: adsorption of strong bases like pyridine or ammonia yield with Brønsted acidic species the corresponding protonated species (pyridinium and ammonium ions, respectively), with unmistakable spectroscopic features, whereas Lewis surface sites coordinate the ligand in a molecular form, with limited, though often very meaningful, changes in frequency.

Thirdly, Brønsted acidity may be measured indirectly as the propensity to engage in H-bonding with molecules with basic properties. The amount of the shift suffered by the O – H stretching mode of the acidic hydroxyl upon H-bonding is a function of the strength of the interaction, so that a measure of the relative acidity of two OH species may be carried out by comparing the shift suffered with the same molecule.

A systematic way of carrying out such a comparison makes use of the so-called Bellamy–Hallam–William plot, a procedure borrowed from solution chemistry, which is as follows. A set of molecules of basic nature is considered. The shift suffered by H-bonding to each molecule in this set is measured by the O – H stretching mode of an acidic hydroxyl (e.g., in H-ZSM-5) and successively plotted against the same type of data for a reference O – H species (e.g., the isolated silanol in H-MCM-41). A proportionality is seen, the slope of the straight line constituting a measure of relative acidity of the two hydroxyl species.

The two methods of measuring Brønsted acidity, i.e., the tendency either to transfer the proton to a strong base or to engage in H-bonding with a mildly basic molecule, constitute different means not necessarily yielding the same results or the same information. Actual H-transfer is a property relevant to catalysis (whereas, basically, propensity to H-bonding is not), and, therefore, catalytic data constitute naturally a reference. The ion pair formed upon proton transfer, however, needs a stabilization from the surroundings, so that the Brønsted acidity in a strict sense is a feature of the acidic species and of its environment. Instead, the ability to form (weak) H-bonds with slightly basic molecules like CO, depends basically on the electric field in the proximity of the acidic proton, so the information acquired is more local and concerns basically the acidic hydroxyl.

3.3.1 The Bare Samples

The most straightforward hypothesis about the Brønsted acidic center in H-[Al]-MTS, as advanced even recently [43, 44], is to assume that it coincides with that of protonic zeolites, the hydroxyl group bridging between an Si and an Al atom. This acidic group will be designated subsequently as bridging OH species and represented as Si(OH)Al: a model is given in Scheme 1.

However, it is known for a long time that the IR spectra of silica-alumina and zeolites are strikingly different [45]. The IR spectra of a series of H-[Al]-

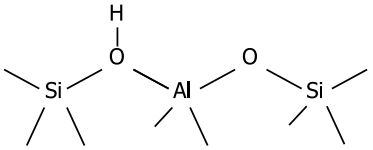

Scheme 1 The commonly accepted structure of Brønsted sites in zeolites

MCM-41 with varying Si/Al ratio (from ∞ to 13), all outgassed at 673 K, is reported in Fig. 4 [46].

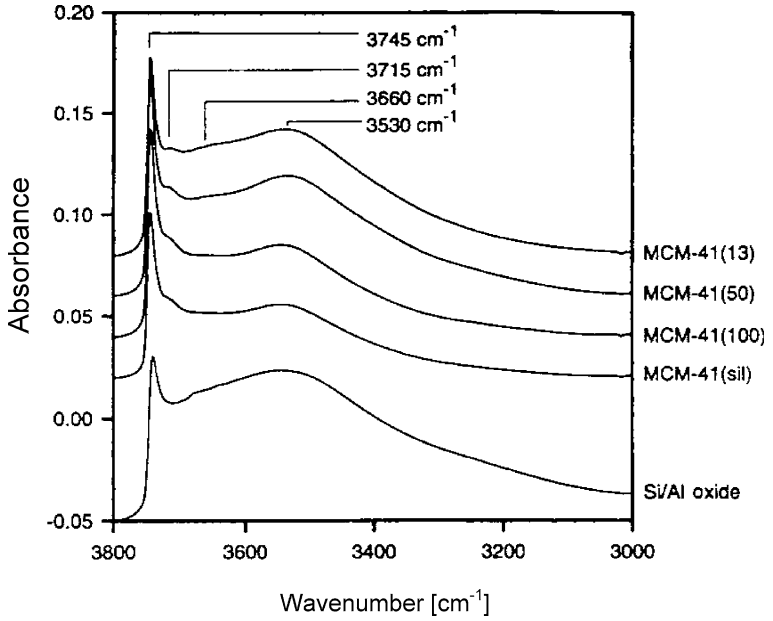

Fig. 4 IR spectra of H-[Al]-MCM-41 samples, differing in Al content (Si/Al ratio in parentheses), outgassed at 673 K. After [46]

The overall spectra are very similar to those of pure amorphous silica, either Aerosil [47] or MCM-41 [48]. Several components are seen, among which predominates the sharp band at 3745 cm^{-1}, due to isolated silanol species (subsequently designated as Sil, Scheme 2a). The couple of bands at 3720–3520 cm^{-1} is due to a pair of silanols mutually interacting via H-bonding (subsequently referred to as Dim-Sil, Scheme 2b), which shifts both vibrations to lower frequencies, that of the H-donor species to a greater extent [47]. A component at 3715 cm^{-1}, not readily distinguishable from the silanol component at 3720 cm^{-1}, is sometimes ascribed to an AlOH species [46], indicated subsequently as AlOH(I), Table 1.

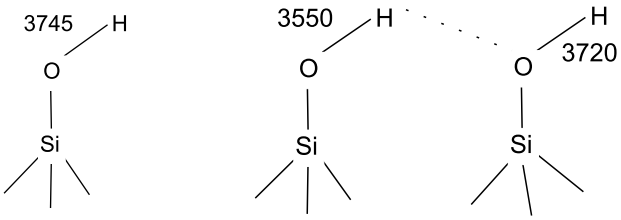

Scheme 2 Structures of Sil (isolated silanol) and Dim-Sil (pair of H-bonded silanols), together with the corresponding O – H stretching modes

Table 1 Acidic centers in H-[Al]-MTS, both Brønsted and Lewis, as revealed by the interaction with CO. Wavenumbers in cm^{-1}: uncertain values with a question mark; frequencies not directly observed in parentheses. Bønsted sites are listed in increasing acidic strengths

Symbol	ν(OH) free	ν(OH) H-bonded	$\Delta\nu$(OH)	ν(CO)	Structure
Brønsted					
Sil	3747	3650–3660	97–87	2156	Scheme 2a
Dim-Sil	3720, 3520	3600	120	2157?	Scheme 2b
AlOH(I)	3715	3570	145		? Related to EFAL debris
AlOH(II)	(3660–3680)	3460	200–220	2173	Scheme 3
AlOH(III)	3610, other modes?	3420	190? probably around 230	2173?	Schemes 4d, 6
$Al\cdots H_2O$	3694, 3609, 1604	3406	245	2174	Schemes 4d, 6
Lewis					
Al^{3+}(S)				2230	Scheme 5
Al^{3+}(I)				2200–2190	? Related to EFAL debris
Al^{3+}(W)				2173	Scheme 5

Figure 5 shows the behavior of a sample H-[Al]-MCM-41(82) with temperature. At high dehydration, the very sharp band near 3747 cm^{-1} predominates, with a tail resisting thermal treatment more than pure silica.

If the acidic species were bridging, zeolite-like Si(OH)Al hydroxyls, a band would be visible around 3600 cm^{-1}. No such band is present in the spectra of Figs. 4 and 5. Only after thermal treatment at highest temperatures, a tiny band appears at ca. 3610 cm^{-1}, actually hardly visible in the figure. The same band has been reported recently [49–52] and sometimes ascribed to Si(OH)Al sites.

The intensity of this band is really minor, so that its presence could be considered as a negligible feature. It has to be recalled, however, that, as discussed

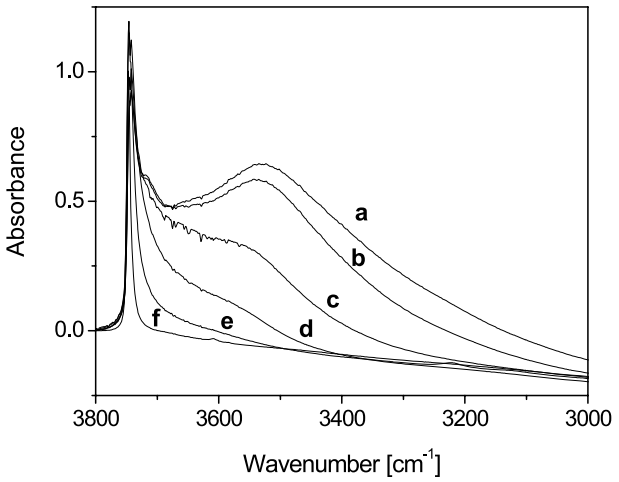

Fig. 5 IR spectra of H-Al-MCM-41(82) at different levels of surface dehydration. Sample outgassed at: **a** room temperature; **b** 373 K; **c** 573 K; **d** 773 K; **e** 923 K; **f** 1073 K

below, direct IR evidence of acidic O – H species is missing, so that very weak bands as the tiny one at ca. 3610 cm^{-1} could be meaningful. Section 3.3.4 below shows, moreover, that such a weak band may be due to Brønsted sites, formed by the adsorption of water on strong Lewis sites, which are not bridging hydroxyl species Si(OH)Al. On the other hand, very recently, Datka and coworkers [53] have observed a very weak band at ca. 3610 cm^{-1} when studying systems similar to those under consideration in this chapter, defined as mesoporous aluminosilicates, and corresponding, roughly speaking, to silicated aluminas. In this very case, as discussed below, the 3610 cm^{-1} could be indeed due to bridging Si(OH)Al species.

The first general conclusion coming from Figs. 4 and 5 is that bridging hydroxyl species do not really show up in the IR spectrum of H-[Al]-MTS, in agreement with what is reported by the majority of workers [54–59], and in full agreement with what is known for ASAs. The second conclusion is that either no acidic hydroxyls are visible at all in the spectrum, or the related absorptions coincide with the only band present, i.e., that around 3745 cm^{-1}, usually ascribed entirely to isolated silanols, Sil. This latter hypothesis has been considered by Busca and coworkers [54, 55, 60], and by Zholobenko et al. [59].

According to Busca, the OH stretching band in silica-aluminas is composite, being made up of two or more components, almost unresolved in the activated sample, ascribable to OH species interacting with a distinctly different strengths with bases. Zholobenko et al. [59] showed that indeed two components are seen around 4550 cm^{-1}, where the combination mode $\nu + \delta$ falls; and propose that two species of silanols actually occur, sharing the same

ν mode at 3745 cm^{-1}, but with δ modes at 825 cm^{-1} (non acidic) and 788 cm^{-1} (acidic), respectively.

3.3.2
Proton Transfer to Strongly Basic Molecules

The occurrence of proton transfer, i.e., of proper Brønsted acidity, is usually revealed by IR spectroscopy, because the vibrational modes of protonated and non-protonated species are remarkably different. This topic, now a standard tool in surface chemistry, is dealt with in detail in other chapters of the present volume, and will not be treated here (cf. also Volume IV, Chapter 1 of the present series "Molecular Sieves – Science and Technology"). A variant of the IR method is the use of quinoline instead of pyridine, which allows the distinction between protonated and non-protonated species by the use of laser-induced fluorescence [32].

Results indicate a definitely higher Brønsted acidity of H-[Al]-MTS with respect to silica, detected, e.g., by protonation of ammonia, pyridine [60], amines [61] and also by the strong H-bonding with nitriles [54]. IR results concerning pyridine adsorption show the presence of Brønsted sites, weaker than those of ASAs and the zeolite USY.

On the other hand, Lewis acid sites are also detected, e.g., by adsorption of pyridine, nitriles and CO [60], which can be remarkably strong. CO adsorption being, as usual, very informative, is reported in detail below. The strength of Lewis sites makes H-[Al]-MTS systems interesting catalysts for Lewis-acid catalyzed reactions, such as, e.g.,, the dehydrochlorination and the steam reforming of halided hydrocarbons [62].

The role of Lewis acidity is particularly clear in the reaction of H-[Al]-MCM-41 with propene (Bonelli B, Garrone E, unpublished results). This reaction was studied to assess whether Brønsted acidity was strong enough to promote polymerization, a reaction clearly visible in the IR. Basically, the result was that, unlike protonic zeolites, H-[Al]-MTS systems do not polymerize propene. Traces of polymerization products observed increased with temperature of pretreatment, thus suggesting that the reaction occurs on Lewis and not on Brønsted sites.

3.3.3
Propensity to Form H-bonded Adducts

Two points arise when studying the interaction of mildly basic molecules with the H-Al-MTS surface with the purpose of identifying the acidic Brønsted centers through the formation of H-bonded adducts. A first point is to check whether the "missing" acidic OH species absorb at the very same frequency of silanols, and are, thus, masked by the latter, being nonetheless characterized by a more marked acidity, as proposed by both Busca and

Zholobenko [59, 60]. Alternatively, it may occur that suitable interactions may evidence "hidden" acidic OH species, prevented, for whatever reason, from showing up in the spectrum.

In our opinion, room-temperature interaction with ammonia provides the former type of evidence, and the interaction at low temperature with CO provides the latter.

Concerning low-temperature infrared spectroscopy, it has to be noted that the coolant employed to reach low temperatures is nearly always liquid nitrogen at its boiling point (77 K). Due to the heating effect of the IR beam, however, the actual temperature of the sample is somewhat higher, the actual increase depending on several parameters, and may also slightly vary along an experiment. For these reasons the temperature of measurement is normally referred to as the nominal value of 77 K.

Figure 6a shows the interaction of ammonia with a specimen of H-[Al]-MCM-41(28) in the O – H stretching region. In the presence of gaseous ammonia, the band at 3745 cm^{-1} decreases, because an H-bond is formed. The broad band at 3060 cm^{-1} is the stretching mode of the O – H species engaged in the H-bonding interaction. The other bands in the spectra are due to ammonia chemisorbed on two types of Lewis sites and to other features not discussed here.

All silanols interact reversibly with ammonia. By measuring the changes in intensity of the 3745 cm^{-1} band as a function of ammonia pressure, the adsorption isotherm may be obtained, as far as only the interaction $SiOH/NH_3$ is concerned. The fraction θ of silanols engaged equals $(A_M - A)/A_M$, A being the intensity of the 3745 cm^{-1} band under a pressure p of ammonia, and A_M the intensity in the absence of interaction. Figure 7b shows that the adsorption isotherm roughly obeys the Langmuir equation $\theta/(1 - \theta) = Kp$, the expected behavior if silanols act as adsorbing centers all equally and are not interacting [63]. The slope of the diagram yields K, the equilibrium constant of the process, which measures the strength of interaction. Section b of Fig. 6 shows that the isotherm for the H-[Al]-MTS sample and that for pure silica samples are indistinguishable, so indicating that no difference in acidity occurs.

It may well occur that with other samples (e.g., at different Al content), or for other pretreatments, silanols may assume a more pronounced acidic character. Data in Fig. 6 indicate, however, that this is not the case with a low Al content, that acidic Brønsted species do not contribute to the absorption at 3745 cm^{-1}, and finally that acidic sites do not appear directly in the IR spectrum.

Several other molecules have been used as basic probes to measure the H-bonding propensity of acidic centers in H-[Al]-MTS, e.g., nitriles, which tend to form relatively strong H-bonds [60]. The interaction with a milder base like CO is more informative, and in our opinion it provides the key to understanding the nature of acidic sites. In the following, the evidence coming from CO adsorption is reported. Table 1 gathers the relevant data.

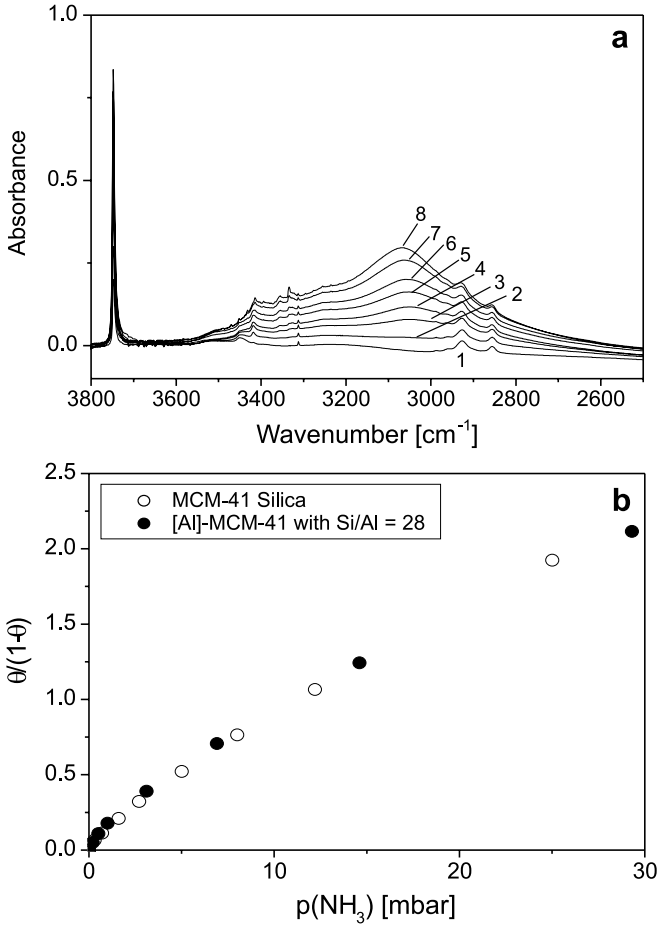

Fig. 6 Spectroscopic data concerning the interaction of ammonia with H-[Al]-MCM-41(28) outgassed at 1073 K in the O – H stretching region. **a** room temperature IR spectra at increasing ammonia equilibrium pressures, i.e., bare sample (spectrum 1), 0.20 (2), 0.50 (3), 1.00 (4), 3.10 (5), 6.90 (6), 14.6 (7) and 29.3 (8) mbar. **b** Check of the Langmuir equation (see text for details) and comparison with pure silica MTS outgassed at the same temperature. In order to allow comparison, spectra have been normalized to the same wafer thickness. θ is the fraction of Sil species interacting with ammonia

We start the review of the IR results concerning the adsorption of CO on oxide systems, containing both Si and Al, by considering first the recent results by Datka and co-workers [53]. Figure 7 depicts the changes occurring in the IR spectra of two samples, because of the low-temperature contact with CO, as difference spectra.

In the case of H-[Al]-MTS, the decrease of the very weak band at ca. 3610 cm^{-1} corresponds to the growth of a complex and broad absorption,

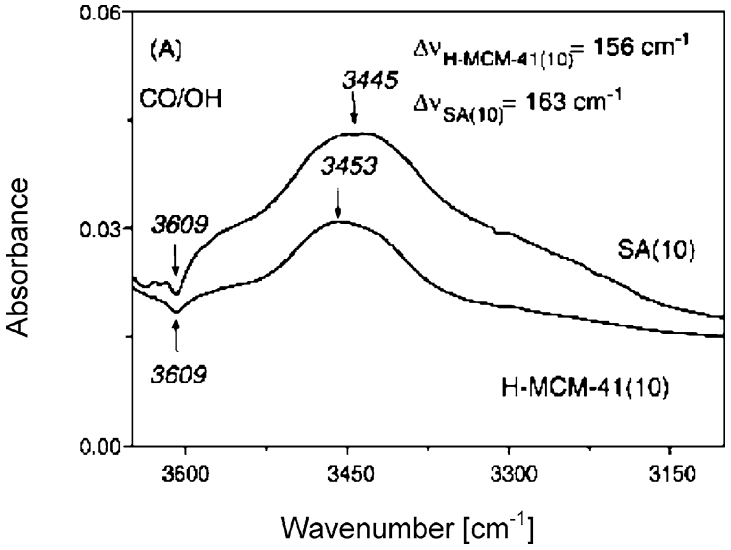

Fig. 7 Comparison of the IR spectra in the O – H stretching region (difference spectra) of an H-[Al]-MCM-41 sample and a silicated alumina after CO contact at nominal 77 K. After [53]

orders of magnitude more intense than the negative band. Two components are seen at ca. 3570 and 3450 cm^{-1}. With the other sample, a silicated alumina, these two bands are more intense, and another component at ca. 3300 cm^{-1} is seen. This latter is of utmost interest, because it could indeed be related to a bridging site, Si(OH)Al, which is characterized by a shift of ca. 300 cm^{-1}. Datka and co-workers interpret the whole positive band envelope as being due to the decrease of the 3610 cm^{-1} band, assumed to be a Brønsted site, which is characterized, however, by a moderate acidity (the overall shift in O – H stretch is only ca. 160 cm^{-1}). This is unconvincing, and therefore we are inclined to interpret the positive band envelope as due to three components, one being the expected contribution of the bridging site Si(OH)Al at ca. 3300 cm^{-1}, and the other two, those at 3570 and 3450 cm^{-1}, being those found rather regularly on H-[Al]-MTS, as detailed below.

Figure 8 shows the IR spectra concerning the adsorption of CO at the nominal temperature of 77 K on an H-[Al]-MCM-41(27) outgassed at the relatively low temperature of 573 K.

Section a of Fig. 8 illustrates the O – H stretching region. Spectra are reported as difference from background, the spectrum of the CO-free sample was obtained at low temperature. Section b depicts the CO stretching region. Contact with CO at increasing pressure brings about the decrease in intensity of the band due to isolated silanols (observed at 3748 cm^{-1}, because of the low temperature of measurement), as well as the decrease of a component at 3720 cm^{-1}, the H-acceptor silanol in Dim-Sil (Scheme 2).

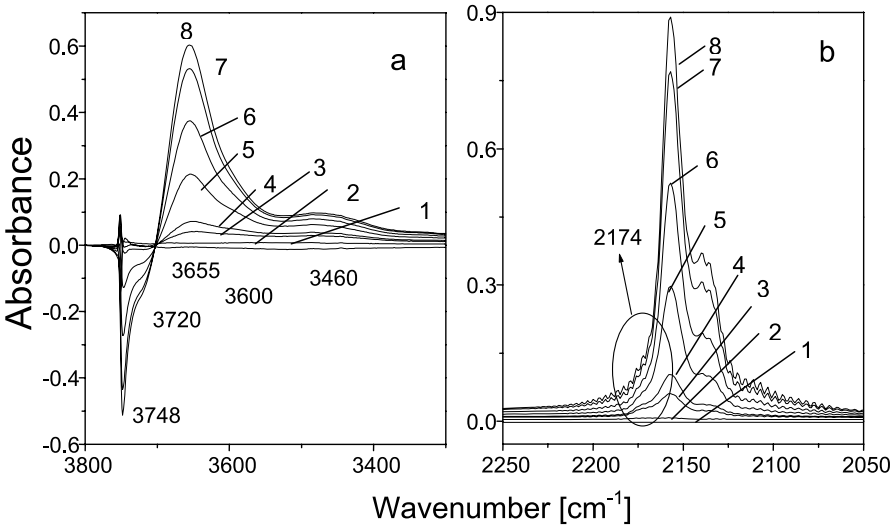

Fig. 8 Difference IR spectra concerning the adsorption of CO at the nominal temperature of 77 K on an H-Al-MCM-41(27) sample outgassed at 573 K. Equilibrium pressures: 0.05 (curve 1); 0.1 (2); 0.5 (3); 1.5 (4); 3.0 (5); 5.0 (6); 10.5 (7); 15.0 (8) mbar. **a** O – H stretching region; **b** CO stretching region

The isolated silanol Sil, when H-bonded to CO, is responsible for the positive band at 3660 cm^{-1} (the corresponding bathochromic shift being ca. 90 cm^{-1}). The Dim-Sil species, when engaged with CO, gives rise to a shoulder at ca. 3600 cm^{-1}. The shift from 3720 cm^{-1} is of about 120 cm^{-1}, in agreement with the relatively larger acidity brought about by H-bonding between the pair of silanols [64].

The puzzling feature of Fig. 8 is the broad band at 3460 cm^{-1}, which is due to some OH species perturbed by CO as indicated by the frequency range. The involved OH species is more acidic than the two types of silanols (Sil and Dim-Sil), because of the definitely smaller wavenumber; moreover, the 3460 cm^{-1} band is formed first. The broadness of this band suggests that probably two components are involved, which are clearly seen in the similar experiment run on the sample outgassed at a higher temperature (Fig. 9).

The corresponding spectra in the CO region show a main band at 2156 cm^{-1}, to which both Sil and Dim-Sil presumably correspond, the difference in the strength of interaction being probably not enough to discriminate between them. The band at ca. 2140 cm^{-1} is due to physisorbed CO and has no relevance here. The features of the weak band at 2174 cm^{-1} indicate that a relatively strong CO species is involved, and suggest correspondence with the absorption centered at 3460 cm^{-1}. Both bands are formed first and located at one end of the respective spectral region. The puzzling point is, however, that no decrease in absorption, seen as a negative band, appears in Fig. 8.

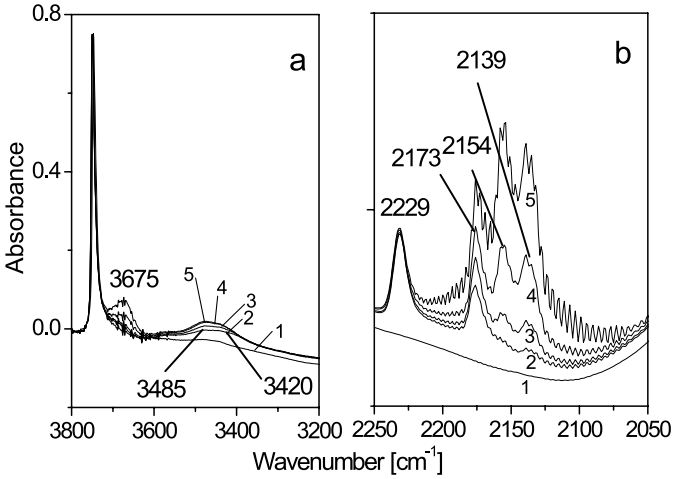

Fig. 9 IR spectra concerning the adsorption of CO at the nominal temperature of 77 K on an H-AL-MCM-41(82) outgassed at 1073 K. Equilibrium pressures: 0.00 (curve 1, bare sample); 0.4 (2); 1.0 (3); 3.0 (4); 14.6 (5) mbar. **a** O – H stretching region; **b** CO stretching region. After [51, 52]

In our opinion, this is further evidence that acidic species, responsible for the Brønsted acidity of the H-[Al]-MTS system, are indeed present but do not appear in the IR spectra. A similar mechanism seems to operate in the case of results by Datka in Fig. 7, as it concerns the two components at 3570 and 3450 cm^{-1}; no corresponding negative band is seen. Also, the apparent giant increase in intensity of the band envelope is not really justified. Intensification of O – H stretching modes upon H-bonding is a usual phenomenon, which depends on the overall strength of interaction, as does the extent of the shift in the O – H mode [65]. The two observables (increase in the intensity of the O – H mode and shift in frequency) are indeed related to each other: the observed intensification is much larger than expected for the range of shifts observed.

A possible explanation is as follows. Because of the amorphous nature of the system and the flexibility of Si – O – Si bonds, Brønsted acidic centers responsible for the 3460 cm^{-1} absorption after interaction may occur in a variety of coordinative environments, so that the corresponding O – H stretch is smeared out and not observed as a definite band in the spectra of the bare sample, nor is it as a negative band in difference spectra like those in section a of Fig. 8. Such is, for instance, the explanation proposed for the species Si(OH)Ga (see Sect. 7). Adsorption would restore homogeneity in the set of the heterogeneously broadened ensemble of acidic species.

Figure 9 shows a similar experiment concerning a more diluted sample outgassed at higher temperatures. Similar features are observed. In the OH stretching region, the isolated silanols give rise to a perturbed band in the ex-

pected position. In the 3500–3400 cm^{-1} region, two components are seen, at ca. 3485 and 3420 cm^{-1}, that at lower frequency being formed first. Again, the lower the frequency of the band, the higher the strength of interaction.

The CO stretching region shows, besides the expected bands at 2139 (physisorbed species) and 2156 cm^{-1} (CO interacting with isolated silanols), a peak at ca. 2175 cm^{-1} shifting to 2173 cm^{-1} with coverage, much more intense than in the previous figure. Also, a substantial band at 2229 cm^{-1} is seen. Both these bands, also visible in spectra taken at room temperature (see below), correspond to CO adsorbed on Lewis sites of different strength, present in several Al-containing systems, such as zeolites [66] and transition aluminas [67]. The band at 2173 cm^{-1} has, therefore, a composite nature. It is due, on the one hand, to Brønsted-type acidic species, the nature of which is still to be determined, and, on the other hand, to weak Lewis acid developed upon thermal treatment. Its increase from the preceding figure to the present one does not correspond to a parallel increase in the intensity of the 3450 cm^{-1} band envelope. It is common knowledge that a frequency of 2173 cm^{-1} is a borderline for CO adsorbed on weak Lewis or H-bonded to strong Brønsted sites.

Brønsted acidity of this H-[Al]-MCM-41 sample is presumably related to these "new" bands absorbing between 3500 and 3400 cm^{-1}. Most probably, no (or negligible) bridging Si(OH)Al species are present. If these were the "hidden" Brønsted sites, the absorption band would occur after adsorption at ca. 3300 cm^{-1}, which is not the case. Other Brønsted species, different from bridging Si(OH)Al species, have to be invoked, in line with the NMR evidence.

Spectra concerning CO adsorption on H-[Al]-MCM-41 were published by Pasqua et al. [68, 69]. Detailed studies on non-porous silica-alumina [70] and H-[Al]-MCM-41 systems [71] have been also reported by Lavalley and co-workers. Both groups of workers found results very similar to those in Figs. 8 and 9, and report in particular the presence of bands at ca. 3400 and 3460 cm^{-1} without any counterpart in the O – H stretching region.

No definite assignment of these two bands was made. Lavalley and co-workers, however, report a correlation between the frequency of CO interacting with a Brønsted center and the shift suffered by the related O – H stretch, which helps in proposing an interpretation for the "hidden" species [70]. From this correlation, it results that the corresponding CO frequency of 2173 cm^{-1} would imply a shift of ca. 200 cm^{-1}. This means that the O – H stretch of the acidic hydroxyls before interaction with CO would fall, roughly speaking, around 3680 and 3620 cm^{-1}, respectively.

The literature on zeolites reports that CO interacting with a Brønsted site originating in zeolites upon dealumination, and characterized by an O – H mode at 3660 cm^{-1}, absorbs at 2173 cm^{-1} [72], while the O – H stretch undergoes a bathochromic shift of ca. 200 cm^{-1}, i.e., shows very close features. A schematic structure of this acidic center, consisting in an aluminol AlOH species grafted to the silica network, is depicted in Scheme 3.

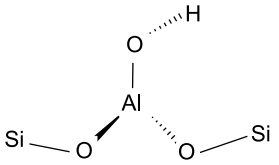

Scheme 3 Tentative structure for of acidic AlOH species, as found in zeolites undergoing dealumination. This species is referred to in the text as AlOH(II). After [51, 52]

A band at 3660 cm^{-1} has also been observed by Jentys et al. [73] on [Al]-MCM-41 systems with a reasonably high Al content, with similar features: the assignment was in this case to OH species on extra-framework debris. It is, therefore, tempting to attribute the absorption at 3485 cm^{-1} to species like that depicted in Scheme 3, or to similar species.

No absorption is, however, clearly visible at 3660 cm^{-1}. Observation of any negative bands in this range is rendered difficult by the growth of the band due to perturbed Sil species. The growth of the two bands at 3485 and 3420 cm^{-1} and that due to perturbed silanols occur, however, at rather different CO pressures, so that it would seem possible to discriminate the two processes of decrease in intensity and successive growth. A possible reason for the "invisibility" of the corresponding band is the same as proposed for the bridging hydroxyls, namely the amorphous nature of the solid and the flexibility of the Si – O – Si bond causing the smearing-out of the related absorption. This species, described by Scheme 3, is designated in Table 1 as AlOH(II).

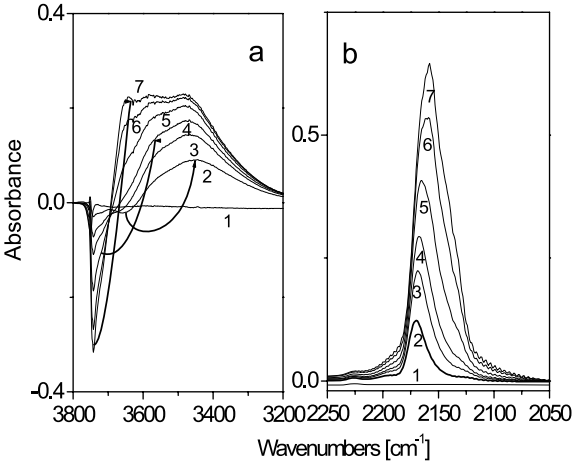

Fig. 10 Difference IR spectra concerning the adsorption of CO at the nominal temperature of 77 K on an Al-rich H-[Al]-MCM-41(2.5) outgassed at 573 K. Equilibrium pressures: 0.005 (curve 1); 0.46 (2); 0.77 (3); 2.0 (4); 4.8 (5); 7.7 (6); 12.0 (7) mbar. **a** O – H stretching region; **b** CO stretching region

As to the species involved in the band at 3420 cm^{-1}, it is proposed in Sect. 4 below that it is related to water molecules sitting on strong Lewis sites.

Data similar to those in Fig. 9 have been reported for an H-[Al]-MTS sample with a higher Al content (Si/Al = 2.5). Figure 10 shows the difference spectra of CO adsorbed on the sample after outgassing at 573 K. In the O – H stretching region, at least three types of hydroxyls are seen as negative bands, at 3660, 3715 and 3747 cm^{-1}, which upon interaction give rise to broad absorptions centered at 3440, 3570, and 3650 cm^{-1}, respectively.

The species absorbing at 3747 cm^{-1} when free, and at 3650 cm^{-1} when interacting with CO is again a more or less isolated silanol. That at 3720 cm^{-1} when free and at 3570 cm^{-1} when H-bonded to CO, is probably a poorly acidic AlOH species, the shift being only 145 cm^{-1}, presumably similar to that invoked by Jentys et al. [46], and referred to in Table 1 as AlOH(I). The band growing at 3440 cm^{-1} and paired to that at 3660 cm^{-1}, seems to correspond to the acidic AlOH species like the one in Scheme 3, because the shift is substantial (220 cm^{-1}) and presumably corresponds to the species AlOH(II).

3.3.4 Lewis Sites: Evidence Provided by CO Adsorption; Conversion into Brønsted Sites

Figure 11 shows the IR spectra [22] concerning the interaction of CO at the nominal temperature of 77 K with H-[Al]-MCM-41(2.5), after outgassing at 573 and 873 K. Basically, three bands are seen, viz. at 2173, 2200 and 2230 cm^{-1}, designated as site W (weak), I (intermediate) and S (strong), be-

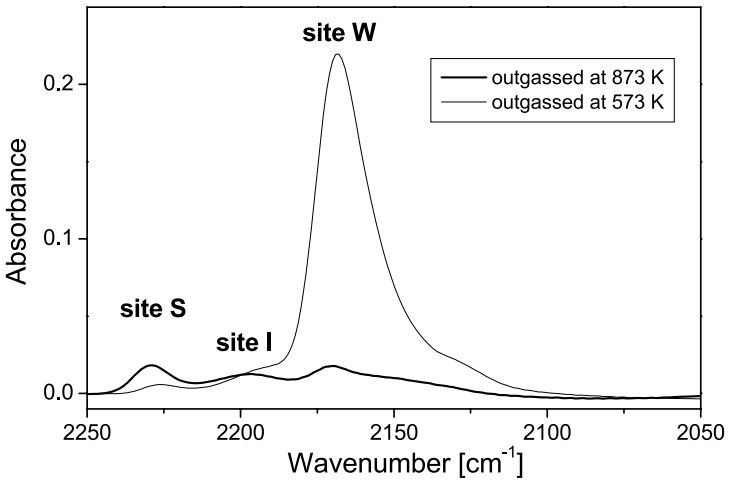

Fig. 11 IR spectra in the CO stretching region concerning the interaction of 0.5 mbar of CO at the nominal temperature of 77 K with H-[Al]-MCM-41 (2.5). After [22]

cause such is the order of interaction strength suggested by the pressure dependence, not reported here.

Increase in the outgassing temperature converts site W into site S. All three sites are related to coordinately unsaturated Al ions. In Al-poor samples, site I is sometimes missing, whereas the other two are invariably present for substantial temperatures of outgassing. On mesoporous alumina, site I predominates and decreases when passing to aluminosilicates, with concomitant increase of site W and S [53]. The related frequencies may be compared with those concerning CO on transition aluminas [67]: site S, e.g.,, is close in nature to the strongest site in transition aluminas characterized by a CO stretching at 2240 cm^{-1}.

Dosage of water on these Lewis sites may convert them into Brønsted sites. This was shown long ago for ASA by Kazansky [74]. The equivalent experiment for mesoporous systems is reported in Fig. 12, which concerns an H-[Al]-MCM-41(13) outgassed at 1073 K [51, 52].

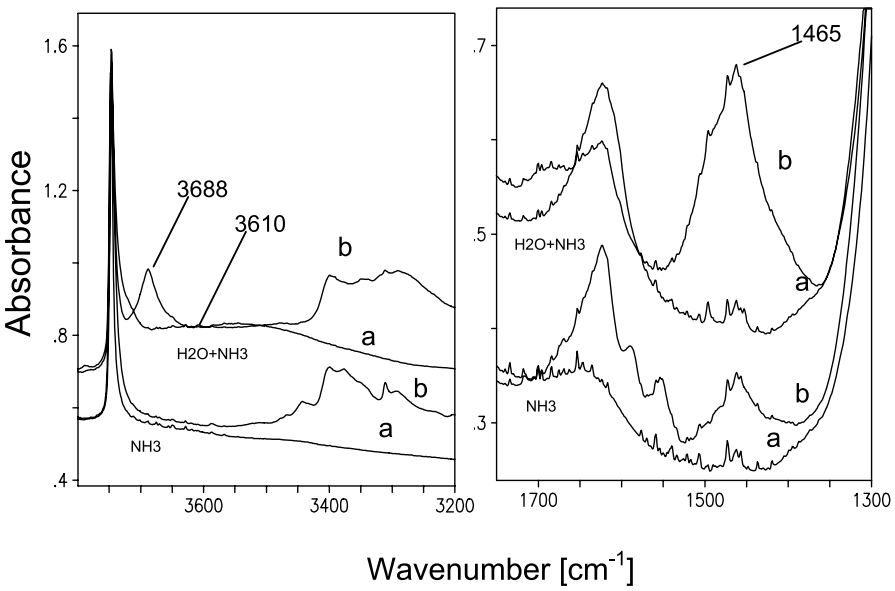

Fig. 12 IR spectra illustrating the conversion of Lewis into Brønsted sites by adsorption of small doses of water (ca. 0.05 mbar). *Left*: OH stretching region; *right*: ammonia deformation region. *Lower spectra*: bare sample as such (spectrum a) and after ammonia adsorption (spectrum b). *Upper spectra*: after chemisorption of a small dose of water (spectrum a) and successive adsorption of ammonia (spectrum b). Sample was H-[Al]-MCM-41(13) outgassed at 1073 K. After [51, 52]

Adsorption of small amounts of water brings about the formation of weak bands at 3685 and 3610 cm^{-1}, which are not due to the same entity, because their intensity ratio varies with different samples. One possibility is that

two different O – H species are formed. Alternatively, it is possible that the 3610 cm^{-1} band is one mode of molecular water, and that the other one, expected around 3690 cm^{-1}, is hidden by the band of clustered water molecules. A frequency of 3680–3690 cm^{-1} may, unfortunately, be due to several species, so that its presence alone is not so meaningful. Whatever the nature of the involved species, successive contact with ammonia shows the formation of ammonium species, i.e., these Brønsted species coming from Lewis sites are acidic enough to transfer a proton to ammonia.

3.4 Catalytic Evidence

H-[Al]-MCM-41 materials have been used as catalysts for the conversion of a large variety of substrates in reactions as diverse as hydrocarbon cracking, hydrocracking and hydroisomerisation, olefin polymerisation, oligomerization and isomerization, Friedel–Crafts aromatic and phenol alkylations and acylations, acetalyzations, Beckmann rearrangements, glycosidation, aldol condensations, polyethylene and polypropylene cracking, Prins condensation. Several reviews have appeared on the subject [75–81].

Analysis of the catalytic results with the objective of comparing the efficiency – and ultimately the nature – of the acid sites of MCM-41s and zeolites is however not straightforward. The reactions investigated over mesostructured aluminosilicates involve generally bulky reactants and/or products or hindered transition states, that cannot be accommodated – or at least under very constrained configurations – inside the micropores of zeolites. In addition, catalyst deactivation by fouling often prevents to draw reliable conclusions on the impact of acidity on activity. Moreover, the nature of the acid sites involved – Lewis or Brønsted – as well as their evolution in the course of the reactions, in the presence of polar reactants and products for instance, are not always well established.

Catalytic cracking and hydrocracking of *n*-alkanes are among the reactions which could overcome some of the above drawbacks, at least with respect to the diffusion constraints imposed to reactants and products. Nevertheless, conflicting conclusions regarding the relative activity of apparently similar materials are commonly attained. Some typical studies, where the catalytic activity of MCM-41 has been compared under strictly identical experimental conditions to that of zeolites, are briefly analyzed below to highlight the above statements.

3.4.1 Cracking of Hydrocarbons

In line with the moderate Brønsted acidity revealed by ammonia and pyridine TPD, Corma et al. [82] reported a much lower activity of MCM-41(Si/Al

= 14, Na_2O = 0.2 wt %) and ASA than USY (Si/Al = 100, Na_2O = 0.03 wt %) for the cracking of *n*-heptane. For this demanding reaction catalyzed by strong acid sites, the authors reported specific first-order rate constants in the range 1 : 4 : 140 for MCM-41, ASA and USY, respectively, at 450 °C. However, in the case of gas oil cracking at 500 °C, increased accessibility to the active centers compensates for the lower intrinsic cracking activity of MCM-41 (with an observed specific activity sequence of 1 : 0.6 : 10 for MCM-41, ASA and USY, respectively), an advantage which is lost after steaming due to the collapse of the mesoporous structure.

A rather different picture of the hydrocarbon cracking activity of MCM-41s is provided by the contributions of the group of Reschetilowski [83–86]. These authors compared the cracking activity of H-forms of MCM-41s (Si/Al = 3 and 17, exchanged three times with NH_4NO_3 solution) and H-Y (Si/Al = 2.6, no analysis for Na given) using *n*-hexadecane and 1,3,5-triisopropylbenzene as reactants at 482 °C in a MAT apparatus (ASTM D-3907). In the cracking of *n*-hexadecane, the results point to a good stability of the MCM-41 catalysts upon repeated reaction-regeneration cycles and to an activity equivalent to that of H-Y. The activity was found higher than that of model and commercial zeolite-Y based cracking catalysts for the transformation of 1,3,5-triisopropylbenzene, where restricted diffusion probably occurs in the case of zeolites. In terms of specific activity, the sites of MCM-41 are therefore 5 to 10 times more efficient than those of H-Y for *n*-alkane cracking.

3.4.2 Alkane Hydroconversion

In order to overcome the limitation associated with the insufficient hydrothermal stability of MCM-41-type materials for catalytic cracking applications, bi-functional catalysts, were a hydro/dehydrogenation metal function is combined to the acidic one, have been prepared. With these systems, isomerization and cracking of alkanes proceeds via the protonation of the olefins formed on the metallic function. Provided that the metal and acid functions are well balanced, the rate limiting step is the rearrangement of the intermediate carbenium ions. With respect to alkane cracking, the reaction is less demanding in terms of acid strength. Over ideal bi-functional catalysts, the activity and selectivity are expected to be determined by both the strength and density of the Brønsted sites of the catalyst.

Figures 13 and 14 are taken from the work of Park and Ihm [87], who investigated the hydroconversion of *n*-hexadecane over a series of Pt/zeolites and zeotypes and a Pt/Al-MCM-41 material in a batch reactor at 350 °C under 103 bar of hydrogen.

The highest activity was observed for catalysts Pt/ZSM-5, Pt/H-β and Pt/ZSM-22, characterized by well-defined high-temperature desorption peaks in the ammonia TPD spectra. Over these catalysts the selectivity at ca. 40%

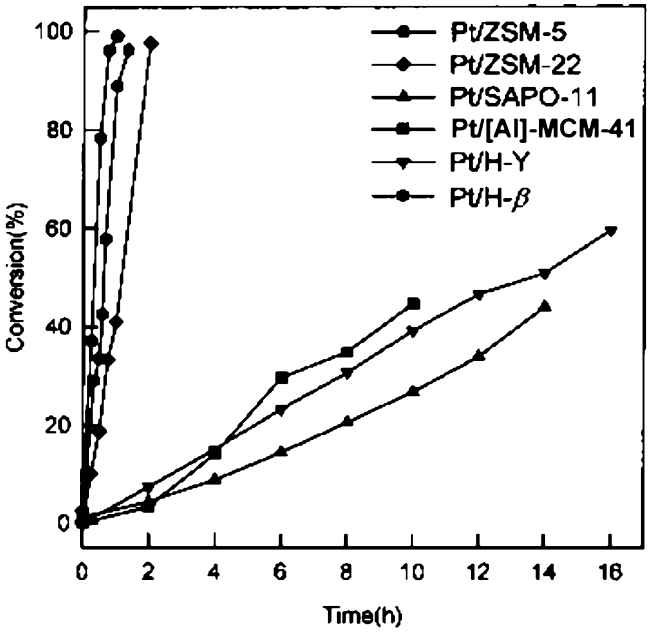

Fig. 13 Catalytic data concerning the hydroconversion of *n*-hexadecane over a series of Pt/zeolites and zeotypes and a Pt/[Al]-MCM-41 material. After [87]

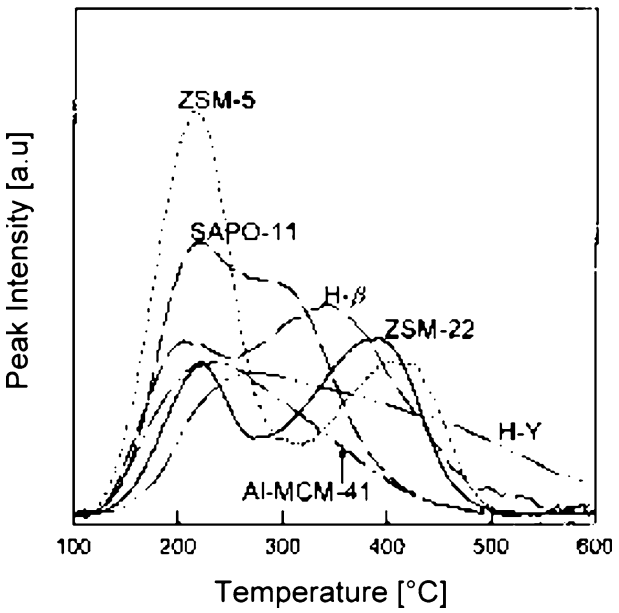

Fig. 14 Ammonia TPD data concerning the samples, Fig. 13 refers to. After [87]

conversion was mostly directed towards hydrocracking products. Pt/SAPO-11 showed low activity, in line with the presence of weaker acid sites. Of particular interest is the comparison of the data obtained over Pt/ H-Y (Si/Al = 2.5) and Pt/[Al]-MCM-41 (Si/Al = 20, pore diameter = 2.6 nm). Both catalysts are highly selective towards hydroisomerization (> 76%), but in spite of the higher density of strong acid sites over the zeolite, the MCM-41 catalysts demonstrated equivalent activity, suggesting higher turn-over frequencies for the acid centers of MCM-41.

In a related study performed in Montpellier [88], *n*-hexadecane hydroconversion was investigated in a series of large-pore zeolites (USY, EMT, EMO, mixed EMT/EMO structures and Beta) and MCM-41 loaded with Pt, using a fixed-bed, down-flow, trickle-bed reactor at 280–300 °C under 20 bar of hydrogen. The acidity of the catalysts was characterized by ammonia microcalorimetry and TPD and infrared spectroscopy of adsorbed pyridine and acetonitrile. Under these conditions, the catalysts proved very selective towards hydroisomerization and the activity was a single function of the total number of acid sites determined by ammonia TPD. The unique correlation existing between the number of sites and the activity, shown in Fig. 15, as well as the plot of the integral heats of ammonia adsorption versus amount adsorbed at low coverage (Fig. 16) suggest that the same type of site operates over the whole solids.

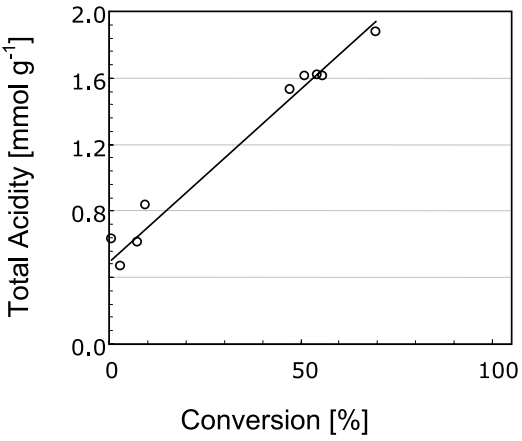

Fig. 15 Catalytic data concerning *n*-hexadecane hydroconversion at 280 °C over large pore zeolites (USY, EMT, EMO, mixed EMT/EMO structures and Beta) and MCM-41 loaded with Pt: correlation between the number of sites and activity. After [88]

The examples presented above demonstrate that acid sites in MCM-41s can be as effective as those of zeolites for hydrocarbon transformations. However, they cannot enable firm conclusions to be drawn regarding their nature and strength, nor to establish the proportion of sites actually involved in the

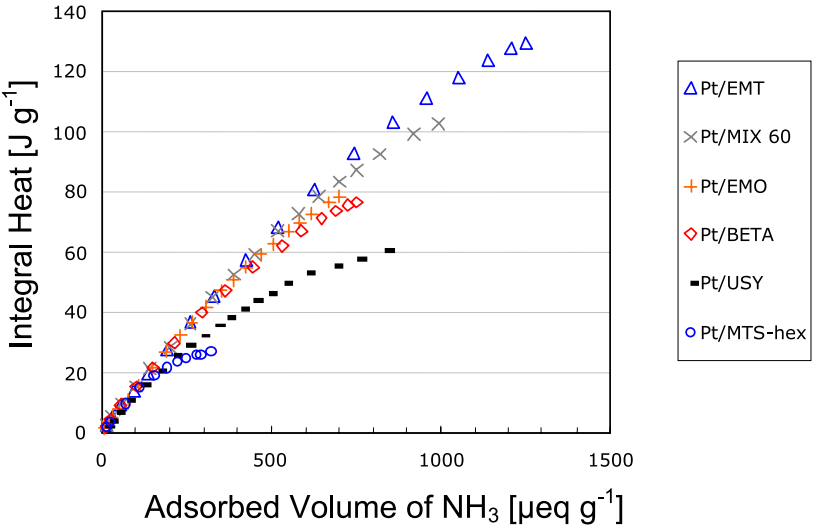

Fig. 16 Integral heats of ammonia adsorption at 150 °C as a function of coverage for the same samples as in the Fig. 15

carbenium-ion chain-reaction process. In that respect catalytic activity cannot serve as acidity diagnostic. The same is true when analyzing catalytic data involving less demanding (in terms of acid strength) reactions. In such cases an additional difficulty arises to discriminate between the contributions of the extensive and intensive factors of the acidity to the catalytic activity. The presence of spectator sites and sites inactive for the target reaction but contributing possibly to deactivation (a general problem in heterogeneous catalysis), adds to the complexity.

3.5 Models for the Acidic Sites of H-Al-MTS (Brønsted and Lewis)

3.5.1 Literature Models for the Brønsted Acidic Sites

Literature results gathered so far provide evidence for a different acidity in silica-aluminas compared to H-zeolites, in agreement with NMR evidence, and for a more complex behavior, highlighted by catalytic results. In particular, as far as it concerns the Brønsted active site, the expected bridging hydroxyl species Si(OH)Al are not observed in the IR spectra.

There are two lines of thoughts in the literature. One invokes nonetheless the presence of the Si(OH)Al species and reasons for its "invisibility" as well as for the decrease in acidity are sought, the other makes the assumption that acidic species different from Si(OH)Al are actually involved.

In the former case, the disordered structure of MTS is assumed to account for both a loss in acidity with respect to protonic zeolites and the absence of IR bands due to Si(OH)Al species. Indeed, in proton-transfer reactions electric fields exerted by the surroundings are vital in stabilizing the ionic species formed. Electric fields at the surface of MTS are most probably less intense than those within zeolites, since at a surface a part of the solid is missing, and a contribution to electric fields is lacking. A further reason, however, could result again from the disordered structure of MTS. This probably means a less ionic system, because ionicity is fully displayed only in ordered crystalline systems. Destabilization of the ionic pair is equivalent to a less marked acidity.

As already quoted, disorder in the structure, due to the flexibility of T – O – T bonds, may cause heterogeneity in the environment of the Si(OH)Al group, bringing about a range of interactions with the surroundings, which causes the smearing-out of the expected Si(OH)Al band.

Spectroscopic IR evidence seems, however, to rule out this interpretation. Were bridging Si(OH)Al sites present, one would expect that, upon interaction with CO, the same bands would be formed as with free bridging species, e.g., that due to the O – H vibration at ca. 3300 cm^{-1}. This is not the case, with the probable exception of the aluminosilicate samples considered by Datka and co-workers [53]. Distinct though broad bands are seen at different locations.

Many proposals have been put forward concerning structures of Brønsted sites differing from the zeolitic Si(OH)Al bridged species. Liepold et al. [83] attributed the high activity of MCM-41 to strongly acidic protons generated by an electron-attracting effect of Lewis acid centers on neighboring Si-OH groups.

A very same description for the acid sites in H-[Al]-MCM-41s has been proposed in more recent works by Savidha et al. [89] and Eswaramoorthi et al. [90]. Such a model for the generation of active acid sites is therefore similar to that anticipated by Uytterhoeven [91] and refined by Mortier [92] to describe the acidity of traditional amorphous silica-aluminas.

Following the same line as Liepold et al., Trombetta et al. [55] and Busca et al. [60] proposed that Brønsted acidic centers of silica-alumina are due to terminal silanols which are somehow modified by neighboring Al cations.

These authors assume that rigidity of the zeolite framework is vital in stabilizing the bridging Si(OH)Al species, and propose that with the flexible MTS structure the bridging of the silanol over a nearest Al ion does not occur, and an open structure is given rise (Scheme 4a). When a base molecule is present, represented as a ligand L in the Scheme, the oxygen atom is assumed to bridge over the nearest Al ions because of the polarization in the O – H bond, and acidic behavior is displayed.

Based on proton NMR data, Heeribout et al. [93] proposed a mechanism for the formation-depletion of Brønsted acid sites in silica-aluminas

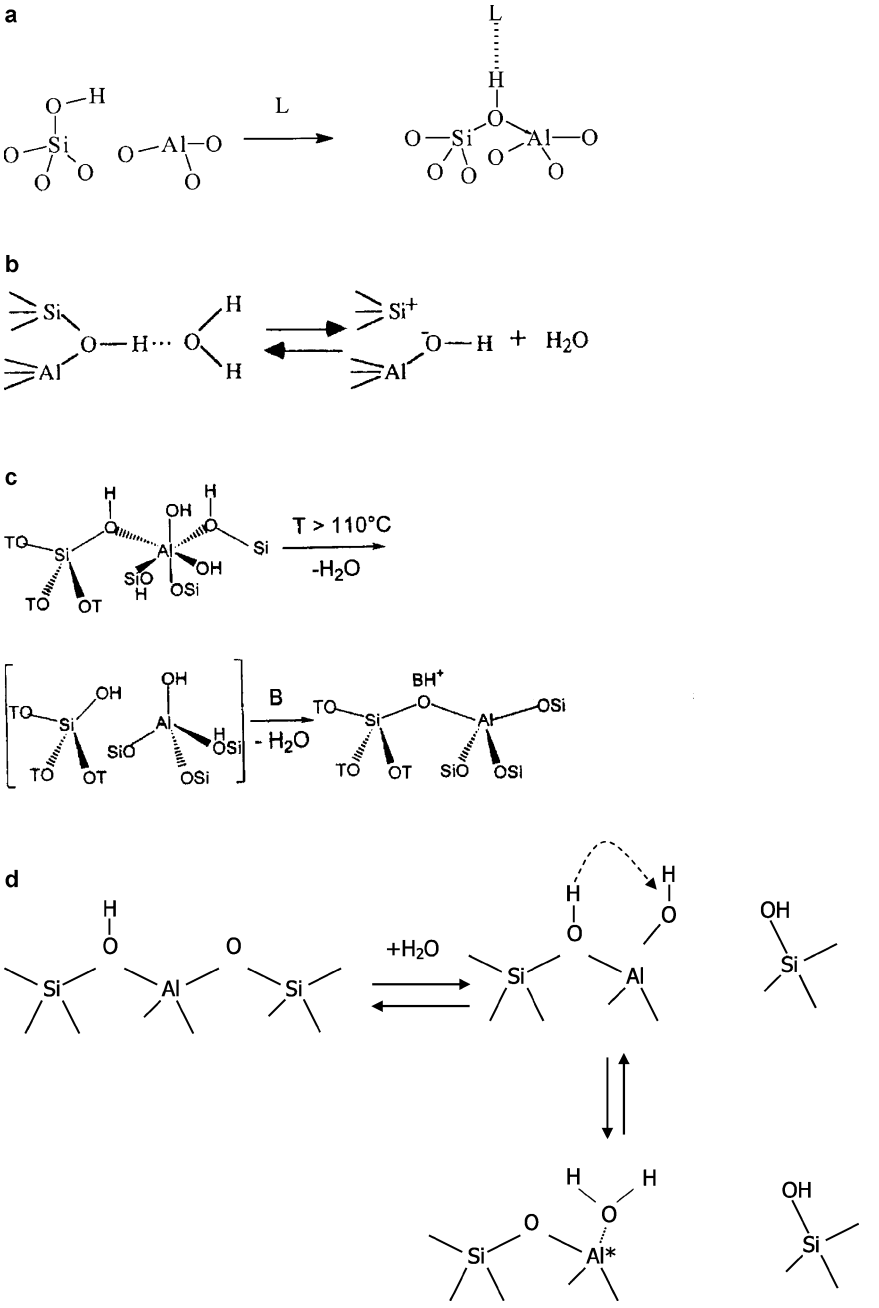

Scheme 4 **a** Structure of acidic centers according to Trombetta and Busca. After [60]. **b** Structure of acidic centers according to Heeribout et al. After [41]. **c** Structure of acidic centers according to Omegna et al. After [42]. **d** Structure of the acidic centers according to Busco and Ugliengo. After [94] (Ugliengo P, personal communication)

by adsorption-desorption of water (Scheme 4b). In this model, bridging Si(OH)Al groups exist only in the presence of some water, giving rise to hydroxonium ions. When water is desorbed, the bridge opens giving rise to Al-OH species, irrespective of the unlikely generation of an unsaturated silicon atom.

As reported above, an AlOH group may be proposed as a model for the acidic species in H-[Al]-MTS, similar to that observed in zeolites undergoing dealumination [72], which usually absorbs at ca. 3660 cm^{-1}. The reason why such a band is not visible in the IR spectra is the same as proposed for the Si(OH)Al species, i.e., heterogeneous interaction with the surroundings. As shown above, this species undergoes a shift with CO of about 200 cm^{-1}, and therefore, the perturbed OH stretch corresponding to this "invisible" species is that at ca. 3450 cm^{-1} observed in the above figure.

Recently, Busco and Ugliengo [94] (Ugliengo P, personal communication) addressed this problem on the base of computational methods. These authors showed that, in a non-zeolitic structure, the bridging OH site is unstable with respect to protonation of a nearby OH group bonded to an Al^{3+} ion, thus yielding a water molecule tightly bound to the Lewis site. The mechanism of generating the non-bridging Brønsted site is shown in Scheme 4d.

3.5.2
Discussion of the Models for Brønsted Acidity

The model by Trombetta and Busca (vide supra) is probably to be discarded. In the first instance, Fig. 6 provides evidence that, at least in some cases, silanols on H-[Al]-MTS systems are not more acidic than on other silica systems. Moreover, the model shows inconsistencies from the energetic point of view. The interaction between the isolated silanol and the Al center is assumed to be repulsive. This is reminiscent of the case of boron-zeolites [95], in which the tetrahedral heteroatom is boron, having a definite propensity towards trigonal coordination. Indeed, interaction with the base molecule makes the boron atom to assume tetrahedral coordination. This is hardly acceptable for Al, which favors either tetrahedral or octahedral coordination and assumes trigonal coordination only exceptionally.

The proposed repulsive interaction between SiOH and the Al atom, as in Scheme 3a, is supposed to be overcome through the action of a base which forces the silanol and the Al atom to interact. Such a mechanism should only work for strong interactions, capable of overcoming the unfavorable energetic feature. We have seen, instead, that even weak interaction like the low-temperature adsorption of CO brings about the formation of SiOH/CO adducts, the O – H stretch of which vibrates at 3450 cm^{-1}. This low frequency is indicative of a good acidic behavior of the related hydroxyls, but implies a reversible and weak interaction from the energetic point of view.

Evidence based on CO adsorption strongly suggests that more than one acidic species may be at the surface of MTS. Two AlOH species, one weak, AlOH(I), and a stronger one AlOH(II) have been already proposed. In Sect. 4 below, experimental evidence is provided that molecular water sitting on strongly polarizing Al species probably are another source of acidity, also occurring at the surface.

3.5.3
Models for Lewis Sites

Up to three different CO bands are seen in Figs. 9 and 11 at ca. 2230, 2200 and 2173 cm^{-1}, which in the present chapter are referred to as site S (strong), I (intermediate) and W (weak), respectively. The information provided by the CO frequency concerns the electric field at the different Al sites. Scheme 5 illustrates two possible situations for sites S and W. Reasons for assuming that they are due to Al species still grafted to the silica network, will be given below. Site I, present on Al-rich systems only and also occurring on aluminas, is probably due to extra-framework Al species.

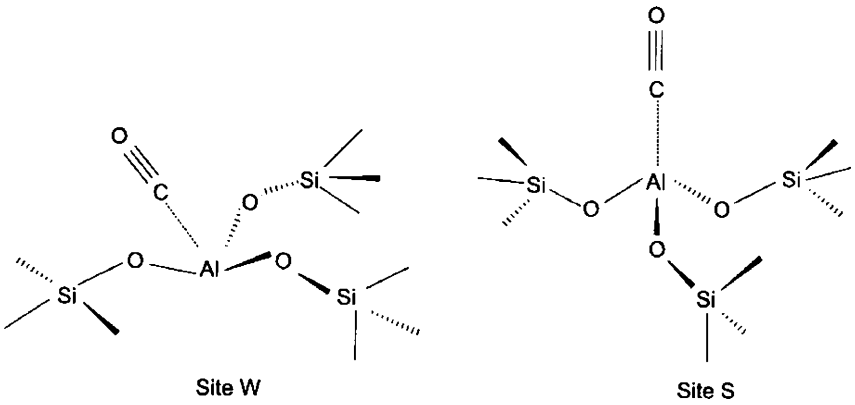

Scheme 5 Models for two Lewis sites on [Al]-MTS, grafted to the silica framework, with different acidity. After [51, 52]

3.6
Comparison with Similar Systems

3.6.1
Outer Surfaces of Zeolites

The external surface of protonic zeolites can play a role in acid catalysis, e.g., in alkylaromatics conversions over H-MFI [96], because H-zeolites pro-

mote the reaction of molecules unable to enter the cavities due to their size. The question arises whether the active sites are qualitatively the same bridged species as within the interior, once the possible difference in the Si/Al ratio between the surface and the bulk is taken into account [97]. Corma et al. [98] reported data on the accessibility of protonic sites of different zeolites to 2,6-di-tert-butyl-pyridine, considered to be "selective" for Brønsted sites and not able to interact with Lewis sites for steric hindrance. Busca and coworkers [99, 100] as well as Otero Areán et al. [101] have investigated the external surfaces of H-FER and H-MFI by spectroscopy of adsorbed sterically hindered nitriles, e.g., adamantane-carbonitrile or diphenylpropionitrile.

The situation seems to show many similarities with the case of zeolites/H-[Al]-MTS systems. Terminal silanols and Lewis acid sites have been identified at the external surface of the zeolites. Very strongly acidic, bridged hydroxyls, however, are only located in the interior.

Onida et al. recently investigated the acidity of samples of ITQ-2 produced by exfoliation of the MCM-22 zeolite, which in principle is an "all surface" zeolite [102]. Upon exfoliation, the band due to bridging Si(OH)Al species decreases strongly in intensity, while the band due to terminal silanols strongly increases. This seems to indicate, that bridging Si(OH)Al species cannot survive the destabilization brought about by the disappearance of the large zeolitic cavity of MCM-22. Acidity still survives, as evidence was given about the existence on the surface of sites with acidity intermediate between silanols and bridging Si(OH)Al species, but not directly detectable in IR spectra [103, 104].

As it concerns Lewis acidity, adsorption of hindered nitriles reveals the presence of such sites at the external surface of H-FER, H-MFI and H-MOR, after outgassing at 673–773 K. Recently, van Bokhoven et al. showed that in these conditions tri-coordinated Al species can be detected by in-situ XANES at the Al-K-edge on H-MOR and H-BEA [105]. These species were proposed to be at framework positions, though it is not possible to determine whether of the internal or external surface.

The overall situation resembles closely that of H-[Al]-MTS, and similar proposals have been made for both H-[Al]-MTS and the external surface of protonic zeolites. For instance, the suggestion has been made that acidic sites at the external surface of protonic zeolites are spectroscopically indistinguishable from terminal silanols [100]. At least for the case of ITQ-2, this hypothesis is disproved in a similar way as done with H-[Al]-MTS, i.e., reversible interaction of ammonia with silanols and the study of the related isotherms show a marginal difference in acidity between silanols in ITQ-2 and pure silica MCM-41 [103, 104]. Onida et al. proposed as acidic centers the AlOH(II) species also for H-[Al]-MTS, absorbing at 3660 cm^{-1} when free, and advanced the same reason for its "invisibility" (interaction with the surroundings).

In conclusion, the external surface of protonic zeolites bears many resemblances with that of silica-alumina. This is because at the external surface of zeolites the rigid nature of the crystalline structure is relaxed, causing instability of the bridging sites.

3.6.2 Dealuminated Zeolites

Without pretension of entering a fairly complicated field, we only wish to report here some evidence that the Brønsted species identified above may occur as well when the regular framework of a zeolitic system is lost not because an external surface is developed (like in Sect. 3.6.1) but because of dealumination, forming internal surfaces, where similar processes may take place. A recent paper by Guisnet and coworkers [106] ascribes: "... the band at 3607 cm^{-1} to bridging O – H groups, that at 3660 cm^{-1} to monomeric and polymeric EFAL species, that at 3680 cm^{-1} to hydroxylated EFAL clusters ...". As already discussed, we prefer to assign the 3660 cm^{-1} band to an AlOH species still attached to the silica framework. Similarities are, however, evident.

Recent work on the low temperature adsorption of CO on a dealuminated mordenite (Bonelli B, Cavani F, Garrone E, unpublished results) has shown a similar situation. Besides expected features, a broad band appears at ca. 3400 cm^{-1}, to which does not correspond any decrease in absorption (negative band).

4 Development of Acidity upon Cation Substitution

Meziani et al. [36] performed calorimetric and volumetric measurements of ammonia adsorption over a series of MCM-41s with varying aluminum contents (Si/Al 8-32) and pore sizes (pore diameter 1.8–2.7 nm) prepared in alkaline media from tetramethylammonium silicate (ex sodium silicate) and aluminum isopropoxide as sources of Si and Al, respectively.

After calcination at 550 °C to decompose the occluded surfactants, the amount of ammonia irreversibly adsorbed leads to a density of acidic sites in the range between 0.04 and 0.09 $\mu mol\ m^{-2}$ corresponding to at most 18–25% of the total surface occupied by the adsorbing basic probe. The acid sites adsorb ammonia with a heat equal to 60–75 kJ mol^{-1}, characteristic of a weak to moderate strength. However, removal of the residual sodium ions by repeated treatments of the samples with ammonium nitrate followed by calcinations at 450 °C led to the formation of octahedrally coordinated aluminum and to a three fold increase of the number of acidic sites with a dramatic increase of their strength, as illustrated in Fig. 17. Infrared spectroscopy of pyridine

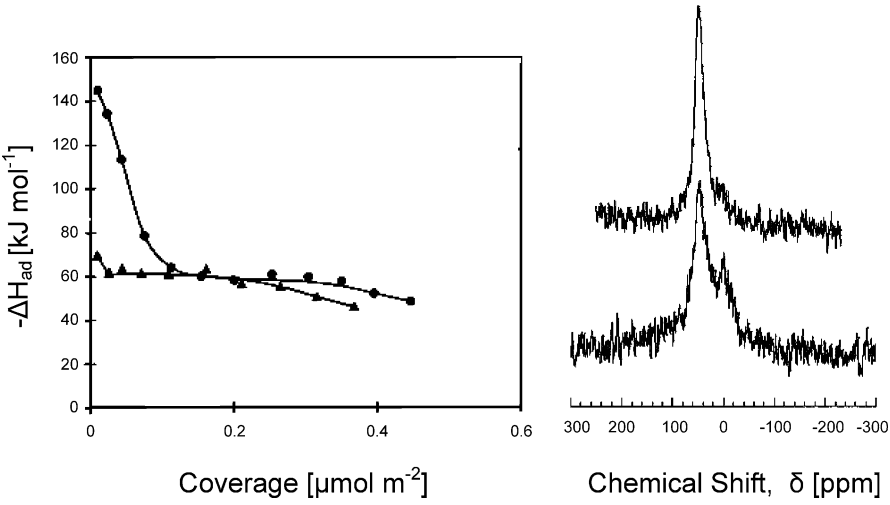

Fig. 17 Development of acidity upon substitution of protons for Na cations. **a** differential heats of adsorption of ammonia on the as-synthesized, Na-rich sample (i) (*triangles*) and on the H-substituted sample (ii) (*dots*); **b** ^{27}Al MAS-NMR spectra of the two specimens. After [36]

adsorption shows that these new strong sites are of Brønsted and Lewis type, with the latter being the strongest.

Though the amount of sodium ions removed by the exchange process is not given, it seems apparent that the phenomena observed and the extent of the changes induced are very similar to those reported in the case of zeolites [107, 108], where residual cations exert a double influence on Brønsted and Lewis acidity.

The arguments developed in the case of zeolites can be summarized as follows. Firstly, sodium ions may provide stabilization to Si – O – Al bridges in T_d configuration (by imposing larger T – O – T bond angles) at the surface or within the pore walls. The distortions generated by the replacement of Na^+ by H^+ and/or the dehydroxylation of the newly formed SiOHAl unit promotes dealumination and migration of electron deficient species to the surface, generating strong Lewis sites. Secondly, the removal of residual Na^+ not only generates much stronger Brønsted sites, but also results in an overall increase of the strength of the existing ones. This effect originates from a cooperative long range re-arrangement of the bond structure of the tri-dimensional lattice spreading over a large number of T–O–T linkages.

The question arises whether these considerations may apply to MTS materials. However the answer cannot be given yet. The dramatic enhancement of the overall acidity upon removal of trace amounts of sodium counterions, revealed by the above study, could nevertheless provide a clarification to the conflicting conclusions reached in some catalytic studies (Sect. 3.4)

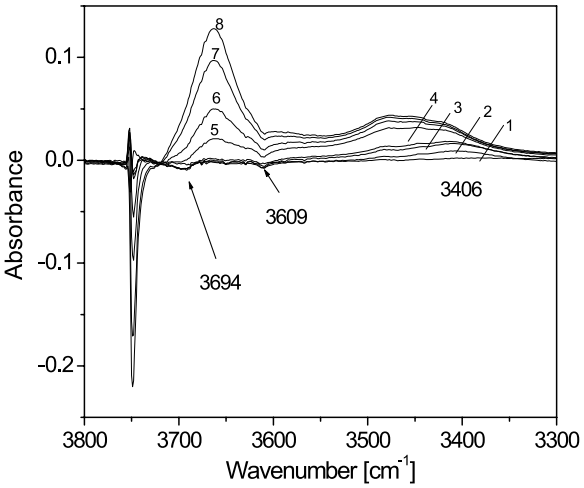

Fig. 18 Difference IR spectra in the O – H stretching region concerning the adsorption of CO at a nominal temperature of 77 K on the sample Fig. 3 refers to, Na-[Al]-MCM-41(20). Equilibrium pressures: 0.05 (curve 1); 0.1 (2); 0.2 (3); 0.5 (4); 1.9 (5); 3.2 (6); 8.0 (7); 12.0 (8) mbar. After [110]

The acidic properties of partially substituted Na(H)-[Al]-MCM-41 samples, to which Fig. 3 refers, have been studied by adsorption of CO at nominal 77 K [109]. The corresponding spectra are reported in Fig. 18 as difference spectra.

Sil species are observed to undergo the expected shift with formation of a band at ca. 3660 cm^{-1}, due to H-bonded species. Other changes in the spectra are most significant instead. The very first doses cause the increase of a band at about 3400 cm^{-1}, which is accompanied by the decrease in intensity at two frequencies, viz. 3694 and 3609 cm^{-1}. The two negative bands are almost equal in intensity, and appear at frequencies typical of water molecules. Moreover, at 1605 cm^{-1} a negative band is seen. This is rather clear evidence that water molecules are acting as reasonably strong acidic sites. To evaluate the related shift in O – H frequency, reference has to be made to the half-sum of the two modes (equal to 3651 cm^{-1}), the uncoupled O – H stretching frequency. The result is 3651 – 3400 = ca.250 cm^{-1}, the highest observed with silica-alumina systems, either amorphous or mesoporous, though yet markedly inferior to the bridging Si(OH)Al site in zeolites.

Because of the substantial presence of Na cations, it remains to be proved that acidic water molecules are those which are, as in the model proposed by Busco and Ugliengo [94] (Ugliengo P, personal communication), coordinated to strongly polarizing Al centers and not to Na cations. Evidence is as follows: i) the involvement of Al is demonstrated by the fact that a similar band at ca. 3400 cm^{-1} was observed on silica-alumina systems in the absence of Na; ii) the acidic properties of water molecules sitting on

Na cations in Na – Y has been measured [109], and the shift in the O – H band caused by CO interaction with the complex Na^+/H_2O does not exceed 100 cm^{-1}.

At higher CO coverages, a band at 3450 cm^{-1} grows, ascribed by us to the AlOH(II) species, which would fall into the range 3660–3680 cm^{-1}, if visible.

It is worth noting that Lavalley and co-workers have observed the same band at ca. 3420 cm^{-1} on amorphous silica-alumina samples without observing any free counterpart, in perfect coincidence with what is reported here concerning H-[Al]-MTS. The spectra in Fig. 18 provide the first example of a connection between a band at 3420–00 cm^{-1} and the acidic behavior of adsorbed water molecules on exposed Al cations, thus providing support to the model proposed by Busco and Ugliengo (cf. ref [94]; Ugliengo P, personal communication). That water molecules strongly polarized by an Al cation may act as a source of Brønsted acidity is a common assumption in surface chemistry of clays [110].

Samples with a high Al content (Si/Al = 2.5) and exchanged with Li and Na cations, the potential basic properties of which have been described in Sect. 2, have been also studied as far as their acidic behavior is concerned. The overall compositions were $H_{0.17}Li_{0.12}Al_{0.29}Si_{0.71}O_2$ and $H_{0.05}Na_{0.24}Al_{0.29}Si_{0.71}O_2$. Because of the extensive substitution, the Na-samples provide less evident results. Figure 19 therefore illustrates the adsorption of CO at nominal 77 K on the Li-samples in the O – H stretching region. Besides the expected bands due to Sil species, low-lying bands are seen.

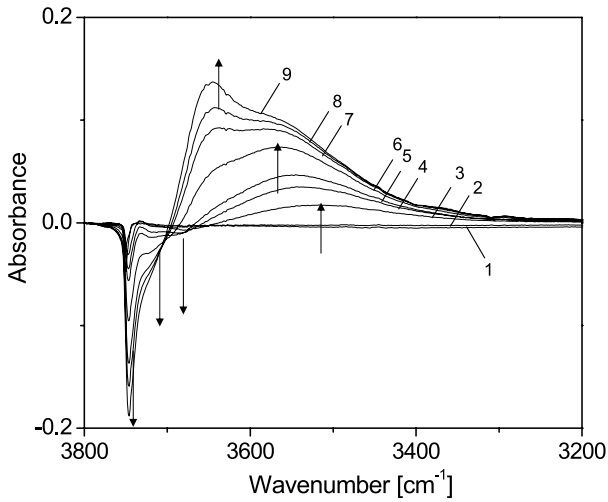

Fig. 19 Difference IR spectra in the O – H stretching region concerning the adsorption of CO at a nominal temperature of 77 K on the sample $H_{0.17}Li_{0.12}Al_{0.29}Si_{0.71}O_2$. Equilibrium pressures: 0.001 (curve 1); 0.14 (2); 0.46 (3); 0.77 (4); 2.0 (5); 4.8 (6); 7.7 (7); 12.0 (8); 19.8 (9) mbar. After [22]

A broad positive band appears at ca. 3500 cm^{-1}, simultaneously with the decrease of a weak band at 3680 cm^{-1}. The growth of the 3500 cm^{-1} band appears to be much more substantial than the corresponding decrease of the partner band. This suggests that only a fraction of the sites giving rise to the 3500 cm^{-1} band do directly appear. The others do not, probably according to the already proposed mechanism of band-smearing out due to the flexibility of the matrix. The species under consideration is close (though perhaps not identical) to species AlOH(II). A component then grows at 3570 cm^{-1}, coupled with the decrease of the band at 3715 cm^{-1}.

This species of moderate acidity (the shift in O – H frequency is only 145 cm^{-1}) is to identify with the species AlOH(I) directly visible in the spectra.

5 Considerations About Acidity/Basicity

In our opinion, Table 1 gathers the available evidence on the types of acidic centers at the surface of H-[Al]-MTS.

There is no evidence of the presence of bridging Si(OH)Al sites. Two weakly acid sites consist of isolated silanol groups (Sil) and pairs of mutually H-bonded silanols (Dim-Sil). In the infrared spectra they give rise to ν(OH) vibrations at 3747 and 3720 cm^{-1}, which shift to 3650–3660 cm^{-1}, respectively, upon CO adsorption. A weak Brønsted site, AlOH(I), characterized by a ν(OH) vibration at 3715 cm^{-1} and shifted to 3570 cm^{-1} in the presence of CO, has been ascribed to extra-framework debris.

The other three Brønsted sites, hardly detectable in the bare samples, give characteristic (broad, multicomponent) signals centered at 3460 cm^{-1} (AlOH(II)), 3420 cm^{-1} (AlOH(III)) and 3406 cm^{-1} (Al$\cdots$$H_2O$). We propose that these species are all associated with aluminum atoms partially linked to the silica matrix, because in this way they may be subjected to spatial reorganization upon interaction of an adsorbate molecule (even a weak one like CO), and only this fact can provide an explanation for their "invisibility" in the bare samples. Also, no comparable acidity is found with alumina particles [67].

Site AlOH(II) is seen as linked to the surface by two Si-O bonds and would correspond to the species observed in dealuminated zeolites, which usually absorbs at 3660 cm^{-1}, being characterized by a moderate-to-strong acidity. The remaining two Brønsted sites probably are variants of the same entity, a water molecule interacting with exposed lattice Lewis sites, although firm evidence is available only for the latter. These are probably the source of strong acidity (though not as strong as in zeolites) in H-[Al]-MTS, and responsible for the controversial ν(OH) vibration appearing around 3610 cm^{-1}, sometimes mistaken for bridged species like in zeolites. Their structure is also in broad agreement with the structures proposed on the basis of NMR results (Scheme 4).

We are facing the rather puzzling result that, when compared to zeolites of similar composition, [Al]-MTS systems are simultaneously weaker acids and weaker bases. On a pure chemical ground, we expect that to a weaker acidity should correspond a more marked basicity and vice versa, if the alkali-substituted forms are regarded as bases conjugated to H-substituted forms.

This appears to be a further proof that the surface species is different in the cation substituted and in the proton substituted [Al]-MTS. In the former case, the prevailing species is a group $Si(O^-)AlNa^+$, the conjugated acid of which is the bridging Si(OH)Al species. In the latter case of H-[Al]-MTS samples, the acidic species are those listed in Table 1.

NMR evidence is that tetrahedral Al does not survive much when the template is removed and the H-forms are generated, because severe reconstructions take place. This is equivalent to saying that the Brønsted sites are unstable, the more so the larger the pore, as reported by Haller and coworkers [111]. This does not apply, however, to samples where the template is substituted by alkali cations, which keep the tetrahedral Al and are, therefore, the conjugated bases of acidic zeolites.

When a proton is in its coordination sphere, instability of tetrahedrally coordinated Al closely resembles the process of dealumination of zeolites or re-arrangements at the outer surfaces of zeolites. It is therefore not surprising that the same species is arrived at in all three cases, i.e., the medium-acidic AlOH(II) species vibrating at 3660 cm^{-1}. It may possible that also the other acidic species are formed on the outer surfaces of zeolites or during dealumination. A possible overall reaction network which accounts for the presence of the two new acidic species is reported in Scheme 6. This

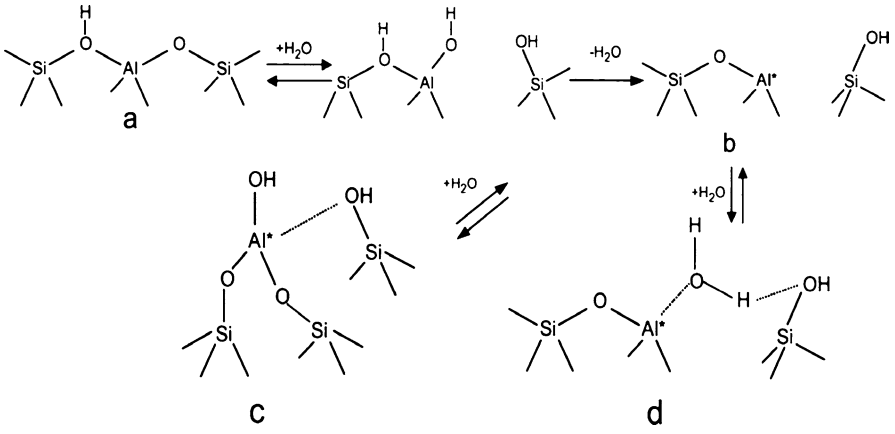

Scheme 6 Mechanism for the water-mediated conversion of bridging sites into acidic non-bridging sites. **a** bridiging site; structure **b** exposed Al cation; structure **c** acidic aluminol of the type AlOH(II) (see text); structure **d** molecular water on an exposed Al cation, an acidic center of the type AlOH(III) (see text). After [103, 104]

scheme is a development of the mechanism proposed by Zecchina and Otero Areán [112] for the formation of Lewis sites in zeolites. Through successive desorption/adsorption of water, two different configurations are arrived at, which correspond to the acidic sites AlOH(II) and AlOH(III). Taking into account that the species $Al\cdots H_2O$ is probably a variant of species AlOH(III) in the presence of Na cations, the mechanism in Scheme 6 might represent a realistic picture of chemical reconstruction at the surface of H-[Al]-MTS. As a minor feature, it has to be noted that structure c in Scheme 6 envisages the intervention of a third Si atom (whereas all other structures only two) because the trigonal Al species given rise is likely to interact with a nearby silanol.

It seems probable that the balance between the various acidic species is dictated by the thermal history of the sample, the conditions of synthesis, etc.

As an overall conclusion, we believe that Brønsted acidity in H-[Al]-MTS is different from that of zeolite, both in nature and in strength. Because several new types of acidic centers may be formed, the strength of Brønsted acidity in H-Al-MTS may vary substantially, though never reaching that of proton zeolites. This opens a field of activity, consisting in the control of the parameters affecting the formation of the various Brønsted acidic species, together with the control of the accompanying Lewis sites.

6
Methods for Improving Acid Strength

6.1
Post-synthesis Alumination

Post-synthesis alumination of siliceous forms of MCM-41 and MCM-48 can be readily achieved by reaction of parent materials at low temperature in nonpolar solvents with various aluminum sources. Among the latter, trimethyl aluminum [113], aluminum trichloride [114], aluminum chlorohydrate [115] aluminum isopropoxide [116, 117] and aluminum acetylacetonate [118, 119] have been used. After calcination, the resulting materials preserve the typical narrow pore distribution of the parent mesophase and ^{27}Al NMR measurements reveal the presence of aluminum atoms in both tetrahedral and octahedral configurations generating Brønsted and Lewis acid sites with a strength comparable to that of mesostructures of similar composition prepared by direct synthesis.

The influence of different post-alumination procedures on the network connectivity of MCM-41s has been analyzed by Burgess et al. [120, 121]. The isopropoxide route was found to be the most effective in incorporating tetrahedral aluminum, probably via the healing of Q^3 sites as suggested by the decrease of the corresponding signal in the ^{29}Si NMR spectra and the changes

in intensity of the narrow (3740 cm^{-1}) and broad (3400 cm^{-1}) features of the IR spectra. No discrete infrared band that could be assigned to bridging Si(OH)Al groups could be, however, detected.

Although materials prepared by post-alumination procedures did not feature acid sites stronger than those obtained by direct synthesis, the catalytic activity of the former (evaluated for cumene cracking [115, 116], isopropanol dehydration [120, 121] or aldehyde condensation [117]) was found systematically higher than that of the latter. Such a result must be attributed to a better accessibility of the acid sites in the case of post-aluminated materials. This fact was actually shown by Collart et al. [118, 119] in the case of [Si]-MCM-48s treated with $Al(acac)_3$. The number of acid sites titrated by ammonia amounted to 100% and 68% of the total number of aluminum atoms deposited in samples containing 1.2 wt % (Si/Al = 37) and 5.1 wt % (Si/Al = 17) Al, respectively.

6.2 Improved Synthesis Procedures

The adjustment of pH, the use of organic and inorganic salts and of highly polymerized silica as silicon sources as well as subsequent hydrothermal treatments, have been successfully applied to produce highly ordered siliceous MTS materials since the very first works in the field. Actually, the chemistry of silicates is fully relevant in those systems, notwithstanding the presence of the surfactants. A better degree of silica condensation (measured for instance by the ratio of the Q^4 to Q^3 peaks in ^{29}Si NMR) leads generally to an increase of the amount of silica incorporated into the solid. The resulting MTSs feature high long-range periodicity, thicker walls and, as a consequence, improved thermal and hydrothermal stabilities. These studies have been comprehensively reviewed [8].

The very same principles have been applied for the preparation of mesostructured aluminosilicates with improved hydrothermal stability and acidity. The idea behind the numerous studies recently performed was to generate a zeolite-like short-range order in the pore walls. Two general strategies have been followed, either the recrystallization of the pore walls in the presence of a zeolite-structure directing agent, or the use of pre-aged aluminosilicate precursors as the source of organic.

MCM-41s with partially zeolitized walls have been tentatively prepared in alkaline medium by post-synthesis recrystallization of MCM-41s in the presence of tetrapropylammonium cations [122] and via simultaneous synthesis of ZSM-5 and MCM-41 using mixtures of C_6 and C_{14} alkyltrimetylammonium templates [123]. The results show that varying amounts of the two structures can actually be obtained by adjusting the synthesis parameters, but the zeolite forms generally as discrete nanocrystals, 2–3 nm in size, segregated from the mesophase. The formation of composite materials and the lack of for-

mation of mesoporous materials with crystallized walls is in line with the thickness of the latter, which rarely exceeds 1 nm under the alkaline conditions applied.

Pinnavaia and his group [124] was the first to report hydrothermally stable and strongly acidic mesoporous aluminosilicate materials (MSU-S) analogs of MCM-41 obtained by the direct assembly of zeolite seeds (otherwise referred to as protozeolites or nanoclusters) of faujasites (FAU) in the presence of alkylammonium surfactants. The procedure was then extended to the self-assembly of precursors of pentasil zeolite such as ZSM-5 (MFI) and beta (BEA) [125]. The resulting materials feature remarkable resistance to high-temperature steaming (800 °C, 20% steam vapor in N_2, 5 h) under conditions which generally lead to complete collapse of well-ordered MCM-41s of similar composition. Moreover, ^{27}Al MAS NMR spectroscopy shows that over 90% of the aluminum atoms in calcined MSU-S are in tetrahedrally coordinated sites and generate strong acid sites, highly efficient for cumene cracking. Though XRD powder patterns of the as-made and calcined materials do not reveal any discernable Bragg diffraction at wide angle, the enhancement of the thermal stability and acidity in MSU-S is attributed to the presence of secondary structural building units in the pore walls, similar to those of microporous zeolites, as suggested by distinct IR vibrations in the range 520–600 cm^{-1}, characteristic of 5-membered rings. The very same explanation was put forward by Xiao and co-workers [126, 127], who prepared a mesoporous aluminosilicate (MAS-5) able to resist severe steaming (800 °C, 100% steam, 2 h) and featuring an acid strength distribution measured by ammonia TPD identical to that of zeolite beta.

The concept of using protozeolites as precursors to generate mesostructures with improved stability and acidity has been then widely expanded and allowed to generate a wide variety of materials including cubic mesophases [128, 129], SBA-15 analogues and foams [130–132]. Progresses in the field have been recently reviewed [133–135]. All these materials share very promising features with regards to catalytic applications such as a narrow (meso)pore size distribution, a high hydrothermal stability and an acid strength comparable to that of the zeolite that would have been obtained after full crystallization of the gel precursor.

7
Trivalent T Atoms Other than Al

The trivalent atoms (other than Al) most commonly used to generate acidity in MTS systems are the same as employed in zeolitic systems, i.e., B, Ga, Fe. In all three cases, the same mechanism of generation of acidity is expected, as well as differences because of the different radius, electronegativity, hardness and so forth. Boron appears, as usual in chemistry, the species

exhibiting a different behavior [136–139]. Al, Ga and Fe have much closer properties [140–147].

7.1 B as T Atom

As it concerns B substitution, Kaliaguine and coworkers [136, 137] achieved framework incorporation into the MCM-41 structure by direct hydrothermal synthesis. The decreased *d* spacing in XRD patterns and the presence of IR bands at 1380 and 940 cm^{-1}, typical of borosilicates, confirm the occupancy of boron in the MCM-41 structure. MAS-NMR results concerning ^{11}B showed that boron atoms are in tetrahedral coordination in the as-synthesized sample, but that removal of the template causes the partial conversion of tetrahedral into trigonal species. This is no surprise, because the tendency of B to favor trigonal coordination is well known in chemistry. Indeed, in zeolites the conversion of tetrahedral into trigonal B and vice versa has been reported to follow dehydration/hydration [138]. Acidity is found, though inferior to that of similar Al-containing samples, i.e., both as Lewis and Brønsted acidity.

Acidity has been characterized much more in detail as it concerns nonporous boria-silica systems. Travert et al. [139] studied the adsorption of CO, pyridine and acetonitrile. CO does not adsorb at all. Pyridine and acetonitrile do adsorb, and spectral features show the proton transfer between the solid and the adsorbate. Spectral features would indicate a quite remarkable strength of interaction. Adsorbed species show instead a labile nature: this apparent conflict is interpreted by assuming that, in the absence of adsorbate, boron atoms prefer trigonal coordination, whereas in the presence of the adsorbate, tetrahedral coordination is necessarily adopted. The conversion from trigonal to tetrahedral coordination is an endothermic step, destabilizing the surface adducts.

7.2 Ga as T Atom

There is a specific interest in Ga-containing MTS, which stems from the high selectivity to aromatics shown by Ga-containing zeolites in the catalytic conversion of hydrocarbons [140–143]. For example, the commercial Cyclar process, where C3-C5 alkanes are dehydrocyclized to yield aromatic hydrocarbons, proceeds over [Ga]-ZSM-5, whereas conventional ZSM-5 aluminosilicates mainly yield paraffins. It has also been shown that Ga-containing MCM-41 is very active for Friedel–Crafts type benzylation and acylation reactions [143, 144].

Kosslick et al. [145] investigated surface acidity by using ammonia as a probe molecule. Adsorbed pyridine and solid state ^{71}Ga MAS-NMR were also used for the same purpose [144, 146]. Otero Areán and co-workers [147]

studied a H-[Ga]-MCM-41 sample with Si/Ga = 16 by IR spectroscopy of adsorbed CO, pyridine and lutidine. One type of Lewis site was found, revealed by a CO band at 2223 cm^{-1}, also found when studying high surface area gallia. The other significant CO band at 2172 cm^{-1} was attributed to CO molecules interacting with a Brønsted site and assumed to have the same nature as the bridged species in gallium-substituted protonic zeolites Si(OH)Ga. Indeed, CO interacting with the acidic proton in H-[Ga]-ZSM-5 absorbs at precisely 2172 cm^{-1} [148].

Whereas in this latter system the Si(OH)Ga species causes a typical absorption at 3617 cm^{-1}, no distinctive band appears around this wavenumber in the blank spectrum of H-[Ga]-MCM-41. The explanation provided by the authors is that the amorphous nature of the MCM-41 system causes the structural heterogeneity of bridging OH groups, so that the corresponding O – H stretching band becomes spread over a large frequency range, and the only observable feature is a raised background in the corresponding spectral region. The OH stretching region is not reported in detail in this paper as it concerns the experiment with CO. It appears, however, that that the absorption expected at 3342 cm^{-1} (stretching mode of the perturbed OH species) [148] does not show up. Similarly, CO adsorption does not bring about the appearance of bands in the region 3400–3500 cm^{-1}, contrary to the Al case. On this bases, it would appear that the acidic surface species may have a different nature in the case of Ga and Al. Other authors, as illustrated below, report different evidence. A further result of this study, coming from the comparative adsorption of pyridine and lutidine, is the remarkable heterogeneity in the strength of Brønsted sites, some of which are able to protonate lutidine (a stronger base) but not pyridine.

It has to be noted that Kosslick et al. [145] report the presence of weak bands at 3605 and 3591 cm^{-1}, ascribed to bridging Si(OH)Ga species. Such an assignment seems doubtful in view of the work of Otero Areán and co-workers [147], and the related bands appear more probably as vestiges of the transformation of unstable bridging species at the surface. Pasqua et al. [68, 69] report a finding in agreement with the general picture drawn for H-[Al]-MS systems: in Ga-containing samples outgassed at 773 K, a band is seen at 3662 cm^{-1}, attributed to the O – H stretch of non-bridging Brønsted sites. The apparent contradiction probably originates from the different handling of the sample as well as the Ga content, which may lead to samples with different behavior.

7.3 Fe as T Atom

As to Fe-containing MTS systems, reference can be made to a paper by Katovic et al. [149]. The samples containing Fe with an Si/Fe ratio of 10–20 are readily prepared, similar to those loaded with Zn atoms. Figure 20 sum-

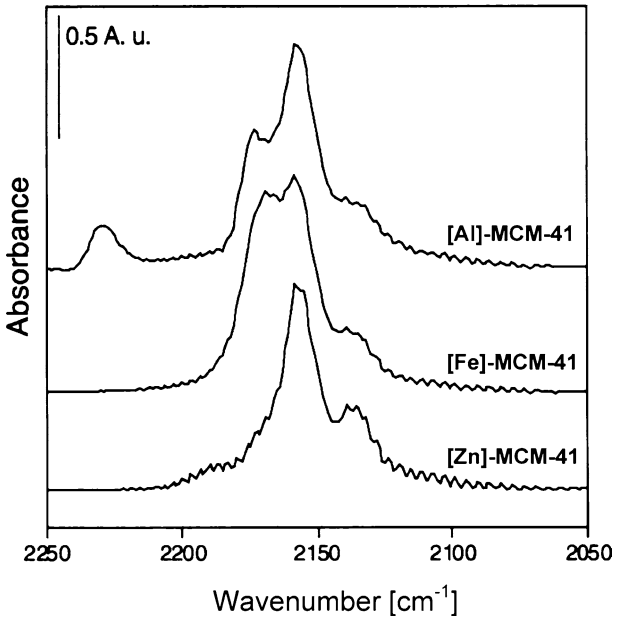

Fig. 20 Comparison of IR spectra in the O – H stretching region concerning the adsorption of 0.5 mbar of CO at a nominal temperature of 77 K on MCM-41 containing Al, Fe and Zn as heteroatoms: see text for explanation. After [146]

marizes the results by comparing the three samples [Al]-, [Fe]- and [Zn]-MCM-41. As noted above, the Al sample shows a strong Lewis site on which adsorbed CO vibrates at 2230 cm^{-1}. A weak site is also noted at ca. 2170 cm^{-1}, probably also partially due to Brønsted species. The Fe sample does not show any strong Lewis site. As adsorption of ammonia indicates that no Brønsted acidity is present, the band at ca. 2170 cm^{-1} is due to a weak Lewis site. The Zn-bearing sample only exhibits the two uninteresting bands at 2156 and 2139 cm^{-1}, due to the interaction with silanols and to physisorbed species.

With regards to the overall acidity, the Brønsted acid scales in the order Al $\gg$ Ga > Fe, as measured both by the number of sites capable of protonating ammonia and by the initial heat of ammonia chemisorption [145]. Such a sequence corresponds to that observed in the case of zeolites. On the other hand, the Lewis acid sites showed an order strength Ga > Al > Fe. The presence of a stronger Lewis acidity over [Ga]-MCM-41 compared to [Al]-MCM-41 has been also reported by Nesterenko et al. [150]. Strong Lewis sites were associated with electron-deficient extra-framework oxide nanoparticles generated upon calcination. It is worth mentioning that recent results [151] on the t-butylation of phenol using the corresponding alcohol as reactant lead to a sequence of activity order as Ga > Al > Fe over MCM-41 and MCM-48 catalysts. This suggests a reaction process catalyzed either by the Lewis

sites or by strong Brønsted sites generated by adsorption of nascent water on the latter.

In conclusion, it is probable that both Fe and Ga are less prone than Al to form isolated acidic species different from the bridging OH species. Once the bridging species, stable in a zeolite framework, is brought to the surface or embedded in a deformable medium, it becomes destabilized and with either Ga or Fe, the process probably preferentially goes to completion, with the yield of extra-framework oxidic species.

8 Concluding Remarks

The objective of this chapter was to review and critically analyze the present state of knowledge of the acidic properties of ordered silica-based mesoporous materials (or MTS) prepared by self-assembly of (alumino) silicates and surfactants and to tentatively identify the nature of the acid sites. The measure of acidity of solids is a delicate task, a statement that fully applies in the present case, where surface properties appear dramatically influenced by the synthesis and thermal history of the material as well as by the conditions under which the measurements are done. Overall methods such as temperature-programmed desorption and microcalorimetry of adsorbed bases reveal very broad distributions of acid strengths covering adsorption energies typical for interaction with silanol groups up to strong bonding with electron-deficient Lewis centers. Identification of the Brønsted sites is a main subject of debate, to which infrared spectroscopy provides most meaningful contributions. Assumptions of the presence of bridging Si(OH)Al sites similar to those of zeolites and their direct observation in bare samples are not sustained by observation of the corresponding O – H bands upon interaction with weak bases nor by proton NMR measurements, thus suggesting that, if present, such sites may contribute only marginally to acidity.

In our opinion, the acid sites in MTS are much diverse and different from those found in zeolites and resemble more those of traditional amorphous aluminosilicates. Adsorption of CO at 77 K allows to reveal at least six types of hydroxyl groups with Brønsted acid character and three types of Lewis sites (Table 1).

Besides Sil and Dim-Sil, all other species appear as the product of the destabilization suffered by tetrahedral Al species, when close at the surface and compensated in charge by protons. Scheme 6 above suggests a possible mechanism for the formation of the two main species, an aluminol grafted to the silica network (Scheme 3) and a water molecule sitting on a strong Lewis site. Most probably, sample composition, conditions of synthesis and activation may generate a broad range of these species and consequently of acid strengths. Such considerations are not limited to [Al]-MTS. Destabilization of

tetrahedral Al also occurs at the external surface of zeolites and at the irregular pores of dealuminated mordenites. Scheme 6 or similar ones could have, therefore, a general significance in describing the evolution of tetrahedral Al species in the presence of protons.

This scheme bears also resemblance to what is reported for clays or pillared clays [110]. Molecular water on strong Al sites is normally assumed as a source of acidity in clays. In [Al]-pillared clays [152], a band was observed with the features of AlOH(II) species, i.e., a stretching mode at 3660 cm^{-1} and a shift upon CO interaction of ca. 200 cm^{-1}. This species arises from the simultaneous presence of the Al pillar and the silica sheet in clays, so it is again proposed to be an Si-O-Al-OH species.

Regarding Lewis acidity, three different ν(CO) bands at 2230, 2200 and 2173 cm^{-1} have been associated with strong, intermediate and weak sites, respectively. Aluminum species attached to the silica network with different degrees of protrusion from the surface and/or extra-lattice species are able to generate this acidity.

Lewis acid sites are the strongest sites detected on MTS materials, and they undoubtedly impact catalytic activity, either directly through electrophilic activation of the substrates or via the generation of strong Brønsted sites by reaction with water. Because of this, it is clear – as already said above – that the thermal history of MTS-based catalysts will determine to a great extent their catalytic behavior.

Similar considerations probably hold for Ga and Fe substituted MTS, though the instability of these tetrahedral heteroatoms is more marked and, consequently, the tendency to yield directly extra-framework debris. This latter, in turn, may readily loose oxygen and promote reactions different from those purely acid-catalyzed.

We hope that this chapter will contribute to a better understanding of the properties of these exciting materials and that our conclusions will nourish the open debate on the nature and origin of their acidity.

References

1. Kresge CT, Leonowicz ME, Roth WJ, Vartuli JC, Beck JS (1992) Nature 359:710
2. Scott BJ, Wirnsberger G, Stucky GD (2001) Chem Mater 13:3140
3. Taguchi A, Schüth F (2005) Microporous Mesoporous Mater 77:1
4. Ganschow M, Wark M, Wöhrle D, Schulz-Ekloff G (2000) Angew Chem Int Ed 39:161
5. Brunel D (1999) Microporous Mesoporous Mater 27:329
6. Thommes M, Kohn R, Fröba M (2002) Appl Surf Sci 196:239
7. Huo Q, Margoles DI, Ciesla U, Demuth D, Feng P, Gier TE, Sieger P, Leon R, Petroff PM, Schüth F, Stucky GD (1994) Nature 368:317
8. Di Renzo F, Galarneau A, Trens P, Fajula F (2002) In: Schüth F, Sing K, Weitkamp J (eds) Handbook of Porous Solids. Wiley-VCH, Weinheim, Germany, p 1311
9. Ottaviani MF, Galarneau A, Desplantier-Giscard D, Di Renzo F, Fajula F (2001) Microporous Mesoporous Mater 44:1

10. Valange S, Gabelica Z, Onida B, Garrone E (1998) In: Treacy MMJ, Marcus BK, Bisher ME, Higgins JB (eds) Proc 12th Int Zeolite Conf, Baltimore, Maryland, USA, July 5–10. Materials Research Society, Warrendale, Maryland, USA, p 2711
11. Sayari A, Kara VR, Reddy JS, Moudrakovski IL (1995) Mat Res Symp Proc 371:81
12. Ziołek M, Nowak I, Lavalley JC (1997) Catal Lett 45:259
13. Chen C-Y, Li H-X, Davis ME (1993) Microporous Mater 2:17
14. Bar MR, Sauer J (1994) Chem Phys Lett 26:405
15. Janicke M, Kumar D, Stucky GD, Chmelka BF (1994) In: Weitkamp J, Karge HG, Pfeifer H, Hölderlich W (eds), Zeolites and related microporous materials: State of the art 1994; Proc 10th Int Zeolite Conf, Garmisch-Partenkirchen, July 17–22, 1994. Elsevier, Amsterdam, 1994, p 243
16. Janicke M, Kumar D, Stucky GD, Chmelka BF (1994) Stud Surf Sci Catal 84:243
17. Luan Z, Cheng C-F, Zhou W, Klinowski J (1995) J Phys Chem 99:1018
18. Kloestra KR, Zandbergen HW, van Bekkum H (1995) Catal Lett 33:157
19. Schmidt R, Akporiaya D, Stöcker M, Ellestad OH (1994) J Chem Soc Chem Comm, p 1493
20. Borade RB, Clearfield A (1995) Catal Lett 31:26
21. Bonelli B, Ribeiro MF, Antunes AP, Valange S, Gabelica Z, Garrone E (2002) Microporous Mesoporous Mater 54:305
22. Bonelli B, Onida B, Chen JD, Galarneau A, Di Renzo F, Fajula F, Garrone E (2004) Microporous Mesoporous Mater 67:95
23. Onida B, Bonelli B, Flora L, Geobaldo F, Otero Arean C, Garrone E (2001) J Chem Soc Chem Comm, p 2216
24. Man Kim J, Hun Kwak J, Shinae J, Ryoo R (1995) J Phys Chem 99:16742
25. Kloestra KL, van Bekkum H (1995) J Chem Soc Chem Comm, p 1005
26. Mokaya R, Jones W (1996) J Chem Soc Chem Comm, p 981
27. Mokaya R, Jones W (1997) J Catal 172:211
28. Mokaya R, Jones W (1998) J Mater Chem 8:2819
29. Tuel A (1999) Microporous Mesoporous Mater 27:151
30. Bonelli B, Onida B, Chen JD, Galarneau A, Di Renzo F, Fajula F, Fubini B, Garrone E (2006) Microporous Mesoporous Mater 87:170
31. Meziani MJ, Zajac J, Douillard JM, Jones DJ, Partyka S, Rozière J (2001) J Coll Inter Sci 233:219
32. Gedeon A, Lassoued A, Bonardet JL, Fraissard J (2001) Microporous Mesoporous Mater 44–45:801
33. Chen C-Y, Li H-X, Davis ME (1993) Microporous Mater 2:17
34. Corma A, Fornès V, Navarro MT, Perez-Pariente J (1994) J Catal 148:569
35. Kosslick H, Lische G, Parlitz B, Storek W, Fricke R (1999) Appl Catal A 184:49
36. Meziani MJ, Zajac J, Jones DJ, Partyka S, Rozière J, Auroux A (2000) Langmuir 16:2262
37. Occelli M, Biz S, Auroux A, Ray GJ (1998) Microporous Mesoporous Mater 26:193
38. Brunner E (1997) Catal Today 38:361
39. Haw JF, Xu T (1998) Adv Catal 42:361
40. Kuroda Y, Mori T, Yoshikawa Y (2001) J Chem Soc Chem Comm, p 1006
41. Heeribout L, Semmer V, Batamack P, Dorémieux-Morin C, Fraissard J (1998) Microporous Mesoporous Mater 21:565
42. Omegna A, van Bokhoven JA, Prins R (2003) J Phys Chem B 107:8854
43. Fraissard J, Petrakis L (eds) (1994) Acidity and basicity of solids: theory, assessment and utility, NATO ASI series. Kluwer Academic Publisher, Dordrecht, The Netherlands
44. Zamaraev KI, Thomas JM (1996) Adv Catal 41:335

45. Boehm HP, Knözinger H (1983) Nature and estimation of functional groups on solid surfaces: In: Anderson JR, Boudart M (eds) Catalysis, Science and Technology 4. Springer, New York, p 39
46. Jentys A, Pham NH, Vinek H (1996) J Chem Soc Faraday Trans 92:3287
47. Morrow BA (1990) In: Fierro JLG (ed) Spectroscopic characterization of heterogeneous catalysts, Part A: Methods of surface analysis. Elsevier, Amsterdam, p 161
48. Chen J, Li Q, Xu R, Xiao F (1995) Angew Chem Int Ed Engl 34:2694
49. Morin S, Ayrault P, El Mouahid S, Gnep NS, Guisnet M (1997) Appl Catal A 159:317
50. Corma A, Grande MS, Gonzalez-Alfonso V, Orchilles AV (1996) J Catal 159:375
51. Di Renzo F, Chiche B, Fajula F, Viale S, Garrone E (1996) In: Hightower JW, Delgass WN, Iglesia E, Bell AT (eds) Proc 11th Congress on Catalysis, Baltimore, Maryland, USA, June 30–July 5, 1996. Elsevier, Amsterdam, p 851
52. Di Renzo F, Chiche B, Fajula F, Viale S, Garrone E (1996) In: Hightower JW, Delgass WN, Iglesia E, Bell AT (eds) Stud Surf Sci Catal 101:851
53. Gora-Marek K, Derewinski M, Sarv P, Datka J (2005) Catal Today 101:131
54. Finocchio E, Busca G, Rossini S, Cornaro U, Piccoli V, Miglio R (1997) Catal Today 33:335
55. Trombetta M, Busca G, Lenarda M, Storaro L, Pavan M (1999) Appl Catal A 182:225
56. Cairon O, Chevreau T, Lavalley JC (1998) J Chem Soc Faraday Trans 94:3039
57. Bonelli B, Onida B, Chen JD, Galarneau A, DiRenzo F, Fajula F, Garrone E (2004) Microporous Mesoporous Mater 67:95
58. Scokart PO, Rouxhet PG (1982) J Colloid Interface Sci 86:96
59. Zholobenko VL, Plant D, Evans AJ, Holmes SM (2001) Microporous Mesoporous Mater 44–45:793
60. Busca G (1998) Catal Today 41:191
61. Ramis G, Busca G (1989) J Mol Struct 193:93
62. Pistarino C, Finocchio E, Larrubia MA, Serra B, Braggio S, Busca G, Baldi M (2001) Ind Eng Chem Res 40:326
63. Allian M, Borello E, Ugliengo P, Spanò G, Garrone E (1995) Langmuir 11:4811
64. Mori T, Kuroda Y, Yoshikawa Y, Nagao M, Kittaka S (2002) Langmuir 18:1595
65. Pimentel GC, Mc Lellan AL (1960) The hydrogen bond. WH Freeman Co., San Francisco, CA
66. Wakabayashi F, Kondo JN, Domen K, Hirose C (1995) J Phys Chem 99:10573
67. Morterra C, Magnacca G (1996) Catal Today 27:497
68. Pasqua L, Testa F, Aiello R (1998) In: Bonneviot L, Beland F, Danumah C, Giasson S, Kaliaguine S (eds) Proc 1st Symp Mesoporous Materials, Baltimore, Maryland, USA, July 10–12, 1998. Elsevier, Amsterdam, p 317
69. Pasqua L, Testa F, Aiello R (1998) In: Bonneviot L, Beland F, Danumah C, Giasson S, Kaliaguine S (eds) Stud Surf Sci Catal 117:317
70. Cairon O, Chevreau T, Lavalley JC (1998) J Chem Soc Faraday Trans 94:3039
71. Ziołek M, Nowak I, Lavalley JC (1997) Catal Lett 45:259
72. Zecchina A, Bordiga S, Spoto G, Scarano D, Petrini G, Leofanti G, Padovan M, Otero Areán C (1992) J Chem Soc Faraday Trans 88:2959
73. Jentys A, Kleerstorfer K, Vinek H (1999) Microporous Mesoporous Mater 27:321
74. Borovkov VY, Alexeev AA, Kazansky VB (1983) J Catal 125:427
75. Sayari A (1996) Chem Mater 8:1840
76. Corma A (1997) Chem Rev 97:2373
77. Corma A, Kumar D (1998) In: Bonneviot L, Beland F, Danumah C, Giasson S, Kaliaguine S (eds) Proc 1st Symp Mesoporous Materials, Baltimore, Maryland, USA, July 10–12, 1998. Elsevier, Amsterdam, p 201

78. Corma A, Kumar D (1998) In: Bonneviot L, Beland F, Danumah C, Giasson S, Kaliaguine S (eds) Stud Surf Sci Catal 117:201
79. Ying JY, Mehnert CP, Wong MS (1999) Angew Chem Int Ed Engl 38:6
80. Linssen T, Cassiers KL, Cool P, Vansant EF (2004) Microporous Mesoporous Mater 103:121
81. Taguchi A, Schüth F (2005) Microporous Mesoporous Mater 77:1
82. Corma A, Grande MS, Gonzalez-Alfaro V, Orchilles AV (1996) J Catal 159:375
83. Liepold A, Roos K, Reschetilowski W (1996) Chem Eng Sci 11:3007
84. Koch H, Reschetilowski W (1998) Microporous Mesoporous Mater 25:127
85. Koch H, Böhmer U, Klemt A, Reschetilowski W, Stöcker MJ (1998) Chem Soc Faraday Trans 94:817
86. Koch H, Liepold A, Roos K, Stöcker M, Reschetilowski W (1999) Chem Eng Technol 22:10
87. Park KC, Ihm SK (2000) Appl Catal A 203:201
88. Perrotin L (2001) PhD Dissertation Thesis, University of Montpellier
89. Savidha R, Pandurangan A, Palaichamy M, Murugesan V (2003) Catal Lett 91:49
90. Eswaramoorthi I, Sundaramurthy V, Lingappan N (2004) Microporous Mesoporous Mater 71:109
91. Uytterhoeven JB, Christner LG, Hall WK (1965) J Phys Chem 69:2117
92. Mortier WJ (1984) In: Olson D, Bisio A (eds) Proc 6th Int Zeolite Conf, Reno, USA, July 10–15, 1983. Butterworth, Guilford, Surrey, UK, p 734
93. Heeribout L, Vincent R, Batamack P, Dorémieux-Morin C, Fraissard J (1998) Catal Lett 53:23
94. Busco C (2003) PhD Thesis, University of Turin
95. Scarano D, Zecchina A, Bordiga S, Geobaldo F, Spoto G, Petrini G, Leofanti G, Padovan M, Tozzola G (1993) J Chem Soc Faraday Trans 89:4123
96. Paparatto G, Moretti E, Leofanti G, Gatti F (1987) J Catal 105:227
97. Kunieda T, Kim JH, Niwa M (1999) J Catal 188:431
98. Corma A, Fornés V, Forni L, Marquez F, Martinez-Triguero J, Moscotti D (1998) J Catal 179:451
99. Trombetta M, Busca G (1999) J Catal 187:521
100. Trombetta M, Armaroli T, Gutiérrez-Alejandre A, Ramírez J, Busca G (2000) Appl Catal A 192:125
101. Otero Areán C, Escalona Platero E, Penarroya Mentruit M, Rodriguez Delgado M, Llabbres i Xamena FX, Garcia Raso A, Morterra C (2000) Mesoporous Microporous Mater 34:55
102. Onida B, Borello L, Bonelli B, Geobaldo F, Garrone E (2003) J Catal 214:191
103. Borello L, Onida B, Bonelli B, Garrone E (2004) In: van Steen E, Callanan LH, Claeys M (eds) Proc 14th Int Zeolite Conf, Cape Town, South Africa, April 25–30, 2004. Elsevier, Amsterdam, 2004, p 1532
104. Borello L, Onida B, Bonelli B, Garrone E (2004) In: van Steen E, Callanan LH, Claeys M (eds) Stud Surf Sci Catal 154:1532
105. van Bokhoven JA, van der Eerden AMJ, Koningsberger DC (2003) J Am Chem Soc 125:7435
106. Marques JP, Gener I, Ayrault P, Bordado JC, Lopes Madeira J, Ramoa Ribeiro F, Guisnet M (2005) CR Chimie 8:399
107. Mishin LV, Klyachko AL, Brueva TR, Nissenbaum VD, Karge HG (1993) Kinet Catal 34:835
108. Muscas M, Dutel JF, Solinas V, Auroux A, Ben Taarit Y (1996) J Mol Cat A Chemical 106:169

109. Garrone E, Onida B, Bonelli B, Busco C, Ugliengo P (2006) J Phys Chem B 110(39):19087
110. Mortland MM, Fripiat JJ, Chaussidon J, Uytterhoeven JB (1963) J Phys Chem 67:248
111. Feng XB, Lee JS, Lee JW, Lee JY, Wei D, Haller GL (1996) Chem Eng J 64:225
112. Zecchina A, Otero Areán C (1996) Chem Soc Rev 187:25
113. Oumi Y, Takagi H, Sumiya S, Mizuno R, Uozumi T, Sano T (2001) Microporous Mesoporous Mater 44:267
114. Chen LY, Ping Z, Chuah GK, Jaenicke S, Simon G (1999) Microporous Mesoporous Mater 27:231
115. Mokaya R, Jones W (1999) J Mater Chem 9:555
116. Mokaya R, Jones W (1999) Phys Chem Chem Phys 1:207
117. Chuah GK, Jaenicke S, Liu SH, Hu XC (2001) Appl Surf Sci 169:253
118. Collart O, Galarneau A, Di Renzo F, Fajula F, van der Voort P, Vansant EF (2001) In: Galarneau A, Di Renzo F, Fajula F, Vedrine J (eds) Zeolites and mesoporous materials at the dawn of the 21st century, Proc 13th Int Zeolite Conf, Montpellier, France, July 8–13, 2001. Elsevier, Amsterdam, 2001, p 29-O-4
119. Collart O, Galarneau A, Di Renzo F, Fajula F, van der Voort P, Vansant EF (2001) In: Galarneau A, Di Renzo F, Fajula F, Vedrine J (eds) Stud Surf Sci Catal 135: 29-O-4
120. Burgess G, Joyner RW, Stockenhuber M (2004) In: van Steen E, Callanan LH, Claeys M (eds) Proc 14th Int Zeolite Conf, Cape Town, South Africa, April 25–30, 2004. Elsevier, Amsterdam, p 446
121. Burgess G, Joyner RW, Stockenhuber M (2004) In: van Steen E, Callanan LH, Claeys M (eds) Stud Surf Sci Catal 154:446
122. Kloestra KR, van Bekkum H, Jansen JC (1997) J Chem Soc Chem Comm, p 2281
123. Verhoelf MJ, Kooyman PJ, van der Waal JC, Rigutto MS, Peters JA, van Bekkum H (2001) Chem Mater 13:683
124. Liu Y, Zhang WZ, Pinnavaia TJ (2000) J Am Chem Soc 122:8791
125. Liu Y, Zhang WZ, Pinnavaia TJ (2001) Angew Chem Int Ed Engl 40:1255
126. Zhang ZT, Han Y, Zhu L, Wang R, Yu Y, Qiu S, Zhao D, Xiao FS (2001) Angew Chem Int Ed Engl 40:1258
127. Zhang ZT, Han Y, Xiao FS, Qiu S, Zhu L, Wang R, Zou B, Sun H, Zhang Z, Zhao D, Yen W (2001) J Am Chem Soc 123:5014
128. Shih PC, Lin HP, Mou CY (2003) In: Park S-E, Ryoo R, Ahn W-S, Lee CW, Chang SH (eds) Nanotechnology in mesostructured materials, Proc 3rd Int Symp Mesostructured Materials, Jeju, Korea, July 8–11, 2002. Elsevier, Amsterdam, p 557
129. Shih PC, Lin HP, Mou CY (2003) In: Park S-E, Ryoo R, Ahn W-S, Lee CW, Chang SH (eds) Stud Surf Sci Catal 146:557
130. Han Y, Wu S, Sun Y, Li D, Xiao FS, Liu J, Zhang X (2002) Chem Mater 14:1144
131. Liu Y, Pinnavaia TJ (2002) Chem Mater 14:3
132. On DT, Kaliaguine S (2002) Angew Chem Int Ed Engl 41:1036
133. Xiao FS (2004) Catal Surveys Asia 8:151
134. Pinnavaia TJ, Kim SS, Zhang WZ, Liu Y (2004) In: van Steen E, Callanan LH, Claeys M (eds) Proc 14th Int Zeolite Conf, Cape Town, South Africa, April 25–30, 2004. Elsevier, Amsterdam, p 14
135. Pinnavaia TJ, Kim SS, Zhang WZ, Liu Y (2004) In: van Steen E, Callanan LH, Claeys M (eds) Stud Surf Sci Catal 154:14
136. Trong On D, Joshi PN, Lemay G, Kaliaguine S (1995) In: Bonneviot L, Kaliaguine S (eds) Zeolites: a refined tool for designing catalytic sites, Proc Int Symp, Québec, Canada, October 15–20, 1995. Elsevier, Amsterdam, p 543

137. Trong On D, Joshi PN, Lemay G, Kaliaguine S (1995) In: Bonneviot L, Kaliaguine S (eds) Stud Surf Sci Catal 97:543
138. School KF, Veeman VS (1985) Zeolites 5:118
139. Travert A, Vimont A, Lavalley JC, Montouillout V, Rodriguez Delgado M, Cuart Pascual JJ, Otero Areán C (2004) J Phys Chem 108:16499
140. Thomas JM, Liu X (1986) J Phys Chem 90:4843
141. Kitagawa H, Sendoda Y, Ono Y (1986) J Catal 101:12
142. Price GL, Kanazirev V (1990) J Catal 126:267
143. Choudary VR, Jana SK, Kiran BP (2000) J Catal 192:257
144. Okumura K, Nishigaki K, Niwa N (2001) Microporous Mesoporous Mater 44:509
145. Kosslick H, Landmesser H, Fricke R (1997) J Chem Soc Faraday Trans 93:1849
146. Trong On D, Nguyen SV, Hulea V, Dumitriu E, Kaliaguine S (2003) Microporous Mesoporous Mater 54:305
147. Turnes Palomino G, Cuart Pascual JJ, Rodriguez Delgado M, Bernardo Parra J, Otero Areán C (2004) Mat Chem Phys 85:145
148. Otero Areán C, Turnes Palomino G, Geobaldo F, Zecchina A (1996) J Phys Chem 100:6678
149. Katovic A, Giordano G, Bonelli B, Onida B, Garrone E, Lentz P, Nagy JB (2001) Microporous Mesoporous Mater 275:44–45
150. Nesterenko NS, Ponomporeva OA, Yuschenko VV, Ivanova II, Testa F, Di Renzo F, Fajula F (2003) Appl Cat A 254:261
151. Dapurkar SE, Selvam P (2004) J Catal 224:178
152. Bodoardo S, Chiappetta R, Onida B, Figueras F, Garrone E (1998) Microporous Mesoporous Mater 20:187
153. Baerlocher C, Meier WM, Olson DH (2001) Atlas of zeolite framework types, 5th edn. Elsevier, Amsterdam, p 302

Author Index Volumes 1–6

Aiello R, see Nagy JB (2006) *5*: 365–478
Anderson PA (2002) Ionic Clusters in Zeolites. *3*: 307–338
Auroux A (2008) Acidity and Basicity: Determination by Adsorption Microcalorimetry. *6*: 45–152

Baerlocher C, see Meier WM (1999) *2*: 141–161
Bauer F, Karge HG (2006) Characterization of Coke on Zeolites. *5*: 249–364
Beck JS, see Vartuli JC (1998) *1*: 97–119
Behrens P (2004) XANES, EXAFS and Related Techniques. *4*: 427–466
Bellussi G, see Perego G (1998) *1*: 187–228
Bennett JM, see Koningsveld van W (1999) *2*: 1–29
Beyer HK, see Karge HG (2002) *3*: 43–201
Beyer HK (2002) Dealumination Techniques for Zeolites. *3*: 203–255
Bonardet J-L, Gédéon A, Springuel-Huet M-A, Fraissard J (2006) NMR of Physisorbed ^{129}Xe Used as a Probe to Investigate Molecular Sieves. *5*: 155–248
Brait A, see Lercher JA (2008) *6*: 153–212
Brunner E, see Hunger M (2004) *4*: 201–293
Brunner E, Pfeifer H (2008) NMR Spectroscopic Techniques for Determining Acidity and Basicity. *6*: 1–43

Coker EN, Jansen JC (1998) Approaches for the Synthesis of Ultra-Large and Ultra-Small Zeolite Crystals. *1*: 121–155
Cool P, Vansant EF (1998) Pillared Clays: Preparation, Characterization and Applications. *1*: 265–288

Depmeier W (1999) Structural Distortions and Modulations in Microporous Materials. *2*: 113–140

Ernst S (1998) Synthesis of more Recent Aluminosilicates with a Potential in Catalysis and Adsorption. *1*: 65–96

Fajula F, see Garrone E (2008) *6*: 213–267
Fitch AN, Jobic H (1999) Structural Information from Neutron Diffraction. *2*: 31–70
Förster H (2004) UV/VIS Spectroscopy. *4*: 337–426
Fraissard J, see Bonardet J-L (2006) *5*: 155–248
Fricke R, see Kosslick H (2006) *5*: 1–66

Gallezot P (2002) Preparation of Metal Clusters in Zeolites. *3*: 257–305
Garrone E, Fajula F (2008) Acidity and Basicity of Ordered Silica-based Mesoporous Materials. *6*: 213–267
Gédéon A, see Bonardet J-L (2006) *5*: 155–248
Geidel E, see Karge HG (2004) *4*: 1–200
Gies H, Marler B, Werthman U (1998) Synthesis of Porosils: Crystalline Nanoporous Silicas with Cage- and Channel-Like Void Structures. *1*: 35–64
Giordano G, see Nagy JB (2006) *5*: 365–478
Grünert W, Schlogl R (2004) Photoelectron Spectroscopy of Zeolites. *4*: 467–515

Harjula R, see Townsend RP (2002) *3*: 1–42
Heidler R, see Weckhuysen BM (2004) *4*: 295–335
Hunger M, Brunner E (2004) NMR Spectroscopy. *4*: 201–293

Jansen JC, see Coker EN (1998) *1*: 121–155
Jentys A, see Lercher JA (2008) *6*: 153–212
Jobic H, see Fitch AN (1999) *2*: 31–70

Karge HG, Beyer HK (2002) Solid-State Ion Exchange in Microporous and Mesoporous Materials. *3*: 43–201
Karge HG, Geidel E (2004) Vibrational Spectroscopy. *4*: 1–200
Karge HG, see Bauer F (2006) *5*: 249–364
Katovic A, see Nagy JB (2006) *5*: 365–478
Kiricsi I, see Nagy JB (2006) *5*: 365–478
Kresge CT, see Vartuli JC (1998) *1*: 97–119
Koningsveld van W, Bennett JM (1999) Zeolite Structure Determination from X-Ray Diffraction. *2*: 1–29
Kónya Z, see Nagy JB (2006) *5*: 365–478
Kosslick H, Fricke R (2006) Chemical Analysis of Aluminosilicates, Aluminophosphates and Related Molecular Sieves. *5*: 1–66

Lercher JA, Jentys A, Brait A (2008) Catalytic Test Reactions for Probing the Acidity and Basicity of Zeolites. *6*: 153–212

Marler B, see Gies H (1998) *1*: 35–64
McCullen SB, see Vartuli JC (1998) *1*: 97–119
Meier WM, Baerlocher C (1999) Zeolite Type Frameworks: Connectivities, Configurations and Conformations. *2*: 141–161
Millini R, see Perego G (1998) *1*: 187–228

Nagy JB, Aiello R, Giordano G, Katovic A, Testa F, Kónya Z, Kiricsi I (2006) Isomorphous Substitution in Zeolites. *5*: 365–478

Pál-Borbély G (2006) Thermal Analysis of Zeolites. *5*: 67–101
Perego G, Millini R, Bellussi G (1998) Synthesis and Characterization of Molecular Sieves Containing Transition Metals in the Framework. *1*: 187–228
Pfeifer H, see Brunner E (2008) *6*: 1–43
Pfenninger A (1999) Manufacture and Use of Zeolites for Adsorptions Processes. *2*: 163–198

Rees LVC (2004) Mossbauer Spectroscopy. *4*: 517–543
Roth WJ, see Vartuli JC (1998) *1*: 97–119
Rymsa U, see Weitkamp J (2002) *3*: 339–414

Schlögl R, see Grünert W (2004) *4*: 467–515
Schoonheydt RA, see Weckhuysen BM (2004) *4*: 295–335
Schulz-Ekloff G, see Weitkamp I (2002) *3*: 339–414
Schunk SA, Schüth F (1998) Synthesis of Zeolite-Like Inorganic Compounds. *1*: 229–263
Schüth F, see Schunk SA (1998) *1*: 229–263
Sealy S, see Traa Y (2006) *5*: 103–154
Springuel-Huet M-A, see Bonardet J-L (2006) *5*: 155–248
Szostak R (1998) Synthesis of Molecular Sieve Phosphates. *1*: 157–185

Terasaki O (1999) Electron Microscopy Studies in Molecular Sieve Science. *2*: 71–112
Testa F, see Nagy JB (2006) *5*: 365–478
Thompsen RW (1998) Recent Advances in the Understanding of Zeolite Synthesis. *1*: 1–33
Townsend RP, Harjula R (2002) Ion Exchange in Molecular Sieves by Conventional Techniques. *3*: 1–42
Traa Y, Sealy S, Weitkamp J (2006) Characterization of the Pore Size of Molecular Sieves Using Molecular Probes. *5*: 103–154

Vansant EF, see Cool P (1998) *1*: 265–288
Vartuli JC, Roth WJ, Beck JS, McCullen SB, Kresge CT (1998) The Synthesis and Properties of M41S and Related Mesoporous Materials. *1*: 97–119

Wark M, see Weitkamp J (2002) *3*: 339–414
Weckhuysen BM, Heidler R, Schoonheydt RA (2004) Electron Spin Resonance Spectroscopy. *4*: 295–335
Weitkamp J, Rymsa U, Wark M, Schulz-Ekloff G (2002) Preparation of Oxide, Sulfide and Other Chalcogenide Clusters in Molecular Sieves. *3*: 339–414
Weitkamp J, see Traa Y (2006) *5*: 103–154
Werthmann U, see Gies H (1998) *1*: 35–64

Subject Index

Accessibility 15
Acetone 98
–, condensation 200
–, diacetone alcohol, base-catalyzed 200
Acetonitrile 68, 76
Acetonylacetone cyclization 196
Acetonylacetone, 2,5-dimethylfuran 197
Acetophenone/malononitrile, Knoevenagel condensation 201
Acetylene 196
Acid sites 156
–, activated samples, strength of acidity 11
–, concentration 10, 158
–, density 189
–, probing 163
Acid strength, catalysis 165
–, improving 255
Acid/basic bifunctional properties 193
Acidity, enhanced strength 7
–, tuning 119
Acidity/basicity 59, 253
Additives 126
Adsorption, acidic sites 223
–, selective 61
Adsorption complexes, geometry 24
Adsorption heat 69
Adsorption temperature 99, 109
Aging 125
Alcohol conversion 195, 198
Alcohol dehydration 185
Alcohol/ketone 204
Alkane hydroconversion 240
Alkane hydrogenolysis 127
Alkanes, superacid (HF) 166
Alkylcarbenium ions 170
Allyl cyanide 203
Al-MTS, ion-exchanged/ion-impregnated samples 220
Alumination, post-synthesis 255
Aluminophosphates (VPI/$AlPO_4$) 130
Ammonia 68
Ammonium hexafluorosilicate 90
Aromatic molecules 77

Bare samples 225
Basic sites 161
Basicity 60
–, NMR 36
–, probing 197
Bellamy–Hallam–William plot 225
Benzene 24, 99
Beta zeolites 119
Boron, T atom 258
Boron-impregnated zeolites 124
Boron-substituted zeolites 120
Brønsted acid sites 4
–, NMR 8
Brønsted acidity 157
Brønsted sites 237
Butene isomerization 193, 198
n-Butylamine 76
Butyrolactones 202

Cal-ad method 55
Calorimetry 56
Carbon–carbon bond cleavage 168
Catalysts, bifunctional 126
Catalytic activity 138
Catalytic test reactions 162
Cation substitution, development of acidity 249
Chemical modification 124
Clusters, zeolite cages 162
CO adsorption 237
CoAPOs 135
Coke deposition 105, 125

Combined rotation and multiple-pulse spectroscopy (CRAMPS) 8
Constant rate thermal analysis (CRTA) 49
Copper 126
Cracking activity 5
CrAPO 134
Crotononitrile 203
Crystallite size 81
Cyclohexene, conversion 168
–, reactions 189
Cyclopentane 99

Dealuminated zeolites 249
Dealumination 64, 102, 113
–, H-Y zeolites 87
Defects 119
Dehydrated samples 28
Diacetone alcohol decomposition 200
Diethylether 98
Differential scanning calorimetry (DSC) 48
Differential thermal analysis (DTA) 48
Differential thermogravimetry (DTG) 48
Diketone cyclization 203
3,3-Dimethyl-1-butene 166
Dimethylether 76
Dimethylfuran 203
2,4-Dimethylpentane, cracking 166
Dinitrogen oxide 32
Diphosphine 22
Disproportionation 179

EDTA 91
Electronegativity 5, 36, 157
– equalization method (EEM) 161
Engelhard titanosilicate-10 123
Erionites 115
Ethylbenzene 99
ETS-10 124
Exchange level 110
Extra-framework alumina species (EFAL) 160, 172

Faujasite-type zeolites 73
Faujasites, thermal stability 79
Fe, T atom 259
Ferrierite-type zeolites 116
Flow microcalorimetry 55
Fluid cracking catalysts (FCCs) 94, 125
–, acidity 94
Fluorine 125
Framework basicity 161

Gallium, T atom 258
Gallium-substituted zeolites 120

H-Al-MTS (Brønsted/Lewis) 243
–, protonic 222
H-bonded adducts 229
H-Rho 116
Heats of adsorption 78
n-Hexane 166
–, cracking activity 5
2,5-Hexanedione (acetonylacetone) 203
Hydrated samples 27
Hydride transfer reactions 192
Hydrocarbons 76
–, cracking 239
Hydrogenation–dehydrogenation 126
Hydroxonium ions 22
Hydroxyl groups 5, 161
3-Hydroxy-3-methyl-2-butanone (HMB)

Indium-substituted zeolites 120
IR spectroscopy 224
Iron-substituted zeolites 120
Isobutene dehydrogenation 129
Isomerization 182
Isomorphous substitution 119
Isopropylamine 49, 70, 75

Knoevenagel condensation 201

Lewis acidity 159, 222
–, NMR 27
Lewis sites 237

Magic angle spinning (MAS) 9
Malononitrile 201
MAS-NMR 224
Mazzite 116
MCM-22 117
MCM-41 136
Mesoporous materials 136
Metal aluminophosphates (MeAPOs) 134
Methacrylonitrile 203
Methanol 23, 138
–, dimethyl ether 198
3-Methyl-2-butenal (PRENAL) 196
3-Methyl-2-cyclopentenone 197

3-Methyl-2-pentene (3M2P) 167
4-Methyl-2-pentene (4M2P) 167
3-Methyl-3-butene-2-one (MIPK) 196
3-Methyl-3-buten-1-yne (MBYNE) 196
2-Methyl-3-butyn-2-ol 196
2-Methylpentane, cracking 166
MgAPO 135
Micelle templated silica (MTS) 216
Microactivity test (MAT) 125
Mobility 24
Molecular sieves 130
Mordenites 107
MWW-based catalysts 117

Neopentane 166, 173
Next-nearest neighbors (NNN) 159
Nickel 126
Nitriles 98
–, interconversion 203
NMR 224
–, ^{27}Al- 27
–, Brønsted acid sites 4
–, MAS- 224
NO 69
Noble metal 126

Occluded clusters 86
Octane number 126
Offretites 115
Outer surfaces 247

Paraffins 77
n-Pentane, protolytic cracking 171
Phosphorus-modified zeolites 124
Piperidine 75
Pore diameter 61
Pore openings 156
Post-synthesis alumination 255
Pretreatment 101, 109
Probe molecules, acidic/basic 65
–, NMR 22
Propan-2-ol 198
Propene 198
Propyne 78
Proton affinities 69
Proton exchange 81, 101
Proton transfer, strongly basic molecules 229
Pt 126
Pyridine 31, 75, 96
Pyridinium ions 22
Pyrrole 67

Rapid exchange 32
Re-USY zeolites 94
REDOR (rotational echo double resonance) 26
Ring exchange reactions 202

SEDOR (spin echo double resonance) 9
Si/Al ratio 63, 102
Silica molecular sieves, isomorphous 105
Silicalite-1 105
Silicoaluminophosphates (SAPOs) 132
Slow exchange 31
Sodium oxide 124
Steaming, dealumination 88
Strength of acidity, acid sites 15
Surface hydroxyl groups, loaded samples, NMR 15
SVK 118

T atoms, tetravalent 122
–, trivalent 120, 257
Tectosilicates 157
Temperature dependence 78
Temperature-programmed desorption (TPD) 94
Tetrachloroethene 99
Tetrahydrofuran 202
Tetrahydrothiophene 202
Thermal analysis techniques 49
Thiobutyrolactones 202
Ti-beta zeolites
Time on stream (TOS) 163
Titanosilicate (TS-1) 122
Toluene 124
– alkylation 194, 199
Trichloroethylene (TCE) 77
1,2,4-Trimethylbenzene 166
2,2,4-Trimethylpentane, cracking 166
Trimethylphosphine 22, 32
Turnover frequency (TOF) 164

o-Xylene, disproportionation 166

Zeolite G/L 118
ZK-4/ZK-5 118
ZSM-5 zeolites 95
–, metal-modified 104